

A PRECIPITATION MODEL AND ITS USE IN REAL-TIME RIVER
FLOW FORECASTING

by

KONSTANTINE P. GEORGAKAKOS
Dipl., National Technical University of Athens
(1977)

M.S., Massachusetts Institute of Technology
(1980)

SUBMITTED IN PARTIAL FULFILLMENT
OF THE REQUIREMENT FOR THE DEGREE OF

DOCTOR OF SCIENCE

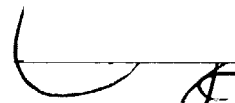
at the

MASSACHUSETTS INSTITUTE OF TECHNOLOGY
July 1982

© Massachusetts Institute of Technology 1982

Signature redacted

Signature of Author


Department of Civil Engineering
July 20, 1982


Signature redacted

Certified by


Rafael L. Bras
Thesis Supervisor

Signature redacted

Accepted by


Francois Morel
Chairman, Department Committee

Archives

MASSACHUSETTS INSTITUTE
OF TECHNOLOGY

NOV 19 1982

LIBRARIES

A PRECIPITATION MODEL AND ITS USE IN
REAL-TIME RIVER FLOW FORECASTING

by

KONSTANTINE P. GEORGAKAKOS

Submitted to the Department of Civil Engineering
on July 26, 1982 in partial fulfillment of the requirements
for the Degree of Doctor of Science in Civil Engineering

ABSTRACT

A one-dimensional, physically based, station precipitation model is proposed and tested. The model state variable is the liquid water equivalent mass in a unit area cloud column. Model inputs are the air temperature, dew-point temperature, and pressure at the ground surface. The precipitation rate at the ground surface is the model output. Simplified cloud microphysics give expressions for the moisture input and output rates in and from the unit area column. Parameterization of the model physical quantities: updraft velocity, cloud top pressure, and average layer cloud-particle diameter is proposed, so that parameters, will remain reasonably constant for different storms.

Conceptual soil and channel routing models were used together with the proposed precipitation model in formulating a general Rainfall-Runoff model.

Hourly data from eleven storms of different types and from two different locations in the US served as the data-base for the station precipitation model tests. Performance in predicting the hourly precipitation rate was good, particularly when a sequential state estimator was used with the model.

The general Rainfall-Runoff model formulated, complemented by a sequential state estimator, was used with six-hourly hydrological data from the Bird Creek basin, Oklahoma, and with six-hourly meteorological data from the somewhat distant Tulsa, Oklahoma, site. Forecasts of both the mean areal precipitation rate and the basin outflow discharge were obtained. Performance indicated the value of the precipitation model in the real-time river flow forecasting.

Thesis Supervisor: Rafael L. Bras

Title: Associate Professor of Civil
Engineering

ACKNOWLEDGEMENTS

I am indebted to my family for their encouragement and support during the time of preparation of this work.

Discussions with many people during the time of my residence at MIT have affected my thoughts and ideas.

The critical attitude and the encouragement of my advisor, Professor Rafael L. Bras, throughout this work, is gratefully acknowledged.

Professors Peter S. Eagleson and John L. Wilson offered many useful comments and suggestions on several occasions.

Discussions with Chris Milly, Lloyd Townley, Telis Mantoglou, Pedro Restrepo-Posada, Jorge Ramirez, Aris Georgakakos, Carlos Puente, Mario Diaz-Granados, Stefanos Andreou, and Diana Kirshen have been useful and they are rightfully acknowledged.

I am grateful to Elaine Healy, Susan Shanahan, and Antoinette DiRenzo for the efficient typing of this thesis.

This work was financially supported by the U. S. Department of Commerce, National Weather Service, Contract Number NA80AA-H-00044.

Administrative support was provided by MIT through the Office of Sponsored Programs, OSP 89310. All the computer work was performed at the MIT Information Processing Center on a Honeywell 6180, Multics Operating System.

TABLE OF CONTENTS

	<u>Page No.</u>
TITLE PAGE	1
ABSTRACT	2
ACKNOWLEDGEMENTS	4
TABLE OF CONTENTS	5
LIST OF FIGURES	10
LIST OF TABLES	17
LIST OF PRINCIPAL SYMBOLS	19
CHAPTER 1 INTRODUCTION	28
1.1 General Framework and Scope of Study	28
1.2 Program of Study	31
CHAPTER 2 STATION PRECIPITATION MODEL OVERVIEW	33
2.1 Introduction	33
2.2 Model Hypothesis	33
2.3 Model Overview	34
CHAPTER 3 WATER VAPOR CONDENSATION	42
3.1 Introduction	42
3.2 General Description of Condensation	42
3.3 Water Mass Rate Condensed	
Per Unit Mass of Moist Air	43

	<u>Page No.</u>
3.4 Input Mass Rate Per Unit Area	50
3.5 Discussion of Assumptions in the Unit Area Column Condensation Equation	52
CHAPTER 4 STORM PRECIPITATION FORMATION AND EVOLUTION	56
4.1 Introduction	56
4.2 Precipitation Formation	57
4.3 Size Distribution of Hydrometeors	59
4.4 Terminal Velocity of Hydrometeors	69
4.5 Steady State Diffusion of Precipitation Particles in Sub-Saturated Air	74
CHAPTER 5 STATION PRECIPITATION MODEL EQUATIONS	86
5.1 Introduction	86
5.2 Unit Area Column Output Rate	86
5.3 Surface Precipitation Mass Rate	89
5.4 Mass Rates Expressed as Functions of the Dimensionless Numbers N_V and N_D	90
5.5 Unit Area Model Parameters	97
5.5.1 Updraft Velocity and Terminal Pressure Parameterization	98
5.5.2 Parameterization of Average Hydrometeor Diameter at Cloud Base	106

	<u>Page No.</u>
CHAPTER 6 A CONCEPTUAL RAINFALL-RUNOFF MODEL	107
6.1 Introduction	107
6.2 Equations of the Soil Moisture Accounting Model	108
6.3 Equations for Channel Routing	118
6.4 Rainfall-Runoff Model	119
6.5 Precipitation, Soil and Channel Models Coupling	123
6.6 The Spatial and Temporal Scales of the Rainfall-Runoff Model Components	124
CHAPTER 7 THE STOCHASTIC RAINFALL-RUNOFF MODEL	131
7.1 Introduction	131
7.2 General Linear Filter for Nonlinear System Equations with Random Inputs	132
7.2.1 Linear Taylor's Series Expansion	142
7.2.2 Statistical Linearization	145
7.3 Linearization of the Rainfall-Runoff Model Equations	147
CHAPTER 8 CASE STUDIES	152
8.1 Introduction	152

	<u>Page No.</u>
8.2 Station Precipitation Model Input	
Data Characteristics	152
8.3 Station Precipitation Model Parameter Determination	195
8.4 Deterministic Station Precipitation Model	206
8.5 Stochastic Station Precipitation Model	216
8.6 Deterministic Rainfall-Runoff Model	227
8.7 Stochastic Rainfall-Runoff Model	231
CHAPTER 9 CONCLUSIONS AND RECOMMENDATIONS	239
9.1 Summary of Results	239
9.2 Future Research	242
9.2.1 Related to Precipitation Forecasting	242
9.2.2 Related to River Flow Forecasting	243
REFERENCES	246
APPENDIX A GLOSSARY OF METEOROLOGICAL TERMS USED	251
APPENDIX B SOLUTION OF THE STATION PRECIPITATION MODEL NONLINEAR ALGEBRAIC EQUATION BY THE NEWTON-RAPHSON ITERATIONS METHOD	254

		<u>Page No.</u>
APPENDIX C	EQUATIONS FOR LARGE RIVER BASIN NETWORKS	260
APPENDIX D	STATION PRECIPITATION MODEL LINEARIZED EQUATIONS	265
APPENDIX E	SOIL MOISTURE ACCOUNTING MODEL LINEARIZED EQUATIONS	287
APPENDIX F	CHANNEL ROUTING MODEL LINEARIZED EQUATIONS	296

LIST OF FIGURES

<u>Figure No.</u>	<u>Title</u>	<u>Page No.</u>
2.1	Schematic representation of the unit area column model variables at time t	39
2.2	Updraft velocity variation with pressure p_s : lifting condensation level pressure p_t : cloud top pressure v : height averaged updraft velocity	41
3.1	Observed (solid lines) saturation vapor pressure over a plane surface of water ($e_{s_w}(T)$) or ice ($e_{s_i}(T)$) vs. temperature T. Fitted $e_s(T)$ in dashed line.	45
4.1	Normalized number concentration n_n , water mass content X_n and precipitation rate P_n due to hydrometeors of diameter in the range $(D, D + dD)$ vs. the normalized diameter cD .	63
4.2a	Height variation of the inverse layer-average diameter c . c_u at cloud top and c_l at cloud bottom	65
4.2b	Height Variation of the layer-average diameter \bar{D} . \bar{D}_u at cloud top and \bar{D}_l at cloud bottom	65
4.3	Observed and fitted terminal velocity as a function of hydrometeor diameter Curve 1: Raindrops, $T = 273.15[^\circ\text{K}]$, $p = 800[\text{MBAR}]$ - Beard (1976) Curve 2: Raindrops, $T = 293.15 [^\circ\text{K}]$, $p = 1013 [\text{MBAR}]$ - Beard (1976) Curve 3: Raindrops, fitted - Eqs. (4.7) and (4.21)	71

- Curve 4: Ice sphere, $\rho = 500$ [KG/M³],
 $T = 273.15$ [°K], $p = 1013$ [MBAR] -
 Beard (1976)
- Curve 5: Lump graupel - Locatelli and
 Hobbs (1974)
- Curve 6: Ice sphere, $\rho = 100$ [KG/M³],
 $T = 273.15$ [°K], $p = 1013$ [MBAR] -
 Beard (1976)
- Curve 7: Hexagonal groupel - Locatelli
 and Hobbs (1974)
- Curve 8: Aggregates of dendritic crystals -
 Locatelli and Hobbs (1974).
- Curve 9: Snow, fitted - Eqs. (4.7) and
 (4.22) 71
- 4.4 Integral F as a function of the water equivalent
 diameter D*
- Curve 1: $T_0 = 273.15$ [°K], $p_0 = 1013$ [MBAR],
 $\rho_p = 1000$ [KG/M³]
- Curve 2: $T_0 = 293.15$ [°K], $p_0 = 1013$ [MBAR],
 $\rho_p = 1000$ [KG/M³]
- Curve 3: $T_0 = 273.15$ [°K], $p_0 = 800$ [MBAR],
 $\rho_p = 1000$ [KG/M³]
- Curve 4: $T_0 = 273.15$ [°K], $p_0 = 1013$ [MBAR],
 $\rho_p = 100$ [KG/M³] 79
- 4.5a Numerical integration results in Pruppacher and
 Klett (1978) used to determine the constant c_1 in
 Eq. (4.42).
 $T_0 = 278.15$ [°K] and $p_0 = 800$ [MBAR]. 83
- 4.5b Initial diameter at cloud base D_0 as a
 function of Z_b for different values of r .
 Solid lines are for numerical integration re-
 sults in Beard and Pruppacher (1971).
 Dashed lines are for Eq. (4.42) with
 $D_F = 0.2$ [MM]. $T_0 = 273.15$ [°K] and
 $p_0 = 765$ [MBAR]. 83

<u>Figure No.</u>	<u>Title</u>	<u>Page No.</u>
4.6	Initial diameter D_c at cloud base, of the largest completely evaporating hydrometeor in a sub-cloud layer of depth Z_b , as a function of Z_b , for different values of the relative humidity r . For raindrops: $T_0 = 293.15 [^{\circ}\text{K}]$, $p_0 = 1013 [\text{MBAR}]$ For snow particles: $T_0 = 273.15 [^{\circ}\text{K}]$, $p_0 = 1013 [\text{MBAR}]$	85
5.1	Reduction factors m_b , m_t and m_p as functions of the number N_v . N_d and γ are parameters of the plots. Curve 1 is for m_b . Curves 1, 2 and 3 are for m_p , for N_d equal to 0, 2, and 4 respectively. Curves 4 and 5 are for m_t for γ equal to 1 and 2 respectively.	92
5.2	Temperature variation of p_t (solid lines) and Q_{TH} (dashed lines) for $p_0 = 1000 [\text{MBAR}]$. Plot parameters are: ϵ_2 , r , $\epsilon_1 \cdot \epsilon_3$ Curve 1: $\epsilon_2 = 700 [\text{MBAR}]$, $r = 0.7$, $\epsilon_1 \cdot \epsilon_3 = 0.01 [\text{SEC/M}]$ Curve 2: $\epsilon_2 = 700 [\text{MBAR}]$, $r = 1$, $\epsilon_1 \cdot \epsilon_3 = 0.01 [\text{SEC/M}]$ Curve 3: $\epsilon_2 = 500 [\text{MBAR}]$, $r = 1$, $\epsilon_1 \cdot \epsilon_3 = 0.01 [\text{SEC/M}]$ Curve 4: $\epsilon_2 = 700 [\text{MBAR}]$, $r = 0.7$ $\epsilon_1 \cdot \epsilon_3 = 0.05 [\text{SEC/M}]$ Curve 5: $\epsilon_2 = 700 [\text{MBAR}]$, $r = 1$, $\epsilon_1 \cdot \epsilon_3 = 0.05 [\text{SEC/M}]$ Curve 6: $\epsilon_2 = 500 [\text{MBAR}]$, $r = 1$, $\epsilon_1 \cdot \epsilon_3 = 0.05 [\text{SEC/M}]$	102
5.3	Pressure \bar{p}_t for $T_0 = 266.16 [^{\circ}\text{K}]$ as a function of the parameter product $\epsilon_1 \cdot \epsilon_3$ with ϵ_2 and r as plot parameters. Curve 1: $\epsilon_2 = 700 [\text{MBAR}]$, $r = 0.7$ Curve 2: $\epsilon_2 = 700 [\text{MBAR}]$, $r = 1$ Curve 3: $\epsilon_2 = 500 [\text{MBAR}]$, $r = 1$.	104

<u>Figure No.</u>	<u>Title</u>	<u>Page No.</u>
6.1a	Outflow $g(\frac{x}{x^0}, u_0)$ from a threshold type reservoir with normalized content $(\frac{x}{x^0})$ and input u_0 .	111
6.1b	Outflow $g_a(\frac{x}{x^0}, u_0)$ from a nonlinear reservoir of exponent m , with normalized content $(\frac{x}{x^0})$ and input u_0 .	111
8.1	Dew point regression hourly predictions (stars) vs. observations (solid line) for storm group 3.	170
8.2	Surface pressure regression hourly predictions (stars) vs. observations (solid line) for storm group 3	171
8.3	Precipitation rate hourly predictions (stars) based on the linear model of Table 8.7 vs. observations (solid line). Storm group 1.	175
8.4	Precipitation rate hourly predictions (stars) based on the linear model of Table 8.7 vs. observations (solid line). Storm group 2	176
8.5	Precipitation rate hourly predictions (stars) based on the linear model of Table 8.7 vs. observations (solid line). Storm group 3.	177
8.6	Precipitation rate hourly predictions (stars) based on the linear model of Table 8.7 vs. observations (solid line). Storm group 4.	178
8.7	Precipitation rate hourly predictions (stars) based on the linear model of Table 8.7 vs. observations (solid line). Storm group 5.	179
8.8	Precipitation rate hourly predictions (stars) based on the linear model of Table 8.8 vs. observations (solid line). Storm group 1.	185
8.9	Precipitation rate hourly predictions (stars) based on the linear model of Table 8.8 vs. observations (solid line). Storm group 2.	186
8.10	Precipitation rate hourly predictions (stars) based on the linear model of Table 8.8 vs. observations (solid line). Storm group 3.	187

<u>Figure No.</u>	<u>Title</u>	<u>Page No.</u>
8.11	Precipitation rate hourly predictions (stars) based on the linear model of Table 8.8 vs. observations (solid line). Storm group 4.	188
8.12	Precipitation rate hourly predictions (stars) based on the linear model of Table 8.8 vs. observations (solid line). Storm group 5.	189
8.13	Absolute proportional average error (E_1). Storm group 2. Contour values: 1 = 0.24, 2 = 0.73, 3 = 1.21, 4 = 1.70, 5 = 2.18.	197
8.14	Proportional standard error (E_2). Storm group 2 Contour values: 1 = 0.942, 2 = 0.948, 3 = 0.954, 4 = 0.960, 5 = 0.966	198
8.15	Cross-correlation coefficient of observations and predictions (E_3). Storm group 2 Contour values: 1 = 0.351, 2 = 0.344, 3 = 0.337, 4 = 0.330, 5 = 0.323	199
8.16	Absolute proportional average error (E_1). Storm group 3 ($c_1 = 1.4 \times 10^5$ [KG/M ³ /SEC]). Contour values: 1 = 0.1, 2 = 0.3, 3 = 0.5, 4 = 0.7, 5 = 0.9	202
8.17	Proportional standard error (E_2). Storm group 3 ($c_1 = 1.4 \times 10^5$ [KG/M ³ /SEC]). Contour values: 1 = 0.84, 2 = 0.87, 3 = 0.90, 4 = 0.93, 5 = 0.96	203
8.18	Absolute proportional average error (E_1). Storm group 3 ($c_1 = 7 \times 10^5$ [KG/M ³ /SEC]). Contour values: 1 = 0.1, 2 = 0.3, 3 = 0.5, 4 = 0.7, 5 = 0.9	204
8.19	Proportional standard error (E_2). Storm group 3 ($c_1 = 7 \times 10^5$ [KG/M ³ /SEC]). Contour values: 1 = 0.84, 2 = 0.87, 3 = 0.90, 4 = 0.93, 5 = 0.96	205
8.20	Deterministic precipitation model hourly predictions (stars) vs. observations (solid line). Storm group 1	208
8.21	Deterministic precipitation model hourly predictions (stars) vs. observations (solid line). Storm group 2	209

<u>Figure No.</u>	<u>Title</u>	<u>Page No.</u>
8.22	Deterministic precipitation model hourly predictions (stars) vs. observations (solid line). Storm group 3	210
8.23	Deterministic precipitation model hourly predictions (stars) vs. observations (solid line). Storm group 4	211
8.24	Deterministic precipitation model hourly predictions (stars) vs. observations (solid line). Storm group 5	212
8.25	Stochastic precipitation model hourly predictions (stars) vs. observations (solid line). Storm group 1.	217
8.26	Stochastic precipitation model hourly predictions (stars) vs. observations (solid line). Storm group 2	218
8.27	Stochastic precipitation model hourly predictions (stars) vs. observations (solid line). Storm group 3.	219
8.28	Stochastic precipitation model hourly predictions (stars) vs. observations (solid line). Storm group 4.	220
8.29	Stochastic precipitation model hourly predictions (stars) vs. observation (solid line). Storm group 5.	221
8.30	Deterministic Rainfall-Runoff model precipitation rate 6-hourly predictions (stars) vs. observations (solid line). Bird Creek, May 1959	228
8.31	Deterministic Rainfall-Runoff model precipitation rate 6-hourly predictions (stars) vs. observations (solid line). Bird Creek, May 1959	229
8.32	Stochastic Rainfall-Runoff model outflow discharge 6-hourly predictions (stars) vs. observations (solid line), for a model error of low intensity. Bird Creek, May 1959	236
8.33	Stochastic Rainfall-Runoff model outflow discharge 6-hourly predictions (stars) vs. observations (solid line), for a model error of high intensity. Bird Creek, May 1959	237

<u>Figure No.</u>	<u>Title</u>	<u>Page No.</u>
C.1	Hypothetical large river basin with five tributary-basins	262
C.2	Flow of computation, indicated by arrows, for the tributary-basin network of Figure C.1. PREC j: Precipitation model computations for basin j SOIL j: Soil model computations for basin j CHANNEL j: Channel routing model computations for basin j.	263

LIST OF TABLES

<u>Table No.</u>	<u>Title</u>	<u>Page No.</u>
6.1	Soil Moisture Accounting Model Variables	113
6.2	Headwater Basin Rainfall-Runoff Model Symbols	121
6.3	Spatial Scales of Atmospheric Motions	126
6.4	Spatial and Temporal Scales of Rainfall-Runoff Model Components	130
7.1	Nonzero Elements of Matrix \overline{N}_F	149
7.2	Nonzero Elements of Matrix \overline{M}_F	150
7.3	Nonzero Elements of Matrix \overline{N}_G	151
7.4	Nonzero Elements of Matrix \overline{M}_G	151
8.1	Case Study Storms	154
8.2	Storm Data Statistics - I	160
8.3	Storm Data Statistics - II	161
8.4	Storm Data Statistics - III	162
8.5	Storm Data Statistics - IV	163
8.6	Dew Point and Surface Pressure Regression Parameters for Storm Group 3	172
8.7	Regression Parameters and Standard Errors. Regression of Precipitation Rate on Temperatures and Pressures	180
8.8	Regression Parameters and Standard Errors. Regression of Precipitation Rate on Temperatures, Pressure, and 1-Hour Lagged Precipitation Rate.	190
8.9	Deterministic Precipitation Model Residual Statistics for Storm Groups 1 to 5	213
8.10	Deterministic Precipitation Model Least Squares Performance Measures for Storm Groups 1 to 5	214

<u>Table No.</u>	<u>Title</u>	<u>Page No.</u>
8.11	Stochastic Precipitation Model Residual Statistics for Storm Groups 1 to 5	222
8.12	Stochastic Precipitation Model Least Squares Performance Measures for Storm Groups 1 to 5	223
8.13	Least Squares Performance Measures for Storm Group 1. Maximum Lead Time 6-hours.	225
8.14	Least Squares Performance Measures for Storm Group 5. Maximum Lead Time 6-hours.	226
8.15	Rainfall-Runoff Initial State Variances and Model Error Spectral Density Matrix Diagonal Elements.	232
8.16	Rainfall-Runoff Model Observation Error Covariance Matrix	233
8.17	Rainfall-Runoff Model Residual Statistics	234

LIST OF PRINCIPAL SYMBOLS

Excluding the symbols in Tables 6.1 and 6.2

<u>Symbol</u>	<u>Description</u>	<u>Equation No.</u>
<u>English Alphabet Symbols:</u>		
A	Drainage basin area	6.25
A_i	Regression parameters (Chapter 8)	
a_i	Parameters of the channel model	6.15
c	Inverse of average layer cloud-particle diameter	4.1
c_1, c_2	Constant coefficients in the diffusion integral approximation	4.35
c_ℓ, c_u	Inverse of average layer cloud-particle diameters at cloud base and cloud top	4.8
c_p	Specific heat of dry air under constant pressure (Chapter 3)	
D	Cloud-particle diameter	4.1
\bar{D}	Average layer cloud-particle diameter	4.10
D_{AB}	Diffusivity of water vapor in air	4.23
D_c	Diffusion critical cloud-particle diameter	4.40
D_{\min}, D_{\max}	Minimum and maximum cloud-particle diameter	4.11
D_ℓ	Minimum diameter of cloud-particles that fall below cloud base	5.2
\bar{D}_ℓ, \bar{D}_u	Average layer cloud-particle diameter at cloud base and cloud top	4.10
D_0, D_F	Cloud-particle diameter at cloud base and at the ground	4.32
$\underline{d}_x(t)$	Parameters of the state vector, current, probability density	7.9
$\underline{d}_u(t)$	Parameters of the input vector, current, probability density	7.9

<u>Symbol</u>	<u>Description</u>	<u>Equation No.</u>
E_1	Absolute proportional average error (Chapter 8)	
E_2	Proportional standard error (Chapter 8)	
E_3	Cross-correlation coefficient of observations and predictions (Chapter 8)	
$e_s(T)$	Saturation vapor pressure over a plane surface of pure water at temperature T	3.1
$F(D)$	Diffusion integral	4.33
$\underline{F}(\underline{x}(t), \underline{u}(t), t)$	Nonlinear vector function of state, input and time in the continuous system dynamics equation	7.1
$\underline{F}_0(\underline{d}_{\underline{x}}(t), \underline{d}_{\underline{u}}(t), t)$	Vector constant in the general linear representation of the vector function $\underline{F}(\bullet)$	7.9
$f(\underline{u}, \underline{a}_I)$	Nonlinear, implicit condensation function of meteorological input and parameters	3.19
$f_v(D)$	Surface averaged ventilation coefficient in sub-cloud diffusion (>1)	4.25
$\underline{G}(\underline{x}(t_k), \underline{u}(t_k), t_k)$	Nonlinear vector function of the state, input and time, in the discrete system observation equation	7.2
$\underline{G}_0(\underline{d}_{\underline{x}}(t_k), \underline{d}_{\underline{u}}(t_k), t_k)$	Vector constant in the general linear representation of the vector function $\underline{G}(\bullet)$	7.10
g	Gravitational acceleration	5.27
$h(\underline{u}, \underline{a}_0)$	Nonlinear, unit-area column output function of meteorological input and parameters	5.25
I	Station precipitation model moisture input rate	2.1
\underline{I}	Unit matrix	7.20
$\underline{\bar{K}}(t_{k+1})$	Filter gain matrix	7.19
$L(T)$	Latent heat of condensation at temperature T	3.14
L_B	Scale length of the drainage basin	6.25
L_c	Scale length of the channel	6.26

<u>Sybmol</u>	<u>Description</u>	<u>Equation No.</u>
$\bar{M}_{-F}(d_{-x}(t), d_{-u}(t), t)$	Matrix coefficient of the input residual in the general linear representation of the vector function $\underline{F}(\cdot)$	7.9
$\bar{M}_{-F_{ij}}$	The (i,j)th element of matrix $\bar{M}_{-F}(\cdot)$ (Appendix D)	
$\bar{M}_{-G}(d_{-x}(t_k), d_{-u}(t_k), t_k)$	Matrix coefficient of the input residual in the general linear representation of the vector function $\underline{G}(\cdot)$	7.10
$\bar{M}_{-G_{ij}}$	The (i,j)th element of matrix $\bar{M}_{-G}(\cdot)$ (Appendix D)	
m	Exponent in the parameterization of the average layer diameter at cloud base $1/c$	5.42
m	Exponent of the nonlinear channel	6.15
N_0	Parameter of the particle size distribution	4.1
N_D	Diffusion strenth number	5.15
$\bar{N}_{-F}(d_{-x}(t), d_{-u}(t), t)$	Matrix coefficient of the state residual in the general linear representation of the vector function $\underline{F}(\cdot)$	7.9
$\bar{N}_{-F_{ij}}$	The (i,j)th element of the matrix $\bar{N}_{-F}(\cdot)$ (Appendix D)	
$\bar{N}_{-G}(d_{-x}(t_k), d_{-u}(t_k), t_k)$	Matrix coefficient of the state residual in the general linear representation of the vector function $\underline{G}(\cdot)$	7.10
$\bar{N}_{-G_{ij}}$	The (i,j)th element of the matrix $\bar{N}_{-G}(\cdot)$ (Appendix D)	
N_{sc}	Schmidt number	4.26
N_v	Cloud base updraft strength number	5.14
$n(D)$	Cloud-particle size distribution per unit volume at cloud base	4.1
$n_n(D)$	Normalized cloud-particle size distribution	4.4
$n_t(D)$	Cloud-particle size distribution per unit volume at cloud top	5.7

<u>Symbol</u>	<u>Description</u>	<u>Equation No.</u>
O	Station precipitation model moisture output rate	2.1
$O_b(D)$	Station precipitation model moisture output rate through the cloud base due to particles of diameter in $(D, dD + D)$	5.1
O_b	Station precipitation model moisture output rate through the cloud base	5.2
$O_t(D)$	Station precipitation model moisture output rate through the cloud top due to particles of diameter in $(D, dD + D)$	5.7
O_t	Station precipitation model moisture output rate through the cloud top	5.8
O_R	Station precipitation reference moisture output rate	5.23
\underline{P}	Precipitation mass rate	5.11
$\underline{P}(D)$	Precipitation mass rate due to particles of diameter in $(D, dD + D)$	4.3
$\underline{P}_n(D)$	Normalized precipitation mass rate due to particles of diameter in $(D, dD + D)$	4.6
\underline{P}_v	Precipitation volume rate	5.31
p	Pressure	3.6
p'	Pressure level of updraft velocity equal to the height averaged updraft velocity	
p_0	Surface pressure	3.1
p_i	Parameters of the channel model	6.15
p_l	Lowest pressure level that the station precipitation model cloud top can attain	5.39
p_s	Pressure at the lifting condensation level	3.8
p_t	Pressure at the cloud top	3.17

<u>Symbol</u>	<u>Description</u>	<u>Equation No.</u>
$\bar{Q}(t)$	Time-varying spectral density matrix of the system model error	7.3
$\bar{Q}'(t)$	Time-varying spectral density matrix of the system model error incremented by the spectral density matrix of the system input residual	7.15
$Q_n(t)$	Drainage basin outflow discharge at time t	6.16
$\bar{Q}_u(t)$	Time-varying spectral density matrix of the system, time-continuous, input residual	7.12
$\bar{Q}_u(t_k)$	Time-varying covariance matrix of the system, time-discrete, input residual	7.12
$\bar{Q}_v(t_{k+1})$	Innovations sequence covariance matrix at time t_{k+1}	7.24
Q_{TH}	Potential thermal energy at pressure p'	5.41
q_h	Specific humidity (Chapter 3)	
R	Gas constant for dry air (Chapter 3)	
$\bar{R}(t_k)$	Observation noise covariance matrix at time t_k	7.4
$\bar{R}'(t_k)$	Observation noise covariance matrix at time t_k incremented by the covariance matrix of the discrete time input residual at time t_k	7.16
R_e	Reynolds number	4.26
R_v	Gas constant for water vapor	4.23
r	Relative humidity	4.42
\underline{r}	Coordinate vector	2.1
$S_i(t)$	Channel state corresponding to the ith reservoir, at time t	6.15
S_i^o	Nominal value for the channel state $S_i(t)$	6.27

<u>Symbol</u>	<u>Description</u>	<u>Equation No.</u>
T	Temperature	3.2
T_0	Surface temperature	3.4
T_d	Dew-point temperature	3.1
T_m	Temperature at pressure p' for pseudo-adiabatic ascent	5.35
T_s	Temperature at the lifting condensation level	3.11
T'_s	Temperature at pressure p' for dry-adiabatic ascent	5.35
T_t	Temperature at the cloud top for pseudo-adiabatic ascent	3.17
T_w	Wet-bulb temperature	4.23
t	Time	2.1
$\underline{v}(t_k)$	Discrete-time observation noise vector at time t_k incremented by the residual noise at t_k	7.14
$\underline{v}(t_k)$	Discrete-time observation noise vector at time t_k	7.2
v	Updraft velocity	3.18
v_p	Terminal velocity of particles with diameter $4/c$	5.16
$v_T(D)$	Terminal velocity of particles with diameter D	4.3
v_β	Updraft velocity at cloud base and at cloud top	5.1
$\underline{W}(t)$	Continuous-time system noise vector at time t incremented by the input residual noise at t	7.13
$\underline{w}(t)$	Continuous-time system noise vector at time t	7.1

<u>Symbol</u>	<u>Description</u>	<u>Equation No.</u>
w_0	Mixing ratio of air at ground surface	3.1
$w_s(T,p)$	Saturation mixing ratio of air at temperature T and pressure p	3.1
X	Station precipitation model state: Mass of liquid water equivalent in the unit area column	2.1
X(D)	Mass of liquid water equivalent per unit volume of air due to particles of diameter in (D, dD + D)	4.2
$X_n(d)$	Normalized mass of liquid water equivalent per unit volume of air due to particles of diameter in (D, dD + D)	4.5
$\underline{x}(t)$	Vector state at time t	7.1
\underline{x}_0	Initial vector state	7.7
Z	Height above ground surface	4.8
Z_b	Height of cloud base above ground	4.9
Z_c	Cloud depth	4.8
Z_t	Height of cloud top above ground surface	4.9
$\underline{z}(t_k)$	Observation vector at time t_k	7.2
$\frac{V}{z_P}$	Accumulated precipitation volume during the observation interval	6.22

<u>Symbol</u>	<u>Description</u>	<u>Equation No.</u>
<u>Greek Alphabet Symbols:</u>		
α	Constant coefficient in the linear expression for the particle terminal velocity	4.7
β	Parameter in the expression for the cloud base and top updraft velocity	5.43
$\Gamma(v, \chi)$	Complementary Gamma function	5.5
γ	Ratio of the average layer particle diameter at cloud base to the average layer diameter at cloud top	4.13
δ	Factor introduced due to the non-uniform height distribution of the average layer particle diameter	4.16
$\delta(t)$	Dirac delta function of t	7.3
δ_{kj}	Kronecker's delta	7.4
$\epsilon_1, \epsilon_2, \epsilon_3, \epsilon_4$	Station precipitation model parameters	5.34, 5.39, 5.42
$\zeta(D)$	Mass reduction factor due to sub-cloud diffusion	4.39
θ	Potential temperature	3.5
θ_e	Equivalent potential temperature	3.14
μ	Dynamic viscosity	4.27
$\underline{v}(t_{k+1})$	Innovations sequence vector at time t_{k+1}	7.23
$(v-1)!$	Factorial: 1.2.3...(v-1)	5.6
$\xi(y)$	Binary function taking only the values 0 and 1	5.30
ρ_a	Mass density of air	4.28
ρ_m	Height averaged cloud air mass density	3.18
ρ_p	Cloud particle mass density	4.23
ρ_w	Liquid water mass density	4.2

<u>Symbol</u>	<u>Description</u>	<u>Equation No.</u>
$\bar{\Sigma}(t)$	State covariance matrix at time t	7.6
$\bar{\Sigma}_0$	Initial state covariance matrix	7.8
τ_{c_i}	Time constant of ith channel reservoir	6.27
τ_p	Time constant of the station precipitation model	6.24
$\phi(\underline{u}, \underline{a}_0)$	Unit area column precipitation rate function of the meteorological input and parameters	5.28
ω_0	Scale constant	6.23

Chapter 1

INTRODUCTION

1.1 General Framework and Scope of Study

In a recent review of the status of the operational precipitation forecasting procedures, the Panel on Precipitation Processes, National Research Council, underlines the significance of development of effective short-range precipitation and flood forecasting and warning procedures to the US safety and economic welfare (NRC, 1980). The importance of the development of probabilistic models for the real-time, local-site, short-term forecasting of floods, based on quantitative precipitation forecasting and multiple sensors (e.g., raingauge, meteorological and flow sensors) observations, is indicated in the same reference.

It is the purpose of this study to develop stochastic models of the precipitation and drainage basin processes suitable for use in the real-time forecasting of precipitation and flow rates.

This study draws heavily on the scientific methods and techniques developed for:

1. the operational forecasting of precipitation,
2. river flow forecasting in real-time, and
3. the optimal blending of system models with observations of the system input and output variables by the use of modern estimation theory.

Considerable work has been done in all three of the above areas with useful, in many ways, results. A brief account of the work, as related to this study, follows.

Operational forecasts of precipitation quantity and time of occurrence over a certain area are based: 1) on the input of large scale models that simulate the atmospheric dynamics, with spatial resolutions of the order of 150 km grid-size and greater (e.g., the Limited area Fine Mesh model, LFM, documented in NWS, 1978), 2) on the use of regression models (Multiple Output Statistics model, MOS, Glahn and Lowry, 1972, and Lowry and Glahn, 1976) that correlate the predictions of the atmospheric models with observations on a smaller scale, and 3) on the experience of local forecasters with local weather patterns.

Recent evaluations (Charba and Klein, 1980, and NRC, 1980) of operational quantitative precipitation forecasts show relatively poor performance.

Large scale atmospheric models fail to adequately consider the meso-scale aspects of precipitation, NRC (1980).

The use of regressions to compensate (at least partially) for systematic errors in the large scale numerical models involves difficulties such as: 1) the identification of all the relevant meteorological variables that will be used as "explanatory" variables for each location, and 2) the absence of high linear correlation in the station precipitation records. In addition, no guarantee is provided regarding the invariance of the regression parameters for different storms, due to the absence of the process physics in the regression.

The process by which local forecasters combine information from different sources to issue operational forecasts varies with each case. They often, however, rely heavily on the LFM and MOS forecasts.

In addition to the procedures described above for the dissemination of operational precipitation forecasts, numerical models simulating some of the convective cloud processes exist in the meteorological literature (e.g., review in Rogers, 1979). Their focus is on the identification of the microphysical cloud processes. Their spatial and temporal scales are significantly finer than those of interest in this work. In addition, their interest is on the moving storm rather than on the effects of the storm processes at a fixed location on the ground.

Recently, advances in satellite technology have given rise to a new group of precipitation models (e.g., review in Ieraham, 1981). Satellite infrared pictures of cloud systems are used to infer storm properties as they develop in space and time (e.g., updraft velocities in clouds, spatial extent and movement characteristics of storm systems). Then, regression models are used to relate these properties with precipitation data from ground observation stations. Although this type of models look promising, they do not avoid the regression parameters calibration problem and they need high quality (and cost) satellite data.

In the past, procedures that combine results in the second and third problem areas have been developed. Conceptual, physically based catchment models and observations of hydrologic variables have been combined, through the use of modern time-domain estimation theory results, to produce improved forecasts of the catchment outflow. Along these lines, the spatially lumped, non-linear, conceptual, soil-moisture accounting scheme of the National Weather Service River Forecast System (NWSRFS) (description in Peck, 1976) together with linear (e.g., Kitanidis and Bras, 1980b, and Restrepo-Posada and Bras, 1982) or non-linear (Georgakakos and Bras, 1982)

channel routing schemes have been successfully used for simulating catchment response. The extended Kalman filter (Kitanidis and Bras, 1980a), and a Gaussian linear filter operating on a statistically linearized model (Georgakakos and Bras, 1982), have been utilized to extract the information contained in the available system observations. The improvement, evident when estimation theory results (filters) are involved, makes the techniques attractive for real time forecasting purposes.

Due to the absence of precipitation models compatible in mathematical structure, and spatial and temporal scales to the hydrologic models of the conceptual type, no work has been reported on the real-time coupling of precipitation and streamflow forecasting models.

1.2 Program of Study

A physically based non-linear precipitation model in the state-space form is formulated first. Based on the meteorological variables (temperature, pressure, and dew point temperature) for a certain ground station, it produces as an output, the precipitation rate at the station location.

The state variable of this model is the liquid water content of the storm clouds at a certain time at the station location. The inflowing and outflowing moisture to the cloud are based on simplified cloud microphysics. The dynamic equations of the precipitation model are coupled together with an improved state-space representation of the stochastic soil moisture accounting model (Kitanidis and Bras, 1980) of the NWSRFS and with the statistically linearized non-linear channel model of Georgakakos and Bras (1982).

Verification of a simple representation of the proposed precipitation model is done with hourly precipitation and meteorological data for Boston, Massachusetts, and Tulsa, Oklahoma. A total of eleven storms of differing severity and type were studied. An application of the full Rainfall-Runoff model developed is also reported for the Bird Creek basin, Oklahoma. Due to the lack of meteorological data in the Bird Creek basin, the Rainfall model utilized information from the somewhat distant Tulsa, Oklahoma, site.

STATION PRECIPITATION MODEL OVERVIEW

2.1 Introduction

This chapter presents the basic ideas and formulation of the conceptual station precipitation model. It avoids mathematical details, but sets the foundation for the more complete discussion of the next chapters.

2.2 Model Hypothesis

The following were the most important considerations in formulating the model:

1. Time series of variables that were either operationally forecasted or observed should be used as model inputs.
2. The model output should be the precipitation rate at a certain location. A forecast lead time of a few hours is of interest.
3. The model equations should be formulated in a state-space form amenable to modern estimation theory techniques.
4. The structure of the model components should be indicated by well established theories and observations, while being as simple as possible.

The fundamental model hypothesis is that the surface temperature (T_o), dew point temperature (T_d), and pressure (p_o) of a certain location

contain considerable amount of information about the concurrent volume precipitation rate (P_v) at the same location.

Accepting the stated hypothesis, the operational precipitation forecasting problem becomes one of forecasting T_o , p_o , T_d . However, the characteristic high linear correlations among those three variables (e.g., hourly auto-correlations of 0.9 are usual) in contrast to the low auto-correlations of the precipitation rate, suggest that simple linear statistical predictors of T_o , p_o , T_d (similar to the ones presently in use by the NWS in the Multiple Output Statistics model) are possible.

2.3 Model Overview

The storm system is conceived as a storage reservoir of condensed water. Its input is the water condensed during the pseudo-adiabatic ascent of moist air. It is depleted 1) through the cloud top by the action of the storm updrafts that carry away the small diameter cloud particles which subsequently evaporate totally in subsaturated air, and 2) through the cloud bottom by the precipitation of the larger particles.

The mass of water in the storm storage varies with time. The formulation is based on the liquid water equivalent mass in the storm clouds; therefore, both rain and snow are treated by the model.

As in every physically based model, a spatial scale should be defined so that the model parameters can be interpreted and associated with observations. Due to the storm movement, a measure of the model

scale is the distance travelled by the storm in the forecast lead time. For example, if the average horizontal storm velocity is 15 km/hour, and the forecast lead time is 1 hour, the horizontal scale is 15 km. The slower the storm and/or the shorter the forecast lead time, the closer the model scale is to the characteristic turbulence scale, that is the storm cells diameter, 0(1 KM). Due to the nature of the nodal points on the ground surface where observations or predictions of the model input and output variables are available, the characteristic model scale will actually be taken equal to the maximum distance between adjacent nodal points.

The characteristic vertical scale is equal to the cloud height. The more vigorous the storm is, the larger this scale becomes.

Storm dynamics are examined within the vertical atmospheric column. The important assumption is that the vertical column is isolated from condensed water transport from the surrounding areas. It is expected that the larger the horizontal scale is the better this assumption becomes.

Within the vertical column of unit horizontal area, there are two, in general, regions of different water particle states. Above the 0°C (32°F) isothermal surface and up to the cloud top, there are ice particles and supercooled rain droplets. As the temperature falls in the upward direction, the ratio of the number of ice particles to the number of the rain droplets increases. There are mainly raindrops under saturated conditions of the ambient air between the melting

level and the cloud base. In the unsaturated layer below the cloud base, falling drops partially evaporate. Depending on the storm type, the season of the year and the geographical location of the storm, some of the layers described above may not exist.

Given time scales of the order of a few hours, this work does not differentiate between the ice and liquid water layers. The storm column is modeled as a single storage reservoir. Evaporation, however, of the water drops or ice particles in the sub-saturated layer is taken into account.

Conservation of mass leads to the following equation for condensed liquid water equivalent in column,

$$\frac{dX(\underline{r},t)}{dt} = I(\underline{r},t) - O(\underline{r},t) \quad (2.1)$$

where,

\underline{r} : the 2-dimensional vector of horizontal coordinates with respect to a coordinate system that is stationary.

t : the time variable.

$X(\underline{r},t)$: mass of liquid water equivalent in the conceptual storage of the unit column at time t (MASS/M²).

$I(\underline{r},t)$: input mass rate due to the condensation of the water vapor in the column at time t (MASS/M²/TIME).

$O(\underline{r},t)$: output mass rate through the top and through the bottom of the unit area column at time t (MASS/M²/TIME).

Of interest in hydrologic applications is the portion of water particles leaving the cloud base which reach the ground. For sub-saturated air below the cloud base, the falling drops undergo a reduction in mass from evaporation.

It should be noted that the quantities in Eq. (2.1) depend both on the horizontal coordinate vector \underline{r} of the unit column and on time t . For simplicity, dependence on \underline{r} or t is not shown when dealing with the unit area column.

Clearly, a complete mathematical description of the whole physical process that produces precipitation would involve statements for the coupled conservation of mass, momentum and heat laws corresponding to the condensed water, the water vapor, and the dry air. For reasons of model simplicity and model compatibility with conceptual hydrologic models (e.g., the National Weather Service River Forecast System (NWSRFS) model, Peck, 1976) the conservation law of Eq. (2.1) is used, while approximations of the heat conservation law for the moist air are used to find expressions for the rates I and O . Comparison of the model predictions with observations will demonstrate the usefulness of this approach given the temporal and spatial scales of the available input data.

The input term I is determined from information on the water vapor content of the inflowing air. Pseudo-adiabatic rising of the air parcels from the cloud base is assumed.

Use of the microphysical structure of the storm clouds (i.e., particle size distribution) and of the terminal fall velocity of the precipitating particles, gives expressions for the output mass rate per unit area O and for the precipitation mass rate per unit area P at ground surface. These quantities are functions of the mass of water in storage: X . Throughout this development it is assumed that the precipitation produced in the unit column reaches the ground within its unit area projection.

Figure 2.1 is a schematic representation of the unit column (shaded regions) and related physical quantities in the storm system. The upper part of the figure is a plan view of the storm clouds moving with horizontal velocity $u(t)$ relative to the ground. The stationary coordinate system has horizontal coordinates r_1^0, r_2^0 and vertical coordinate Z . It is assumed that the origin of the coordinate system stays at ground level at all times. dA is the unit area of the column located at (r_1, r_2) .

The lower part of Figure 2.1 represents a vertical cross-section in the storm system along the dashed line a-a. All the quantities shown are functions of the coordinate vector \underline{r} and of time t . The variables X, I have been defined in Eq. (2.1). The output mass rate O has been divided into O_t and O_b to denote output from the top and the bottom of the clouds in the unit area column, respectively. P is the ground surface precipitation mass rate per unit area. The cloud height averaged updraft velocity is denoted by v . The normalized particle size distribution $n(D)/N_0$ is also shown as a function of the liquid water equivalent

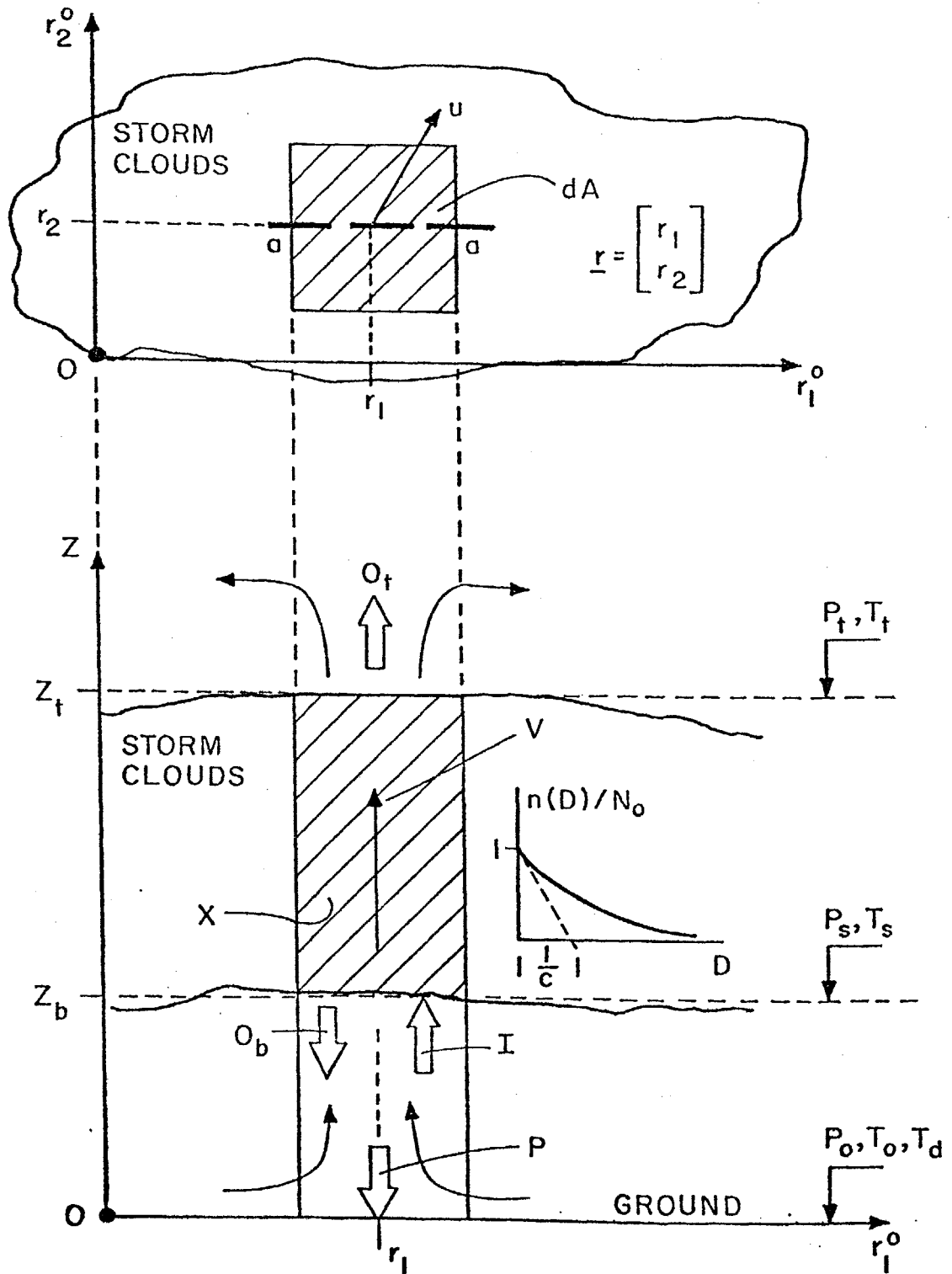


FIGURE 2.1 Schematic representation of the unit area column model variables at time t

diameter D . The inflowing air at the ground level is characterized by pressure p_o , temperature T_o and dew-point temperature T_d . The pressure and temperature at cloud base are p_s and T_s . The same quantities at the cloud top are p_t and T_t . The quantities p_s , T_s are those resulting from heat adiabatic ascent, while p_t , T_t are those resulting from further pseudo-adiabatic rising. The cloud bottom is at elevation Z_b , while the cloud (and column) top is at Z_t . The unit column model related input variables are: p_o , T_o , T_d . The physical model parameters are: v , p_t , c . The quantity c is the characteristic scale of the assumed exponential particle-size distribution.

The updraft velocity is assumed to vary as in Figure 2.2 along the vertical, reaching a maximum v_{max} at the elevation where the average of top and bottom pressures occurs. Its values at the cloud top and bottom are equal to a portion β of its vertically averaged value v . The value of v is the value of the updraft velocity at the height defined by the pressure level $p_s - \frac{1}{4}(p_s - p_t)$.

A parameterization of v , p_t and c will be proposed so that they are functions of the input variables T_o , p_o and T_d . This is done in an effort to obtain a model with parameters that are reasonably constant for different storms. The details of the model formulation are given in the next three chapters.

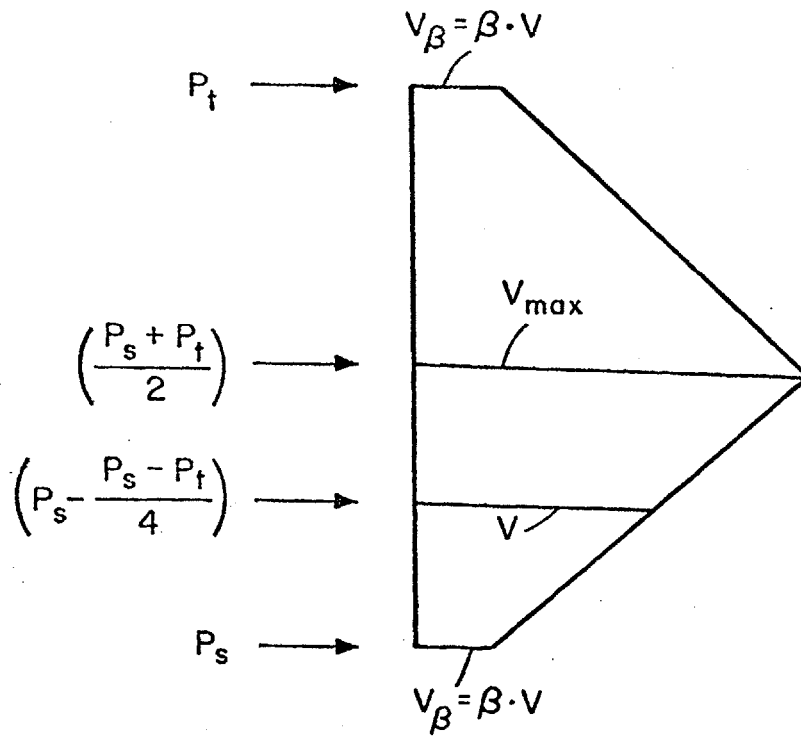


FIGURE 2.2 Updraft velocity variation with pressure
 p_s : lifting condensation level pressure
 p_t : cloud top pressure
 v : height averaged updraft velocity

Chapter 3

WATER VAPOR CONDENSATION

3.1 Introduction

The water mass supply of the vertical unit area column is the moist-laden inflowing air that rises in it. This work assumes conservation of heat of the air masses, as they rise. There is no heat exchange between rising air parcels and the ambient air. The parcels are warmed, however, by the release of the latent heat of condensation when they are above the cloud base. The relevant theory is well established in the literature and pseudo-adiabatic charts have been constructed to facilitate the calculations. It is the purpose of this Chapter to derive an efficient numerical algorithm for the computation of the condensed water mass rate input I . Appendix A gives the definitions of the relevant meteorological terms used.

3.2 General Description of Condensation

Moist, unsaturated air with temperature T_o , pressure p_o and dew point temperature T_d is lifted in the storm. As it ascends, it immediately adjusts to the pressure reduction with height and expands. Given that the atmospheric moist air follows closely the ideal gas law, it cools adiabatically. Since the saturation vapor pressure is an increasing function of temperature, and the saturation mixing ratio is an increasing function of the saturation pressure, at some point during its rise, the

air becomes saturated. This is the lifting condensation level (LCL). Further lifting will result in supersaturated air (supersaturations up to 1% have been observed). However, the excess vapor condenses onto the atmospheric nuclei, suspended in the air, to form water droplets. Within the storm clouds the air is saturated with water vapor.

Below the lifting condensation level, the air rises heat-adiabatically with constant potential temperature. Above the level of condensation the rising air is warmed by the latent heat of condensation and it is assumed that it follows the pseudo-adiabatic rate, with constant equivalent potential temperature up to the level of pressure p_t where the condensation ceases.

The next two sections derive the set of equations that define the input mass rate I per unit horizontal area. The last section discusses some of the assumptions involved.

3.3 Water Mass Rate Condensed per Unit Mass of Moist Air

What is the mass of liquid water equivalent condensed per unit mass of dry air, when an air parcel with initial temperature T_o , initial pressure p_o and dew point temperature T_d is lifted up to a terminal pressure level p_t ?

The initial mixing ratio w_o is known from the input parameters

$$w_o = w_s(T_d, p_o) = \epsilon \cdot \frac{e_s(T_d)}{p_o - e_s(T_d)} \quad (3.1)$$

where $w_s(T_d, p_o)$ is the saturation mixing ratio at temperature T_d and pressure p_o and

$$\epsilon = 0.622$$

$e_s(T_d)$ = saturation vapor pressure over
a plane surface of pure water.

The saturation vapor pressure e_s is a nonlinear convex function of temperature (solid lines in Figure 3.1). It is convenient to fit a nonlinear function of the type

$$e_s(T) = A_1 \cdot (T - 223.15)^{3.5} \quad (3.2)$$

since:

$$c_p/R = 3.5$$

with

$$R = 287 \quad [\text{Joule}/(\text{kg} \cdot ^\circ\text{K})]$$

$$c_p = 1004 \quad [\text{Joule}/(\text{kg} \cdot ^\circ\text{K})]$$

A value of $8 \times 10^{-4} \text{ [kg}/(\text{m} \cdot \text{sec}^2 \cdot ^\circ\text{K}^{3.5})]$ for A_1 gives the fit shown in Figure 3.1 (dashed line). It is seen that the function of Eq. (3.2) provides an excellent fit to the observed data (Mason, 1971, pg. 615) for values of temperature in the range: $-30^\circ\text{C} \leq T \leq 10^\circ\text{C}$.

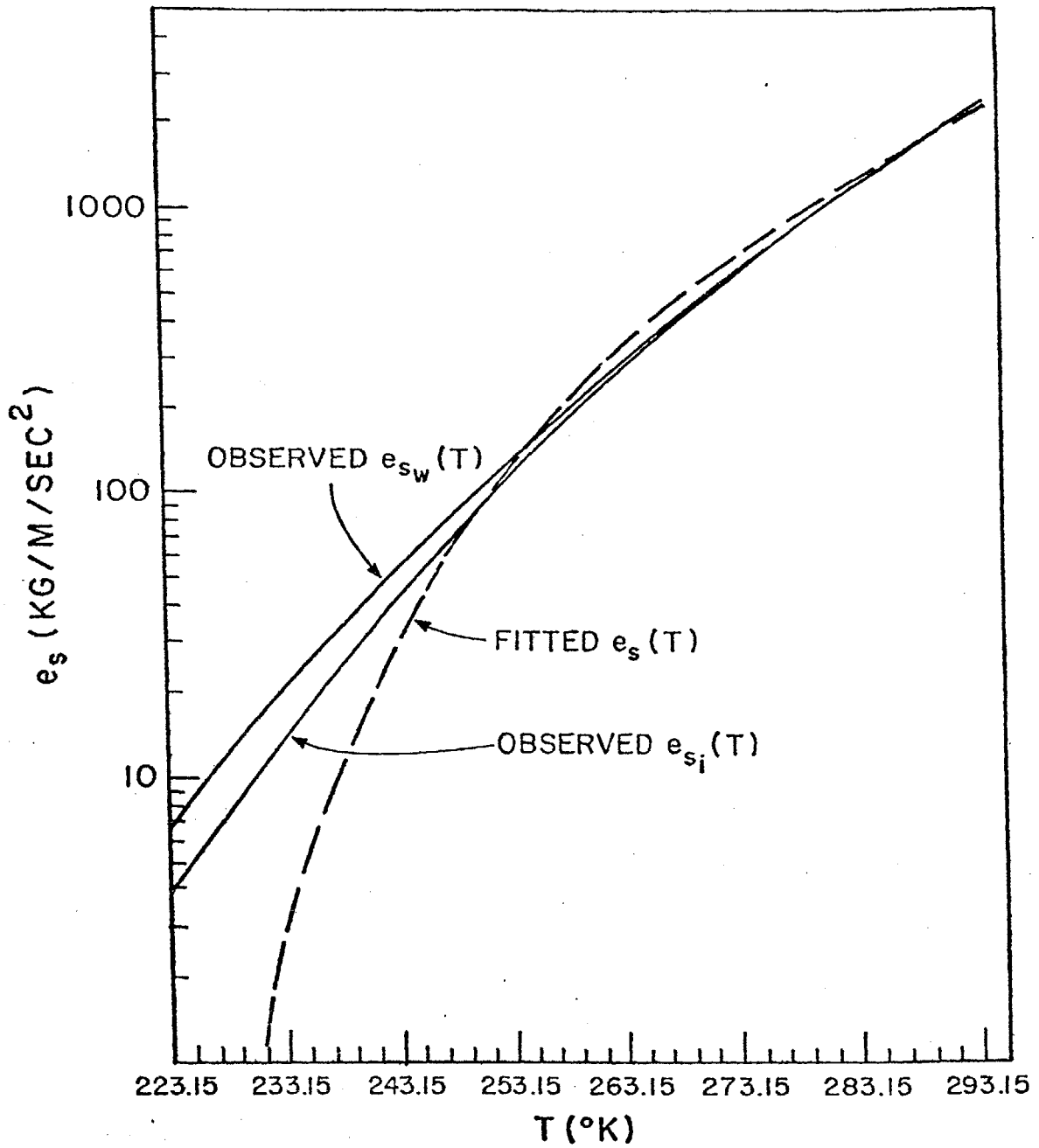


FIGURE 3.1

Observed (solid lines) saturation vapor pressure over a plane surface of water ($e_{sw}(T)$) or ice ($e_{si}(T)$) vs. temperature T .

Fitted $e_s(T)$ in dashed line.

From Eqs. (3.1) and (3.2) it follows that ($p_o \gg e_s(T_d)$),

$$w_o = \epsilon \cdot \frac{A_1 \cdot (T_d - 223.15)^{3.5}}{p_o} \quad (3.3)$$

Similarly, the saturation mixing ratio at temperature T_o and pressure p_o (i.e., if the air were saturated at T_o) is,

$$w_s(T_o, p_o) = \epsilon \cdot \frac{A_1 \cdot (T_o - 223.15)^{3.5}}{p_o} \quad (3.4)$$

If $w_o < w_s(T_o, p_o)$, equivalently if $T_d < T_o$, the air is not saturated. During the ascent, the temperature and pressure will follow the dry adiabat that originates at T_o, p_o . When the air becomes saturated, the pseudo-adiabat, passing through the level at which saturation was first reached, will be followed for the rest of the ascent.

If $w_o = w_s(T_o, p_o)$, equivalently $T_o = T_d$, the air is saturated and the pseudo-adiabat will be followed throughout the rising.

During the dry-adiabatic rising, the potential temperature θ of the air stays constant at the value given by the Poisson's equation (Wallace and Hobbs, 1977),

$$\theta = T_o \cdot \left(\frac{p_n}{p_o}\right)^{R/c_p} \quad (3.5)$$

where $p_n = 10^5$ [KG/(M·SEC²)]

Along the θ adiabat given by (3.5), temperature T and pressure p change according to,

$$T = \left(\frac{1}{0.286} \right) \cdot \theta \cdot p^{0.286} \quad (3.6)$$

since, $R/c_p = 0.286$.

The dry adiabatic rising continues until the air parcel becomes saturated. The point (T_s, p_s) where this takes place is the solution of the system of Eqs. (3.6) and

$$T - 223.15 = \left(\frac{w_o \cdot p}{A_1 \cdot \epsilon} \right)^{0.286} \quad (3.7)$$

Eq. (3.7) has been inferred from Eqs. (3.2) and (3.1).

The system of equations leads to

$$\left(\frac{p_s}{p_n} \right)^{0.286} \left[- \left(\frac{p_n \cdot w_o}{A_1 \cdot \epsilon} \right)^{0.286} + \theta \right] = 223.15 \quad (3.8)$$

The solution of Eq. (3.8) depends on whether the function

$$f_1(T_o, p_o, T_d) = \theta - \left(\frac{p_n \cdot w_o}{A_1 \cdot \epsilon} \right)^{0.286} \quad (3.9)$$

is equal to zero or not.

By virtue of Eqs. (3.3) and (3.5)

$$f_1(T_o, p_o, T_d) = \left(\frac{p}{p_o}\right)^{0.286} \cdot (T_o - T_d + 223.15) \quad (3.10)$$

By definition, for all values of T_o and T_d the function f_1 in Eq. (3.10) is different from zero.

Substitution of Eq. (3.10) in Eq. (3.8) results in,

$$\frac{T_s}{T_o} = \left(\frac{p_s}{p_o}\right)^{0.286} = \frac{1}{\frac{T_o - T_d}{223.15} + 1} \quad (3.11)$$

So the lifting condensation level pressure p_s and temperature T_s are given by

$$p_s = \left(\frac{1}{\frac{T_o - T_d}{223.15} + 1}\right)^{3.5} \cdot p_o \quad (3.12)$$

$$T_s = \left(\frac{1}{\frac{T_o - T_d}{223.15} + 1}\right) \cdot T_o \quad (3.13)$$

It should be noted that the choice of the exponent in Eq. (3.2) is responsible for the simple form of Eqs. (3.12) and (3.13).

Ascent of the air parcel above the level (T_s, p_s) results in the condensation of the water vapor to liquid water. The released latent heat of condensation will warm the air parcel. Consequently, further rising will not be heat-adiabatic. It is assumed that the latent

heat released does not cross the boundaries of the ascending air mass, and that the condensate is liquid water and it precipitates immediately so that the heat content of the condensed material (small compared to the heat content of the air mass) need not be considered when calculating temperature changes.

Under the above assumptions, the characteristic equivalent potential temperature θ_e of the pseudo-adiabat followed is (Wallace and Hobbs, 1977),

$$\theta_e = \theta \cdot \exp\left\{ \frac{L(T_s) \cdot w_s(T_s, p_s)}{c_p \cdot T_s} \right\} \quad (3.14)$$

where $L(T)$ is the latent heat of condensation, which depends weakly on the temperature. Eagleson (1970) suggests a linear function for $L(T)$ of the type

$$L(T) = A - B \cdot (T - 273.15) \quad (3.15)$$

where $A = 2.5 \cdot 10^6$ [JOULE/KG] and $B = 2.38 \cdot 10^3$ [JOULE/(KG \cdot °K)].

Expressing θ in terms of p and T using Eq. (3.6) and substituting in Eq. (3.14) leads to the following description of the variation of T and p along a constant θ_e , pseudo-adiabatic rising

$$\theta_e = T \cdot \left(\frac{p_n}{p}\right)^{0.286} \cdot \exp\left\{ \frac{L(T) \cdot w_s(T, p)}{c_p \cdot T} \right\} \quad (3.16)$$

Given a terminal pressure level, p_t , it is then possible to obtain the corresponding temperature T_t , using Eq. (3.16). The final saturation mixing ratio can be computed and is $w_s(T_t, p_t)$. The difference

$$\Delta w = w_o - w_s(T_t, p_t) \quad (3.17)$$

is the mass of liquid water resulting from the condensation during the pseudo-adiabatic ascent of a unit mass of dry air. Since the specific humidity q_h is related to the mixing ratio w by (Eagleson, 1970) $w \cong q_h$, it follows that Δw is also approximately equal to the mass of liquid water resulting from the ascent of a unit mass of moist air.

The steps outlined above are in fact an analytical version of the pseudo-adiabatic chart used in meteorology.

Due to the nonlinearity in Eq. (3.16) with respect to the temperature T , Δw cannot be found explicitly. Rather, it must be obtained using iterative methods of root determination (e.g., the Newton-Raphson method). The necessary derivatives and starting value are given in Appendix B.

3.4 Input Mass Rate Per Unit Area

Assuming that the water content of a volume of air entering the cloud base vertically per unit time will not leave the unit area column from the sides, the input mass rate of condensate is

$$I = \Delta w \cdot \rho_m \cdot v \cdot dA \quad (3.18)$$

ρ_m : a vertically (from pressure p_s to pressure p_t)
averaged density of moist air,

v : the vertically averaged updraft velocity of the
inflowing air,

dA : the unit area measure (=1).

Eq. (3.18) can be written as,

$$I = f(\underline{u}, \underline{a}_I) \quad (3.19)$$

where \underline{u} is the vector of input variables

$$\underline{u}^T = [T_o \ p_o \ T_d]$$

and \underline{a}_I is a parameter vector

$$\underline{a}_I^T = [p_t \ v]$$

with the symbol "T", when used as an superscript, defining the
transpose of a vector or matrix quantity. A discussion on the parameters
 p_t and v is given in Chapter 5.

An important conclusion is that the input rate I is not (in
general) a linear function of the water vapor mass content of the
inflowing (in the storm) air.

3.5 Discussion of Assumptions in the Unit Area Column Condensation Equation

Several assumptions have led to the form of the unit area column condensation equations presented in Sections 3.3 and 3.4. When possible, the effect of each assumption on the model behavior is assessed in terms of existing observations of the physical process. It should be kept in mind, however, that the model equations will be verified as adequate, if a good fit of the model output with observed data gives physically reasonable (observed) values for the model state and parameters.

Due to the large spatial extent and time duration of the storms of significance to hydrologic basins (areas of 1000 km^2), very few (mostly radar based) observations of the characteristics of the storm dynamics are available (e.g., discussions in Rogers, 1979, Fletcher, 1962). For the past years, observations of the storm dynamics have been almost exclusively in small scale convective storms. The discussion of the model assumptions based on these observations is justified, by evidence of existence of convection regions within large scale stratiform cloud development (Hobbs and Houze, 1976, Fujiwara, 1976, Rogers, 1979).

Observations of the liquid water content of convective clouds by aircraft, summarized by Byers (1965), showed that it is significantly less in most cases than the value realized by pseudo-adiabatic parcel ascent. The ratio of observed to theoretical water content ranged from 0.1 for observations on West Indian hurricanes to 0.4 for observations on trade-wind cumulus in the Caribbean, decreasing with height

in the cloud. This was explained by the supposition that dry environmental air mixes into the cloud, thus reducing its water content. The extent to which entrainment is important to the types of storm systems of interest in this work cannot be determined based on existing observations. Nevertheless, it can be stated that if entrainment is important, the model will tend to over-estimate the precipitation rate.

Byers (1965) discusses the use of the pseudo-adiabatic ascent to describe the dynamics of condensation. He concludes that the mutually exclusive assumptions:

1. water is precipitated as fast as it is condensed
(the process is irreversible),
2. water stays in the parcel during ascent (the process
is reversible),

lead to similar numerical results.

Direct deposition from the vapor phase to the solid phase is not taken into account during condensation, therefore the latent heat of sublimation is not used in Eqs. (3.14), (3.15), and (3.16). Observations of large numbers of supercooled liquid water droplets at -15°C or colder (Rogers, 1979) render this assumption reasonable. Nevertheless, even for very low temperatures, the latent heats of condensation and sublimation differ by less than 10% (Byers, 1965).

In using adiabatic transitions it is implicitly assumed that the air below the cloud base is well mixed. That is, the temperature lapse rate is the dry adiabatic and that the cloud base is at the lifting condensation level (Rogers, 1979). Coulman's and Warner's (1976)

aircraft observations in convective clouds indicate that this assumption is reasonable.

Condensation of the water vapor at saturation conditions, not allowing supersaturation, is supported by 1) the presence of hygroscopic nuclei in the atmosphere in vast quantities and sizes, and 2) the long time intervals of interest in this work (of the order of a few hours).

The errors due to considering the dry air and the water vapor in moist air, as ideal gases are rather small. Dufour and Defay (1963) prove that, in humid air at pressures less than 1000 [MBAR], the error for the dry air is less than 0.1%, and that for the water vapor is less than 1%.

In some cases the so-called virtual temperature is used in place of the ordinary one, so that the properties of the dry air as an ideal gas can be used when dealing with moist air. The correction is a function of the mixing ratio. For mixing ratios observed in the earth's atmosphere (less than 0.04), the correction adds less than 1% to the temperature (Byers, 1965).

Eq. (3.18) utilizes vertically averaged values of ρ_m and v . Given the uncertainty associated with estimates of v in the unit area column, the increased complexity introduced by using

$$I = \int_{w_s(T_s, p_s)}^{w_s(T_t, p_t)} v(p) \cdot \rho(p, T) \cdot (dA) \cdot dw_s(p, T)$$

was not considered necessary. Integration in the above is for values of p , T along the pseudo-adiabat. $\rho(p, T)$ is the air density at pressure p and temperature T .

STORM PRECIPITATION FORMATION AND EVOLUTION

4.1 Introduction

It is the next task to obtain expressions for the unit area column output mass rate O of Eq. (2.1) and for the precipitation mass rate, P , per unit area, that reaches the ground. Expressions for these quantities are obtained by examination of the cloud micro-physical structure.

Theories of precipitation formation and evolution are reviewed to establish a working background. It should be noted that due to the immense variety of temporal and spatial scales involved in the dynamics of precipitation, observations are difficult to obtain and even more difficult to interpret (Mason, 1971; Braham, 1965; Pruppacher and Klett, 1978). Consequently, the following is a brief account of the contemporary theories on precipitation, based on currently available instrumentation which is far from being adequate for all purposes.

The macroscale processes accompanying forced lifting of moist air masses, described in the previous chapter, result in an amount of liquid condensed water. This is in the form of minute hydrometeors of various sizes created by the adherence of the H_2O molecules onto small ($<1,10 \mu m$) particles (condensation nuclei) that are available in vast quantities and different sizes in the lower atmosphere. Various growth processes, to be described in section 4.2, lead to a broad spectrum of drop sizes in the cloud. A portion of the drops, those big enough

to fall toward the ground against the updraft of velocity v , precipitate through the cloud base at some terminal velocity. Given unsaturated conditions below the cloud base, evaporation reduces the precipitating mass.

Following a brief account on the in-cloud growth of the precipitation particles, observations on the distribution of particles with size are presented in section 4.3. Next, observations on the terminal velocity v_T , are used to establish the v_T versus particle diameter D relationship. Evaporation is dealt with in Section 4.5.

4.2 Precipitation Formation

Detailed reviews of the theories of precipitation formation can be found in Braham (1965), Sulakvelidze (1969), Mason (1971) and Pruppacher and Klett (1978). All of those authors summarize observations of cloud systems that support, for the most part, the following.

The dominant precipitation generating mechanism in clouds whose tops extend in regions of freezing temperatures is the growth of ice crystals at the expense of the existing supercooled water droplets. It is hypothesized that the water vapor pressure in such clouds assumes an intermediate value between the saturated vapor pressures over ice and over water. Therefore, freezing takes place on ice crystals while the droplets evaporate. This process continues until the liquid phase disappears completely. In the mean time, large ice crystals begin to fall, coalesce with smaller particles and grow in volume. Generally,

if surface temperatures are above 0°C , ice particles melt on their way down the atmosphere, resulting in rainfall on the ground. The first ice crystals in a supercooled liquid-droplet cloud are formed on minute freezing nuclei, active in temperatures from -10°C to -20°C .

For clouds whose tops are below the level where active freezing nuclei can be found, precipitation formation is explained by the so-called chain reaction theory. Droplets grow in a cloud by gravitational coalescence. When the drops reach a critical diameter above which they become aerodynamically unstable, or due to collisions with other drops, they splinter to form a few large drops and many small droplets. Each of the large drops generated grow by gravitational coalescence until the critical diameter is reached or a collision occurs, when it splinters and the cycle is repeated. The chain effect leads to the formation of the raindrops in precipitation.

Houghton (1968) suggests that the precipitation mechanism in stratiform, cyclonic systems is largely based on the ice crystal growth. He used the observed exponential increase of ice crystal concentration with decreasing temperature to explain the height uniformity of the level of precipitation initiation, over the spatial and temporal storm extent. This uniformity and the high efficiency of the ice crystal process to remove the products of vapor condensation or deposition, is used to explain the steady, highly efficient, precipitation observed in stratiform clouds.

The same author suggests that convective storms are the result of high liquid water presence due to the strong updrafts, and the chain reaction process. He explains the low precipitation efficiency (ratio of precipitation to condensate, expressed as a percentage) of convective clouds using the hypothesis that the accretional growth process is incomplete in those clouds.

4.3 Size Distribution of Hydrometeors

Since a hydrometeor (also referred to as a cloud particle) will start falling toward the ground if its terminal velocity is greater than the updraft velocity, and since the terminal velocity depends on the hydrometeor size (subject of section 4.4), it is necessary to have a description of the hydrometeor size spectrum in order to find the number of particles large enough to precipitate.

Conclusions on hydrometeor size distribution are shaded by the characteristics of existing data collection methods (Mason, 1971).

A few important drawbacks are:

1. Calibration of instruments is difficult.
2. Measurements of particles with sizes of lengths less than about 5 μm are not reliable.
3. Instantaneous measurements of different locations in the storm cloud are not feasible with present day instrumentation.
4. Observations in clouds containing ice particles are troubled by icing on the instruments.

Observations summarized by Mason (1971), and Pruppacher and Klett (1978) from a wide range of storm cloud types and locations throughout the world, reveal a common characteristic of the particle size distribution as expressed by the number of particles, $n(D)$, of water equivalent diameter D , per unit volume, per unit diameter range $(D, dD + D)$. That is, $n(D)$ increases steeply for small D to reach a maximum and possesses a very mild slope for large D .

Log-normal, Pearson Type III (Mason, 1971), and the so-called Khrgian-Mazin (Pruppacher and Klett, 1978) distributions have been proposed and used to describe the observed characteristics of $n(D)$, in cloud physics research.

A simpler, exponential function of the type:

$$n(D) = N_0 \cdot e^{-c \cdot D} \quad (4.1)$$

is adopted in this work. N_0 and c are parameters.

The reasons for such a choice are:

1. It is a much simpler function.
2. The exponential shape for relatively large D has been established from observations of precipitation particles.

For example, the raindrop distribution in Marshall and Palmer (1948) and snowflake distribution in Gunn and Marshall (1958) are of the type in Eq. (4.1) with N_0 , c parameters possibly depending on the precipitation rate. Those dis-

tributions have been shown to fit rather well observations of precipitation, for a variety of storm types and meteorological conditions (e.g., observations by Dingle and Hardy (1962) and by Ohtake (1965)).

3. There is uncertainty as to the shape of the distribution for small D due to errors in the sampling of the smallest particles. In addition, there is some evidence (Eldridge, 1957) that droplets with diameters less than $1 \mu\text{m}$ occur in much greater proportions than have been detected by ordinary methods.
4. Droplets with small diameters are carried away due to the action of the updraft in the model developed in this work. Small droplets predicted by the exponential in Eq. (4.1) will then play a minor role in the actual precipitation rate.

Given the size distribution of Eq. (4.1), the water equivalent mass $X(D)$ due to particles of diameters in the interval $(D, dD + D)$, per unit volume is:

$$X(D) = \rho_w \cdot n(D) \cdot \frac{\pi}{6} D^3 \quad (4.2)$$

The precipitation mass rate $P(D)$ due to the same particles is:

$$P(D) = \rho_w \cdot n(D) \cdot \frac{\pi}{6} D^3 (v_T(D) - v) \quad (4.3)$$

where,

- ρ_w : liquid water density [KG/M³],
 $v_T(D)$: terminal velocity of particles of diameter D [M/SEC],
 v : updraft velocity [M/SEC].

The relative importance of the different diameters to $n(D)$, $X(D)$ and $p(D)$ can be readily seen in Figure 4.1. There, the normalized variables:

$$n_n(D) = n(D)/N_0 \quad (4.4)$$

$$X_n(D) = \frac{X(D) \cdot c^3}{\frac{\pi}{6} \cdot \rho_w \cdot N_0} \quad (4.5)$$

$$P_n(D) = \frac{P(D) \cdot c^4}{\frac{\pi}{6} \cdot \rho_w \cdot N_0 \cdot \alpha} \quad (4.6)$$

are plotted together in a common scale. It has been assumed that $v_T(D)$ is of the type:

$$v_T(D) = \alpha \cdot D \quad (4.7)$$

and v is equal to zero. The next sub-section will justify the use of a linear function for $v_T(D)$ and will determine the constant α .

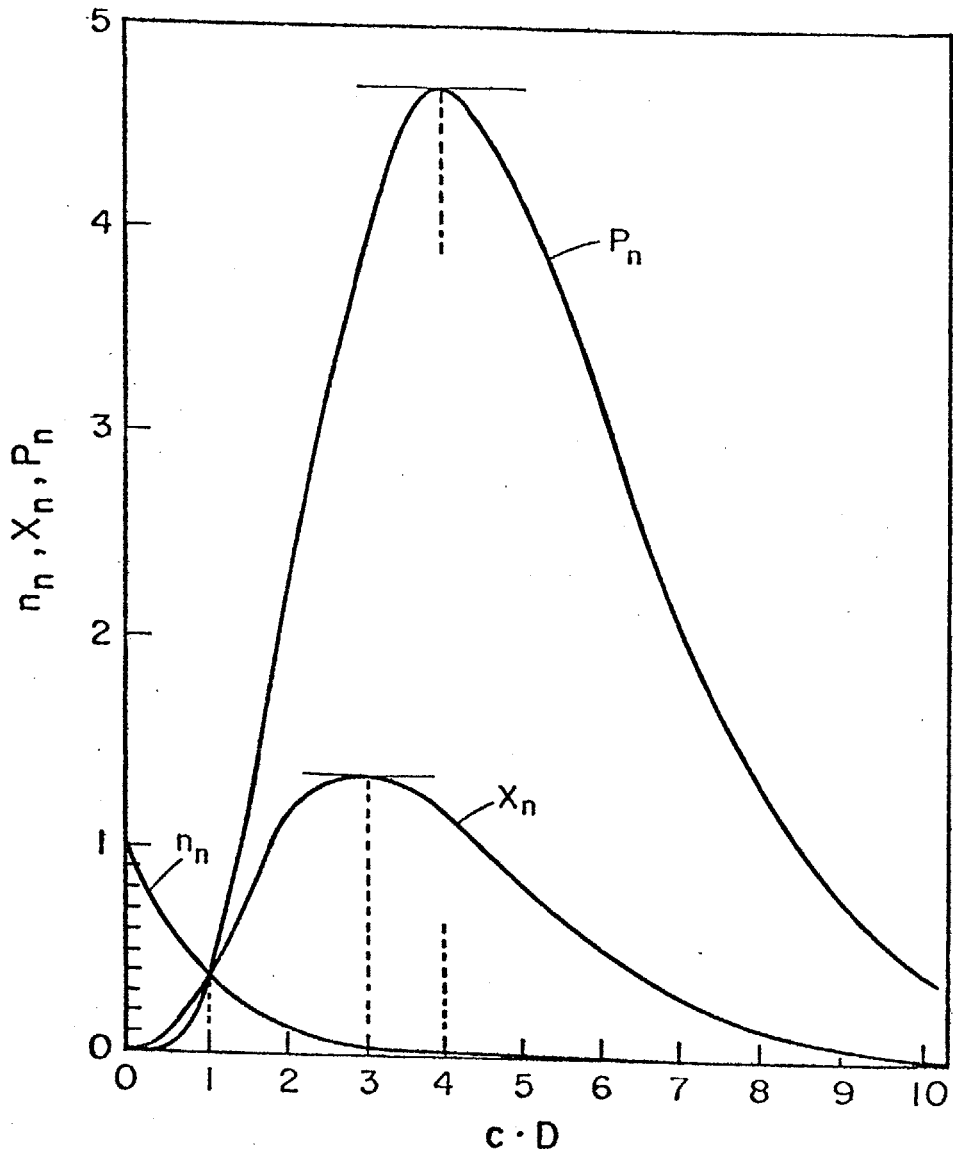


FIGURE 4.1

Normalized number concentration n_n , water-mass content X_n and precipitation rate P_n due to hydrometeors of diameter in the range $(D, D^n + dD)$ vs. the normalized diameter cD .

Figure 4.1 shows that the diameter that contributes the maximum water equivalent mass is equal to $3/c$, while the one that contributes the maximum water equivalent mass precipitation rate is equal to $4/c$. In addition, the proportion of the water equivalent mass contributed by particles less than $1/c$ in diameter is 0.019 and the portion of the water equivalent mass rate contributed by particles less $1/c$ in diameter is 0.0037.

The proportions are respectively 0.1429 and 0.0527 for particles of size diameter less than or equal to $2/c$.

The parameter c in Eq. (4.1) is equal to the inverse of the average diameter. The parameter N_0 reflects the number of small diameter droplets that have a small contribution to the precipitation rate (e.g., Figure 4.1). For simplicity it is taken to be a constant throughout the height of the column. A simple linear function of height is adopted for c :

$$c = c_l + \frac{Z}{Z_c} (c_u - c_l) \quad (4.8)$$

with Z_c given by:

$$Z_c = Z_t - Z_b \quad (4.9)$$

and where c_l , c_u , Z are shown in the definition sketch in Figure 4.2a. Figure 4.2b represents the resultant height variation of the inverse

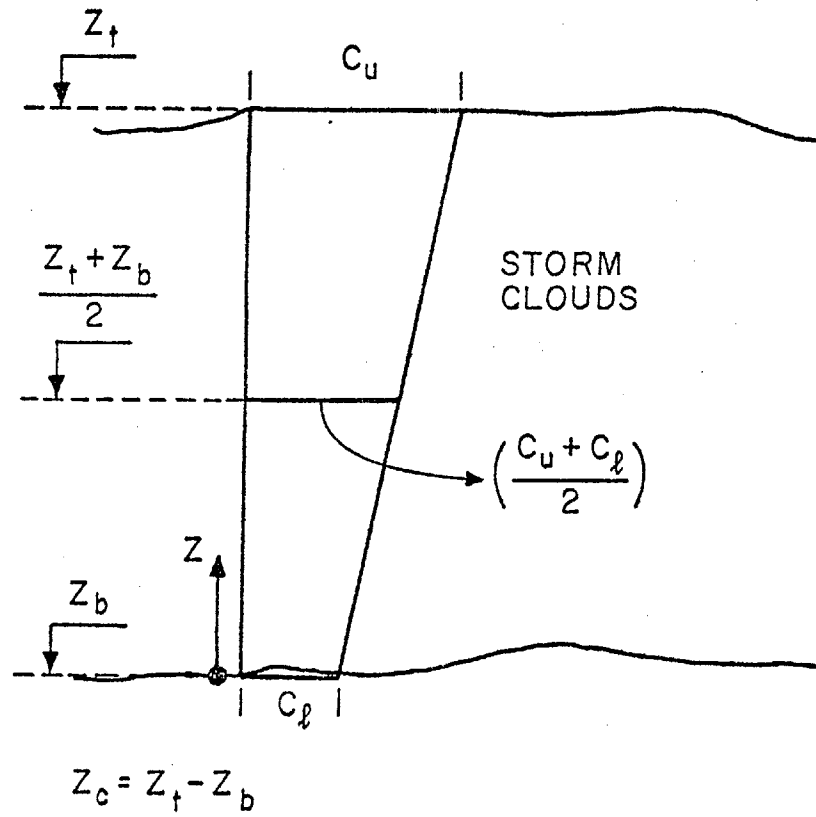


FIGURE 4.2a

Height variation of the inverse layer-average diameter c_u at cloud top and c_ℓ at cloud bottom

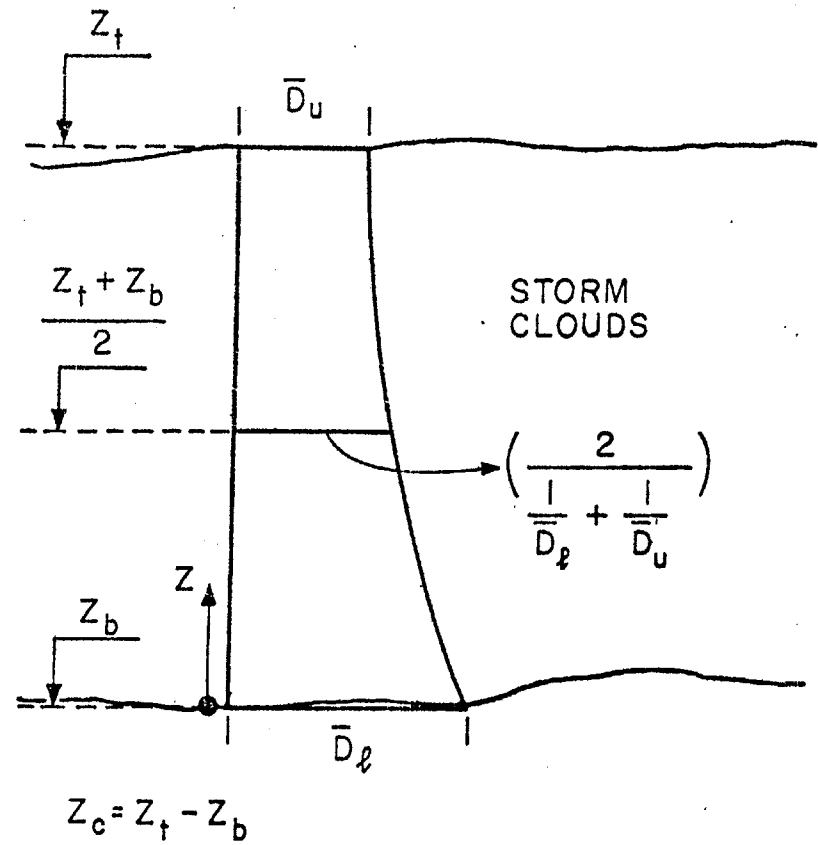


FIGURE 4.2b

Height Variation of the layer-average diameter \bar{D}_u at cloud top and \bar{D}_ℓ at cloud bottom

of c , that is the average particle diameter \bar{D} , given by:

$$\bar{D} = \frac{1}{\left(1 - \frac{Z}{Z_c}\right) \cdot \frac{1}{D_\ell} + \frac{Z}{Z_c} \cdot \frac{1}{D_u}} \quad (4.10)$$

Figures 4.2a and 4.2b indicate that larger particles are expected as one moves from the top of the cloud toward the cloud base. This is consistent with the growth processes of collision and coalescence.

The mass of liquid water equivalent in storage, X , in the column is given by:

$$X = \int_0^{Z_t - Z_b} \frac{1}{6} \pi \rho_w N_0 \left\{ \int_{D_{\min}}^{D_{\max}} D^3 \cdot e^{-D \left[c_\ell + \frac{Z}{Z_c} (c_u - c_\ell) \right]} \cdot dD \right\} \cdot dZ \quad (4.11)$$

where Z_t , Z_b are the heights of the top and the bottom of the unit area column cloud, and D_{\min} , D_{\max} are the minimum and maximum diameters in the cloud.

For D_{\min} , D_{\max} taken as 0 and ∞ respectively, Eq. (4.11) gives:

$$X = \frac{1}{3} \pi \rho_w \cdot N_0 \cdot Z_c \cdot \frac{1}{c_\ell^4} \left(\frac{c_\ell}{c_u} + \left(\frac{c_\ell}{c_u}\right)^2 + \left(\frac{c_\ell}{c_u}\right)^3 \right) \quad (4.12)$$

Denoting by γ the ratio of the average diameter at cloud base to the average diameter at cloud top, or equivalently:

$$c_u = \gamma \cdot c_\ell ; \quad \gamma \geq 1 \quad (4.13)$$

results in:

$$X = \pi \cdot \rho_w \cdot N_0 \cdot Z_c \cdot \frac{1}{c} \left\{ \frac{1}{3} \left(\frac{1}{\gamma} + \frac{1}{\gamma^2} + \frac{1}{\gamma^3} \right) \right\} \quad (4.14)$$

with c_ℓ replaced by c for notational convenience. For a uniform c distribution with height, the result is:

$$X = \pi \cdot \rho_w \cdot N_0 \cdot Z_c \cdot \frac{1}{c} \quad (4.15)$$

The effect of a linear variation of c with height is the introduction of the factor δ given by:

$$\delta = \frac{1}{3} \left(\frac{1}{\gamma} + \frac{1}{\gamma^2} + \frac{1}{\gamma^3} \right) \quad (4.16)$$

Some values for δ are:

$$\begin{aligned} \gamma = 1 & \quad \delta = 1 \\ \gamma = 2 & \quad \delta = 0.291 \\ \gamma = 10 & \quad \delta = 0.037 \end{aligned}$$

Eq. (4.14) relates the microphysical cloud structure as represented by the parameters N_0 , c , γ to the macrophysical state of the

system, the mass of liquid water equivalent in the unit area column X.

At this point, a choice has to be made as to which parameter, N_0 or c , one should keep in the model equations. The decision is between possibly easier parameter estimation but non-linear model versus harder estimation with a state-linear formulation. Marshall and Palmer's (1948) observations of rainfalls support a dependence of c on the precipitation rate and no precipitation rate dependence for N_0 . This would argue for keeping N_0 in the formulation since it might be easier to estimate. On the other hand, eliminating N_0 and keeping c in the formulation leads to a convenient linear equation for the state X. In the following presentation, both the linear and non-linear formulations will be shown; however, in application, the linear model choice will be made.

From Eq. (4.14), N_0 can be expressed in terms of c as:

$$N_0 = \frac{c^4}{\pi \rho_w \cdot Z_c \cdot \delta} \cdot X \quad (4.17)$$

with corresponding size distribution:

$$n(D) = \frac{c^4}{\pi \rho_w \cdot Z_c \cdot \delta} e^{-cD} \cdot X \quad (4.18)$$

Expressing c in terms of N_0 , Eq. (4.14) is written as:

$$c = \left[\frac{\pi \rho_w \cdot N_0 \cdot Z_c \cdot \delta}{X} \right]^{1/4} \quad (4.19)$$

with corresponding size distribution:

$$n(D) = N_0 \cdot e^{-\left[\frac{\pi \rho_w \cdot N_0 \cdot Z_c \cdot \delta^{1/4}}{X}\right] \cdot D} \quad (4.20)$$

4.4 Terminal Velocity of Hydrometeors

The fall velocity of the precipitation particles (hydrometeors) of a certain size is the means by which the discrete mass flux of particles is transformed to the observable continuous precipitation rate (see Eq. (4.3)).

Pruppacher and Klett (1978) present experimental evidence that justifies the assumption of a constant terminal velocity during the fall of isolated cloud particles in quiet air.

Determining the motion of a particle during free fall in the atmosphere are the gravitational force corrected for buoyancy and the drag force. Due to difficulties of the solution of the Navier-Stokes equations for Reynolds number greater than 1, approximate numerical solutions and field or laboratory observations have been used to determine the terminal velocity of an isolated cloud particle as a function of its size and shape.

Beard (1976) compiled observations of the free fall of liquid water drops of a wide range of diameters (from 1 μM to 7 MM) and presented expressions for the terminal velocity v_T as a function of the diameter D , the particle density ρ_p and the temperature and pressure, T and p , of the ambient air. The high accuracy of the suggested

expressions depends on the diameter range. Based on Beard's expressions, the terminal velocity of liquid water drops was calculated for a variety of conditions and diameters. For illustration purposes, the results for $T = 273.15^{\circ}\text{K}$, $p = 800 \text{ MB}$ (curve 1) and $T = 293.15^{\circ}\text{K}$, $p = 1013 \text{ MB}$ (curve 2) are shown in Figure 4.3. Intermediate conditions lie between the two curves in such a way that v_T decreases as the pressure and temperature increase. This variation of T, p is representative of the conditions expected in the sub-cloud layer where the precipitation rate is sought. A simple linear approximation to the function $v_T(D)$ is fitted to the results of Beard shown in dashed line in Figure 4.3 (curve 3). The fitted curve represents v_T reasonably well for diameters in the range of 1 to 2 MM, which is the size of most raindrops. It underestimates v_T for diameters in the range of 0.2 to 1 MM (maximum percent error less than 20%), and it overestimates v_T for diameters greater than 2 MM. The approximation takes the form of Eq. (4.7) with α given by:

$$\alpha = 3500 \text{ [1/SEC]} \quad (4.21)$$

Contrary to liquid precipitation drops, solid precipitation particles of same mass display a wide variety of terminal velocities. For the most part this is due to their highly irregular shape. Spherical ice particles of densities 100 to 900 KG/M^3 and highly irregular aggregates of dendritic crystals can be found in precipitation. The interested

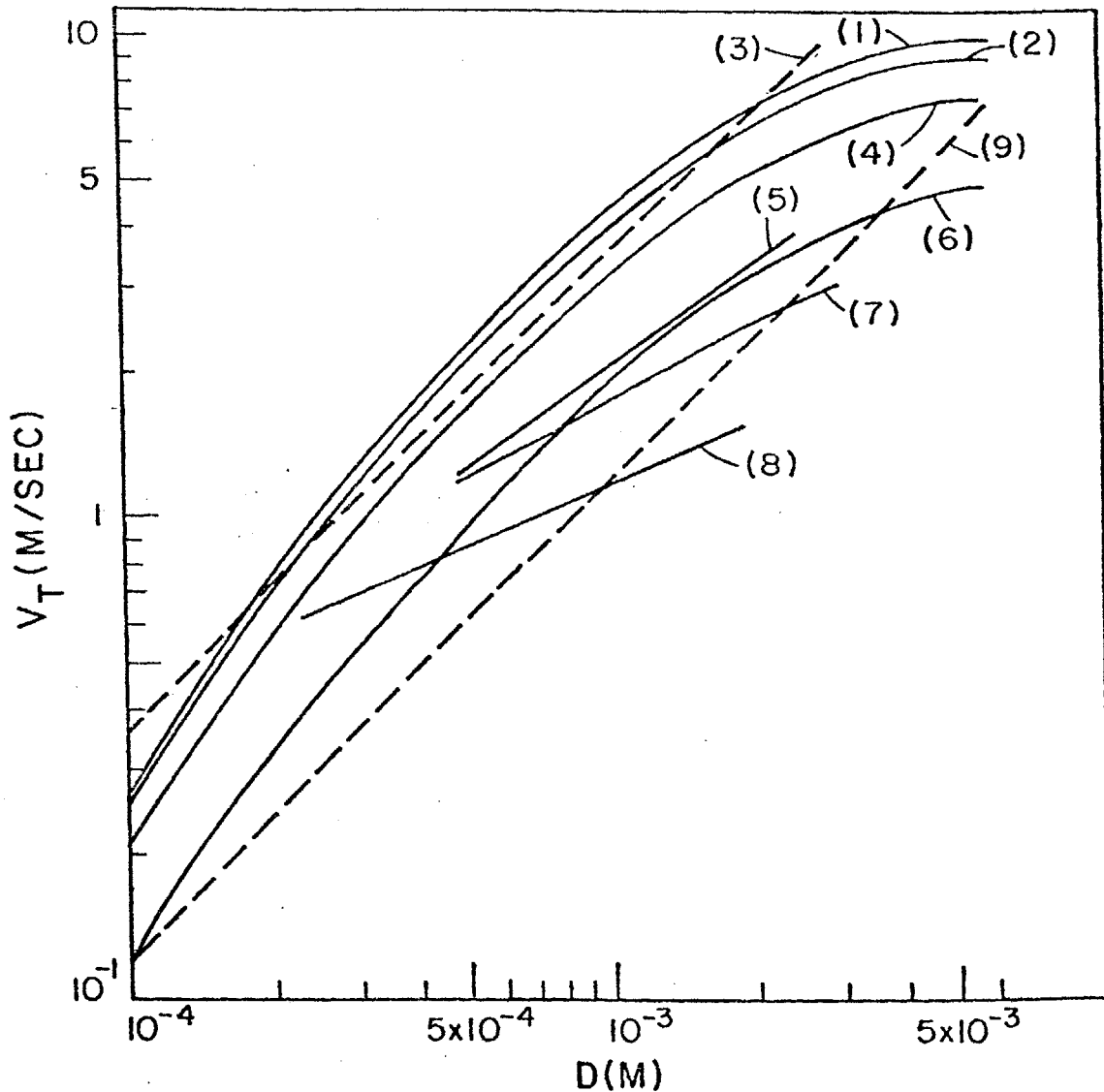


FIGURE 4.3

Observed and fitted terminal velocity as a function of hydrometeor diameter

- Curve 1: Raindrops, $T = 273.15$ [°K], $p = 800$ [MBAR] - Beard (1976)
- Curve 2: Raindrops, $T = 293.15$ [°K], $p = 1013$ [MBAR] - Beard (1976)
- Curve 3: Raindrops, fitted - Eqs. (4.7) and (4.21)
- Curve 4: Ice sphere, $\rho = 500$ [KG/M³], $T = 273.15$ [°K], $p = 1013$ [MBAR] Beard (1976)
- Curve 5: Lump graupel - Locatelli and Hobbs (1974)
- Curve 6: Ice sphere, $\rho = 100$ [KG/M³], $T = 273.15$ [°K], $p = 1013$ [MBAR] Beard (1976)
- Curve 7: Hexagonal groupel - Locatelli and Hobbs (1974)
- Curve 8: Aggregates of dendritic crystals Locatelli and Hobbs (1974)
- Curve 9: Snow, fitted - Eqs. (4.7) and (4.22)

reader is referred to Magono and Lee (1966) for a classification of the snow crystals, and to Hobbs, Chang and Locatelli (1974) for a discussion of the dependence of shape and size spectra on the conditions prevailing in the place of formation.

Locatelli and Hobbs (1974) fitted observations of terminal velocity and mass of precipitating solid particles on the Cascade Mountains of Washington with simple power laws. The scatter of the data is considerable and no trend was obvious for many classes of shapes.

Figure 4.3 depicts the regression relationships given in Locatelli and Hobbs (1974) for "lump graupel" (curve 5), "hexagonal graupel" (curve 7) and aggregates of dendritic crystals (curve 8). Curves 4 and 6 are Beard's (1976) results for solid spheres of densities 500 and 100 (KG/M^3) respectively. The results of Locatelli and Hobbs (1974) shown are those for which the regression correlation coefficient was higher than 0.69. The dashed line (curve 9) was "fitted" to all curves corresponding to solid precipitation particles. All curves represent function $v_T(D)$ where D is the diameter of the liquid water drop with the same mass as the solid precipitation particle.

The dashed line is a reasonable approximation to conditions found in 1) dendritic aggregates for D in the range 0.5 to 1.5 MM, 2) "graupel" particles for D in the range 1.5 to 2.5 MM, and 3) ice spheres of densities 100 to 500 KG/M^3 for D greater than 2.5 MM. For D smaller than 0.5 MM, the dashed curve approximates the low density

ice spheres, curve 6. It is expected that the approximation is better than suggested from Locatelli and Hobb's (1974) curves in Figure 4.3 since they correspond to low air density conditions (observations at altitudes 750 and 1500 m above sea level). Thus, they tend to overestimate the terminal velocities of the snow crystals at lower altitudes.

The dashed line for solid precipitation is of the type in Eq. (4.7) with α given by:

$$\alpha = 1500 \text{ [1/SEC]} \quad (4.22)$$

Based on Eqs. (4.21) and (4.22), the terminal velocity of snow particles appears to be about one-third that of the liquid water drops with equal mass.

Due to insufficient data in the literature, the velocity of isolated particles is assumed equal to the velocity of a system of particles. Experiments documented in Sulakvelidze (1969) show, however, an increase of fall velocity for a system of particles of common dimension as compared to an isolated particle of the same dimension.

The increase depends on the distance of the particles expressed in number of diameters, the Reynolds number, and the total number of particles. For Reynolds number of order 10^{-1} , for particle center distances of the order of 15 diameters, the increase is about 25%.

As the distance between the particle centers increases, the difference in velocity between the system of particles and a single particle drops rapidly to zero (its value for a distance greater than 30 to 35 diameters). Using the single isolated particle velocity, therefore, would tend to underestimate the precipitation rate especially during high intensity periods.

Determination of the type of precipitation (rain/snow) is based on the surface temperature T_0 , such that snow occurs when T_0 is less than 274.50°K (Eagleson, 1970).

4.5 Steady-State Diffusion of Precipitation Particles Falling in Subsaturated Air

Consider a spherical precipitation particle of diameter D_0 at the cloud base (corresponding to the lifting condensation level LCL). Denote by Z_b the height above ground of the cloud base (Figure 2.1). Assume that the particle undergoes an isothermal and isobaric free fall at its terminal velocity $v_T(D)$. The ambient temperature is T_0 , the ambient pressure p_0 and the ambient water vapor pressure is $e_s(T_d)$ with T_d the dew point temperature ($T_d \leq T$).

The particle will lose a portion of its mass due to the difference in the water vapor pressure at the surface of the particle and $e_s(T_d)$.

Steady-state diffusion from a motionless particle, assuming that the particle surface vapor is at the wet-bulb temperature T_w , gives (Byers, 1965):

$$\rho_p \cdot D \cdot \frac{dD}{dt} = \frac{4D_{AB}}{R_v} \left(\frac{e_s(T_d)}{T_0} - \frac{e_s(T_w)}{T_w} \right) \quad (4.23)$$

where:

D = particle diameter during free fall [M]

t = time [SEC]

ρ_p = particle density [KG/M³]

R_v = gas constant for water vapor = 461 [JOULE/(KG · °K)]

D_{AB} = diffusivity of water vapor in air [M²/SEC]

Pruppacher and Klett (1978) give:

$$D_{AB} = 2.11 \cdot 10^{-5} \left(\frac{T_0}{T^*} \right)^{1.94} \left(\frac{p^*}{p_0} \right) \quad (4.24)$$

with

$$T^* = 273.15 \text{ [}^\circ\text{K]}$$

$$p^* = 101325 \text{ [KG/(M} \cdot \text{SEC}^2\text{)]}$$

and D_{AB} in [M²/SEC]

Eq. (4.24) is valid for temperatures between 233.15 °K (-40°C) and 313.15 °K (+40°C).

For a particle of diameter D falling freely in air with terminal velocity $v_T(D)$, diffusion is enhanced due to the ventilation effect on the moving particle.

Denote by $\overline{f}_v(D)$ the mean ventilation coefficient (>1), defined as the ratio of the water mass fluxes from a moving and a motionless particle. Then, the differential equation of vapor diffusion becomes:

$$\rho_p \cdot D \cdot \frac{dD}{dt} = \frac{4D_{AB} \cdot \overline{f}_v(D)}{R_v} \left(\frac{e_s(T_d)}{T_0} - \frac{e_s(T_w)}{T_w} \right) \quad (4.25)$$

Experimental studies published by Beard and Pruppacher (1971) for spherical particles suggest that $\overline{f}_v(D)$ depends on the Reynolds number R_e as:

$$\overline{f}_v(D) = \begin{cases} 1 + 0.108 N_{sc}^{2/3} \cdot R_e; & N_{sc}^{1/3} \cdot R_e^{1/2} \leq 1.4 \\ 0.78 + 0.308 N_{sc}^{1/3} \cdot R_e^{1/2}; & N_{sc}^{1/3} \cdot R_e^{1/2} \geq 1.4 \end{cases} \quad (4.26)$$

with

$$R_e = \frac{D \cdot v_T(D) \cdot \rho_a}{\mu} \quad (4.27)$$

and

$$N_{sc} = \frac{\mu}{\rho_a \cdot D_{AB}} \quad (4.28)$$

where

ρ_a : air density at temperature T_0 and pressure p_0 [KG/M³]

μ : air dynamic viscosity at temperature T_0 [KG/(M·SEC)]

For μ , Rogers (1979) gives the empirical relationship:

$$\mu = 1.72 \cdot 10^{-5} \left(\frac{393}{T_0 + 120}\right) \left(\frac{T_0}{273}\right)^{3/2} \quad (4.29)$$

with T_0 in [$^{\circ}$ K], μ in [KG/(M · SEC)].

If the subcloud layer average updraft velocity is negligible, as is the case of most storms with appreciable precipitation, then the kinematic equation for particle movement is:

$$\frac{dZ}{dt} = -v_T(D) \quad (4.30)$$

where Z is the vertical axis coordinate whose origin is at ground level with upwards positive direction (Figure 2.1).

Elimination of dt between the diffusion and the kinematic equation results in:

$$\rho_P \frac{D \cdot v_T(D)}{\bar{F}_V(D)} \cdot dD = \frac{4D_{AB}}{R_v} \left(\frac{e_s(T_w)}{T_w} - \frac{e_s(T_d)}{T_0} \right) \cdot dZ \quad (4.31)$$

Denote by D_F the particle diameter, when it reaches the ground. Then:

$$\rho_P \int_{D_F}^D \frac{D \cdot v_T(D)}{\bar{F}_V(D)} \cdot dD = \int_0^{Z_b} \frac{4D_{AB}}{R_v} \left(\frac{e_s(T_w)}{T_w} - \frac{e_s(T_d)}{T_0} \right) \cdot dZ \quad (4.32)$$

Due to the nature of the functions $v_T(D)$ and $\overline{f_v}(d)$ as they are given in Beard (1976) and Beard and Pruppacher (1971), respectively, it is not possible to analytically solve Eq. (4.32) for the diameter D_F when D_0 is given. Nevertheless, a closed form explicit solution is desirable for the computation of the precipitation rate that reaches the ground. Therefore, some approximation is in order.

It is only necessary to approximate the integral $F(D^*)$ given by:

$$F(D^*) = \rho_p \int_0^{D^*} \frac{D \cdot v_T(D)}{\overline{f_v}(D)} \cdot dD \quad (4.33)$$

since Eq. (4.32) can be written as:

$$F(D_0) - F(D_F) = \int_0^{z_b} \frac{4D_{AB}}{R_v} \left(\frac{e_s(T_w)}{T_w} - \frac{e_s(T_d)}{T_0} \right) \cdot dz \quad (4.34)$$

The temperature and pressure dependence of $F(D^*)$ is established in Figure 4.4 for liquid water. There, results of numerical computation of $F(D^*)$ are displayed for selected temperature T_0 and p_0 , to be expected in the subcloud layer. Curve 1 corresponds to $T_0 = 273.15$ °K, $p_0 = 1013$ MB; curve 2 corresponds to $T_0 = 293.15$ °K, $p_0 = 1013$ MB; curve 3 corresponds to $T_0 = 273.15$ °K, $p_0 = 800$ MB. Also $F(D^*)$ is displayed for a low density ($\rho_p = 100$ KG/M³) particle when $T_0 = 273.15$ °K and $p_0 = 1013$.

It can be stated that $F(D^*)$ increases as temperature increases or as pressure decreases. For values of D in the range of 0.5 to 1.5 MM,

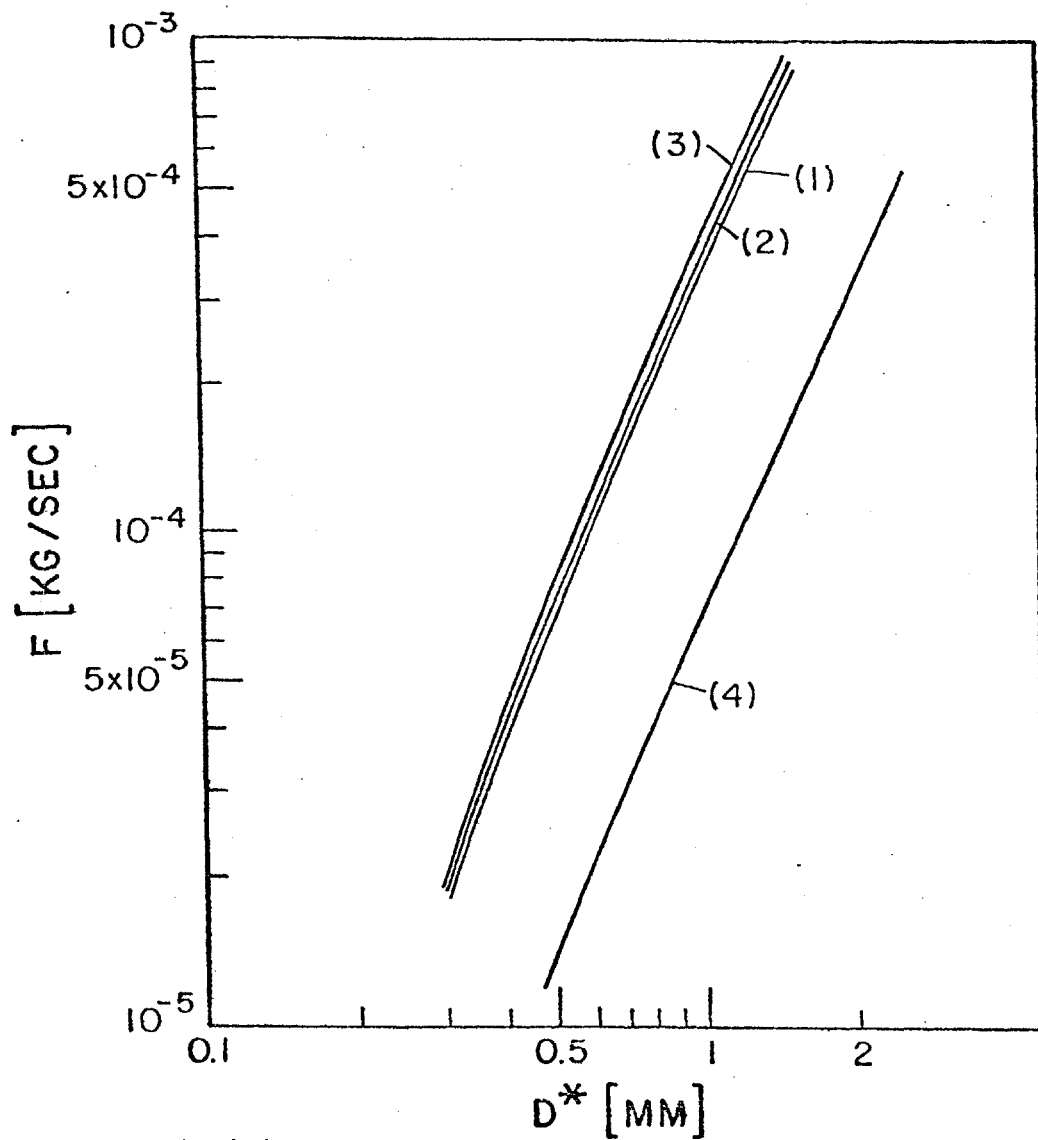


FIGURE 4.4

Integral F as a function of the water equivalent diameter D^*

Curve 1: $T_0 = 273.15$ [$^{\circ}$ K], $p_0 = 1013$ [MBAR], $\rho_p = 1000$ [KG/M 3]

Curve 2: $T_0 = 293.15$ [$^{\circ}$ K], $p_0 = 1013$ [MBAR], $\rho_p = 1000$ [KG/M 3]

Curve 3: $T_0 = 273.15$ [$^{\circ}$ K], $p_0 = 800$ [MBAR], $\rho_p = 1000$ [KG/M 3]

Curve 4: $T_0 = 273.15$ [$^{\circ}$ K], $p_0 = 1013$ [MBAR], $\rho_p = 100$ [KG/M 3]

of interest in precipitation, the dependence of F on T_0 , p_0 is weak relative to its dependence on D and it is ignored in this work.

A cubic relationship of F on D^* is adopted. That is, in general,

$$F(D^*) = c_2 + c_1 \cdot D^{*3} \quad (4.35)$$

with c_2 , c_1 constants.

Then, Eq. (4.34) becomes:

$$c_1(D_0^3 - D_F^3) = \int_0^{Z_b} \frac{4D_{AB}}{R_v} \left(\frac{e_s(T_w)}{T_w} - \frac{e_s(T_d)}{T_0} \right) \cdot dz \quad (4.36)$$

Assuming isothermal and isobaric free fall, Eq. (4.36) takes the form:

$$D_F^3 = D_0^3 - \frac{1}{c_1} \cdot \frac{4D_{AB}}{R_v} \left(\frac{e_s(T_w)}{T_w} - \frac{e_s(T_d)}{T_0} \right) \cdot Z_b \quad (4.37)$$

The wet-bulb temperature can be obtained, under equilibrium conditions (Byers, 1965) from:

$$T_w = T_0 - \frac{L(T_w)}{c_p} (w_s(T_w, p_0) - w_s(T_d, p_0)) \quad (4.38)$$

through the use of iteration techniques. In Eq. (4.38) $L(T_w)$ is the latent heat of vaporization (Eq. (3.15)), c_p is the specific heat of dry air, and $w_s(T, p)$ is the saturation mixing ratio at temperature

T and pressure p (Eq. (3.4)). Usually, in surface meteorological stations T_w is observed through a wet-bulb thermometer.

The final versus initial mass ratio for a particle, $\zeta(D_0)$, is

$$\zeta(D_0) = \left(\frac{D_F}{D_0}\right)^3 \quad (4.39)$$

By means of Eq. (4.37), this gives:

$$\zeta(D_0) = 1 - \left(\frac{D_c}{D_0}\right)^3 \quad (4.40)$$

with

$$D_c = \left[\frac{1}{c_1} \cdot \frac{4D_{AB}}{R_v} \cdot z_b \cdot \left(\frac{e_s(T_w)}{T_w} - \frac{e_s(T_d)}{T_0} \right) \right]^{1/3} \quad (4.41)$$

It can be observed that D_c represents the diameter of the particle that leaves the cloud base and evaporates completely when it is just reaching the ground. Particles of diameter less than or equal to D_c at the cloud base do not contribute to the precipitation rate at ground level.

Use of Eq. (4.40) requires estimation of the constant c_1 . An estimate of c_1 is obtained from published data corresponding to Eq. (4.37) with the assumption $T_w \approx T_0$ (reasonable during a storm period). Under this condition, Eq. (4.37) gives:

$$D_F = [D_0^3 - \frac{4D_{AB} \cdot e_s(T_0)}{c_1 R_v T_0} \cdot (1 - r) \cdot Z_b]^{1/3} \quad (4.42)$$

with the fractional relative humidity r given by

$$r = \frac{e_s(T_d)}{e_s(T_0)} \quad (4.43)$$

The value of c_1 adopted is the one that gives the best fit of the diameter D_F , computed from Eq. (4.42), to the results in Pruppacher and Klett (1978) shown in Figure 4.5a. D_F is presented as a function of the distance, $-Z_b$, of the ground surface below cloud base. In this figure, the cloud base is located at the 0 mark of the ordinate axis. Therefore, at this level $D_F = D_0$. The fitted c_1 value was $7 \cdot 10^5$ [KG/(M³ · SEC)].

The behavior of D_0 in Eq. (4.42) is shown with dashed lines in Figure 4.5b for different T_0 , p_0 , r values. There, the value of D_F is set equal to 0.2 [MM] and Eq. (4.42) is solved for D_0 with c_1 at its estimated value. In this case, the 0 mark in the ordinate axis represents the ground surface. The solid lines are the results of numerical computation of D_0 from Eq. (4.32) with $T_w \approx T_0$, published in Beard and Pruppacher (1971). The approximation is rather good, particularly when the cloud base is low. There is, however, a tendency to overestimate the mass loss due to evaporation, especially for small initial diameters D_0 .

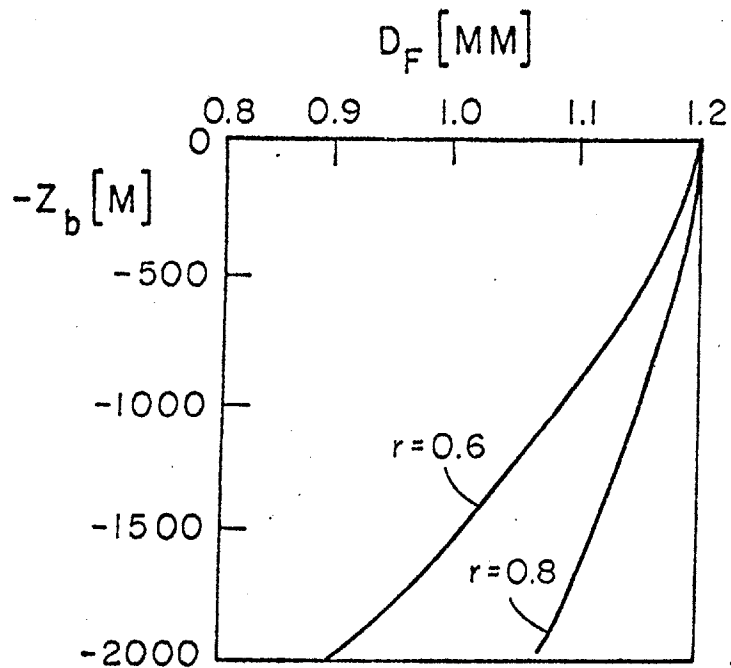


FIGURE 4.5a

Numerical integration results in Pruppacher and Klett (1978) used to determine the constant c_1 in Eq. (4.42). $T_0 = 278.15$ [°K] and $p_0 = 800$ [MBAR].

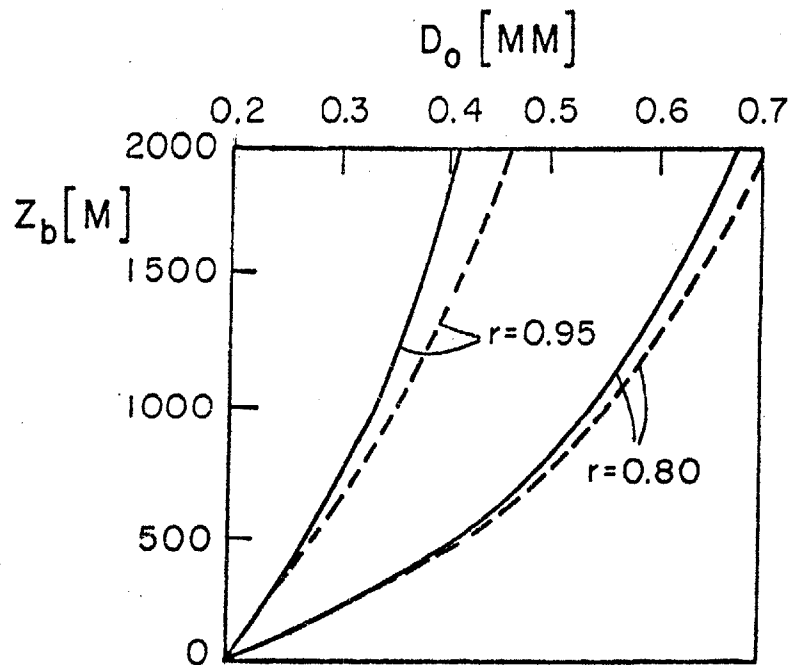


FIGURE 4.5b

Initial diameter at cloud base D_0 as a function of Z_b for different values of r . Solid lines are D_0 for numerical integration results in Beard and Pruppacher (1971). Dashed lines are for Eq. (4.42) with $D_F = 0.2$ [MM]. $T_0 = 273.15$ [°K] and $p_0 = 765$ [MBAR].

The results presented correspond to liquid water drops. A value of c_1 for snow particles can be obtained as follows.

Denote by R_F the ratio of the integral of type F for liquid water particles to the same one for ice particles of low density, $100 \text{ [KG/M}^3\text{]}$. Then, Eq. (4.35) and Figure 4.4 give, for small c_2 , a value of R_F equal to 5. This results in a value of c_1 equal to $1.4 \cdot 10^5$ for snowfall. Clearly, this is but a rough estimate of c_1 for snowfall and fitting to input-output data is required to give an accurate c_1 -snow value.

Summarizing, the value of c_1 is given, in SI units, by:

$$c_1 = \begin{array}{l} 7 \cdot 10^5 \text{ -- RAIN} \\ 1.4 \cdot 10^5 \text{ -- SNOW} \end{array} \quad (4.44)$$

The dependence of D_c on Z_b and r ($T_w = T_0$), for an isothermal and isobaric descent of liquid water ($\rho_p = 1000 \text{ [KG/M}^3\text{]}$) and snow ($\rho_p = 100 \text{ [KG/M}^3\text{]}$) spherical particles is shown in Figure 4.6. For raindrops the variables are $T_0 = 293.15 \text{ [}^\circ\text{K]}$, $p_0 = 1013 \text{ [MBAR]}$. For snow particles they are $T_0 = 273.15 \text{ [}^\circ\text{K]}$ and $p_0 = 1013 \text{ [MBAR]}$.

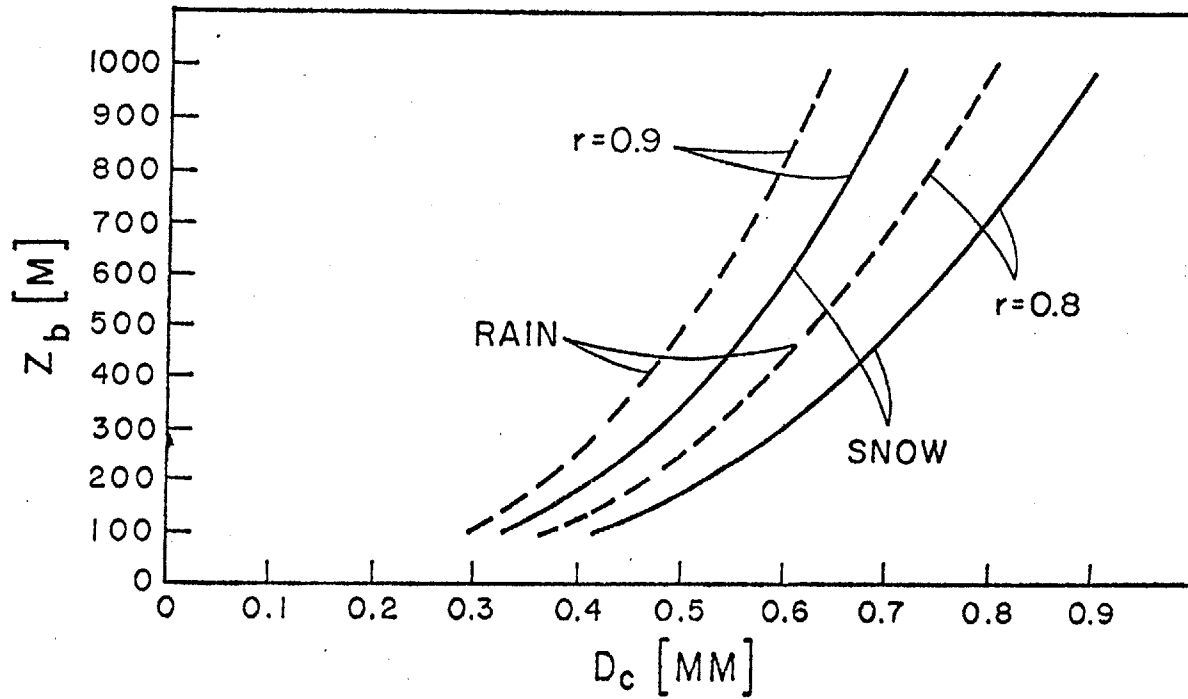


FIGURE 4.6 Initial diameter D_c at cloud base, of the largest completely evaporating hydrometeor in a sub-cloud layer of depth Z_b , as a function of Z_b , for different values of the relative humidity r . For raindrops: $T_0 = 293.15$ [°K], $p_0 = 1013$ [MBAR] For snow particles: $T_0 = 273.15$ [°K], $p_0 = 1013$ [MBAR]

Chapter 5

STATION PRECIPITATION MODEL EQUATIONS

5.1 Introduction

Based on the results of the three previous chapters, the equations corresponding to the unit area atmospheric column are formulated in sections 5.2 through 5.4. In order to arrive at a physically meaningful model form, two dimensionless numbers, N_v and N_D , are identified, related to the updraft strength and to the magnitude of the sub-cloud evaporation, respectively. They play a crucial role in the present formulation. The updraft velocity v_β ($v_\beta \leq v$) at the top and bottom of the cloud column (see Figure 2.2) is used in the derivation of the output mass rates O_b and O_t .

Section 5.5 expresses the model physical parameters c , v and p_t as functions of the input variables T_0 , p_0 and T_d , such that a storm invariant parameterization results.

5.2 Unit Area Column Output Rate

The output mass rate per unit area through the storm cloud base, in the diameter interval $(D, D + dD)$, is:

$$O_b(D) \cdot dD = \frac{\pi}{6} \cdot D^3 \cdot \rho_w (v_T(D) - v_\beta) n(D) \cdot dD \quad (5.1)$$

Therefore, the total mass rate per unit area through the cloud base is:

$$O_b = \int_{D_\ell}^{D_{\max}} \frac{\pi}{6} \cdot \rho_w \cdot D^3 (v_T(D) - v_\beta) n(D) \cdot dD \quad (5.2)$$

where

D_{\max} , D_ℓ are the maximum and minimum liquid water diameters found among the particles that fall to the ground.

Due to the basic exponential decay of $n(D)$ with increasing D , D_{\max} is set equal to $+\infty$. D_ℓ is such that the difference $(v_T(D) - v_\beta)$ is non-negative for all D in Eq. (5.2).

Therefore, substituting for $v_T(D)$ and $n(D)$ from Eqs. (4.7) and (4.1), respectively, one obtains,

$$O_b = \int_{\frac{v_\beta}{\alpha}}^{+\infty} \frac{\pi}{6} \cdot \rho_w \cdot N_0 \cdot D^3 (\alpha \cdot D - v_\beta) e^{-cD} \cdot dD \quad (5.3)$$

Direct integration yields:

$$O_b = \frac{\pi}{6} \cdot \rho_w \cdot \frac{N_0}{c} \left[\frac{\alpha}{c} \Gamma\left(5, \frac{cv_\beta}{\alpha}\right) - v_\beta \cdot \Gamma\left(4, \frac{cv_\beta}{\alpha}\right) \right] \quad (5.4)$$

where the complementary Gamma function $\Gamma(v, \chi)$, for χ a real number, is defined by:

$$\Gamma(v, \chi) = \int_{\chi}^{+\infty} e^{-t} \cdot t^{v-1} \cdot dt \quad (5.5)$$

and, for ν an integer, is computed by:

$$\Gamma(\nu, \chi) = (\nu-1)! e^{-\chi} \left(1 + \chi + \frac{\chi^2}{2!} + \dots + \frac{\chi^{\nu-1}}{(\nu-1)!} \right) \quad (5.6)$$

The output mass rate per unit area due to the action of the updraft velocity v_β on the smallest water particles in the interval $(D, D + dD)$ is:

$$O_t(D) \cdot dD = \frac{\pi}{6} \cdot \rho_w \cdot D^3 (v_\beta - v_T(D)) n_t(D) \cdot dD \quad (5.7)$$

with $n_t(D)$ the size distribution at the cloud top, where the parameter of the size distribution takes the value $\gamma \cdot c$ (see also Eq. (4.13)).

Setting the lower limit of integration equal to 0 and the upper to $\frac{v_\beta}{\alpha}$, to prevent negative $(v_\beta - v_T(D))$, the total output mass rate per unit area is:

$$O_t = \int_0^{\frac{v_\beta}{\alpha}} \frac{\pi}{6} \cdot \rho_w \cdot N_0 \cdot D^3 (v_\beta - \alpha \cdot D) e^{-\gamma c D} \cdot dD \quad (5.8)$$

Direct integration yields:

$$O_t = \pi \cdot \rho_w \frac{N_0}{c^4} \frac{\alpha}{c \cdot \gamma^5} \left\{ \frac{1}{6} \left[\Gamma\left(5, \gamma \frac{v_\beta \cdot c}{\alpha}\right) - \left(\gamma \frac{v_\beta \cdot c}{\alpha}\right) \cdot \Gamma\left(4, \gamma \frac{v_\beta \cdot c}{\alpha}\right) \right] + \gamma \frac{v_\beta \cdot c}{\alpha} - 4 \right\} \quad (5.9)$$

The total mass output rate O per unit area is then given by:

$$O = O_b + O_t \quad (5.10)$$

5.3 Surface Precipitation Mass Rate

Due to evaporation in the subcloud layer, the precipitation rate at ground level is generally only a portion of O_b . Denote by P the mass precipitation rate per unit area of liquid water equivalent at ground level. It is given as:

$$P = \int_{D_\ell}^{+\infty} \frac{\pi}{6} \cdot \rho_w \cdot D^3 \cdot \zeta(D) (v_T(D) - v_\beta) n(D) \cdot dD \quad (5.11)$$

where the limit D_ℓ is now defined as:

$$D_\ell = \max \left\{ D_c, \frac{v_\beta}{\alpha} \right\} \quad (5.12)$$

with $\zeta(D)$ and D_c given in Eqs. (4.40) and (4.41), respectively.

Substitution of $\zeta(D)$, $v_T(D)$ and $n(D)$ in Eq. (5.11) and integration yields:

$$P = \frac{\pi}{6} \cdot \rho_w \cdot \frac{N_0}{c} \left[\frac{\alpha}{c} \cdot \Gamma(5, c D_\ell) - v_\beta \cdot \Gamma(4, c D_\ell) - D_c^3 \cdot \alpha \cdot c^2 \cdot \Gamma(2, c D_\ell) + D_c^3 \cdot v_\beta \cdot c^3 \cdot e^{-c D_\ell} \right] \quad (5.13)$$

5.4 Mass Rates Expressed as Functions of the Dimensionless

Numbers N_v and N_D

Define N_v , N_D and v_p as:

$$N_v = \frac{v_\beta \cdot c}{\alpha} \quad (5.14)$$

$$N_D = c \cdot D_c \quad (5.15)$$

$$v_p = 4 \cdot \alpha \cdot \frac{1}{c} \quad (5.16)$$

The number N_v is indicative of the updraft strength at the cloud base since it is the ratio of the diameter $(\frac{v_\beta}{\alpha})$ of the particles that possess terminal velocity equal to v_β , to the average diameter $(\frac{1}{c})$ of the cloud particles. As N_v increases, the updraft strength increases.

The number N_D is a measure of the relative strength of the diffusion process (Eq. (4.41)) in the sub-cloud layer. Diffusion losses increase with increasing N_D .

The velocity v_p corresponds to particles of diameter $(\frac{4}{c})$ which are the ones that contribute the maximum rate to the total precipitation rate (Figure 4.1).

Use of Eqs. (5.14), (5.15) and (5.16) in Eqs. (5.4), (5.9) and (5.13) results in:

$$O_b = \frac{X}{24 \cdot \delta \cdot Z_c} v_p \cdot [\Gamma(5, N_V) - N_V \cdot \Gamma(4, N_V)] \quad (5.17)$$

$$O_t = \frac{X}{4 \cdot \delta \cdot Z_c} v_p \cdot \frac{1}{5} \cdot \left\{ \frac{1}{6} \cdot [\Gamma(5, N_V \gamma) - \gamma N_V \cdot \Gamma(4, \gamma N_V)] \right. \\ \left. + \gamma N_V - 4 \right\} \quad (5.18)$$

$$P = \frac{X}{24 \cdot \delta \cdot Z_c} v_p \cdot [\Gamma(5, N_D) - N_V \cdot \Gamma(4, N_D) - N_D^3 \cdot \Gamma(2, N_D) \\ + N_V \cdot N_D^3 \cdot e^{-N_D}] \quad ; \quad N_D \geq N_V \quad (5.19a)$$

$$P = \frac{X}{24 \cdot \delta \cdot Z_c} v_p \cdot [\Gamma(5, N_V) - N_V \cdot \Gamma(4, N_V) - N_D^3 \cdot \Gamma(2, N_V) \\ + N_V \cdot N_D^3 \cdot e^{-N_V}] \quad ; \quad N_V \geq N_D \quad (5.19b)$$

Further simplification is possible through the use of Eq. (5.6).

Then,

$$O_b = \frac{X}{\delta \cdot Z_c} v_p \left[\frac{1 + \frac{3}{4} N_V + \frac{N_V^2}{4} + \frac{N_V^3}{24}}{e^{N_V}} \right] \quad (5.20)$$

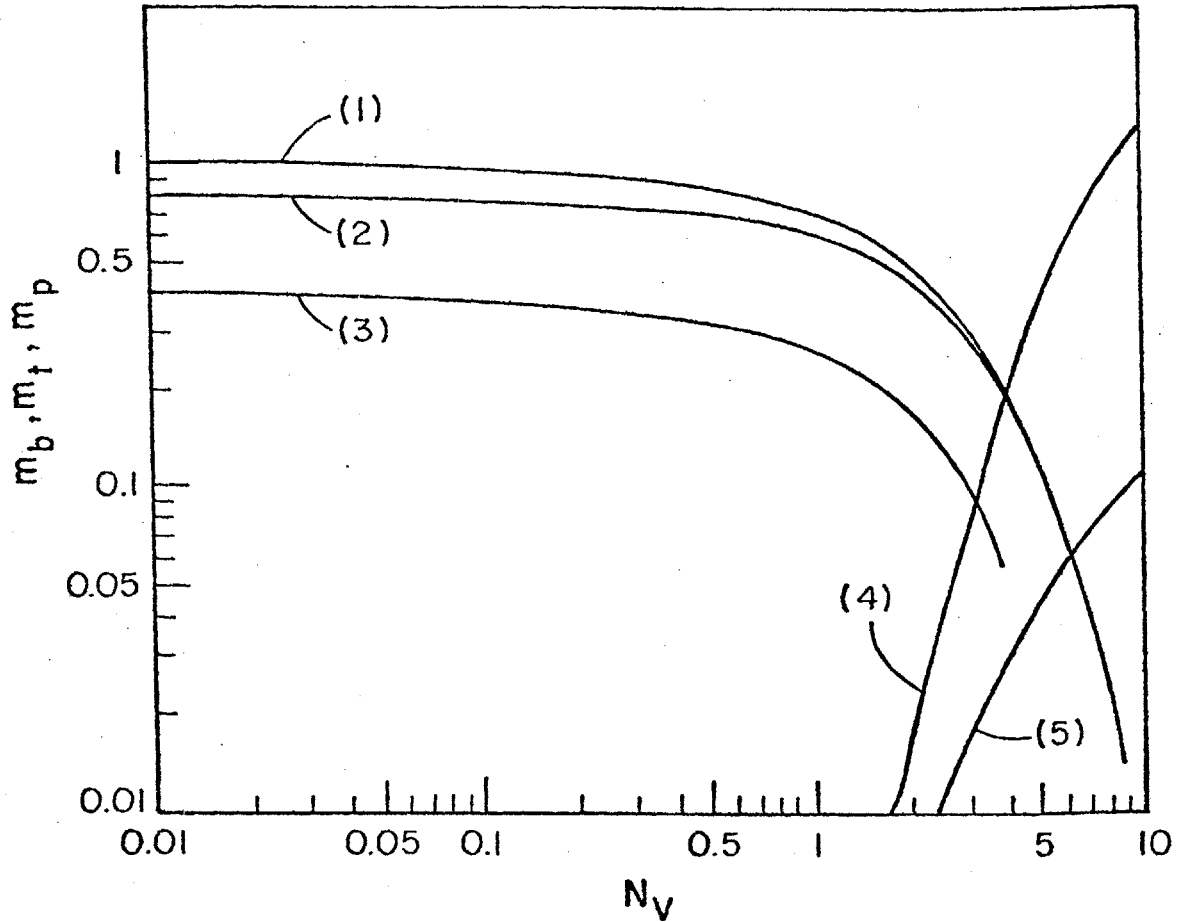


FIGURE 5.1

Reduction factors m_b , m_t and m_p as functions of the number N_v . N_d and γ are parameters of the plots. Curve 1 is for m_b . Curves 1, 2 and 3 are for m_p , for N_d equal to 0, 2, and 4 respectively. Curves 4 and 5 are for m_t for γ equal to 1 and 2 respectively.

$$O_t = \frac{X}{\delta \cdot Z_c} v_p \cdot \frac{1}{\gamma} \left[\frac{1 + \frac{3}{4} (\gamma N_v) + \frac{(\gamma N_v)^2}{4} + \frac{(\gamma N_v)^3}{24}}{e^{\gamma N_v}} + \frac{\gamma N_v}{4} - 1 \right] \quad (5.21)$$

$$P = \frac{X}{\delta \cdot Z_c} v_p \left[\frac{(1 - \frac{N_v}{4}) (1 + N_D + \frac{N_D^2}{2}) + \frac{N_D^3}{8}}{e^{N_D}} \right] ; \quad N_D \geq N_v \quad (5.22a)$$

$$P = \frac{X}{\delta \cdot Z_c} v_p \left[\frac{(1 + \frac{3}{4} N_v + \frac{N_v^2}{4} + \frac{N_v^3}{24} - \frac{N_D^3}{24}}{e^{N_v}} \right] ; \quad N_v \geq N_D \quad (5.22b)$$

Denote by O_R the reference mass rate per unit area defined by:

$$O_R = \frac{X}{\delta \cdot Z_c} v_p \quad (5.23)$$

Then one can define the reduction factors m_b , m_t and m_p as the ratios of the rates O_b , O_t and P to the reference rate O_R .

Figure 5.1 shows plots of m_b , m_t , m_p as functions of N_v , N_D , and γ . Curve 1 represents m_b as a function of N_v . Curves 1, 2, 3 represent m_p as a function of N_v , for N_D equal to 0, 2 and 4, respectively. The reduction factor m_t is represented in curves 4 and 5 for γ equal to 1 and 2, respectively. Based on Figure 5.1:

1. Losses through the cloud top (i.e., O_t rate) become significant for $N_v > 3$ if γ is equal to 1 or 2. The larger the γ , the smaller m_t becomes.
2. For low N_D numbers ($N_D < 1$) the precipitation rate that reaches the ground is practically equal to the output rate, O_b , through the cloud base (curves 1 and 2).
3. As N_v decreases, the precipitation rate P increases reaching a maximum as N_v tends to 0 (no updraft at the cloud base).
4. For instances of insignificant diffusion losses and for small N_v numbers ($N_v < 0.5$), the precipitation rate P is given by:

$$P = \frac{X}{\delta \cdot Z_c} v_p \quad (5.24)$$

The rates O_b , O_t and P are functions of c and not of N_0 in Eqs. (5.20), (5.21) and (5.22). Therefore, if c is retained as a model parameter, those equations are linear in the state variable X . In this "convenient" case, the results of this section can be put in the following format.

$$0 = h(\underline{u}, \underline{a}_0) \cdot X \quad (5.25)$$

where O is the total output rate from the unit area column and the nonlinear function $h(\cdot)$ is defined as:

$$h(\underline{u}, \underline{a}_0) = \frac{v_p}{Z_c \cdot \delta} \left[\frac{1 + \frac{3}{4} N_v + \frac{N_v^2}{4} + \frac{N_v^3}{24}}{e^{N_v}} + \frac{1 + \frac{3}{4} (\gamma N_v) + \frac{(\gamma N_v)^2}{4} + \frac{(\gamma N_v)^3}{24}}{\gamma^5 \cdot e^{\gamma N_v}} + \frac{N_v}{4 \cdot \gamma^4} - \frac{1}{\gamma^5} \right] \quad (5.26)$$

with \underline{u} defined in section 3.4 and \underline{a}_0 defined by:

$$\underline{a}_0^T = [p_t \ v \ c]$$

Dependence of the function $h(\cdot)$ on the parameter p_t comes from the definition equations for Z_c in a hydrostatic atmosphere. The height Z above a fixed pressure level p_0 and the pressure p at that height (Z) are related through the hypsometric equation (Wallace and Hobbs, 1977):

$$Z = \frac{R \cdot \bar{T}}{g} \cdot \ln \left(\frac{p_0}{p} \right) \quad (5.27)$$

with \bar{T} the average temperature in the layer of height Z , R the dry air gas constant, and g the gravitational acceleration.

The precipitation rate P is:

$$P = \phi(\underline{u}, \underline{a}_0) \cdot X \quad (5.28)$$

with the function $\phi(\cdot)$ given by (Eqs. (5.22)):

$$\begin{aligned} \phi(\underline{u}, \underline{a}_0) = & \frac{v_P}{Z_c \cdot \delta} \left[\xi\left(\frac{N_D}{N_V}\right) \frac{(1 - \frac{N_V}{4}) (1 + N_D + \frac{N_D^2}{2}) + \frac{N_D^3}{8}}{e^{N_D}} \right. \\ & \left. + (1 - \xi\left(\frac{N_D}{N_V}\right)) \frac{1 + \frac{3}{4} N_V + \frac{1}{4} N_V^2 + \frac{1}{24} N_V^3 - \frac{1}{24} N_D^3}{e^{N_V}} \right] \quad (5.29) \end{aligned}$$

The step function $\xi(\cdot)$ is defined by:

$$\xi(y) = \begin{cases} 1 & \text{if } y \geq 1 \\ 0 & \text{if } y < 1 \end{cases} \quad (5.30)$$

Usually, the input to hydrologic soil moisture accounting models is the water equivalent volume rate P_v of precipitation. The mass rate P can be converted to volume rate P_v by the transformation:

$$P_v = \frac{P}{\rho_w} \quad (5.31)$$

where ρ_w is the density of liquid water.

Then, the dynamics equation describing the evolution of moisture in the column is:

$$\frac{dX}{dt} = f(\underline{u}, \underline{a}_T) - h(\underline{u}, \underline{a}_0) \cdot X \quad (5.32)$$

and the output equation is:

$$P_v = \frac{\phi(\underline{u}, \underline{a}_0)}{\rho_w} \cdot X \quad (5.33)$$

In the case when one wants to retain N_0 instead of c as a model parameter, the functions $h(\cdot)$ and $\phi(\cdot)$ become dependent on the state X due to the substitution of c by the expression in Eq. (4.19). For computational convenience the linear formulation in Eqs. (5.32) and (5.33) is used in this work.

An important conclusion that follows from Eq. (5.33) is that the precipitation rate is directly analogous to the average liquid water content $\frac{X}{Z_c}$ of the cloud.

5.5 Unit Area Model Parameters

The following have been identified as model physical parameters: the vertically averaged updraft velocity in the unit area column v , the terminal pressure level of the column p_t and the average water equivalent particle diameter $\frac{1}{c}$ at the cloud base. Nevertheless, it

is desirable to express the model equations in terms of parameters that are storm invariant so that robust parameter estimates can be obtained.

5.5.1 Updraft Velocity and Terminal Pressure Parameterization

Work presented in Sulakvelidze (1969) indicates that v obeys a law of the type:

$$v = \epsilon_1 \cdot \sqrt{c_p \cdot \Delta T} \quad (5.34)$$

where:

$$\Delta T = T_m - T_s' \quad (5.35)$$

In the previous equations, ϵ_1 is a constant parameter, c_p is the specific heat of dry air under constant pressure [Joule/(kg · °K)], T_m is the cloud temperature [°K] at a certain level p' [mbar] assuming pseudo-adiabatic ascent and T_s' is the corresponding ambient air temperature [°K]. The quantity ϵ_1^2 is analogous to the ratio of kinetic to thermal energy per unit mass of ascending air, at the level p' . Therefore, ϵ_1 is dimensionless.

Due to the difficulty of obtaining radiosonde data for the locations of interest in real time, T_s' is taken as the temperature at level p' that results from dry-adiabatic ascent. The pressure level p' is taken where the updraft velocity is equal to the height

averaged v . Given the assumed vertical distribution of updraft velocity (Figure 2.2), p' becomes:

$$p' = p_s - \frac{1}{4} (p_s - p_t) \quad (5.36)$$

with p_s and p_t defined as the pressures at the cloud base and cloud top, respectively.

Using the results of Chapter 3, Eqs. (3.6) and (3.16), expressions for T_s' and T_m can be obtained. These are:

$$T_s' = \frac{T_0}{p_0^{0.286}} \left(\frac{3}{4} p_s + \frac{1}{4} p_t \right)^{0.286} \quad (5.37)$$

and

$$T_m \left(\frac{p_n}{p'} \right)^{0.286} \cdot \exp \left\{ \frac{L(T_m) \cdot w_s(T_m, p')}{c_p \cdot T_m} \right\} = \theta_e \quad (5.38)$$

Equation (5.34) and the definitions, Eqs. (5.35) through (5.38), provide an implicit relationship between p_t and v .

Independently, and based on observations of the development of storm clouds, another equation relating p_t and v is suggested. It is based on the well-known fact that the stronger the updraft, the more vigorous the storm clouds development and consequently the lower p_t is. However, the value of p_t also depends on the past history of the storm. Thus, as the storm persists for several hours,

even for low updraft velocities, p_t is expected to be relatively low (e.g., in precipitation processes from stratiform clouds). Since no information of the lifetime of the storm system before reaching the drainage basin boundaries is assumed, the new p_t versus v relationship is parameterized as follows:

$$\frac{p_t - p_\ell}{\epsilon_2 - p_\ell} = \frac{1}{1 + \epsilon_3 \cdot v} \quad (5.39)$$

where p_ℓ is the lowest value that p_t can attain, and ϵ_2, ϵ_3 are constant parameters.

Parameter p_ℓ can be set equal to the pressure value at the troposphere-stratosphere boundary since very few storms penetrate into the stratosphere. That is:

$$p_\ell = 200 \text{ [MBAR]}$$

Parameter ϵ_2 has dimensions of pressure and depends on the history of the storm before it reaches the basin boundaries. Parameter ϵ_3 has dimensions of inverse velocity and controls the p_t versus v relationship. Note that as v tends to zero, p_t tends to ϵ_2 , and as v tends to infinity, p_t tends to p_ℓ in agreement with the qualitative arguments described above. Simplification of the set of Eqs. (5.34) through (5.39) is possible by substitution of the velocity v from Eq. (5.39) into the expression for T_m resulting from Eqs. (5.34)

through (5.37). Thus, one obtains:

$$T_m = \frac{1}{c_p (\epsilon_1 \cdot \epsilon_3)^2} \cdot \left(\frac{\epsilon_2 - p_t}{p_t - p_\ell} \right)^2 + \frac{T_0}{p_0^{0.286}} \left(\frac{3}{4} p_s + \frac{1}{4} p_t \right)^{0.286} \quad (5.40)$$

The set of Eqs. (5.38) and (5.40) define the terminal pressure p_t in terms of ϵ_2 , p_ℓ , ϵ_1 , ϵ_3 , and the model inputs. Due to the nonlinearity in Eq. (5.38), iteration methods are utilized for the determination of its p_t root. The necessary derivatives and the starting value of p_t for use with a Newton Raphson method, are given in Appendix B. Use of those results is made to examine the behavior of the solution p_t when ϵ_1 , ϵ_2 , ϵ_3 , T_0 and T_d change, for a nominal pressure p_0 equal to 1000 [MBAR]. In this case, T_0 is equal to the potential temperature θ .

Figure 5.2 presents the function $p_t(T_0)$, solid lines, for $p_0 = 1000$ [MBAR], and for different values of ϵ_2 , r and $(\epsilon_1 \cdot \epsilon_3)$; r is the fractional relative humidity defined by Eq. (4.43). The parameter ϵ_2 takes the values 700 [MBAR] and 500 [MBAR], r takes the values 0.7 and 1 and the product $(\epsilon_1 \cdot \epsilon_3)$ is set to 0.01 and 0.05.

In the same figure, the potential thermal energy Q_{TH} per unit mass of air at pressure p' (dashed lines) is plotted against T_0 for the same values of the parameters and r . Q_{TH} is defined by:

$$Q_{TH} = c_p (T_m - T_s') \quad (5.41)$$

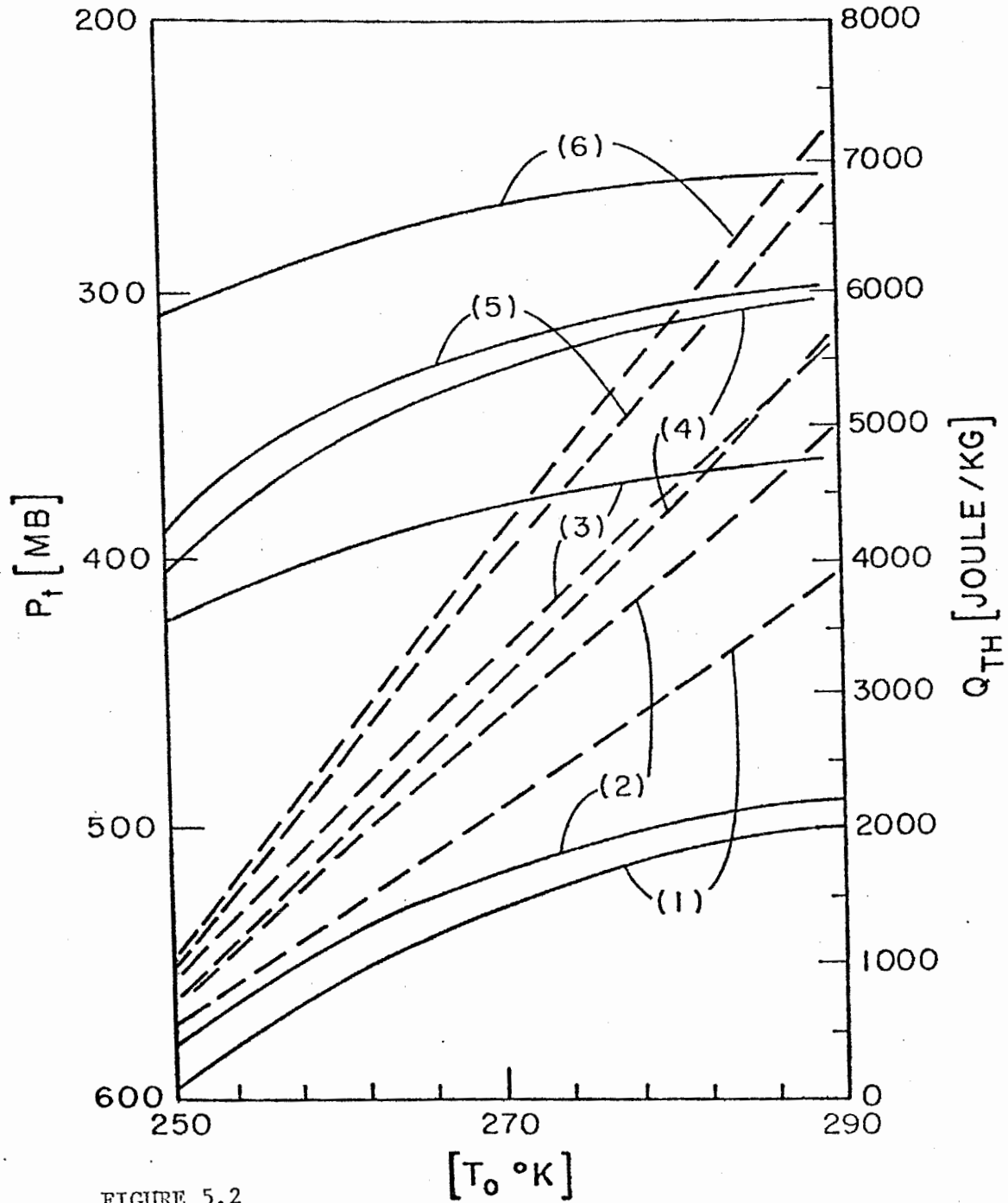


FIGURE 5.2

Temperature variation of p_t (solid lines) and Q_{TH} (dashed lines) for $p_0 = 1000$ [MBAR]. Plot parameters are: ϵ_2 , r , $\epsilon_1 \cdot \epsilon_3$

- Curve 1: $\epsilon_2 = 700$ [MBAR], $r = 0.7$, $\epsilon_1 \cdot \epsilon_3 = 0.01$ [SEC/M]
- Curve 2: $\epsilon_2 = 700$ [MBAR], $r = 1$, $\epsilon_1 \cdot \epsilon_3 = 0.01$ [SEC/M]
- Curve 3: $\epsilon_2 = 500$ [MBAR], $r = 1$, $\epsilon_1 \cdot \epsilon_3 = 0.01$ [SEC/M]
- Curve 4: $\epsilon_2 = 700$ [MBAR], $r = 0.7$, $\epsilon_1 \cdot \epsilon_3 = 0.05$ [SEC/M]
- Curve 5: $\epsilon_2 = 700$ [MBAR], $r = 1$, $\epsilon_1 \cdot \epsilon_3 = 0.05$ [SEC/M]
- Curve 6: $\epsilon_2 = 500$ [MBAR], $r = 1$, $\epsilon_1 \cdot \epsilon_3 = 0.05$ [SEC/M]

The range of temperatures used in the figure is from 250 °K to 290 °K and includes the freezing point. The pressure p_t took values in the range from 600 [MBAR] to 200 [MBAR] (left ordinate), while Q_{TH} varied from 500 [JOULE/KG] to 7500 [JOULE/KG] (right ordinate).

Figure 5.2 supports the following comments:

1. For the range of input and parameter values examined, p_t is closer to the lower limit p_ℓ (= 200 [MBAR]) for lower ϵ_2 , higher r and higher $(\epsilon_1 \cdot \epsilon_3)$.
2. For constant parameters ϵ_2 and $(\epsilon_1 \cdot \epsilon_3)$, the higher the vapor content of the air, the lower p_t becomes for all T_0 .
3. The lower the pressure parameter ϵ_2 is, the more insensitive to T_0 , p_t becomes.
4. The pressure p_t is much more sensitive to changes in the parameters ϵ_2 and $(\epsilon_1 \cdot \epsilon_3)$, than it is to changes in the input variables, T_0 , T_d .
5. In response to variations in ϵ_2 , $(\epsilon_1 \cdot \epsilon_3)$, T_0 and r , Q_{TH} displays the same behavior as the pressure p_t does. For T_0 at the freezing point, Q_{TH} ranges from 2200 [JOULE/KG] to about 4500 [JOULE/KG].

The terminal pressure p_t for given T_0 is a function of the product $(\epsilon_1 \cdot \epsilon_3)$ for different values of ϵ_2 and r , as shown in Figure 5.3. There the quantity \bar{p}_t , which is the value of p_t for the average temperature 266.15 [°K] in the temperature range of Figure 5.2, is plotted against $(\epsilon_1 \cdot \epsilon_3)$, for the same pairs of values of ϵ_2 and

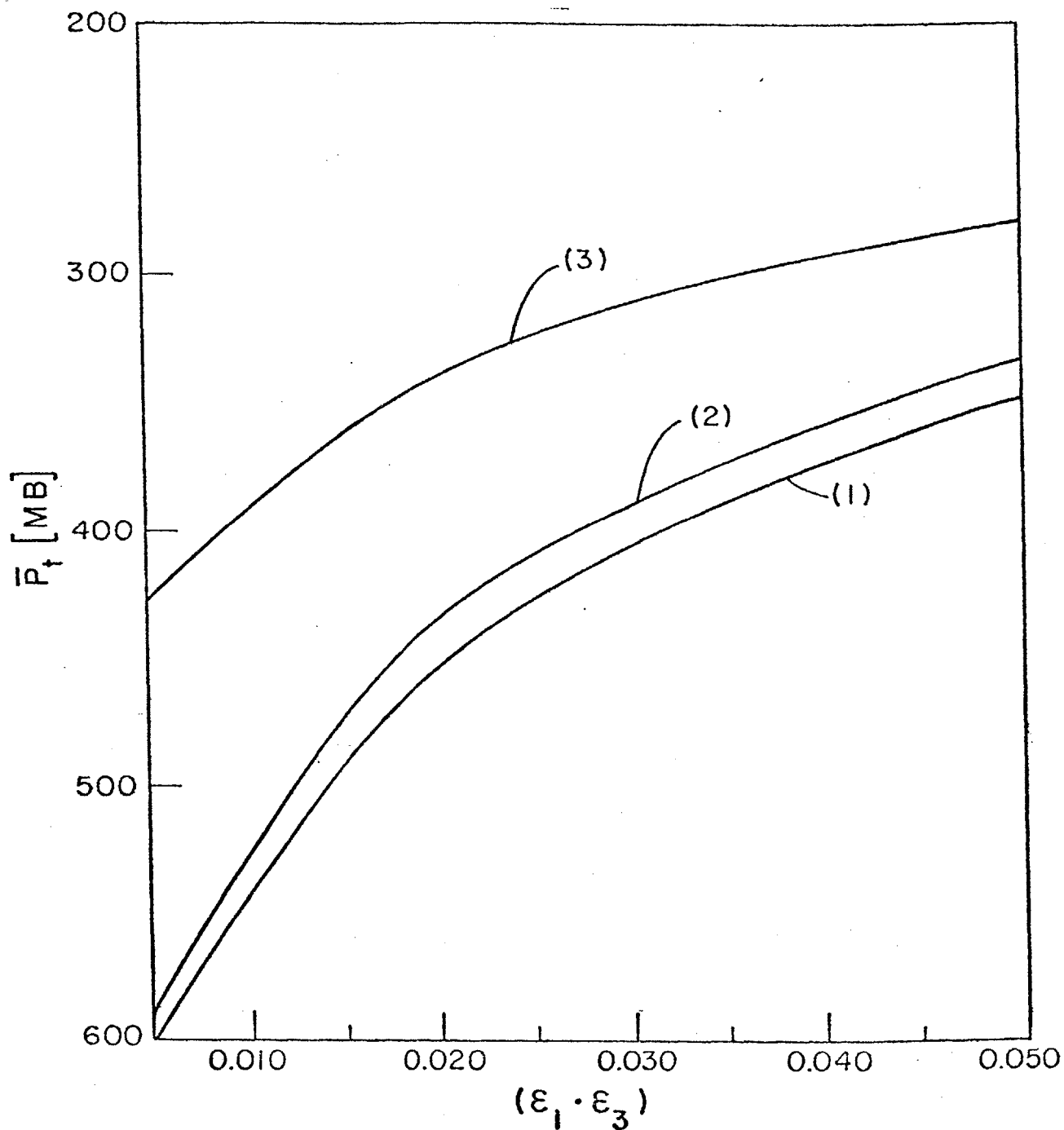


FIGURE 5.3

Pressure \bar{p}_t for $T_0 = 266.16$ [$^{\circ}\text{K}$] as a function of the parameter product $\epsilon_1 \cdot \epsilon_3$ with ϵ_2 and r as plot parameters.

Curve 1: $\epsilon_2 = 700$ [MBAR], $r = 0.7$

Curve 2: $\epsilon_2 = 700$ [MBAR], $r = 1$

Curve 3: $\epsilon_2 = 500$ [MBAR], $r = 1$.

r used in the previous figure. A low value of the parameter ϵ_2 and a high value of r push \bar{p}_t closer to p_ℓ ($= 200$ [MBAR]). It can also be seen that with decreasing ϵ_2 , the sensitivity of \bar{p}_t on $(\epsilon_1 \cdot \epsilon_3)$ is reduced. It is important to note that figures like 5.3, with perhaps more values for p_0 , ϵ_2 , and r, can be valuable in parameter estimation, when observations of p_t are available together with observations of T_0 , p_0 and T_d . Thus, given T_0 , p_0 , T_d , curves of equal T_0 , p_0 and r (since r is obtained from T_0 and T_d) can be constructed; for example, curves (2) and (3) in Figure 5.3, with only varying parameter: ϵ_2 . Then, the pairs of $[(\epsilon_1 \cdot \epsilon_3), \epsilon_2]$ that correspond to the observed p_t can be identified by the crossings of a parallel to the abscissa at p_t - observed value and of curves similar to (2) and (3) in Figure 5.3. This way, a relationship between ϵ_2 and $(\epsilon_1 \cdot \epsilon_3)$, that the feasible $\epsilon_1, \epsilon_2, \epsilon_3$ should obey, is constructed which will serve as an additional aid in the parameter estimation.

Once p_t , T_m and T_s' are expressed in terms of parameters ϵ_1 , ϵ_2 and ϵ_3 (Eqs. (5.40), (5.38), and (5.37), v is obtained directly from Eq. (5.34). Given p_t , the terminal temperature T_t , necessary to determine Δw from Eq. (3.17), is obtained by the Newton-Raphson method from Eq. (3.16) for $p = p_t$ and $T = T_t$.

5.5.2 Parameterization of Average Hydrometeor Diameter at Cloud Base

Several processes contribute to determine the parameter c . Based on past work, Pruppacher and Klett (1978) identify as most important: the condensation; the collision-coalescence and; the collisional breakup of the larger particles. They indicate that the stronger the updraft velocity is, the larger the number of the larger particles is. That implies increasing the average diameter ($\frac{1}{c}$) as v increases. In addition, based on theoretical work they suggest that even a mild updraft (e.g., of v equal to 0.10 m/sec) has a pronounced effect on the particle distribution. For the purposes of this work, it is assumed that c is solely determined by v from a relationship of the type:

$$\frac{1}{c} = \epsilon_4 \cdot v^m \quad (5.42)$$

where ϵ_4 and m are constant parameters. The dimensions of ϵ_4 are: $\frac{(\text{SEC})^m}{M^{(m-1)}}$, while m is dimensionless.

In summary, the storm invariant model parameters are: ϵ_1 , ϵ_2 , ϵ_3 , ϵ_4 and m . In addition, the values of γ and β defined by Eq. (4.13) and

$$v_\beta = \beta \cdot v \quad (5.43)$$

have to be determined. Parameter estimation based on physical arguments and input-output data is undertaken in Chapter 8.

Chapter 6

A CONCEPTUAL RAINFALL-RUNOFF MODEL

6.1 Introduction

This chapter formulates the equation of a general rainfall runoff model in state space form. The model is suitable for use in operational river flow forecasting. It couples the storm, soil and channel states in an extended state vector, and produces as an output flow rates at the drainage basin outlet. The soil moisture accounting scheme of the National Weather Service River Forecast System (NWSRFS) is utilized as the soil response simulator. The precipitation model developed in the previous chapters and the channel routing model of Georgakakos and Bras (1982) are used to provide the input and to propagate downstream the output of the soil model, respectively.

The proposed general rainfall-runoff model uses, as its input, real time forecasts of the meteorological variables T_o , p_o , T_d and of the evapotranspiration potential u_e . It produces as outputs the precipitation rate for the area corresponding to the forecasted T_o , p_o , and T_d , and the discharge output at the drainage basin outlet.

Formulation of the model equations for the case of a headwater basin with no upstream inflows is undertaken in Section 6.4.

Discussions on the coupling of the model components and on the relevant spatial and temporal scales are presented in Sections 6.5 and 6.6.

6.2 Equations of the Soil Moisture Accounting Model

The soil moisture accounting scheme of the NWSRFS has been successfully used with modern estimation theory techniques for the real time forecasting of river flows (Kitanidis and Bras, 1980a-b, Georgakakos and Bras, 1979, Georgakakos and Bras, 1982, Restrepo-Posada and Bras, 1982). It is a conceptual model of the reservoir type that monitors the volume of water in the different soil layers. Description of the deterministic model is given in Peck (1976). Armstrong (1978) gives the physical interpretation of the model components in terms of the observable soil characteristics. The differential equations for the time evolution of the model states, which are the contents of each conceptual reservoir, have been formulated in Kitanidis and Bras (1980a). A more complete formulation is given in Georgakakos, Restrepo-Posada and Bras (1980).

Characteristic to all up-to-date formulations is that they represent outflow from certain conceptual reservoirs as a discontinuous function of their contents. For instance, the upper zone tension water reservoir, modeling upper soil layer and interception storage, produces zero outflow until its contents reach its capacity. Once full the reservoir output is equal to its net input. This type of behavior is very difficult to handle within the linear framework of the most powerful modern estimation techniques. Kitanidis and Bras (1980a), in their formulation of the

linearized system, use describing function techniques to avoid the problem, while keeping the discontinuous formulation when computing the system response.

This work substitutes the threshold type behavior of the reservoir outflow (wherever applicable in the model) with a nonlinear reservoir response. This way the reservoir produces outflow even if it is not full, and its outflow depends on the degree of saturation. From a physical point of view, this is consistent with the spatially lumped nature of the model given the soil-property inhomogeneity of the basin. Thus, even if each soil column behaves as a threshold-type reservoir, the basin produces continuous outflow to groundwater and to the channel due to the spatial variation of the threshold value. In this work, the model parameter that defines the threshold (reservoir capacity) is considered to be a basin wide maximum capacity of the soil columns. The substitution of threshold-type reservoirs by a nonlinear power law-type one is illustrated in the following.

Denote by $g(\frac{x}{x^0}, u_0)$ the outflow function of the reservoir for a non-negative input u_0 . Then $g(\frac{x}{x^0}, u_0)$ given by

$$g(\frac{x}{x^0}, u_0) = \begin{cases} -u_0 & \text{if } \frac{x}{x^0} = 1 \\ 0 & \text{otherwise} \end{cases} \quad (6.1)$$

is a function of $\frac{x}{x_0}$ of the type shown with thick line in Figure 6.1a. Note the discontinuity in $x=x_0$.

The approximation in Figure 6.1b is used in place of Eq. (6.1).

That is,

$$g_a\left(\frac{x}{x_0}, u_0\right) = -u_0\left(\frac{x}{x_0}\right)^m \quad (6.2)$$

The higher the value of m the closer $g_a\left(\frac{x}{x_0}, u_0\right)$ approximates $g\left(\frac{x}{x_0}, u_0\right)$. Note that the domain of definition of x for the approximation is still the closed interval $[0, x_0]$.

Apart from the removal of the discontinuities, the following were important model modifications.

The moisture input to the soil moisture accounting scheme is taken from the precipitation model output (Eq. (5.33)), written in the form

$$P_v = \phi \cdot X \quad (6.3)$$

with P_v the volume rate per unit area and X the volume in cloud storage. The dependence of ϕ on \underline{u} and \underline{a}_0 has been omitted for notational convenience.

The distribution function for allocation of the percolating water between the lower zone free water reservoirs has been substituted with a numerically better behaving one. Use of the function in the original NWS model within a state estimation algorithm is liable to produce incorrect results (TASC, 1980). The modification is presented in Georgakakos, Restrepo-Posada and Bras (1980), and the result is:

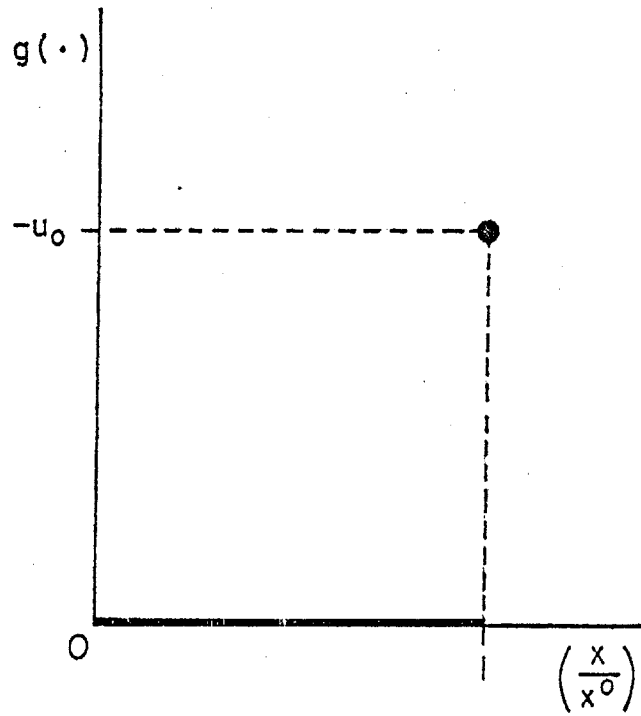


FIGURE 6.1a
 Outflow $g\left(\frac{x}{x_0}, u_0\right)$ from a threshold type reservoir with normalized content $\frac{x}{x_0}$ and input u_0 .

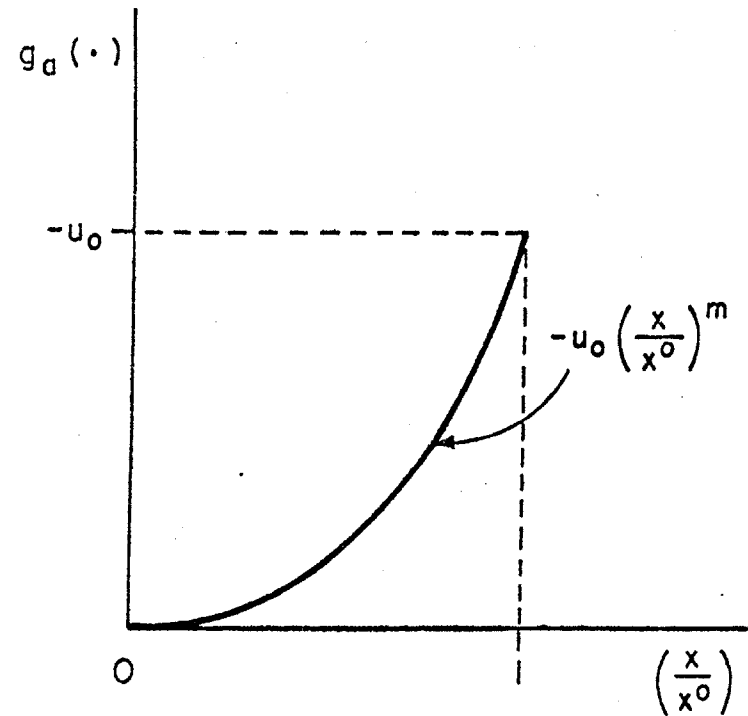


FIGURE 6.1b
 Outflow $g_a\left(\frac{x}{x_0}, x_0\right)$ from a nonlinear reservoir of exponent m , with normalized content $\left(\frac{x}{x_0}\right)$ and input u_0 .

Portion allocated to primary storage: $(C_2 \cdot \frac{x_5}{x_5^0} - 1) \cdot \frac{x_4}{x_4^0} + 1$

Portion allocated to secondary storage: $(1 - C_2 \cdot \frac{x_5}{x_5^0}) \cdot \frac{x_4}{x_4^0}$

with C_2 defined by,

$$C_2 = \frac{d'_l \cdot x_4^0}{d'_l \cdot x_4^0 + d''_l \cdot x_5^0} \quad (6.4)$$

Table 6.1 is a list of symbols used in the soil moisture accounting equations together with their description. It is mostly based on the notation introduced by TASC (1980) (see also Kitanidis and Bras, 1980a).

A difference between the present formulation and the one published in Kitanidis and Bras (1980a) is that the equations to follow include the surface runoff outflow from the additional impervious area. In this aspect the present formulation agrees with the one in Georgakakos, Restrepo-Posada and Bras (1980). Depending on the hydro-geomorphologic characteristics of the basin under study, this component of outflow may or may not be significant.

Table 6.1

SOIL MOISTURE ACCOUNTING MODEL VARIABLES

<u>Symbol</u>	<u>Description</u>
	<u>States:</u>
x ₁	upper zone tension water content [MM]
x ₂	upper zone free water content [MM].
x ₃	lower zone tension water content [MM].
x ₄	lower zone primary free water content [MM].
x ₅	lower zone secondary free water content, [MM].
x ₆	additional impervious storage [MM].
	<u>Inputs:</u>
u _e	instantaneous evapotranspiration demand [MM/HOUR].
	<u>Parameters:</u>
x ₁ ⁰	upper zone tension water capacity [MM].
x ₂ ⁰	upper zone free water capacity [MM].
x ₃ ⁰	lower zone tension water capacity [MM].
x ₄ ⁰	lower zone primary free water capacity [MM].
x ₅ ⁰	lower zone secondary free water capacity [MM].
d _u	upper zone instantaneous drainage coefficient [1/HOURS].
d'	lower zone primary instantaneous drainage coefficient [1/HOURS].
d''	lower zone secondary instantaneous drainage coefficient [1/HOURS].

Table 6.1 (continued)

<u>Symbol</u>	<u>Description</u>
ϵ	parameter in percolation function
θ	exponent in percolation function
P_f	fraction of percolated water assigned to the lower zone free water aquifers
μ	fraction of base flow not appearing in river flow
β_1	fraction of basin that becomes impervious when tension water requirements are met
β_2	fraction of basin permanently impervious
m_1	exponent of the upper zone tension water nonlinear reservoir
m_2	exponent of the upper zone free water nonlinear reservoir
m_3	exponent of the lower zone tension water nonlinear reservoir

To facilitate notation define the quantities y and C_1 as

$$y = 1 - \frac{x_3 + x_4 + x_5}{x_3^0 + x_4^0 + x_5^0} \quad (6.5)$$

and

$$C_1 = d'_l \cdot x_4^0 + d''_l \cdot x_5^0 \quad (6.6)$$

The applicable differential equations are then:

Upper zone tension water element:

$$\frac{dx_1}{dt} = \left[1 - \left(\frac{x_1}{x_1^0} \right)^{m_1} \right] \cdot \phi \cdot X - u_e \frac{x_1}{x_1^0} \quad (6.7)$$

Upper zone free water element:

$$\begin{aligned} \frac{dx_2}{dt} = & \left(\frac{x_1}{x_1^0} \right)^{m_1} \cdot \phi \cdot X \cdot \left[1 - \left(\frac{x_2}{x_2^0} \right)^{m_2} \right] - d_u \cdot x_2 - \\ & - C_1 \cdot (1 + \epsilon \cdot y^\theta) \cdot \frac{x_2}{x_2^0} \end{aligned} \quad (6.8)$$

Lower zone tension water element:

$$\begin{aligned} \frac{dx_3}{dt} = & C_1 \cdot (1 + \varepsilon \cdot y^\theta) \cdot \frac{x_2}{x_2^o} \cdot (1 - P_f) \left[1 - \left(\frac{x_3}{x_3^o} \right)^{m_3} \right] - \\ & - u_e \left(1 - \frac{x_1}{x_1^o} \right) \cdot \frac{x_3}{x_1^o + x_3^o} \end{aligned} \quad (6.9)$$

Lower zone primary water element:

$$\begin{aligned} \frac{dx_4}{dt} = & -d'_\ell \cdot x_4 + C_1 \cdot (1 + \varepsilon y^\theta) \cdot \frac{x_2}{x_2^o} \cdot [1 - (1 - P_f) \cdot [1 - \left(\frac{x_3}{x_3^o} \right)^{m_3}]] \\ & \cdot \left[\left(C_2 \cdot \frac{x_5}{x_5^o} - 1 \right) \cdot \frac{x_4}{x_4^o} + 1 \right] \end{aligned} \quad (6.10)$$

Lower zone secondary water element:

$$\begin{aligned} \frac{dx_5}{dt} = & -d''_\ell \cdot x_5 + C_1 \cdot (1 + \varepsilon y^\theta) \cdot \frac{x_2}{x_2^o} [1 - (1 - P_f) \cdot [1 - \left(\frac{x_3}{x_3^o} \right)^{m_3}]] \cdot \\ & \cdot \left(1 - C_2 \cdot \frac{x_5}{x_5^o} \right) \cdot \frac{x_4}{x_4^o} \end{aligned} \quad (6.11)$$

Additional impervious area water element:

$$\begin{aligned} \frac{dx_6}{dt} = & \left[1 - \left(\frac{x_6 - x_1}{x_3^o} \right)^2 \cdot \left(\frac{x_1}{x_1^o} \right)^{m_1} \right] \cdot \phi \cdot X - u_e \left(1 - \frac{x_1}{x_1^o} \right) \cdot \left(\frac{x_6 - x_1}{x_3^o + x_1^o} \right) - \\ & - u_e \cdot \frac{x_1}{x_1^o} - \left[1 - \left(\frac{x_6 - x_1}{x_3^o} \right)^2 \right] \cdot \left(\frac{x_2}{x_2^o} \right)^{m_2} \cdot \left(\frac{x_1}{x_1^o} \right)^{m_1} \cdot \phi \cdot X \end{aligned} \quad (6.12)$$

The output u_c from the soil moisture accounting model, referred to as total channel inflow per unit time, is given by,

$$\begin{aligned}
 u_c = & (d_u \cdot x_2 + \frac{d'_l \cdot x_4 + d''_l \cdot x_5}{1 + \mu}) \cdot (1 - \beta_1 - \beta_2) + \\
 & + \phi \cdot X \cdot \beta_2 + (\frac{x_6 - x_1}{x_3^o})^2 \cdot \phi \cdot X \cdot (\frac{x_1}{x_1^o})^{m_1} \cdot \beta_1 + \\
 & + \phi \cdot X \cdot (\frac{x_1}{x_1^o})^{m_1} \cdot (\frac{x_2}{x_2^o})^{m_2} \cdot (1 - \beta_1 - \beta_2) + \\
 & + [1 - (\frac{x_6 - x_1}{x_3^o})^2] \cdot (\frac{x_2}{x_2^o})^{m_2} \cdot (\frac{x_1}{x_1^o})^{m_1} \cdot \phi \cdot X \cdot \beta_1 \quad (6.13)
 \end{aligned}$$

The following constraints determine the definition domain of the state variables x_i^o .

$$0 \leq x_i \leq x_i^o; \quad i = 1, 2, \dots, 5 \quad (6.14)$$

It should be noted that Eqs. (6.7) and (6.8) are mathematical approximations in that the nonlinear reservoir outflow does not depend on the current net input, but rather on the non-negative portion of it. This

may result, for example, in a situation where the filled upper zone tension water element will be depleted by evapotranspiration even though the current precipitation rate might be greater than the actual evapotranspiration rate. Given, however, the small time increments in which the integration of the differential equations will proceed, the error introduced will be well within the overall model structure errors.

6.3 Equations for Channel Routing

Georgakakos and Bras (1982) presented a conceptual, nonlinear reservoir-type channel routing model, which when tested with the soil moisture accounting scheme of the NWSRFS, showed improved performance over linear black-box type models. Their model is simple to implement on a digital computer and it does not require high quality and quantity input data, as the models based on the full momentum and continuity equation do.

The idea is to represent the channel as a collection of n reservoirs in series. Let $S_i(t)$ be the volume of water in storage at the i^{th} reservoir and $u_c(t)$ the total channel inflow per unit time (for example, the output of the soil moisture accounting scheme presented in Section 6.2). Then for a headwater basin with no upstream inflows, the model differential equations are

$$\frac{d S_i(t)}{dt} = P_i u_c(t) + a_{i-1} S_{i-1}^m(t) - a_i S_i^m(t); \quad i=0,1,\dots,n \quad (6.15)$$

$$a_0 \triangleq 0$$

and the instantaneous discharge $Q_n(t)$ at the basin outlet is given by:

$$Q_n(t) = a_n \cdot S_n^m(t) \quad (6.16)$$

Parameters of the model are: $p_i, a_i, i=1,2,\dots,n, m$ and n . Georgakakos and Bras (1980) give the details of model formulation as well as ways of estimating model parameters from 1) the basin observable hydro-morphologic characteristic, and 2) input-output time series data.

6.4 Rainfall-Runoff Model

The differential equations of Chapter 5 for the station precipitation model together with the equations of Sections 6.2 and 6.3 of this chapter constitute a general rainfall-runoff model. Based on the current and local moisture content states of the atmosphere, soil and channel, and on forecasts of the meteorological variables T_o, T_d, p_o and u_e (evapotranspiration potential), the model equations are capable of producing rainfall and runoff forecasts for the basin of interest.

The general model equations are presented next, for a headwater basin (with no upstream inflows). It is assumed that the basin is characterized by one set of forecasts T_o, p_o, T_d and u_e at each time. Present day operational atmospheric models with spatial scales of grid sizes 200km and greater, render this assumption reasonable.

The rainfall-runoff model equations, in the notation of Table 6.2, are:

$$\frac{d}{dt} (\underline{x}_p) = f_p(\underline{x}_p, \underline{u}; \underline{a}_p) \quad (6.17)$$

$$\frac{d}{dt} (\underline{x}_s) = f_s(\underline{x}_p, \underline{x}_s, \underline{u}, u_e; \underline{a}_p, \underline{a}_s) \quad (6.18)$$

$$\frac{d}{dt} (\underline{x}_c) = f_c(\underline{x}_p, \underline{x}_s, \underline{x}_c, \underline{u}, u_e; \underline{a}_p, \underline{a}_s, \underline{a}_c) \quad (6.19)$$

The concurrent precipitation and basin-outlet discharge rates are the instantaneous model outputs, given by

$$z_p = h_p(\underline{x}_p, \underline{u}; \underline{a}_p) \quad (6.20)$$

$$z_c = h_c(\underline{x}_c; \underline{a}_c) \quad (6.21)$$

Current observation networks give measurements of the instantaneous discharge rate z_c . However, the accumulated precipitation volume z_p^V over a time interval Δt is sampled instead of the instantaneous rate z_p . Given the time-discrete nature of the input forecasts, Eq. (6.20) is utilized, with the instantaneous rate z_p related to the volume z_p^V by

Table 6.2

HEADWATER BASIN RAINFALL-RUNOFF MODEL SYMBOLS

<u>Symbol</u>	<u>Description</u>
	<u>Functions:</u>
$f_p(\cdot)$	Function to represent the right hand side of Eq. (5.32)
$\underline{f}_s(\cdot)$	Vector function whose i^{th} component represents the right hand side of the differential equation for x_i ($i=1,2,\dots,6$) in Section 6.2.
$\underline{f}_c(\cdot)$	Vector function whose i^{th} component represents the right hand side of the differential equation for S_i ($i=1,2,\dots,n$) in Section 6.3.
$h_p(\cdot)$	Function to represent the right hand side of Eq. (6.3).
$h_c(\cdot)$	Function to represent the right hand side of Eq. (6.16).
	<u>States:</u>
x_p	Precipitation model state
\underline{x}_s	Vector of the soil moisture accounting model states.
\underline{x}_c	Vector of channel states
	<u>Input:</u>
\underline{u}	Precipitation model input: T_o, P_o, T_d
u_e	Potential evapotranspiration rate.
	<u>Parameters:</u>
\underline{a}_p	Vector of precipitation model storm invariant parameters.
\underline{a}_s	Soil model parameters.
\underline{a}_c	Channel routing model parameters.

Table 6.2 (continued)

<u>Symbol</u>	<u>Description</u>
	<u>Output:</u>
z_p	Precipitation rate per unit area in the drainage basin.
z_c	Discharge rate at the drainage basin outlet.

$$z_p = \frac{v}{\Delta t} \quad (6.22)$$

Equations (6.20) and (6.21) are valid for discrete times t , $t+\Delta t$, $t+2\Delta t$, ..., $t+k\cdot\Delta t$.

The relevant equations for a large river basin with several tributary-basins are given in Appendix C.

6.5 Precipitation, Soil and Channel Models Coupling

The previous formulation presents the coupling of the equations corresponding to three different models of the storm-basin system. Thus, consideration of the set of Eqs. (6.17) through (6.19), shows that the state of the precipitation model, x_p , directly affects the equations of time-evolution of the soil states, x_s . Both x_p and x_s affect the channel states differential equation (Eq. (6.19)). Coupling is due to the enforcement of the conservation of water-mass (or volume) law at the boundaries of each model. Note, however, that it is a one-way coupling. That is, the states of the channel or the soil models do not affect the precipitation state. Therefore, information on those states cannot be passed, with the present deterministic formulation, to the precipitation model. It is this open link in the overall rainfall-runoff model that modern estimation theory techniques close, using observations on all the model outputs (Eqs. (6.20), (6.21)). Statistical filters will effectively couple the state variables of the soil and channel models with those of the precipitation one. This is a different coupling than the one due to the

conservation of water-mass law. The effect that each state variable has on the overall storm-basin model outputs, is monitored through the filter equations. Each state variable is updated, from the system observations, based on the degree of its correlation to the model outputs and to the rest of the model variables. In this way, the errors in predicting the discharge at the catchment outlet have a bearing on the specification of the initial conditions of the precipitation model variables. Similarly, observations of the precipitation state variables and parameters have an effect on the determination of the drainage basin related state variables. This assures co-ordination in the operation of the coupled storm and basin models in real-time. Chapter 7 develops the formulation of the stochastic rainfall-runoff model in a linear statistical filter framework.

6.6 The Spatial and Temporal Scales of the Rainfall-Runoff Model Components

The specification of the applicable scales of a mathematical model and of its inputs is of primary importance in the determination of the maximum forecast lead time and maximum forecast area up to which reliable forecasts can be expected. In many cases, effective model simplification results by comparison of the scales of its components. For example, components with small time or space constants compared to those of the overall system, can be substituted by their time or space average behavior. The model input scale specification, in addition, determines the spatial and temporal averaging that the observations of the input variables have to undergo before they are suitable for use with a particular model.

If the equation describing the evolution of a system state x in time or space ω , with no external inputs, is

$$\frac{dx(\omega)}{d\omega} = - \frac{1}{\omega_0} x(\omega) \quad (6.23)$$

with ω_0 a positive constant and with initial condition x_0 , the scale of the $x(\omega)$ variations in the time or space ω is ω_0 .

It is very seldom, however, that physically based hydrologic models have the form of Eq. (6.23). They usually are nonlinear differential equations both in the system state $x(\omega)$ and in the external inputs. Therefore, the concept of scale, as defined in Eq. (6.23) is not directly applicable. An estimate of the system scale can result from linearization about a nominal trajectory $x^0(\omega)$. Then, ω_0 is the inverse of the coefficient of linearization and it is a variable dependent both on the nominal $x^0(\omega)$ and on the system inputs. In this case the range of possible ω_0 can be obtained based on representative values of $x^0(\omega)$ and on the range of possible inputs.

The characteristic spatial scales of the precipitation model have been given in Chapter 2. The horizontal scale depends on the characteristics of the storm movement and on the discretization interval of the meteorological T_0 , p_0 , T_d input observations. This scale is bounded above by the horizontal storm scale given in Table 6.3 (Holton, 1979) for different types of storms. In the same table, additional spatial scales of atmospheric motions are included for comparison. The vertical

Table 6.3

SPATIAL SCALES OF ATMOSPHERIC MOTIONS
(After Holton, 1979)

<u>Type of Motion</u>	<u>Horizontal Scale [M]</u>
Molecular mean free path	10^{-7}
Minute turbulent eddies	10^{-2} to 10^{-1}
Small eddies	10^{-1} to 1
Dust devils	1 to 10
Gusts	10 to 100
Tornadoes	10^2
Cumulonimbus clouds	10^3
Fronts, squall lines	10^4 to 10^5
Hurricanes	10^5
Synoptic cyclones	10^6
Planetary waves	10^7

precipitation model scale is equal to the average storm clouds depth during the storm passage. They range from 4-5 [KM] to more than 10 [KM] for the most vigorous storms.

An estimate of the response time of the precipitation model is given by the inverse of the function $h(\underline{u}, \underline{a}_0)$ given in Eq. (5.26). Neglecting the small (see discussion of Figure 5.1) cloud top contribution, the response time estimate, τ_p , is given by

$$\tau_p = \frac{Z_c \cdot \delta}{v_p} : \left[\frac{1 + \frac{3}{4} N_v + \frac{N_v^2}{4} + \frac{N_v^3}{24}}{e^{N_v}} \right]^{-1} \quad (6.24)$$

For $\frac{1}{c}$ of the order 10^{-1} [MM] at cloud base and for a Z_c of about 6 [KM] (at the 500 (MBAR) level), Eq. (6.24) gives ($\delta = 1$),

$$\tau_p = 1.2 \cdot \left[\frac{1 + \frac{3}{4} N_v + \frac{N_v^2}{4} + \frac{N_v^3}{24}}{e^{N_v}} \right]^{-1}$$

Thus, τ_p ranges from a value of about 1 [HOUR] during intense precipitation activity (low updraft, $N_v = 0$, at the cloud base due to the existence of downdrafts), to a value of about 10 [HOURS] for a strong average updraft of 2 [M/SEC] at cloud base.

The horizontal scale of the soil model components is equal to the scale length L_B of the drainage basin. Thus, if the basin area is denoted by A ,

$$L_B = \sqrt{A} \quad (6.25)$$

For $A = 10^3 [\text{KM}^2]$, $L_B = 31 [\text{KM}]$.

The vertical scale of the soil model extends from the soil surface down to the bottom of the groundwater aquifers and is of order $10^2 [\text{M}]$.

The time constants of each one of the soil models of Section 6.2, with respect to their contribution to the channel input u_c , range from near zero (e.g., the rainfall on impervious areas is instantaneously routed downstream) to a maximum equal to the inverse of the linear coefficient of the lower zone primary water element (order of 10^2 days).

The horizontal channel routing model scale is equal to the channel length, L_c , given by, Eagleson, (1970),

$$L_c [\text{MILES}] = 1.40 \{ A [\text{MILES}^2] \}^{0.568} \quad (6.26)$$

with A the catchment area. For $A = 10^3 [\text{KM}^2]$, $L_c = 70 [\text{KM}]$. The vertical channel scale ranges from a few meters for the first order streams to several tens of meters for the highest order streams.

The response time of the channel routing model of Section 6.3 is the sum of the time constants τ_{c_i} of its nonlinear reservoirs. To a first

order approximation, τ_{c_i} is given by

$$\tau_{c_i} = \frac{1}{m \cdot a_i \cdot S_i^o(m-1)} \quad (6.27)$$

with S_i^o a nominal value for the state S_i . Using $n=3$, $m=0.8$, $a_i = 10^{-3} [M^3(1-m)/SEC]$ (Georgakakos and Bras, 1982) and for a nominal outflow discharge equal to $100 [M^3/SEC]$, use of an Eq. (6.16)-type relationship gives $S_i^o = 2 \times 10^6 [M^3]$. Then, Eq. (6.27) results in a value of τ_{c_i} of the order of 6[HOURS].

Table 6.4 summarizes the rainfall-runoff model component spatial and temporal scales estimates for a typical drainage basin of area $10^3 [KM^2]$.

The meteorological storm input, T_o , p_o , and T_d , scales should be comparable to the precipitation model ones. The evapotranspiration potential spatial scale should be the characteristic length of the basin, while the corresponding time constant is of the order of 1 day (equal to the period of the radiation forcing).

Table 6.4

SPATIAL AND TEMPORAL SCALES OF RAINFALL-RUNOFF MODEL COMPONENTS

<u>Description</u>	<u>Horizontal Scale</u>	<u>Vertical Scale</u>	<u>Temporal Scale</u>
Precipitation Model:	1 - 10 ² [KM]	1 - 10[KM]	1 - 10 [HOURS]
Soil Model Components:	10 - 10 ² [KM]	1 - 10 ² [M]	0 - 10 ² [DAYS]
Channel Model Components:	10 - 10 ² [KM]	1 - 10 [M]	1 - 10 [HOURS]

THE STOCHASTIC RAINFALL-RUNOFF MODEL7.1 Introduction

It is well-established that the use of modern estimation theory techniques to process system output observations improves the performance of the hydrologic deterministic models (e.g., Kitanidis and Bras, 1980b, Georgakakos and Bras, 1982). In addition, techniques to handle the nonlinearities present in the physical hydrologic systems, which are not directly amenable to estimation theory processing, have been successfully used with conceptual models in real world applications. The extended Kalman filter (Gelb, 1974) and a Gaussian filter based on statistical linearization (Georgakakos and Bras, 1982) depend on the linearization of the system nonlinear function. The first uses a Taylor's series expansion about the current best estimate of the system states, keeping the linear terms in the series. The latter develops generalized least squares linear approximations to nonlinear functions of the states. Both assume implicitly or explicitly Gaussian probability distributions for the system states. The first is easier to derive and implement, especially for multidimensional functions. The second, however, has the advantage of producing unbiased estimates, if the underlying probability distribution is known.

A general linear filter formulation is presented in the next section. The formulation accommodates both the extended Kalman filter and the one based on statistical linearization. Section 7.3 gives the linearized equations for the station precipitation, the soil moisture accounting and the channel routing models. As a first step towards the development of a stochastic hydrologic system, the simpler linearization procedure (by Taylor's series expansion) is used for the precipitation and soil models. The formulation of Georgakakos and Bras (1982) is given for the channel routing model, where statistical linearization is used. Throughout the development it is assumed that the meteorological input and the potential evapotranspiration are Gaussian random processes with known first and second moments.

7.2 General Linear Filter for Nonlinear System Equations with Random Inputs

It is assumed that the system random variables are approximately Gaussian. Further, it is assumed that the system vector state obeys a first order differential equation while observations of the system vector output are available in discrete time.

The system dynamics equation is written as:

$$\frac{dx(t)}{dt} = F(x(t), u(t), t) + w(t) \quad (7.1)$$

and the observation equation as:

$$\underline{z}(t_k) = \underline{G}(\underline{x}(t_k), \underline{u}(t_k), t_k) + \underline{v}(t_k) \quad ; \quad k = 1, 2, 3 \dots \quad (7.2)$$

where:

- $\underline{x}(t)$: vector state at time t , $(n \cdot 1)$
- $\underline{u}(t)$: vector of random inputs to the system which are uncorrelated to the state and noises, $(p \cdot 1)$
Note that $\underline{u}(t)$ includes the evapotranspiration potential.
- $\underline{z}(t_k)$: vector of observations of the system output, $(m \cdot 1)$
- t_k : discrete time
- $\underline{F}(\cdot)$: nonlinear vector function, $(n \cdot 1)$
- $\underline{G}(\cdot)$: nonlinear vector function, $(m \cdot 1)$
- $\underline{w}(t)$: a continuous time white noise process of mean zero and covariance parameter (time varying spectral density) $\overline{Q}(t)$
- $\underline{v}(t_k)$: a discrete time white noise sequence with covariance matrix $\overline{R}(t_k)$ and mean zero

$$E \{ \underline{w}(t) \cdot \underline{w}^T(\tau) \} = \overline{Q}(t) \cdot \delta(t-\tau) \quad (7.3)$$

$$E \{ \underline{v}(t_k) \cdot \underline{v}^T(t_j) \} = \underline{R}(t_k) \cdot \delta_{kj} \quad (7.4)$$

δ_{kj} : the Kronecker's delta, nonzero at $k=j$ where it takes the value 1

$\delta(t)$: the Dirac Delta function being zero everywhere except at $t=0$ where it becomes infinite

$E\{\cdot\}$: the expectation operator

In general one needs a prediction estimate (to be used for the hydrologic forecast) $\hat{\underline{x}}(t|t_k)$ with associated covariance matrix $\underline{\Sigma}(t|t_k)$, for times after the observation time t_k and before the one at time t_{k+1} . A so-called filtered estimate $\hat{\underline{x}}(t_{k+1}|t_{k+1})$ is obtained at time t_{k+1} when the new observation becomes available. The associated covariance matrix is denoted by $\underline{\Sigma}(t_{k+1}|t_{k+1})$. The current mean of $\underline{x}(t)$ is obtained from:

$$\hat{\underline{x}}(t) = E \{ \underline{x}(t) \} \quad (7.5)$$

where depending on the available measurements, the expectation is over the appropriate conditional density. Also:

$$\underline{\Sigma}(t) = E \{ (\underline{x}(t) - \hat{\underline{x}}(t)) (\underline{x}(t) - \hat{\underline{x}}(t))^T \} \quad (7.6)$$

with the same convention for the expectation operator.

The filter equations are given in recursive form and require initial conditions both for the state estimate and for the state covariance. Set:

$$\hat{\underline{x}}(t_0|t_0) = \underline{x}_0 \quad (7.7)$$

$$\bar{\Sigma}(t_0|t_0) = \bar{\Sigma}_0 \quad (7.8)$$

It is also assumed that the system noises $\underline{w}(t)$ and $\underline{v}(t_k)$ have known second moment matrices $\bar{Q}(t)$ and $\bar{R}(t_k)$. Also, the mean vector and the covariance parameter matrix of the continuous input vector are denoted by $\hat{\underline{u}}(t)$ and $\bar{Q}_u(t)$, respectively.

In order to use the powerful linear filter developed by Kalman and Bucy (1961), one needs linear system equations. In the following, a general linear representation of the system is assumed and the filter equations are derived based on it. Then, reference to the ordinary linearization and to statistical linearization is made and the associated linear coefficients and constants are given.

Let a general linear representation of $F(\cdot)$ and $G(\cdot)$ be:

$$\begin{aligned} \underline{F}(\underline{x}(t), \underline{u}(t), t) &= \underline{F}_0(\underline{d}_{\underline{x}(t)}, \underline{d}_{\underline{u}(t)}, t) \\ &+ \bar{N}_F(\underline{d}_{\underline{x}(t)}, \underline{d}_{\underline{u}(t)}, t) (\underline{x}(t) - \hat{\underline{x}}(t)) \\ &+ \bar{M}_F(\underline{d}_{\underline{x}(t)}, \underline{d}_{\underline{u}(t)}, t) (\underline{u}(t) - \hat{\underline{u}}(t)) \end{aligned} \quad (7.9)$$

and

$$\begin{aligned}
\underline{G}(\underline{x}(t_k), \underline{u}(t_k), t_k) &= \underline{G}_0(\underline{d}_{\underline{x}}(t_k), \underline{d}_{\underline{u}}(t_k), t_k) \\
&+ \overline{\underline{N}}_G(\underline{d}_{\underline{x}}(t_k), \underline{d}_{\underline{u}}(t_k), t_k) (\underline{x}(t_k) - \hat{\underline{x}}(t_k)) \\
&+ \overline{\underline{M}}_G(\underline{d}_{\underline{x}}(t_k), \underline{d}_{\underline{u}}(t_k), t_k) (\underline{u}(t_k) - \hat{\underline{u}}(t_k))
\end{aligned} \tag{7.10}$$

where $\underline{d}_{\underline{x}}(t)$, $\underline{d}_{\underline{u}}(t)$ represent the vectors of the parameters of the probability contributions of the random processes $\underline{x}(t)$ and $\underline{u}(t)$, respectively, at time t . For instance, for ordinary Taylor's series expansion $\underline{d}_{\underline{x}}(t)$, $\underline{d}_{\underline{u}}(t)$ will be the mean vectors $\hat{\underline{x}}(t)$ and $\hat{\underline{u}}(t)$. In statistical linearization and for Gaussian distributions they will include the elements of the respective second moment matrices, provided they exist. For statistical linearization with non-Gaussian distributions, higher order moments will be added to the vectors $\underline{d}_{\underline{x}}(t)$ and $\underline{d}_{\underline{u}}(t)$. Depending on the kind of linearization procedure, different expressions for the vectors $\underline{F}_0(\cdot)$, $\underline{G}_0(\cdot)$ and the matrices $\overline{\underline{N}}_F(\cdot)$, $\overline{\underline{M}}_F(\cdot)$, $\overline{\underline{N}}_G(\cdot)$, $\overline{\underline{M}}_G(\cdot)$ will result. Later in this section, expressions for those quantities are derived for Taylor's linearization and statistical linearization.

At this point, one should distinguish between the continuous process $\underline{u}(t)$ and its discrete counter part $\underline{u}(t_k)$. Even though they are both uncorrelated in time they have, in general, different means and covariance matrices. The mean of $\underline{u}(t)$ can be obtained at each time t with $t_k \leq t \leq t_{k+1}$, $\forall k$, from:

$$\hat{\underline{u}}(t) = \hat{\underline{u}}(t_k) + \left(\frac{t - t_k}{t_{k+1} - t_k} \right) (\hat{\underline{u}}(t_{k+1}) - \hat{\underline{u}}(t_k)) \quad (7.11)$$

where $\hat{\underline{u}}(t_k)$, $\hat{\underline{u}}(t_{k+1})$ are equal to the mean vectors of the time-discrete process \underline{u} . In the case of the rainfall runoff model presented they will be meteorological forecasts of \underline{u} at times t_k and t_{k+1} . Note that Eq. (7.11) expresses a linear interpolation between $\hat{\underline{u}}(t_k)$, $\hat{\underline{u}}(t_{k+1})$ for times t in the interval $[t_k, t_{k+1}]$.

It is assumed that $(\underline{u}(t) - \hat{\underline{u}}(t))$ is a continuous white noise with covariance parameter $\overline{\underline{Q}}_u(t)$. If the corresponding discrete time covariance matrix is $\overline{\underline{Q}}_u(t_k)$, then (Gelb, 1974):

$$\overline{\underline{Q}}_u(t) \cong \Delta t \cdot \overline{\underline{Q}}_u(t_k) \quad (7.12)$$

with $\Delta t = t_{k+1} - t_k$, assumed constant.

Note that by making the assumption of no time correlation for $\underline{u}(t_k)$, one is assuming that one obtains the mean vector $\hat{\underline{u}}(t_k)$ by a forecast procedure with time-uncorrelated prediction residuals.

Since most of the meteorological forecasts of temperature and pressure are based on linear regressions, (i.e., Multiple Output Statistics Model) the assumption is reasonable for the case of the rainfall-runoff model of the previous chapter.

Due to the assumption of no correlation between the input and the system states, the terms:

$$\underline{W}(t) = \overline{M}_F(d_{\underline{x}(t)}, d_{\underline{u}(t)}, t) (\underline{u}(t) - \hat{\underline{u}}(t)) + \underline{w}(t) \quad (7.13)$$

and

$$\underline{V}(t_k) = \overline{M}_G(d_{\underline{x}(t_k)}, d_{\underline{u}(t_k)}, t_k) (\underline{u}(t_k) - \hat{\underline{u}}(t_k)) + \underline{v}(t_k) \quad (7.14)$$

are white noises, with zero means and second moments defined by:

$$\begin{aligned} E \{ \underline{W}(t) \cdot \underline{W}^T(\tau) \} &= \{ \overline{M}_F(d_{\underline{x}(t)}, d_{\underline{u}(t)}, t) \cdot \underline{Q}_u(t) \\ &\quad \cdot \overline{M}_F^T(d_{\underline{x}(t)}, d_{\underline{u}(t)}, t) + \overline{Q}(t) \} \cdot \delta(t-\tau) \\ &= \underline{Q}'(t) \cdot \delta(t-\tau) \end{aligned} \quad (7.15)$$

and

$$\begin{aligned}
E \{ \underline{V}(t_k) \cdot \underline{V}^T(t_j) \} &= [\bar{M}_G(\underline{d}_x(t_k), \underline{d}_u(t_k), t_k) \cdot \bar{Q}_u(t_k) \\
&\cdot \bar{M}_G^T(\underline{d}_x(t_k), \underline{d}_u(t_k), t_k) + \bar{R}(t_k)] \cdot \delta_{kj} \\
&= \bar{R}'(t_k) \cdot \delta_{kj}
\end{aligned} \tag{7.16}$$

In addition, since $\underline{u}(t)$, $\underline{w}(t)$, $\underline{v}(t_k)$ have been assumed Gaussian for all times, linear combinations of them, like $\underline{W}(t)$ or $\underline{V}(t_k)$, are also Gaussian.

The filter equations for the interval $[t_k, t_{k+1}]$ then take the form:

Linear Filter Equations:

State Estimate Propagation

$$\frac{d(\hat{\underline{x}}(t|t_k))}{dt} = \underline{F}_0(\underline{d}_x(t|t_k), \underline{d}_u(t), t) ; t \in [t_k, t_{k+1}] \tag{7.17}$$

Error Covariance Propagation

$$\begin{aligned}
\frac{d(\bar{\Sigma}(t|t_k))}{dt} &= \bar{N}_F(t|t_k) \bar{\Sigma}(t|t_k) + \bar{\Sigma}(t|t_k) \cdot \bar{N}_F^T(t|t_k) \\
&+ \bar{Q}'(t|t_k) ; t \in [t_k, t_{k+1}]
\end{aligned} \tag{7.18}$$

State Estimate Update

$$\hat{\underline{x}}(t_{k+1}|t_{k+1}) = \hat{\underline{x}}(t_{k+1}|t_k) + \bar{\underline{K}}(t_{k+1}) \cdot (\underline{z}(t_{k+1}) - \underline{G}_0(\frac{d}{dt}\underline{x}(t_{k+1}), \frac{d}{dt}\underline{u}(t_{k+1}), t_{k+1})) \quad (7.19)$$

Error Covariance Update

$$\begin{aligned} \bar{\underline{\Sigma}}(t_{k+1}|t_{k+1}) &= [\bar{\underline{I}} - \bar{\underline{K}}(t_{k+1}) \cdot \bar{\underline{N}}_G(t_{k+1}|t_k)] \cdot \bar{\underline{\Sigma}}(t_{k+1}|t_k) \\ &\cdot [\bar{\underline{I}} - \bar{\underline{K}}(t_{k+1}) \cdot \bar{\underline{N}}_G(t_{k+1}|t_k)]^T + \bar{\underline{K}}(t_{k+1}) \cdot \bar{\underline{R}}'(t_{k+1}) \cdot \bar{\underline{K}}^T(t_{k+1}) \end{aligned} \quad (7.20)$$

Filter Gain

$$\begin{aligned} \bar{\underline{K}}(t_{k+1}) &= \bar{\underline{\Sigma}}(t_{k+1}|t_k) \cdot \bar{\underline{N}}_G^T(t_{k+1}|t_k) \\ &\cdot [\bar{\underline{N}}_G(t_{k+1}|t_k) \cdot \bar{\underline{\Sigma}}(t_{k+1}|t_k) \cdot \bar{\underline{N}}_G^T(t_{k+1}|t_k) + \bar{\underline{R}}'(t_{k+1})]^{-1} \end{aligned} \quad (7.21)$$

where $\bar{\underline{I}}$ is the $n \cdot n$ unit matrix.

With the initial conditions of Eqs. (7.7) and (7.8) the set of Eqs. (7.17) through (7.21) is solved recursively in time, until

all available observations have been processed.

The following are some comments regarding the filter equations.

1. Due to the dependency of $\underline{F}_0(\cdot)$ and $\overline{\underline{N}}_F(\cdot)$ on the best available estimate of the system state, Eqs. (7.17) and (7.18) are coupled differential equations.
2. Care should be exercised to prevent the covariance matrix $\overline{\underline{\Sigma}}(t|t_k)$ from becoming negative at the propagation step. Positive definiteness should be enforced.
3. To ensure the positive definiteness of $\overline{\underline{\Sigma}}(t_{k+1}|t_{k+1})$, Eq. (7.20) is used, rather than the simpler expression:

$$\overline{\underline{\Sigma}}(t_{k+1}|t_{k+1}) = [\overline{\underline{I}} - \overline{\underline{K}}(t_{k+1}) \cdot \overline{\underline{N}}_G(t_{k+1}|t_k)] \cdot \overline{\underline{\Sigma}}(t_{k+1}|t_k) \quad (7.22)$$

4. The linearization vectors $\underline{F}_0(\cdot)$, $\underline{G}_0(\cdot)$ and matrices $\overline{\underline{N}}_F(\cdot)$, $\overline{\underline{N}}_G(\cdot)$ always use the parameter of the current probability distribution for the vector $\underline{x}(t)$. This is made explicit through the notation.
5. The vector $\underline{v}(t_{k+1})$ defined by:

$$\underline{v}(t_{k+1}) = \underline{z}(t_{k+1}) - \underline{G}_0(\underline{d}_{\underline{x}}(t_{k+1}), \underline{d}_{\underline{u}}(t_{k+1}), t_{k+1}) \quad (7.23)$$

is called the innovations sequence vector. Under optimal filter performance with correct noise statistics,

it is an uncorrelated sequence of zero mean Gaussian variables with variance $\bar{Q}_v(t_{k+1})$ given by:

$$\bar{Q}_v(t_{k+1}) = \bar{N}_G(t_{k+1} | t_k) \cdot \sum_{-} (t_{k+1} | t_k) \cdot \bar{N}_G^T(t_{k+1} | t_k) + \bar{R}'(t_{k+1}) \quad (7.24)$$

Comparison of the statistical properties of the residuals of the type in the right-hand side of Eq. (7.23) during actual filter operation, with the theoretical properties of the innovations sequence, just described, is used to make assessments about the optimality of the filter performance. Note that the inverse of the expression in Eq. (7.24) appears in Eq. (7.21).

6. The number of basic calculations necessary to compute the state mean and error covariance varies as: n^3 .

In the following, expressions for the vectors $\underline{F}_0(\cdot)$, $\underline{G}_0(\cdot)$ and for the matrices $\bar{N}_F(\cdot)$, $\bar{M}_F(\cdot)$, $\bar{N}_G(\cdot)$, $\bar{M}_G(\cdot)$ are presented for the following linearization procedures: 1) linear Taylor's series expansion, and 2) statistical linearization.

7.2.1 Linear Taylor's Series Expansion

The idea is to expand the nonlinear functions about the current best estimates of the relevant random variables and then keep the first two terms in the expansion.

Then:

$$\begin{aligned}
 \underline{F}(\underline{x}(t), \underline{u}(t), t) &= \underline{F}_0(\hat{\underline{x}}(t), \hat{\underline{u}}(t), t) \\
 &+ \bar{\underline{N}}_F(\hat{\underline{x}}(t), \hat{\underline{u}}(t), t) (\underline{x}(t) - \hat{\underline{x}}(t)) \\
 &+ \bar{\underline{M}}_F(\hat{\underline{x}}(t), \hat{\underline{u}}(t), t) (\underline{u}(t) - \hat{\underline{u}}(t))
 \end{aligned} \tag{7.25}$$

with the ij^{th} element of $\bar{\underline{N}}_F(\cdot)$, $\bar{\underline{M}}_F(\cdot)$ given by:

$$\left. \begin{aligned}
 \{\bar{\underline{N}}_F(\hat{\underline{x}}(t), \hat{\underline{u}}(t), t)\}_{ij} &= \frac{\partial F_i(\underline{x}(t), \underline{u}(t), t)}{\partial x_j(t)} \\
 &\left| \begin{array}{l} \underline{x}(t) = \hat{\underline{x}}(t) \\ \underline{u}(t) = \hat{\underline{u}}(t) \end{array} \right.
 \end{aligned} \right. \tag{7.26}$$

$$\left. \begin{aligned}
 \{\bar{\underline{M}}_F(\hat{\underline{x}}(t), \hat{\underline{u}}(t), t)\}_{ij} &= \frac{\partial F_i(\underline{x}(t), \underline{u}(t), t)}{\partial u_j(t)} \\
 &\left| \begin{array}{l} \underline{x}(t) = \hat{\underline{x}}(t) \\ \underline{u}(t) = \hat{\underline{u}}(t) \end{array} \right.
 \end{aligned} \right. \tag{7.27}$$

where $\frac{\partial}{\partial}$ denotes partial derivative, $F_i(\cdot)$ is the i^{th} element of the vector function $\underline{F}(\cdot)$, $x_j(t)$ is the j^{th} element of the state vector $\underline{x}(t)$, and $u_j(t)$ is the j^{th} element of the input vector $\underline{u}(t)$. The right-hand side of Eqs. (7.26) and (7.27) implies that the derivatives are evaluated at the current mean value (best estimate) of the state and the input vectors.

Also:

$$\underline{F}_0(\underline{\hat{x}}(t), \underline{\hat{u}}(t), t) = \underline{F}(\underline{\hat{x}}(t), \underline{\hat{u}}(t), t) \quad (7.28)$$

Similarly:

$$\left. \begin{aligned} \{\underline{N}_G(\underline{\hat{x}}(t_k), \underline{\hat{u}}(t_k), t_k)\}_{ij} &= \frac{\partial G_i(\underline{x}(t_k), \underline{u}(t_k), t_k)}{\partial x_j(t_k)} \Big|_{\substack{\underline{x}(t_k) = \underline{\hat{x}}(t_k) \\ \underline{u}(t_k) = \underline{\hat{u}}(t_k)}} \end{aligned} \right\} \quad (7.29)$$

$$\left. \begin{aligned} \{\underline{M}_G(\underline{\hat{x}}(t_k), \underline{\hat{u}}(t_k), t_k)\}_{ij} &= \frac{\partial G_i(\underline{x}(t_k), \underline{u}(t_k), t_k)}{\partial u_j(t_k)} \Big|_{\substack{\underline{x}(t_k) = \underline{\hat{x}}(t_k) \\ \underline{u}(t_k) = \underline{\hat{u}}(t_k)}} \end{aligned} \right\} \quad (7.30)$$

$$\underline{G}_0(\underline{\hat{x}}(t_k), \underline{\hat{u}}(t_k), t_k) = \underline{G}(\underline{\hat{x}}(t_k), \underline{\hat{u}}(t_k), t_k) \quad (7.31)$$

The important features of the linearization procedure are:

1. The linearization matrices and vectors are only functions of the state and input mean vectors. That is:

$$\frac{d}{dt} \underline{x}(t) = \underline{\hat{x}}(t) \quad (7.32)$$

$$\frac{d}{dt} \underline{u}(t) = \underline{\hat{u}}(t) \quad (7.33)$$

$$\underline{d}_u(t_k) = \hat{\underline{u}}(t_k) \quad (7.34)$$

2. When used with the filter equations (the so-called extended Kalman filter, Gelb (1974)) they produce biased estimates due to the fact that in general:

$$E \{ \underline{F}(\underline{x}(t), \underline{u}(t), t) \} \neq \underline{F}(\hat{\underline{x}}(t), \hat{\underline{u}}(t), t)$$

3. Taylor expansions are easy if the nonlinear functions of interest are differentiable. If not, this procedure cannot be applied.

7.2.2 Statistical Linearization

The idea in this case is to assume a general linear approximation of the type in Eqs. (7.9) and (7.10) and then obtain the constant and coefficient matrices by minimizing the expected value of the weighted, squared deviations from the nonlinear function.

In this case, the equations for the $\bar{\underline{N}}_F(\cdot)$, $\bar{\underline{N}}_C(\cdot)$, $\bar{\underline{M}}_C(\cdot)$ matrices and $\bar{\underline{F}}_0(\cdot)$, $\bar{\underline{G}}_0(\cdot)$ vectors are:

$$\bar{\underline{N}}_F \left(\frac{d}{d\underline{x}(t)}, \frac{d}{d\underline{u}(t)}, t \right) = E \{ \underline{F}(\underline{x}(t), \underline{u}(t), t) \cdot \underline{r}_x^T(t) \} \cdot \int_{-1}^{-1} (t) \quad (7.35)$$

$$\bar{N}_G(\underline{d}_{\underline{x}(t_k)}, \underline{d}_{\underline{u}(t_k)}, t_k) = E\{G(\underline{x}(t_k), \underline{u}(t_k), t_k) \cdot \underline{r}_{\underline{x}}^T(t_k)\} \cdot \bar{\Sigma}^{-1}(t_k) \quad (7.36)$$

$$\bar{M}_G(\underline{d}_{\underline{x}(t_k)}, \underline{d}_{\underline{u}(t_k)}, t_k) = E\{G(\underline{x}(t_k), \underline{u}(t_k), t_k) \cdot \underline{r}_{\underline{u}}^T(t_k)\} \cdot \bar{Q}_{\underline{u}}^{-1}(t_k) \quad (7.37)$$

$$\bar{F}_0(\underline{d}_{\underline{x}(t)}, \underline{d}_{\underline{u}(t)}, t) = E\{F(\underline{x}(t), \underline{u}(t), t)\} \quad (7.38)$$

$$\bar{G}_0(\underline{d}_{\underline{x}(t_k)}, \underline{d}_{\underline{u}(t_k)}, t_k) = E\{G(\underline{x}(t_k), \underline{u}(t_k), t_k)\} \quad (7.39)$$

Due to the white noise nature of the continuous process $\underline{u}(t)$, its covariance matrix does not exist, therefore $\bar{M}_F(\cdot)$ is defined as in Eq. (7.27).

For this linearization procedure, it is important to note the following:

1. The linearization matrices and vectors are functions of the state and input first and second moment properties given the Gaussian assumption. In general they are functions of all the parameters of their probability distributions.
2. Equations (7.17) and (7.19) together with Eqs. (7.38) and (7.39) show that this procedure used with a linear filter produces unbiased estimates. This fact may be of crucial importance when one is doing parameter estimation through state augmentation (e.g., Georgakakos and Bras, 1982).

3. An assumption about the underlying probability distribution is necessary to compute the linearization matrices and vectors. Usually a Gaussian assumption suffices for good performance, while providing the state mean and covariance recursively if this procedure is used with the linear filter.
4. To avoid the burden of multidimensional integral evaluation necessary for the computation of the expectations, Georgakakos and Bras (1982) devised an approximate analytical procedure for the determination of the expected value of general multidimensional nonlinear functions. Their solution is particularly useful when one has to compute the linearization matrices and vectors recursively, as in a filter operation.
5. No assumption regarding function differentiability is made for the statistical linearization procedure. Kitanidis and Bras (1980a) show an example where a nondifferentiable nonlinear function was statistically linearized.

7.3 Linearization of the Rainfall-Runoff Model Equations

Linearization is based on the Taylor's series expansion (section 7.2.1) for the precipitation and soil models and on statistical linearization (section 7.2.2) for the channel routing model. The state vector corresponding to the precipitation, soil and channel models is such that the storm water content state X is the first element, and the soil states x_1, \dots, x_6 follow in the order presented

in Table 6.1. The channel states occupy the last positions in the state vector. The input vector \underline{u} is defined as:

$$\underline{u} = [T_0 \ P_0 \ T_d \ u_e]^T$$

In the derivation of the linearized equations for the channel, the input u_c is linearized through an ordinary Taylor's series expansion. Appendices D, E and F determine the necessary derivatives corresponding to the precipitation, soil and channel models, respectively. Tables 7.1, 7.2, 7.3, and 7.4 indicate the a priori non-zero elements of the matrices \bar{N}_F , \bar{M}_F , \bar{N}_G , and \bar{M}_G , respectively. In those tables and for the ij^{th} element of a matrix, the corresponding state, input or output variable to i and j are also presented.

The present formulation utilizes the set of equations presented in section 6.4 for a headwater basin.

Table 7.1

NON-ZERO ELEMENTS OF MATRIX \overline{N}_F

i/j	1,X	2,x ₁	3,x ₂	4,x ₃	5,x ₄	6,x ₅	7,x ₆	8,S ₁	...	7+n,S _n
1,X	✓									
2,x ₁	✓	✓								
3,x ₂	✓	✓	✓	✓	✓	✓				
4,x ₃		✓	✓	✓	✓	✓				
5,x ₄			✓	✓	✓	✓				
6,x ₅			✓	✓	✓	✓				
7,x ₆	✓	✓	✓				✓			
8,S ₁	✓	✓	✓		✓	✓	✓	✓		
⋮	⋮	⋮	⋮	⋮	⋮	⋮	⋮			
⋮	⋮	⋮	⋮	⋮	⋮	⋮	⋮			
⋮	⋮	⋮	⋮	⋮	⋮	⋮	⋮			
7+n,S _n	✓	✓	✓		✓	✓	✓		⋯	✓

Table 7.2

NON-ZERO ELEMENTS OF MATRIX \overline{M}_F

i/j	1, T ₀	2, p ₀	3, T _d	4, u _e
1, X	✓	✓	✓	
2, x ₁	✓	✓	✓	✓
3, x ₂	✓	✓	✓	
4, x ₃				✓
5, x ₄				
6, x ₅				
7, x ₆	✓	✓	✓	✓
8, S ₁	✓	✓	✓	
⋮				
7+n, S _n	✓	✓	✓	

Table 7.3

NON-ZERO ELEMENTS OF MATRIX \bar{N}_G

i/j	1,X	2,x ₁	3,x ₂	4,x ₃	5,x ₄	6,x ₅	7,x ₆	8,S ₁	...	7+n,S _n
1,P _v	✓									
2,Q _n										✓

Table 7.4

NON-ZERO ELEMENTS OF MATRIX \bar{M}_G

i/j	1,T ₀	2,P ₀	3,T _d	4,u _e
1,P _v	✓	✓	✓	
2,Q _n				

Chapter 8

CASE STUDIES

8.1 Introduction

This chapter documents tests of the station precipitation and of the full rainfall-runoff models. Hourly meteorological data (T_o, P_o, T_d) and hourly precipitation data from Boston, Massachusetts, and Tulsa, Oklahoma, corresponding to several storms of different types were the basis of the precipitation model tests. The full rainfall-runoff model runs used 6-hourly hydrological data (mean areal precipitation, evapotranspiration and instantaneous discharge) for the Bird Creek basin, near Sperry, Oklahoma, together with meteorological data from Tulsa.

The next section discusses some important characteristics of the data used as an input to the station precipitation model. Section 8.3 presents the parameter estimation procedures. Runs of the deterministic precipitation model (the precipitation model developed using as an input observed T_o, P_o, T_d) are presented in Section 8.4. The stochastic precipitation model (the precipitation model together with a filter) operation is illustrated in Section 8.5, Sections 8.6, and 8.7 show the full rainfall-runoff model operation for the Bird Creek basin, for the excessively wet month of May 1959, with meteorological input from Tulsa.

8.2 Station Precipitation Model Input Data Characteristics

The National Climatic Center (NCC) in Asheville, North Carolina, is the source of the meteorological and precipitation data in the

United States. The meteorological data are archived in the tape-series TDF-14. They are based on airways surface observations. Hourly data exist for periods prior to the year 1965. Currently a 3-hourly observation interval is in use. The hourly precipitation data are archived in tape-series TD-9657. Both meteorological and precipitation data can also be found in the Local Climatological Data sheets published once a month by the National Oceanic and Atmospheric Administration (NOAA), Environmental Data and Information Service.

The Boston-data used were taken from the Local Climatological Data sheets. The Tulsa-data are from the tape archives in NCC under the code numbers TD-1440, 13968 for the meteorological data, and TD-9657, 34-8992 for the hourly precipitation data. The Fortran program documented in Restrepo-Posada and Eagleson (1979) was used for the interpretation of the hourly precipitation data.

Eight storms at the Boston area and three storms at Tulsa were studied. The storm dates, storm number and comments regarding their nature and the meteorological conditions at the time of their occurrence are given in Table 8.1. The same Table also gives the identification characteristics of the observation locations. For the purpose of processing the data and in view of the presumed storm-invariance property of the precipitation model parameters, the storms were grouped in five groups (also indicated in Table 8.1) with the number of data points (i.e., hourly values) ranging from 60 to 100. The storms in each group have similar characteristics. In the following, each group is referred to by the group number.

Table 8.1

CASE STUDY STORMS

<u>STORM NO.</u>	<u>INITIAL DATE (YYMMDDHH)</u>	<u>FINAL DATE (YYMMDDHH)</u>	<u>DURATION (HOURS)</u>	<u>GROUP NUMBER</u>	<u>COMMENTS</u>
1.	62092707	62092818	36	1	Convective line-storm with heavy rains and damaging northeasterly gales. -- BOSTON
2.	62100506	62100721	64	1	The combination of a coastal storm on the 5-6th of October immediately followed by tropical storm Daisy, passing distantly offshore on the 7th, yielded 7.01 inches of rainfall. This was the 3rd greatest storm total of record. -- BOSTON
3.	63110619	63110906	60	2	Low pressure followed by persistent rainfall. The surface wind direction shifted from Southeast on the 6th of November to North on the 9th. This November was especially wet. Rainfall was the greatest for November since 1895. -- BOSTON

Table 8.1 (continued)

CASE STUDY STORMS

<u>STORM NO.</u>	<u>INITIAL DATE (YYMMDDHH)</u>	<u>FINAL DATE (YYMMDDHH)</u>	<u>DURATION (HOURS)</u>	<u>GROUP NUMBER</u>	<u>COMMENTS</u>
4.	63012600	63012715	16	3	Snowstorm. This January was the 7th consecutive colder than normal month. Wind direction shifted from East to North East. -- BOSTON
5.	63030117	63030211	19	3	Snowstorm, heaviest of the season. It yielded 8.7 inches of snow. Wind direction shifted from East to North East. -- BOSTON
6.	63032004	63032110	31	3	Snowstorm. Wind direction shifted from East to North East. -- BOSTON
7.	62120508	62120620	37	4	Low pressure system in a 6th consecutive colder than normal month. Wind direction shifted from a North Easterly to an Easterly direction. -- BOSTON

Table 8.1 (continued)

CASE STUDY STORMS

<u>STORM NO.</u>	<u>INITIAL DATE (YYMMDDHH)</u>	<u>FINAL DATE (YYMMDDHH)</u>	<u>DURATION (HOURS)</u>	<u>GROUP NUMBER</u>	<u>COMMENTS</u>
8.	63112906	63113004	23	4	Caused by a deep low pressure center which traveled northward through western New England during the morning of the 30th. Excessive and flooding rains and high southerly winds caused widespread damage inland while erosion and flooding from high waves and abnormal tides added to coastal losses. Wind direction shifted from North-East to East to South. -- BOSTON
9.	50050913	50051106	42	5	Heaviest of the season. Wind direction shifted from North to North East. -- TULSA
10.	50070909	50071015	31	5	Showers with long no-rain hours in between. Wind was from a South Easterly direction. -- TULSA
11.	50072106	50072208	27	5	Showers with long no-rain hours in between. Wind direction shifted from North to North East. -- TULSA

Table 8.1 (continued)

CASE STUDY STORMS

<u>OBSERVATION AREA</u>	<u>LATITUDE</u>	<u>LONGITUDE</u>	<u>ELEVATION[M]</u>
Boston, Massachusetts Logan International Airport	42° 22' N	71° 01' W	5
Tulsa, Oklahoma International Airport	36° 12' N	95° 54' N	200

The selected storms include different types (convective, frontal, snowstorms) of hydrologically significant (large amounts of rainfall) storms. The Boston climatological precipitation record offered several examples. The dates prior to 1965 were used because of the 1-hour time resolution.

Typical in the Tulsa record were short periods of significant amount of rainfall with long dry periods in between. Pronounced rainfall activity in Tulsa takes place from May to September. Rainfall for the Boston area is uniformly distributed throughout the year.

The following parameters were available for all storms:

- 1) the hourly precipitation rate [INCHES/HOUR]
- 2) the air temperature [°F]
- 3) the dew point temperature [°F]
- 4) the wet bulb temperature [°F]
- 5) the surface pressure [INCHES of Hg]

The units were converted to [MM/HOUR] for the precipitation rate, [°K] for the temperatures and [Pascals] for the pressure. These units are used throughout this chapter.

Errors of 0.01 [INCHES] for the precipitation rate, 1[°F] for the temperatures and 0.01 [INCHES Hg] for the pressure are expected because of truncation during data recording. No estimate of the observation error was available for the recorded variables. However, the following are generally applicable (Linsley, Kohler and Paulhus, 1975):

- 1) The tipping-bucket and weighing rain and snow gages in use for the precipitation rate recording underestimate light precipitation (especially snow) in the presence of wind.
- 2) Measurement of the dew point and/or wet bulb temperatures is one of the least accurate instrumental procedures in meteorology.

The average precipitation rate expressed in [MM/HOUR] of water equivalent is shown in Table 8.2, for each group. Also shown in the total accumulation of precipitation in [MM] for each group. The convective group 1 had the highest average precipitation rate and the highest accumulation. The snowstorms, group 3, had the lowest corresponding figures.

The coefficient of variation and the skewness coefficients are shown in Table 8.3. Table 8.4 gives the cross-correlations of the temperature and pressure variables to the concurrent precipitation rate. The hourly auto-correlation coefficients for each variable, for each storm group, up to lag 6 hours are given in Table 8.5.

Tables 8.2 to 8.5 indicate the following:

- 1) The scale of fluctuations of the precipitation variable, as it is expressed by the coefficient of variation (ratio of standard deviation to the mean), is at least two orders of magnitude greater than those of the temperature and pressure variables for all storm groups.

Table 8.2

STORM DATA STATISTICS - I

<u>Storm Group No.</u>	<u>Average Precipitation Rate [MM/HOUR]</u>	<u>Accumulated Precipitation [MM]</u>
1	2.59	259
2	1.585	95
3	0.950	62.7
4	2.193	131.6
5	1.831	183.1

Table 8.3

STORM DATA STATISTICS - II

Storm Group No.	<u>Coefficient of Variation</u>					<u>Skewness Coefficient</u>				
	T _o	P _o	T _d	T _w	P _v	T _o	P _o	T _d	T _w	P _v
1	0.005	0.008	0.007	0.006	1.066	-0.216	-0.710	-1.106	-0.460	1.691
2	0.002	0.007	0.003	0.002	1.157	0.139	1.125	-0.578	-0.467	1.303
3	0.005	0.009	0.006	0.005	1.266	-0.489	0.746	-0.547	-0.483	2.926
4	0.012	0.009	0.011	0.011	1.418	1.707	-0.614	1.205	1.590	3.061
5	0.012	0.002	0.010	0.010	1.609	-0.141	-0.034	-0.221	-0.198	2.53

Table 8.4

STORM DATA STATISTICS -- III

<u>Storm Group No.</u>	<u>Cross-Correlations to Precipitation Rate</u>			
	<u>T_o</u>	<u>P_o</u>	<u>T_d</u>	<u>T_w</u>
1	-0.066	0.087	0.170	0.086
2	0.315	-0.101	0.392	0.347
3	0.185	0.204	0.340	0.283
4	0.253	-0.228	0.337	0.303
5	-0.474	0.161	-0.394	-0.431

Table 8.5

STORM DATA STATISTICS - IV

<u>Variable</u>	<u>Lag (HOURS):</u>	Group 1 Auto-Correlations					
		<u>1</u>	<u>2</u>	<u>3</u>	<u>4</u>	<u>5</u>	<u>6</u>
T _O		0.928	0.840	0.738	0.626	0.513	0.411
P _O		0.976	0.945	0.908	0.867	0.823	0.775
T _d		0.914	0.814	0.706	0.611	0.525	0.460
T _w		0.928	0.837	0.746	0.656	0.554	0.473
P _v		0.641	0.441	0.313	0.188	0.066	0.031

Table 8.5 (continued)

STORM DATA STATISTICS - IV

Group 2 Auto-Correlations

<u>Variable</u>	<u>Lag (HOURS):</u>	<u>1</u>	<u>2</u>	<u>3</u>	<u>4</u>	<u>5</u>	<u>6</u>
T _o		0.839	0.719	0.625	0.491	0.383	0.263
P _o		0.954	0.898	0.838	0.775	0.713	0.646
T _d		0.804	0.703	0.587	0.492	0.490	0.413
T _w		0.831	0.744	0.636	0.517	0.469	0.400
P _v		0.408	0.174	0.110	0.104	-0.008	-0.180

Table 8.5 (continued)

STORM DATA STATISTICS - IV

<u>Variable</u>	<u>Lag (HOURS):</u>	<u>Group 3 Auto-Correlations</u>					
		<u>1</u>	<u>2</u>	<u>3</u>	<u>4</u>	<u>5</u>	<u>6</u>
T _o		0.831	0.550	0.292	0.134	0.128	0.145
P _o		0.861	0.706	0.540	0.380	0.234	0.096
T _d		0.804	0.578	0.400	0.284	0.206	0.074
T _w		0.836	0.559	0.324	0.172	0.134	0.116
P _v		0.600	0.400	0.269	0.194	0.082	0.002

Table 8.5 (continued)

STORM DATA STATISTICS - IV

Group 4 Auto-Correlations

<u>Variable</u>	<u>Lag (HOURS):</u>	<u>1</u>	<u>2</u>	<u>3</u>	<u>4</u>	<u>5</u>	<u>6</u>
T _O		0.938	0.839	0.718	0.600	0.485	0.373
P _O		0.883	0.750	0.601	0.449	0.306	0.183
T _d		0.876	0.750	0.652	0.539	0.431	0.327
T _w		0.931	0.826	0.709	0.589	0.473	0.364
P _v		0.372	0.119	0.092	0.132	-0.153	-0.152

Table 8.5 (continued)

STORM DATA STATISTICS - IV

Group 5 Auto-Correlations

<u>Variable</u>	<u>Lag (HOURS):</u>	<u>1</u>	<u>2</u>	<u>3</u>	<u>4</u>	<u>5</u>	<u>6</u>
T _o		0.939	0.872	0.806	0.740	0.693	0.655
P _o		0.926	0.852	0.775	0.707	0.638	0.565
T _d		0.943	0.894	0.843	0.785	0.753	0.729
T _w		0.949	0.899	0.846	0.788	0.749	0.721
P _v		0.609	0.361	0.166	0.084	0.087	0.066

- 2) Strong positive skewness is characteristic of the precipitation rate. The skewness coefficient of the other variables were both negative and positive.
- 3) Low cross-correlations of the temperatures and of the pressure to the concurrent hourly precipitation rate were observed, ranging from 0.066 to 0.474 in absolute value. This highlights the difficulty of using the temperatures and pressure as explanatory variables in a linear regression for the precipitation rate prediction.
- 4) Characteristically high lag-1 (1 hour) auto-correlations were obtained for the temperatures and the pressure variables. They ranged from about 0.8 to about 0.98, suggesting that the current value of those variables contains considerable amount of information on their value 1 hour later. Therefore, simple linear regression predictors can be used to forecast those variables at least for 1 hour lead time. In some cases, groups 1, 2 and 5, the correlations are of a high value even for lags of 6 hours (up to about 0.77). In group 3, the snowstorms group, correlations dropped relatively fast with lag.
- 5) Auto-correlations of the precipitation rate were lower than those of the other variables for all lags and for all groups. One hour auto-correlations lag ranged from a value of about 0.6 (groups 1, 3, and 5) to a value of about 0.37 (group 4). The auto-correlations dropped fast at higher lags and became negative in some cases (groups 2 and 4).

- 6) A variety of intrinsic statistical character can be observed for the different groups. Therefore, none was considered redundant for the purposes of the precipitation model tests. Most importantly, this indicates that the optimal parameters of linear, purely statistical, predictors of those variables based on past values of the same variables, would be calibration period dependent. This holds true especially when predictions of the precipitation rate are sought.
- 7) No significant difference of statistical character was observed between Boston and Tulsa storms. The relatively strong negative cross-correlation of the temperatures to concurrent hourly precipitation rate in Tulsa hold some promise for linear regressions at this site.

The use of simple linear predictors of the temperature and pressure variables of the type in Table 8.6 is illustrated in the next two Figures. Figure 8.1 displays plots of the observed (solid lines) hourly dew-point temperature together with the corresponding one-hour lead time predictions (dashed line) for the snowstorm group 3. This is the worst case in terms of dew point prediction among the different groups. Analogous plots are shown in Figure 8.2 for the surface pressure of group 3. Again, shown is the worst case among all the different groups. Table 8.6 gives the explanatory variables for the regression together with the associated optimal parameters and standard errors. It is stressed that the parameter estimates were obtained for the periods

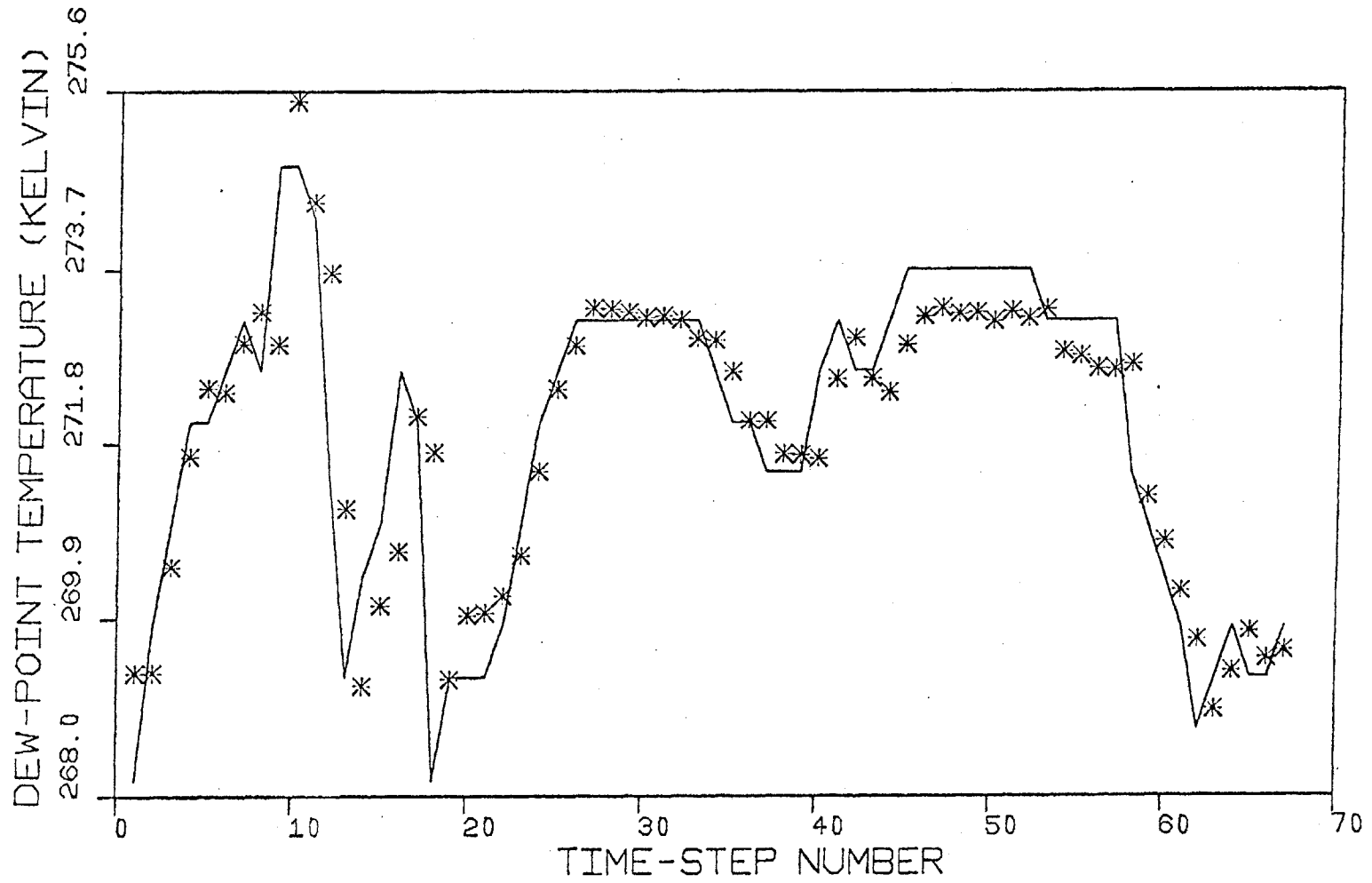


FIGURE 8.1 Dew point regression hourly predictions (stars) vs. observations (solid line) for storm group 3.

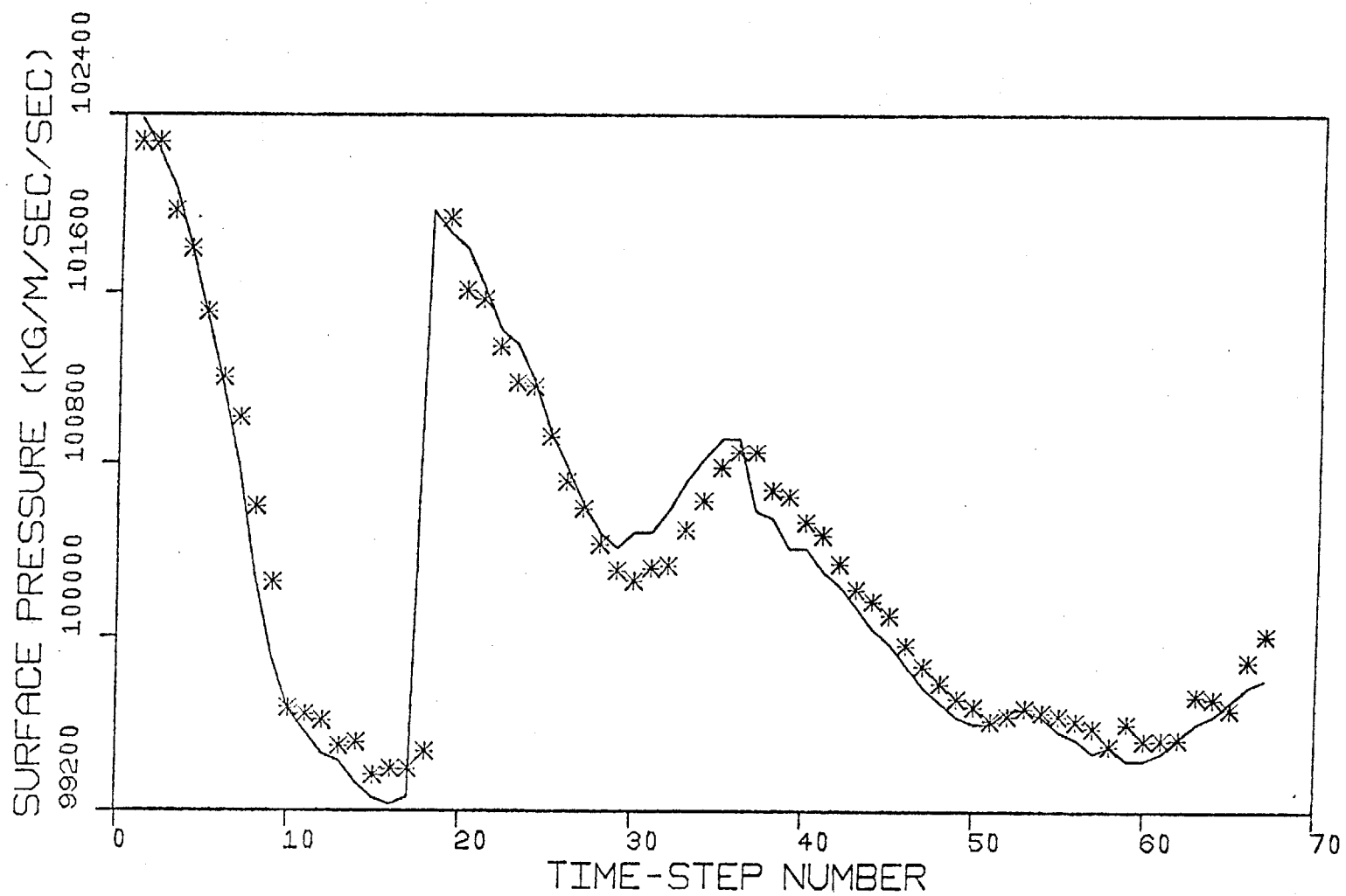


FIGURE 8.2 Surface pressure regression hourly predictions (stars) vs. observations (solid line) for storm group 3

Table 8.6

DEW POINT AND SURFACE PRESSURE REGRESSION PARAMETERS
FOR STORM GROUP 3

$$T_d(k) = A_1 \cdot T_o(k-1) + A_2 \cdot T_d(k-1) + A_3 \cdot p_o(k-1) + A_4 \cdot T_w(k-1) \\ + A_5 \cdot P_v(k-1) + A_0$$

Hourly Dew Point Temperature

<u>Explanatory Variables</u>	<u>Parameter Estimates</u>	<u>Standard Errors in Parameter Estimates</u>
Temperature (1 HOUR LAG):	-0.07546	0.49409
Dew Point Temperature (1 HOUR LAG):	0.67435	0.29255
Surface Pressure (1 HOUR LAG):	0.00029	0.00014
Wet Bulb Temperature (1 HOUR LAG):	0.30341	0.77911
Precipitation Rate (1 HOUR LAG):	0.15549	0.10542
Constant of Regression:	-2.4044	33.242

Table 8.6 (continued)

$$p_o(k) = A_1 \cdot T_o(k-1) + A_2 \cdot T_d(k-1) + A_3 \cdot p_o(k-1) + A_4 \cdot T_w(k-1) \\ + A_5 \cdot P_v(k-1) + A_o$$

Hourly Surface Pressure

<u>Explanatory Variables</u>	<u>Parameter Estimates</u>	<u>Standard Errors in Parameter Estimates</u>
Temperature (1 HOUR LAG):	-29.097	201.54
Dew Point Temperature (1 HOUR LAG):	-120.09	119.33
Surface Pressure (1 HOUR LAG):	0.87747	0.0565
Wet Bulb Temperature (1 HOUR LAG):	164.19	317.80
Precipitation Rate (1 HOUR LAG):	-45.452	43.
Constant of Regression:	8155.9	13559.

of Figures 8.1 and 8.2. Variation of optimal parameters for different calibration periods is expected. The magnitude of the standard errors indicates large parameter uncertainty, for some of the explanatory variables. Nevertheless the behavior of the models is good.

The performance of a linear regression of the type in Table 8.7 in predicting precipitation is illustrated in Figures 8.3 to 8.7 for storm groups 1 through 5 respectively. Again, shown are the calibration periods in each case. The parameter estimates and the associated standard errors are given in Table 8.7.

Characteristic to this set of regressions is the great variation of the parameter estimates (indicated also by the high standard errors) from one calibration period (storm group) to the other. The fit is best in storm groups 2 and 3. However, the predicted curve lacks the large fluctuations about the mean that characterizes the observed values. Due to the unconstrained nature of the regressions, unrealistic negative values of precipitation rate were also predicted. The predictions in dashed lines in Figures 8.3 to 8.7 will be compared to the predictions of the deterministic station precipitation model developed in this work. Both the regression and the physically based model use the same variables as their input.

The performance during the calibration period of a second set of regressions of the type in Table 8.8 is presented in Figures 8.8 to 8.12. The precipitation rate lagged by one hour was added to the list of explanatory variables for this set of regressions. The corresponding parameter estimates and standard errors are given in

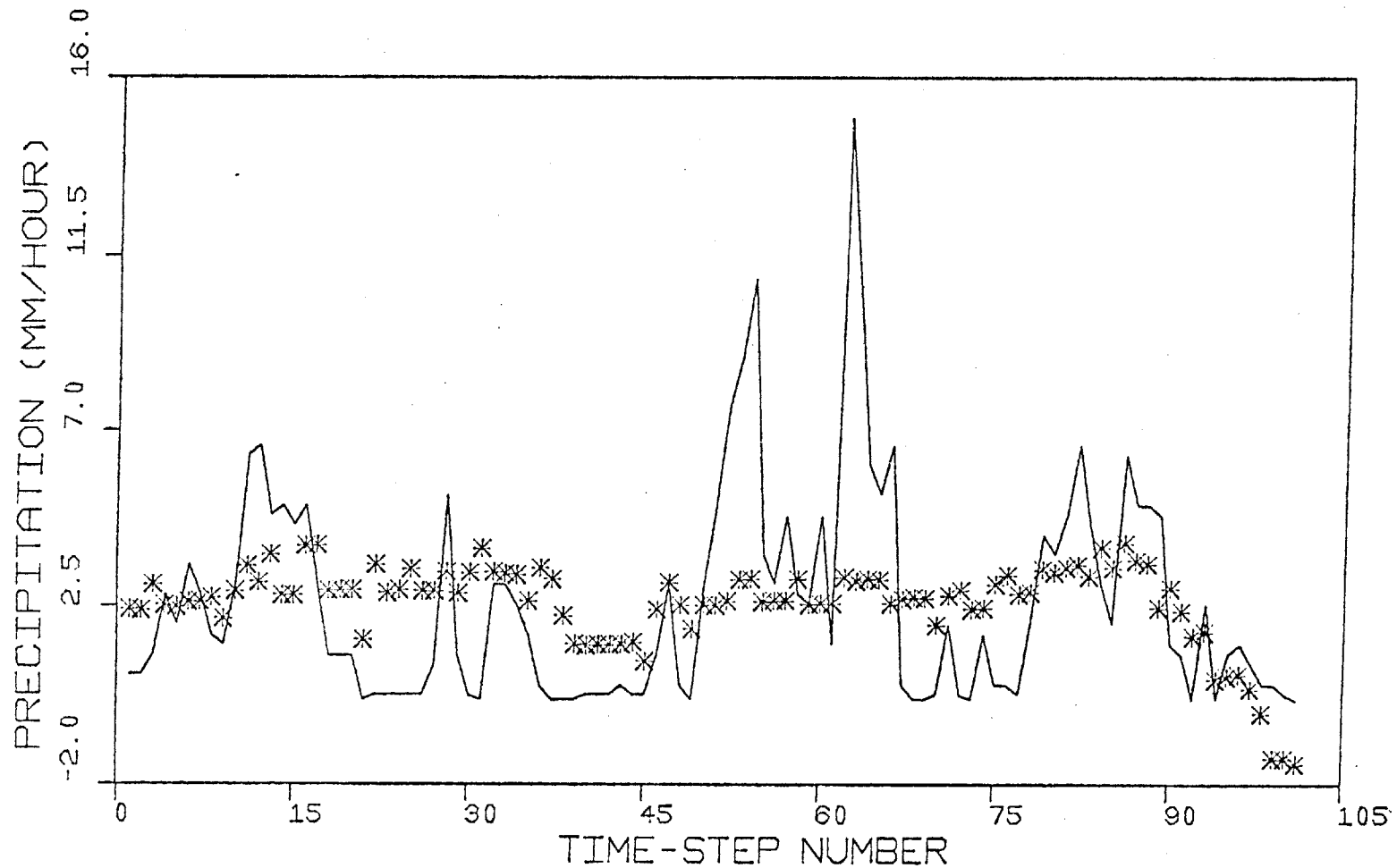


FIGURE 8.3 Precipitation rate hourly predictions (stars) based on the linear model of Table 8.7 vs. observations (solid line). Storm group 1.

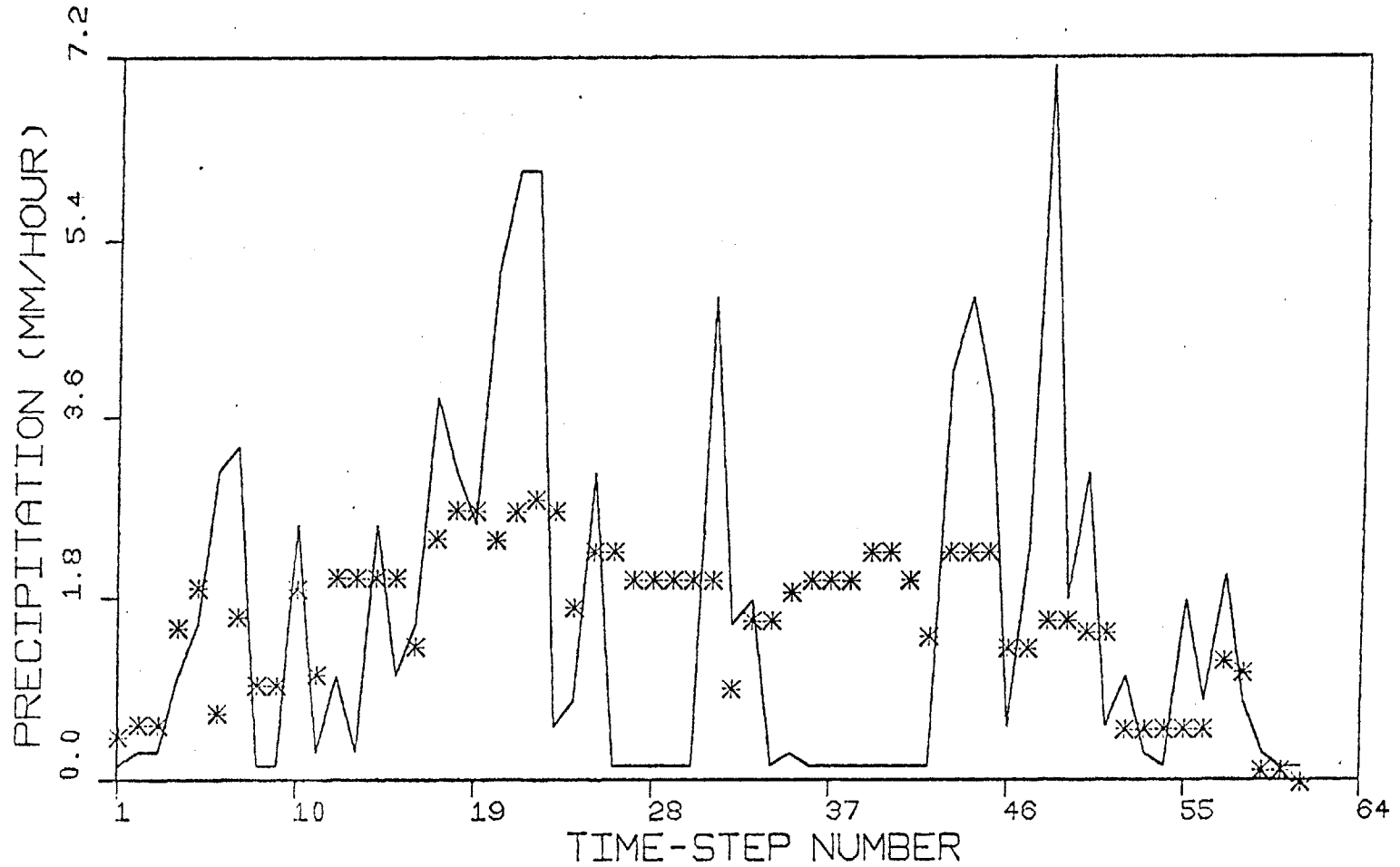


FIGURE 8.4 Precipitation rate hourly predictions (stars) based on the linear model of Table 8.7 vs. observations (solid line). Storm group 2.

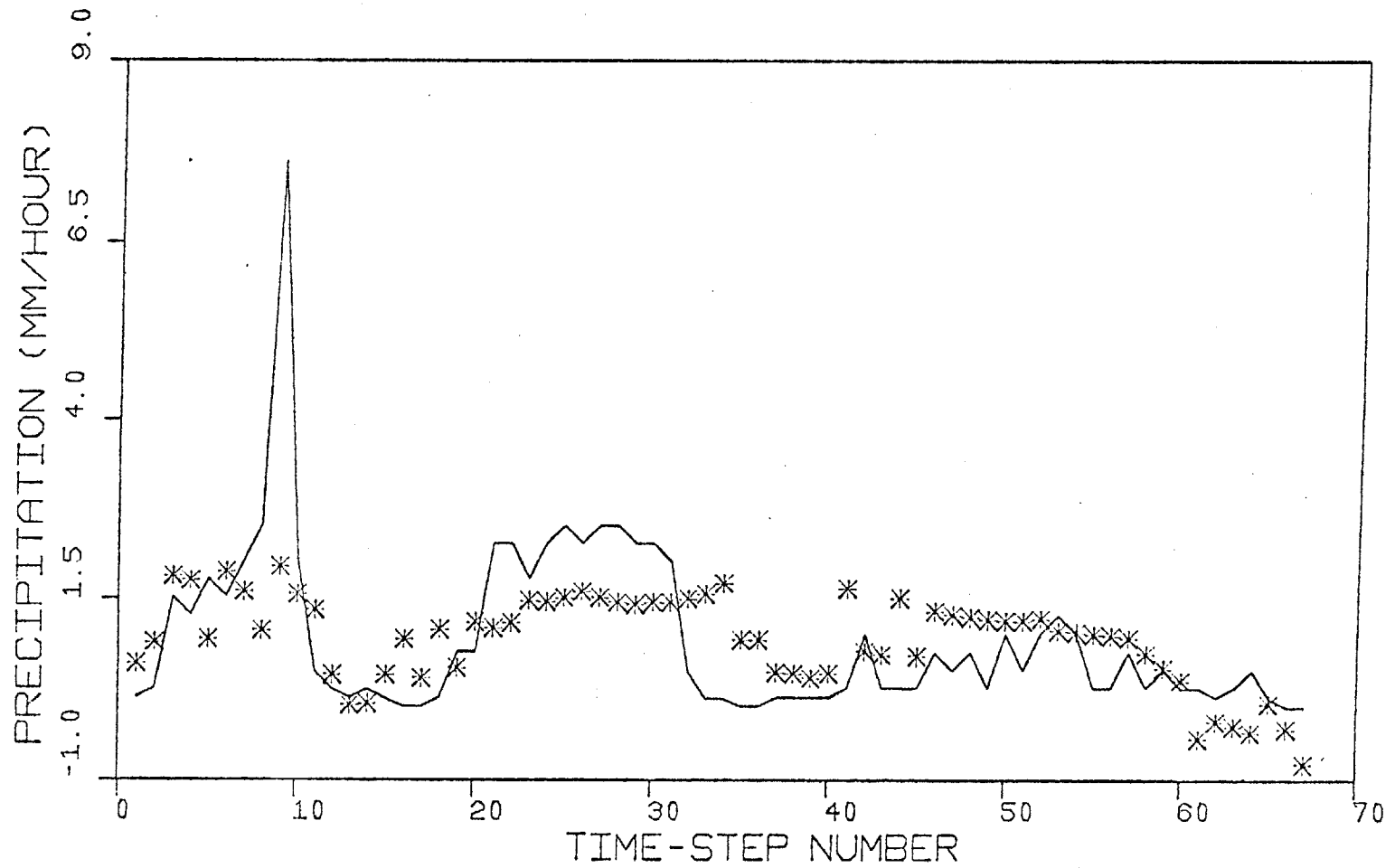


FIGURE 8.5 Precipitation rate hourly predictions (stars) based on the linear model of Table 8.7 vs. observations (solid line). Storm group 3.

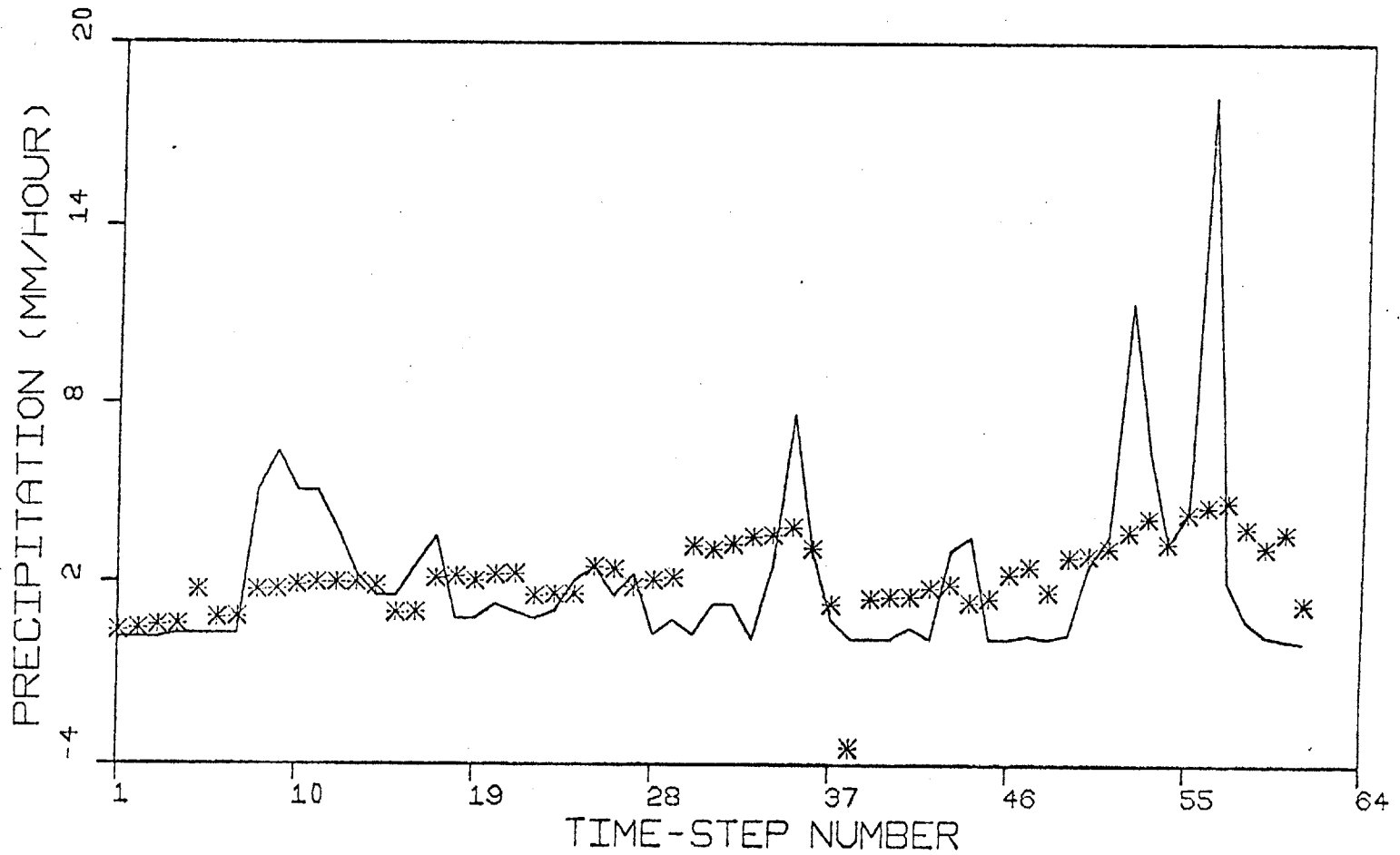


FIGURE 8.6 Precipitation rate hourly predictions (stars) based on the linear model of Table 8.7 vs. observations (solid line). Storm group 4.

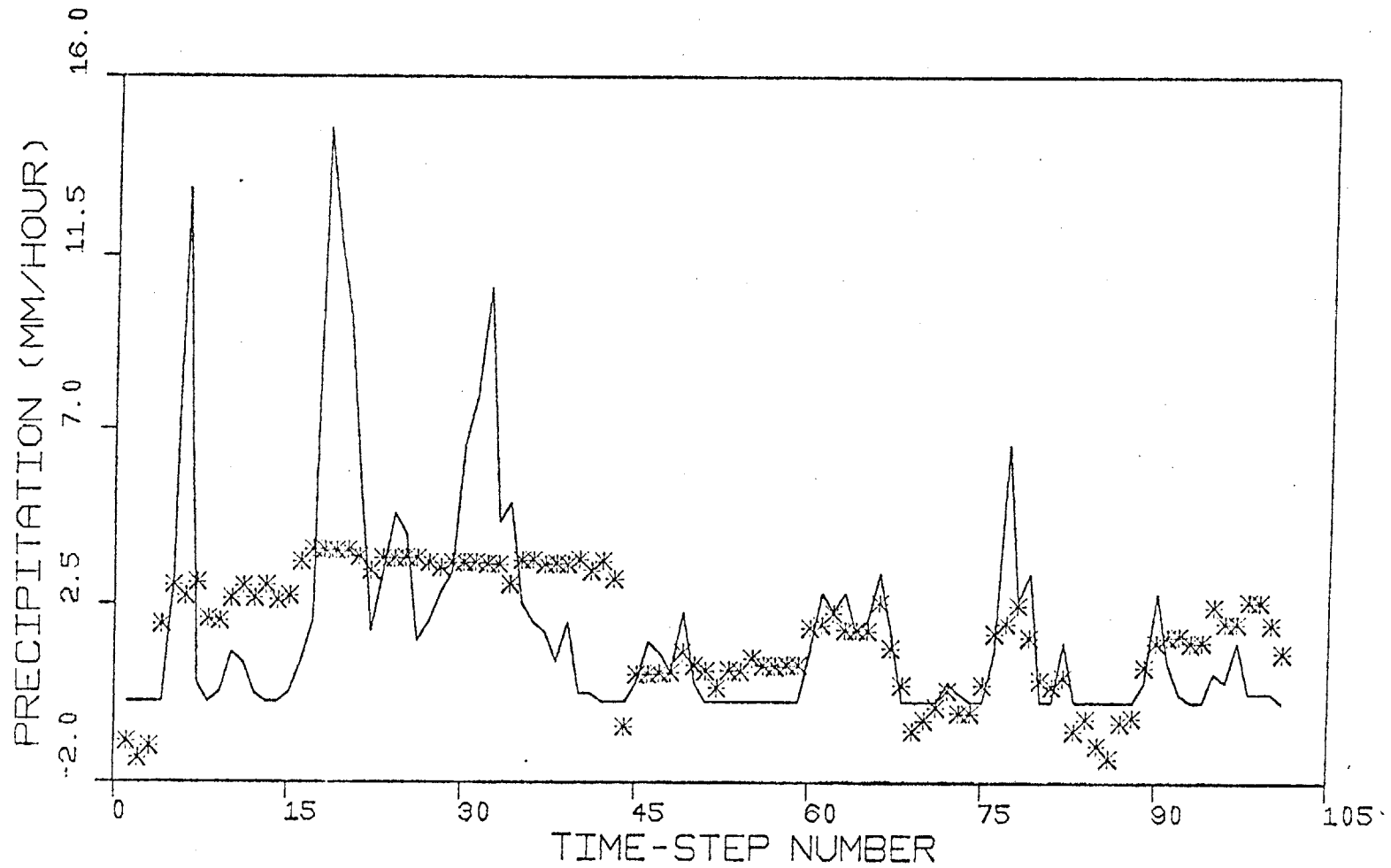


FIGURE 8.7 Precipitation rate hourly predictions (stars) based on the linear model of Table 8.7 vs. observations (solid line). Storm group 5.

Table 8.7

REGRESSION PARAMETERS AND STANDARD ERRORS
REGRESSION OF PRECIPITATION RATE ON TEMPERATURES AND PRESSURES

$$P_v(k) = A_1 \cdot T_o(k) + A_2 \cdot T_d(k) + A_3 \cdot P_o(k) + A_4 \cdot T_w(k) + A_0$$

Storm Group 1

<u>Explanatory Variable</u>	<u>Parameter Estimate</u>	<u>Standard Error</u>
Temperature:	-0.67677	0.70792
Dew Point Temperature:	1.18	0.72597
Surface Pressure:	-0.00028	0.00045
Wet Bulb Temperature:	-0.66274	1.3217
Constant of Regression:	77.420	62.888

Table 8.7 (continued)

	<u>Storm Group 2</u>	
<u>Explanatory Variable</u>	<u>Parameter Estimate</u>	<u>Standard Error</u>
Temperature:	0.81306	0.79902
Dew Point Temperature:	-1.6129	0.9228
Surface Pressure:	0.00001	0.00029
Wet Bulb Temperature:	2.3238	1.4324
Constant of Regression:	-433.66	113.44

Table 8.7 (continued)

Storm Group 3

<u>Explanatory Variable</u>	<u>Parameter Estimate</u>	<u>Standard Error</u>
Temperature:	-0.95569	0.59705
Dew Point Temperature:	-0.06964	0.36834
Surface Pressure:	0.00059	0.00016
Wet Bulb Temperature:	1.1979	0.95236
Constant of Regression:	-105.55	38.139

Table 8.7 (continued)

Storm Group 4

<u>Explanatory Variable</u>	<u>Parameter Estimate</u>	<u>Standard Error</u>
Temperature:	-2.3187	1.1131
Dew Point Temperature:	-0.98358	1.0464
Surface Pressure:	-0.00052	0.00072
Wet Bulb Temperature:	3.5262	2.0683
Constant of Regression:	-8.8449	119.03

Table 8.7 (continued)

Storm Group 5

<u>Explanatory Variable</u>	<u>Parameter Estimate</u>	<u>Standard Error</u>
Temperature:	-0.21898	0.65217
Dew Point Temperature:	1.7385	1.044
Surface Pressure:	-0.00046	0.00112
Wet Bulb Temperature:	-1.8472	1.6473
Constant of Regression:	143.63	117.37

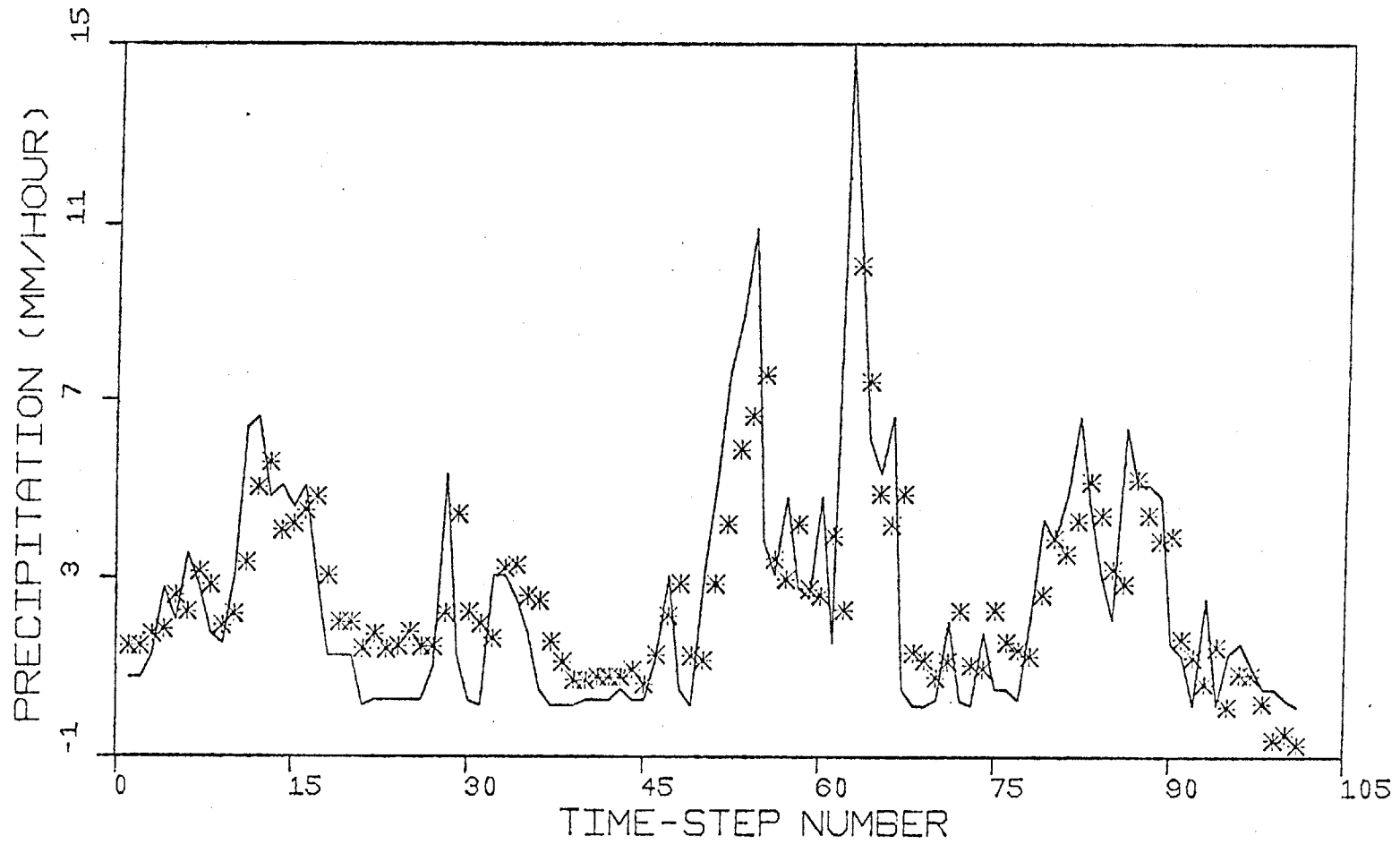


FIGURE 8.8 Precipitation rate hourly predictions (stars) based on the linear model of Table 8.8 vs. observations (solid line). Storm group 1.

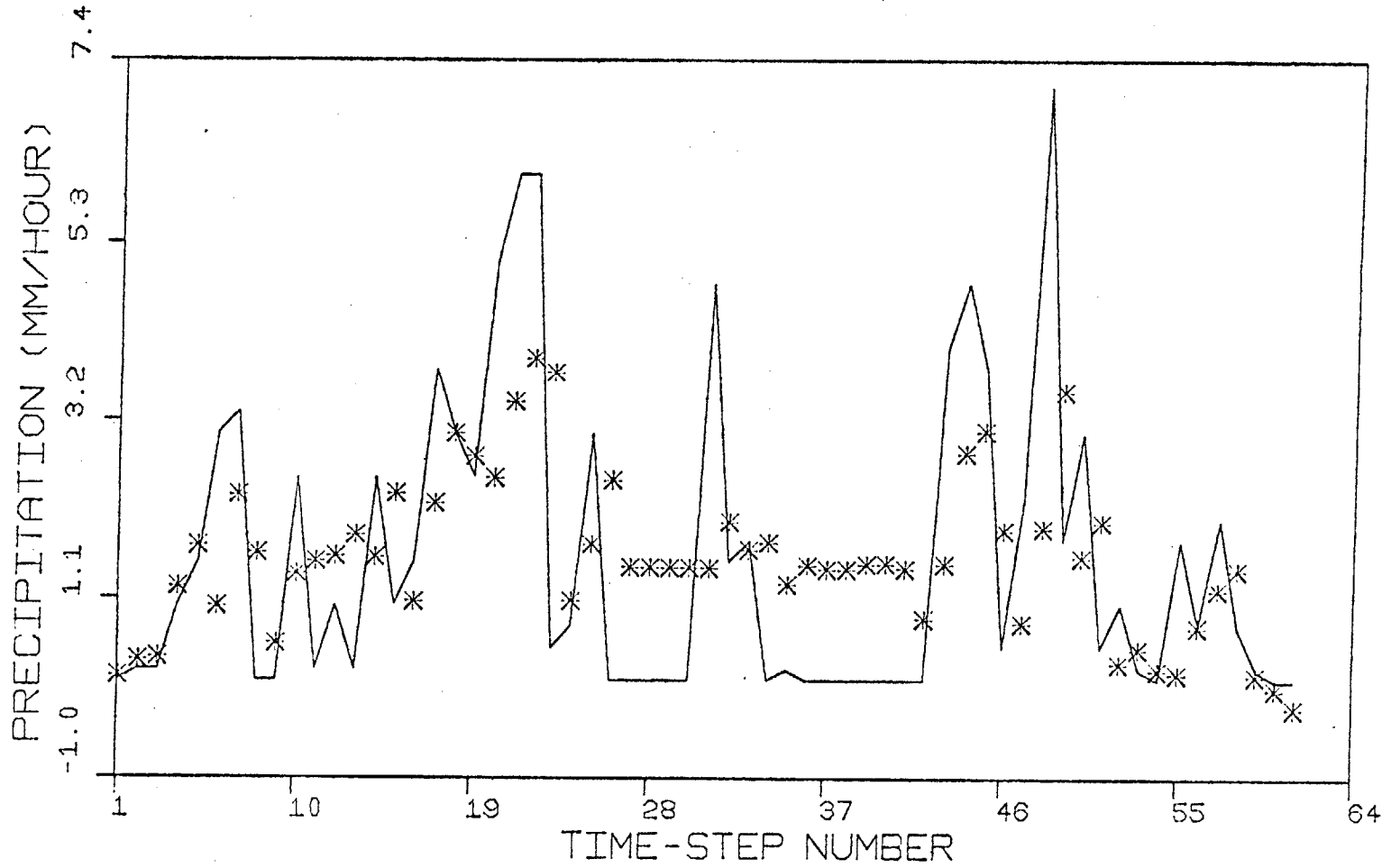


FIGURE 8.9 Precipitation rate hourly predictions (stars) based on the linear model of Table 8.8 vs. observations (solid line). Storm group 2.

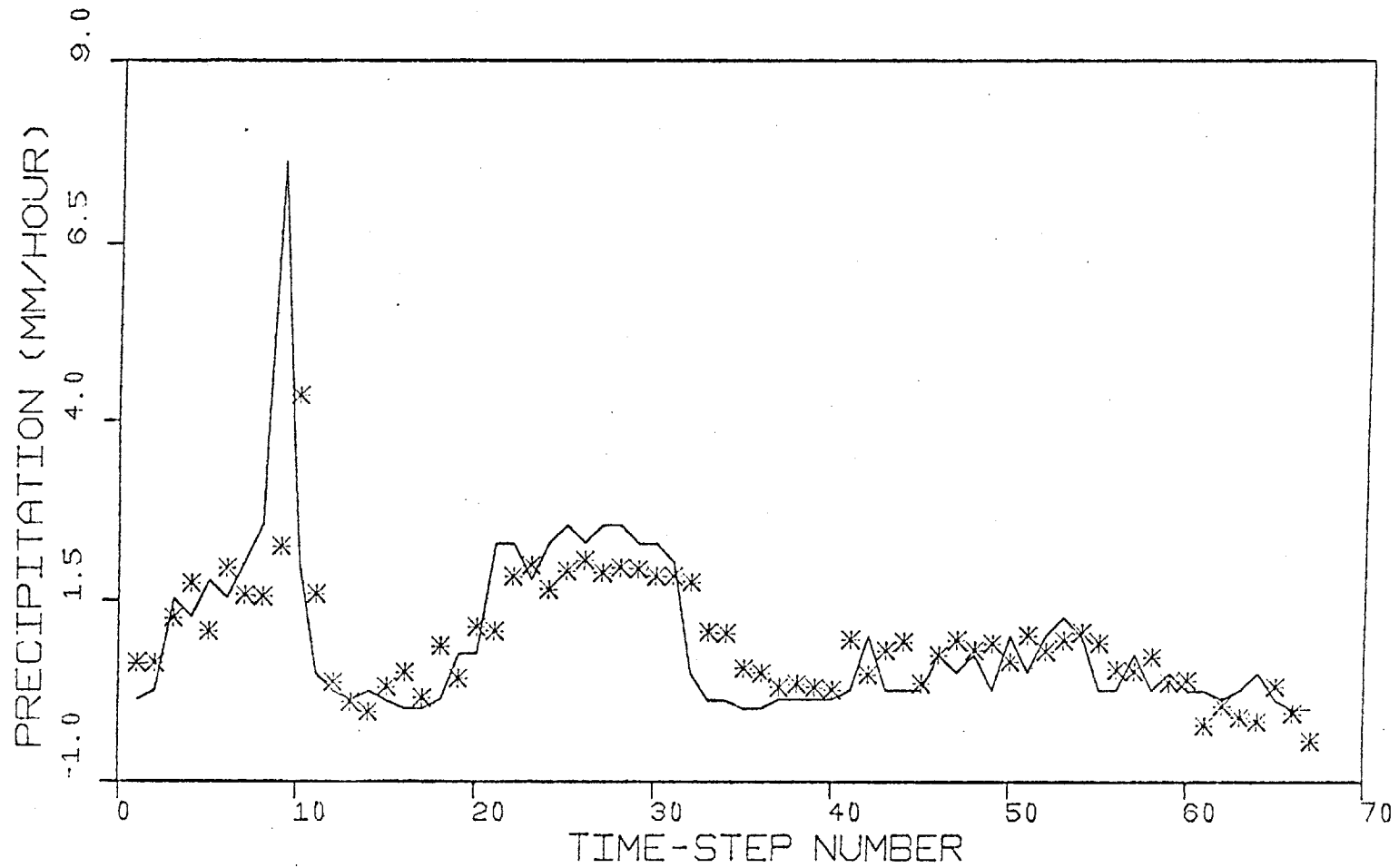


FIGURE 8.10

Precipitation rate hourly predictions (stars) based on the linear model of Table 8.8 vs. observations (solid line). Storm group 3.

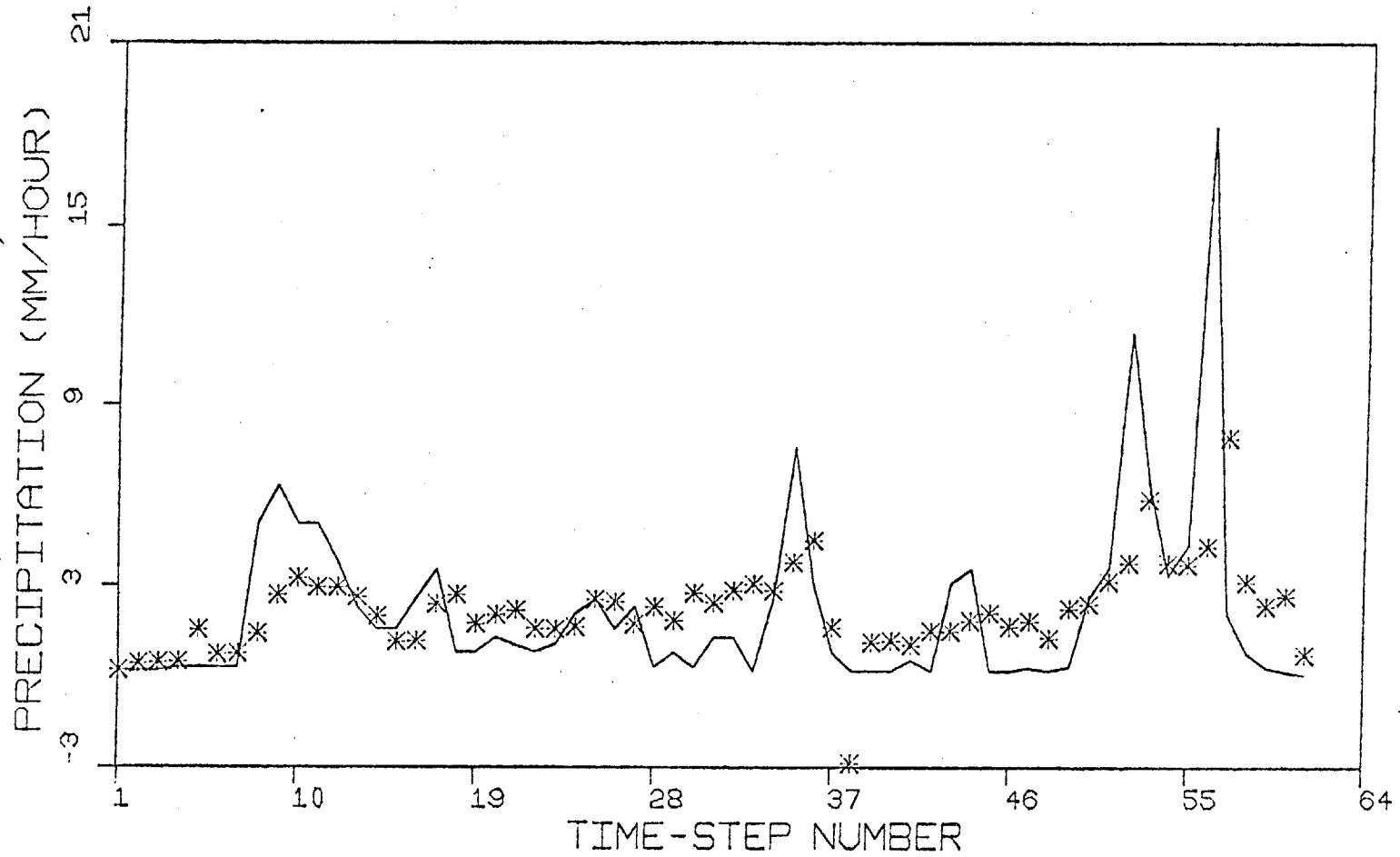


FIGURE 8.11 Precipitation rate hourly predictions (stars) based on the linear model of Table 8.8 vs. observations (solid line). Storm group 4.

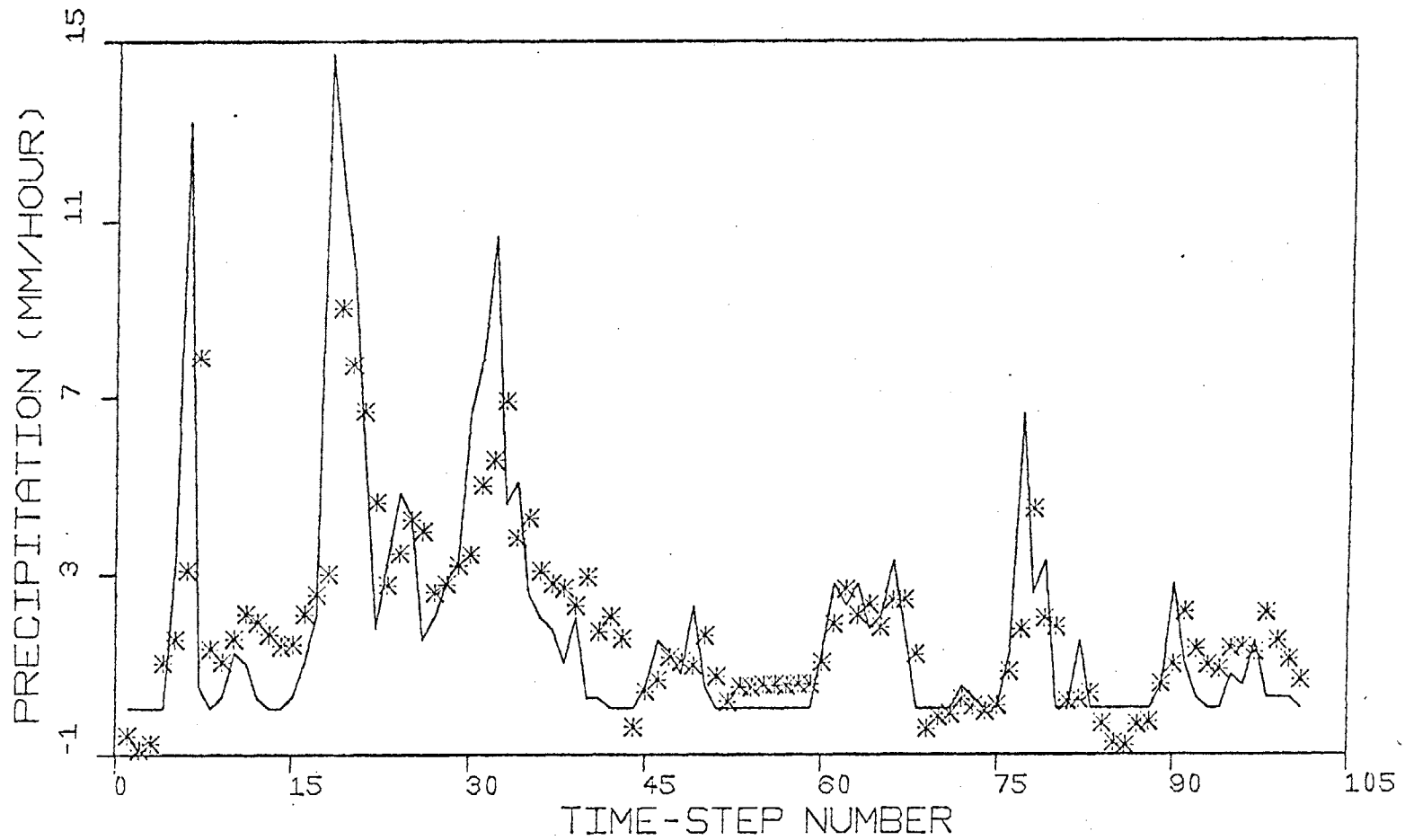


FIGURE 8.12 Precipitation rate hourly predictions (stars) based on the linear model of Table 8.8 vs. observations (solid line). Storm group 5.

Table 8.8

REGRESSION PARAMETERS AND STANDARD ERRORS
REGRESSION OF PRECIPITATION RATE ON TEMPERATURES
PRESSURE AND 1-HOUR LAGGED PRECIPITATION RATE

$$P_v(k) = A_1 \cdot T_o(k) + A_2 \cdot T_d(k) + A_3 \cdot P_o(k) + A_4 \cdot T_w(k) \\ + A_5 \cdot P_v(k-1) + A_0$$

Storm Group 1

<u>Explanatory Variable</u>	<u>Parameter Estimate</u>	<u>Standard Error</u>
Temperature:	0.14092	0.57909
Dew Point Temperature:	0.55297	0.58901
Surface Pressure:	0.00009	0.00036
Wet Bulb Temperature:	-0.7196	1.0611
Precipitation Rate (1 HOUR LAG):	0.6186	0.0842
Constant of Regression:	-1.0403	51.602

Table 8.8 (continued)

Storm Group 2

<u>Explanatory Variable</u>	<u>Parameter Estimate</u>	<u>Standard Error</u>
Temperature:	0.63004	0.73828
Dew Point Temperature:	-2.2879	0.87435
Surface Pressure:	0.000005	0.00027
Wet Bulb Temperature:	2.8935	1.3309
Precipitation Rate (1 HOUR LAG):	0.38864	0.11737
Constant of Regression:	-351.70	107.42

Table 8.8 (continued)

<u>Explanatory Variable</u>	<u>Parameter Estimate</u>	<u>Standard Error</u>
Temperature:	-0.2361	0.54064
Dew Point Temperature:	0.02507	0.32011
Surface Pressure:	0.00033	0.00015
Wet Bulb Temperature:	0.22086	0.85250
Precipitation Rate (1 HOUR LAG):	0.53395	0.11535
Constant of Regression:	-35.513	36.373

Table 8.8 (continued)

Storm Group 4

<u>Explanatory Variable</u>	<u>Parameter Estimate</u>	<u>Standard Error</u>
Temperature:	-1.9360	1.0909
Dew Point Temperature:	-1.1063	1.0139
Surface Pressure:	-0.00025	0.00071
Wet Bulb Temperature:	3.2149	2.0061
Precipitation Rate (1 HOUR LAG):	0.29207	0.13298
Constant of Regression:	-21.357	115.30

Table 8.8 (continued)

Storm Group 5

<u>Explanatory Variable</u>	<u>Parameter Estimate</u>	<u>Standard Error</u>
Temperature:	0.24412	0.58033
Dew Point Temperature:	1.4350	0.92043
Surface Pressure:	-0.00031	1.4496
Precipitation Rate (1 HOUR LAG):	0.48477	0.09007
Constant of Regression:	89.642	103.77

Table 8.8. Examination of the parameter estimates of Table 8.8 shows considerable differences from one storm group to another. The figures show improvement over the previous set of regressions, although some prediction delays are still observed. Some negative values were also predicted. This set of predictions will be compared to the predictions of the stochastic station precipitation model.

8.3 Station Precipitation Model Parameter Determination

For the purposes of this work and as a first step toward the testing of the precipitation model developed, uniform vertical velocity profile with height is assumed. Similarly, the distribution of the parameter c (inverse average level diameter) with height was taken to be uniform. Under those assumptions $\beta = 1$ (Eq. 5.43), and $\gamma = 1$ (Eq. 4.13). No dependency of the parameter c on the updraft velocity was considered, $m = 0$ (Eq. 5.42). This implies constant average level diameter for all storms and at all times. The value of parameter ϵ_3 (Eq. 5.39) was taken equal to 1 [SEC/M] which is the order of magnitude of the inverse updraft velocity v . Parameter ϵ_2 (Eq. 5.39) was set at the 700 [MBAR] level. Therefore, the cloud top was allowed to vary from the level of 700 [MBAR] to a level of 200 [MBAR] for all cases. For all the model runs to follow, the initial condition X_0 of the state (mass of condensed liquid water equivalent in cloud storage) was taken equal to 1 [KG/M²]. With those values for β , γ , ϵ_3 , ϵ_2 , and X_0 , the model was used with input-output data

to determine the values of the remaining two parameters: ϵ_1 (Eq. 5.34) and ϵ_4 (Eq. 5.42). Storm group 2 consisting of only one storm, was selected as the calibration period.

Three model performance criteria were considered. The average error in predicting the precipitation rate, the residual standard deviation and the cross-correlation coefficient, E_3 , between the model prediction and the observations. The first indicates the extent to which the model produces the volume of precipitation observed. The second is the standard least squares criterion. The third was included to indicate undesirable lags between observations and predictions. Its value ranges from -1, for worst performance, to 1, for perfect performance. Normalized quantities for the first and second criteria were used for calibration. Those were the absolute proportional average error E_1 and the proportional standard error E_2 . E_1 is obtained by dividing the residual mean by the observed mean precipitation rate mean and taking the absolute value of the ratio. Perfect performance leads to a value of E_1 equal to zero. E_2 results by division of the residual standard deviation with the observed precipitation rate standard deviation. Perfect performance yields a value of E_2 equal to zero. Figures 8.13 to 8.15 present contours of E_1 , E_2 , and E_3 , respectively, in the space of the parameters ϵ_1 (ordinate) and ϵ_4 (abscissa). Parameter ϵ_1 ranged from 10^{-4} to 1.5×10^{-2} , while parameter ϵ_4 ranged from 10^{-5} [M] to 10^{-4} [M]. The computational discretization intervals, corresponding to the

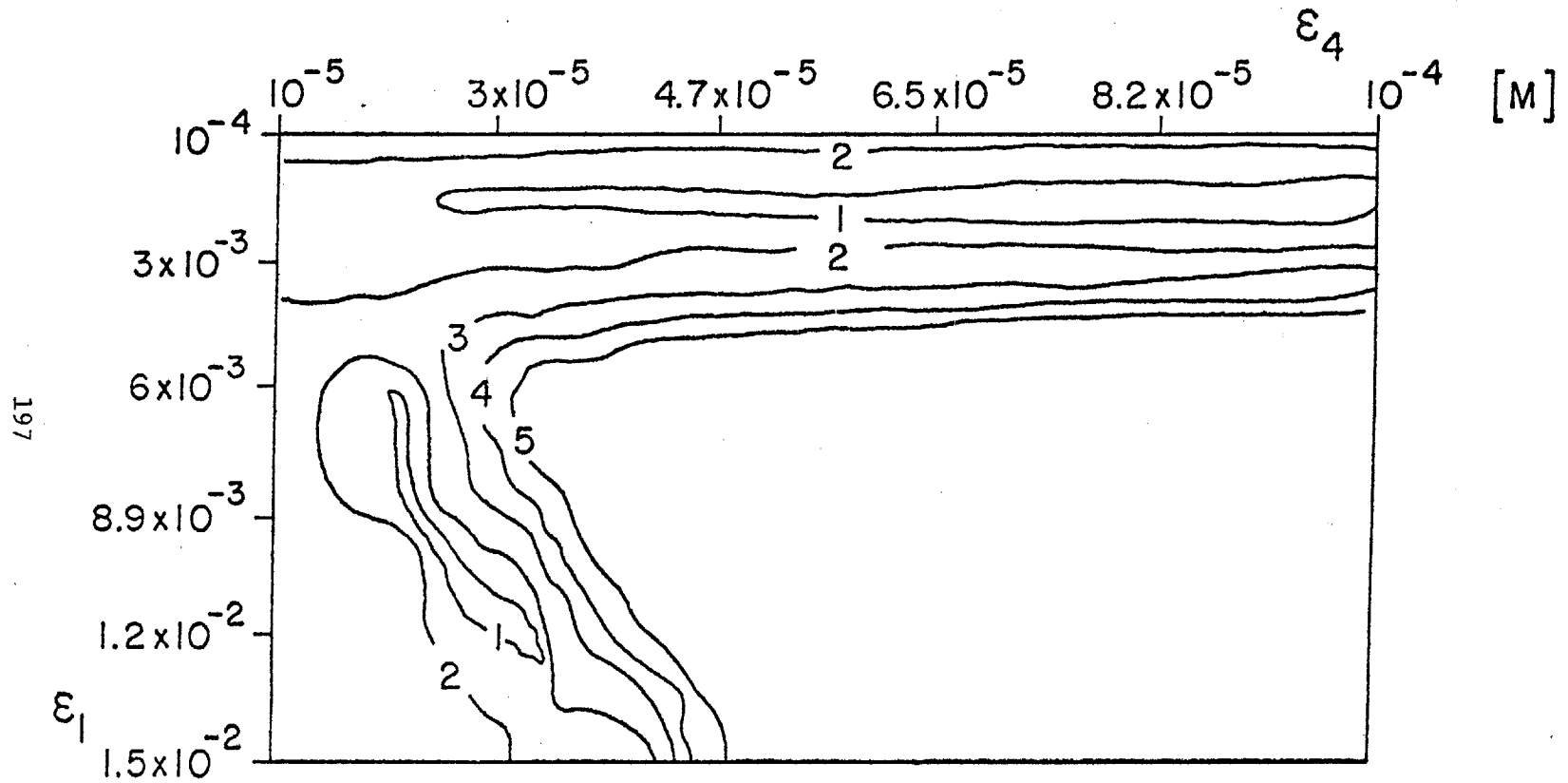


FIGURE 8.13 Absolute proportional average error (E_1). Storm group 2.
 Contour values: 1 = 0.24, 2 = 0.73, 3 = 1.21, 4 = 1.70, 5 = 2.18.

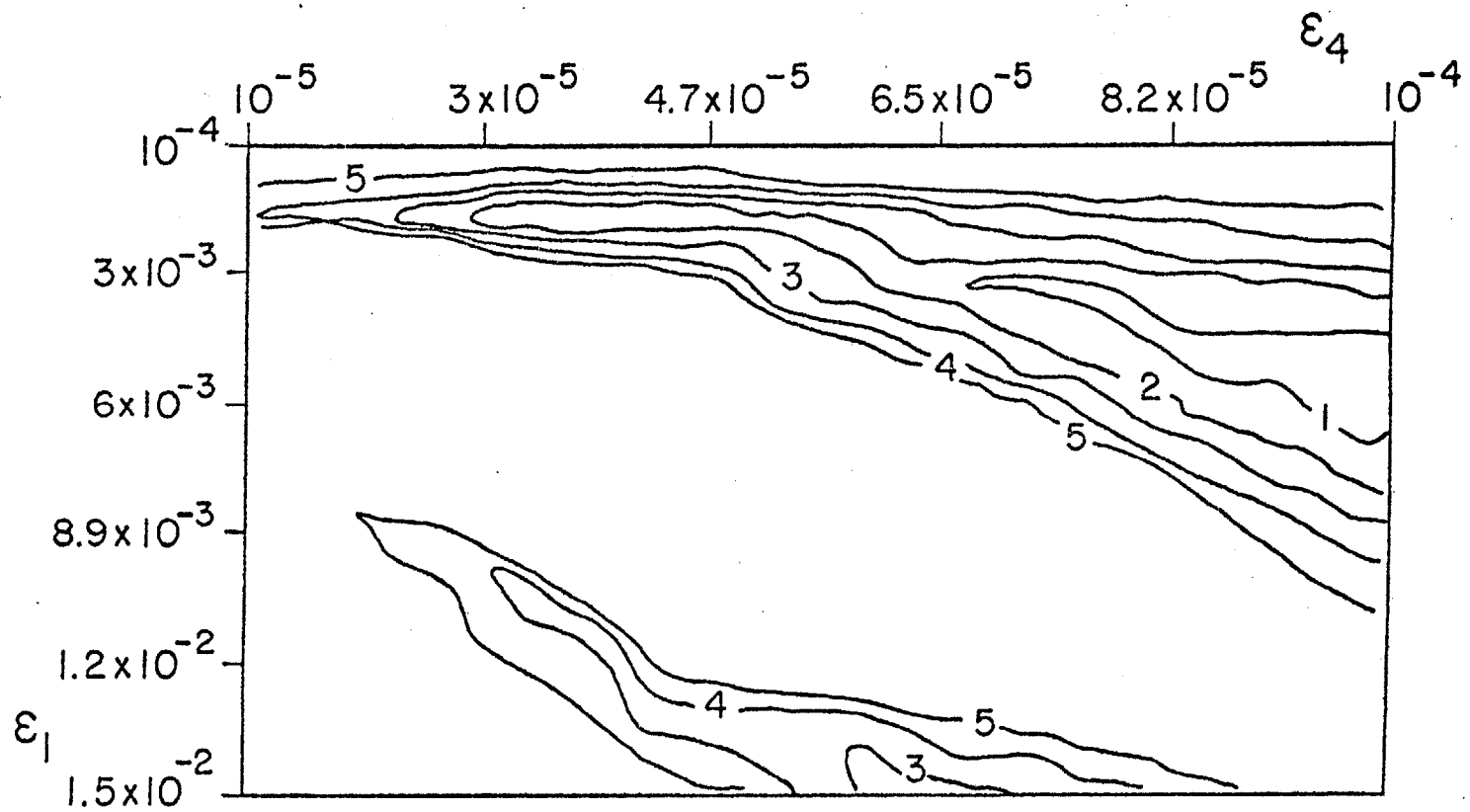


FIGURE 8.14 Proportional standard error (E_2). Storm group 2 Contour values: 1 = 0.942, 2 = 0.948, 3 = 0.954, 4 = 0.960, 5 = 0.966

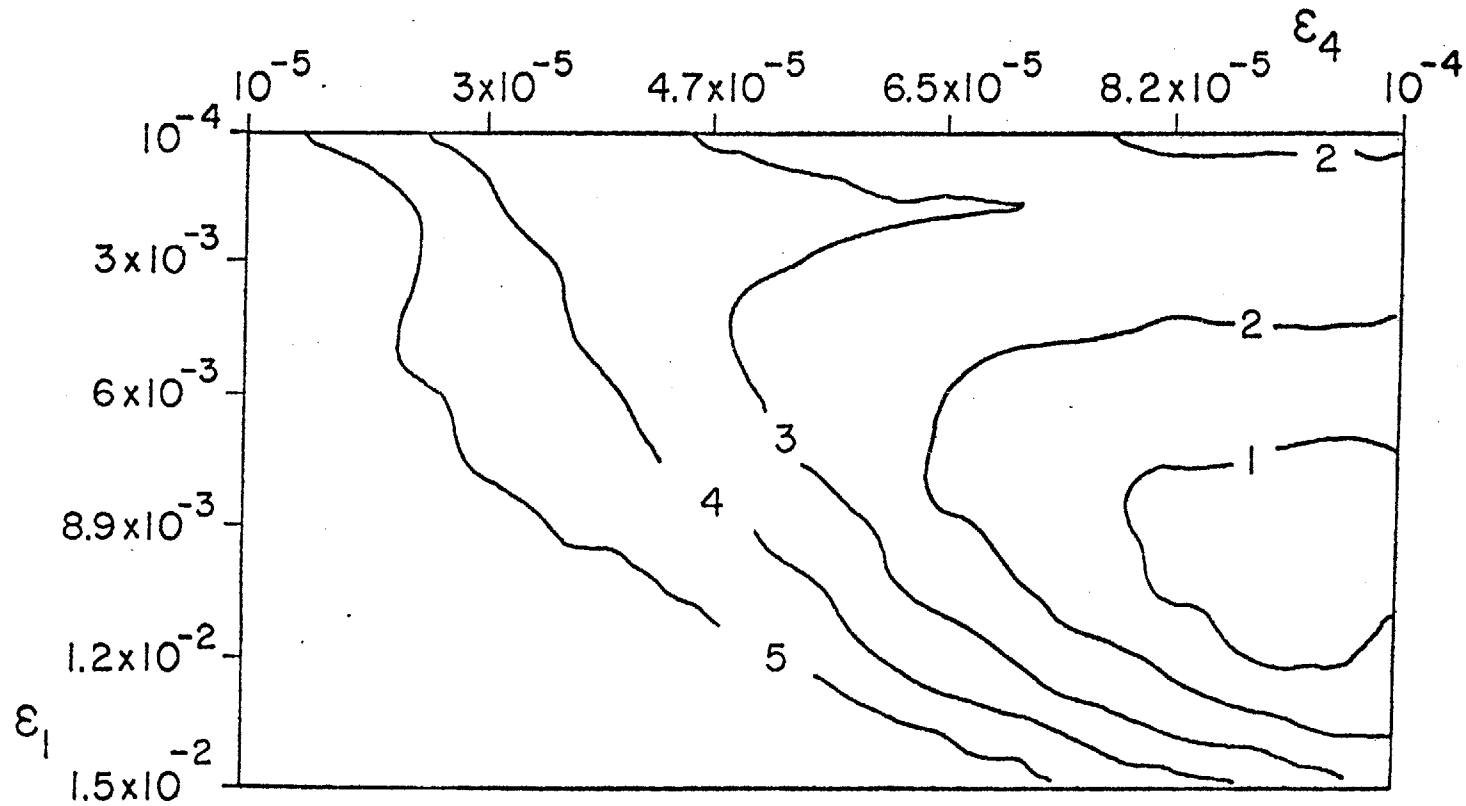


FIGURE 8.15 Cross-correlation coefficient of observations and predictions (E_3). Storm group 2 Contour values: 1 = 0.351, 2 = 0.344, 3 = 0.337, 4 = 0.330, 5 = 0.323

estimation accuracy in this case, were 1.4×10^{-3} for ϵ_1 and 9.8×10^{-6} [M] for ϵ_4 . Note that given $m = 0$, ϵ_4 is the average diameter, assumed constant.

Examination of Figures 8.13 to 8.15 reveals that different parameter sets optimize the different criteria for the selected calibration period. Thus, good least squares performance does not guarantee equally good performance in the cross-correlation coefficient E_3 .

Notable is also the fact that changes in the value of one of the parameters result in drastic changes in the gradient of the performance index E_1 with respect to the other parameter. Thus, a value of about 2×10^{-3} for ϵ_1 gives regions of very mild E_1 gradient with respect to ϵ_4 . For E_1 near 9×10^{-3} sharp changes in E_1 occur by changing ϵ_4 . Multiple optima occur for E_1 and possibly (for high values of ϵ_1) for E_2 . Index E_3 was used to decide between these optima. For example, the depressions in the lower left part of Figures 8.13 and 8.14 were excluded due to their lower value of E_3 .

Even with the exclusion of the lower left part of all figures as a possible optimum, a choice between the parameter sets that optimize the different performance indices has to be made.

E_1 was heavily weighted due to the importance of preserving total precipitation volume and due to its sensitivity to parameter ϵ_1 . The region of the limited ϵ_1 , ϵ_4 space that gives both good performance with respect to E_1 and to E_2 is the one defined by

ϵ_1 in the range 1.5×10^{-3} to 2.5×10^{-3} and ϵ_4 in the range 3×10^{-5} [M] to 5.5×10^{-5} [M]. A choice of $\epsilon_1 = 2 \times 10^{-3}$ and $\epsilon_4 = 4.5 \times 10^{-5}$ [M] in the prespecified region was arbitrarily made.

The sensitivity to the value of the ill defined constant c_1 for snow diffusion losses (Eq. 4.41) was studied next for the case of the snowstorm group 3. Two values of c_1 , the one obtained in Section 4.5 for rain, $c_1 (= 7 \times 10^5 \text{ [KG/(M}^3\text{SEC)]}$), and the one estimated for snow, $c_1 (= 1.4 \times 10^5 \text{ [KG/M}^3\text{SEC)]}$ were examined. Contours of E_1 and E_2 for ϵ_1 in the range 10^{-4} to 1.3×10^{-2} and ϵ_4 in the range 1.2×10^{-5} to 10^{-4} were obtained for both values of c_1 . Those are shown in Figures 8.16 through 8.19. The computational discretization interval was 2.6×10^{-3} for ϵ_1 and 1.8×10^{-5} [M] for ϵ_4 .

No significant changes are observed among the different plots corresponding to E_1 and E_2 other than a shift to a higher optimal value of ϵ_4 when c_1 changes from 7×10^5 to $1.4 \times 10^5 \text{ [KG/(M}^3\text{SEC)]}$. Choosing a value of $c_1 = 1.4 \times 10^5$ for snowstorm, group 3, leads to parameters ϵ_1 and ϵ_4 similar to the ones already obtained using group 2 (rainfall) data.

In summary, c_1 was taken as 1.4×10^5 for group 3 and 7×10^5 for all other groups. Parameters ϵ_1 and ϵ_4 took values of 2×10^{-3} and 4.5×10^{-5} , respectively, for all groups.

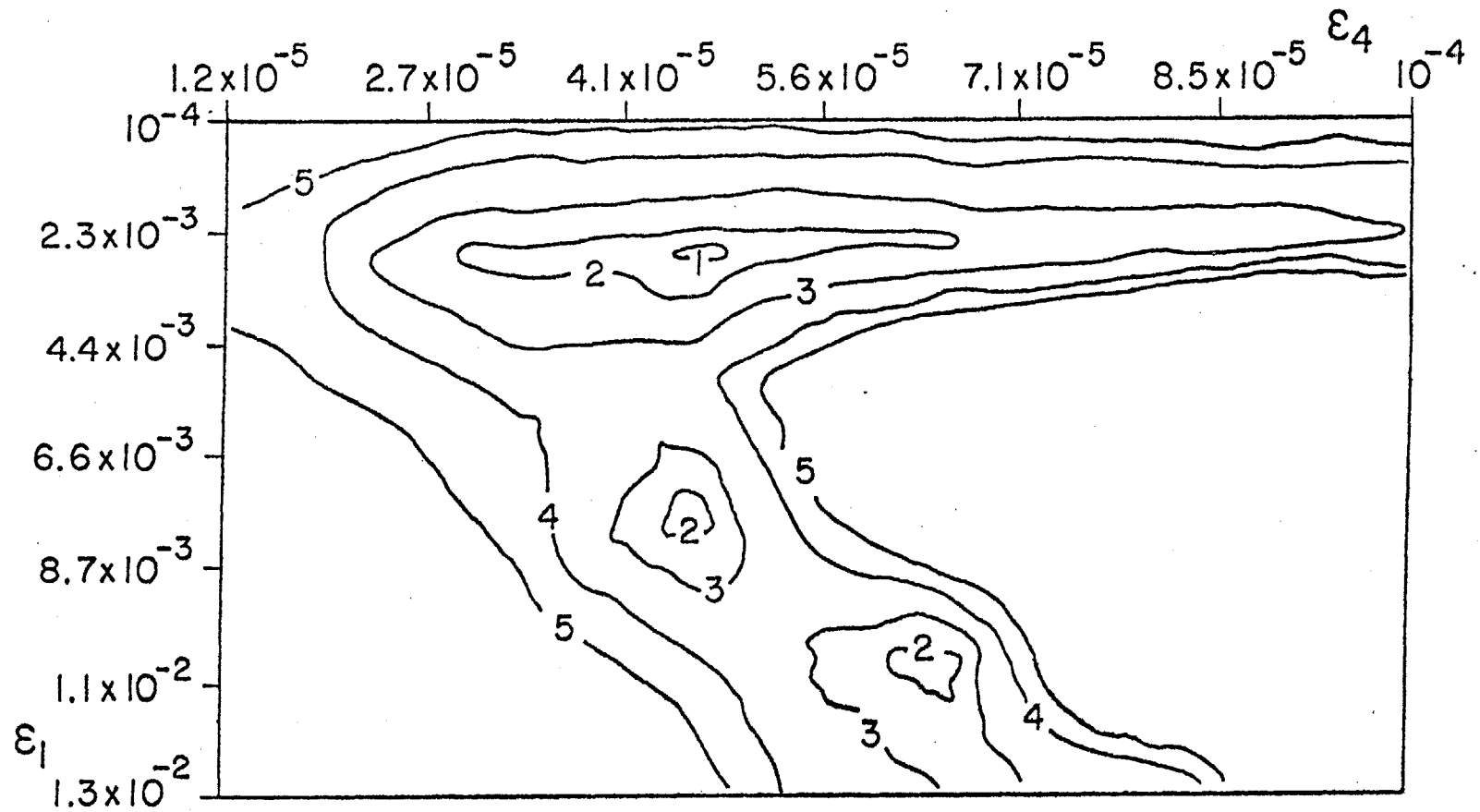


FIGURE 8.16 Absolute proportional average error (E_1). Storm group 3 ($c_1 = 1.4 \times 10^5$ [KG/M³/SEC]). Contour values: 1 = 0.1, 2 = 0.3, 3 = 0.5, 4 = 0.7, 5 = 0.9

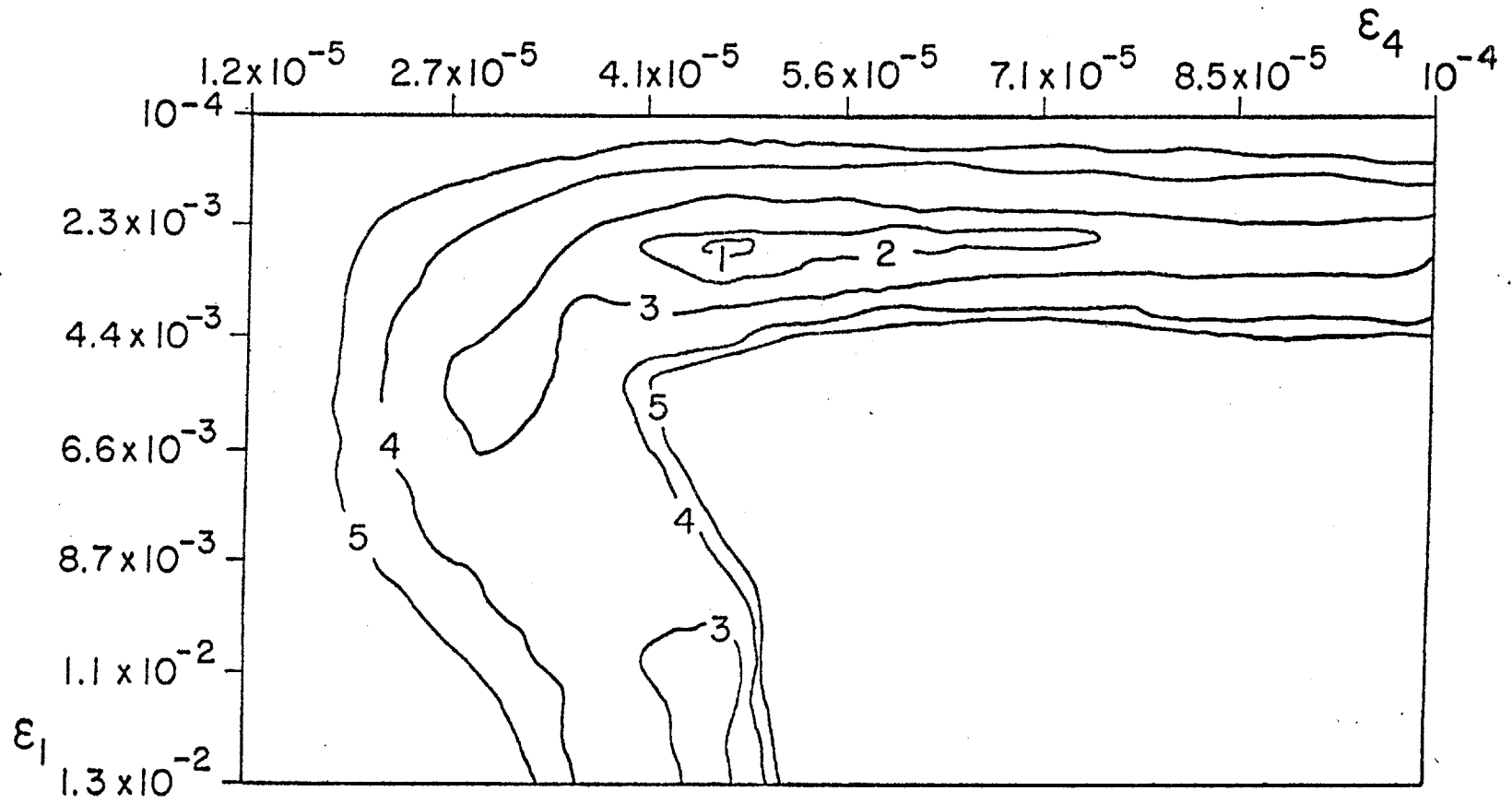


FIGURE 8.17 Proportional standard error (E_2). Storm group 3 ($c_1 = 1.4 \times 10^5$ [KG/M³/SEC]).
Contour values: 1 = 0.84, 2 = 0.87, 3 = 0.90, 4 = 0.93, 5 = 0.96

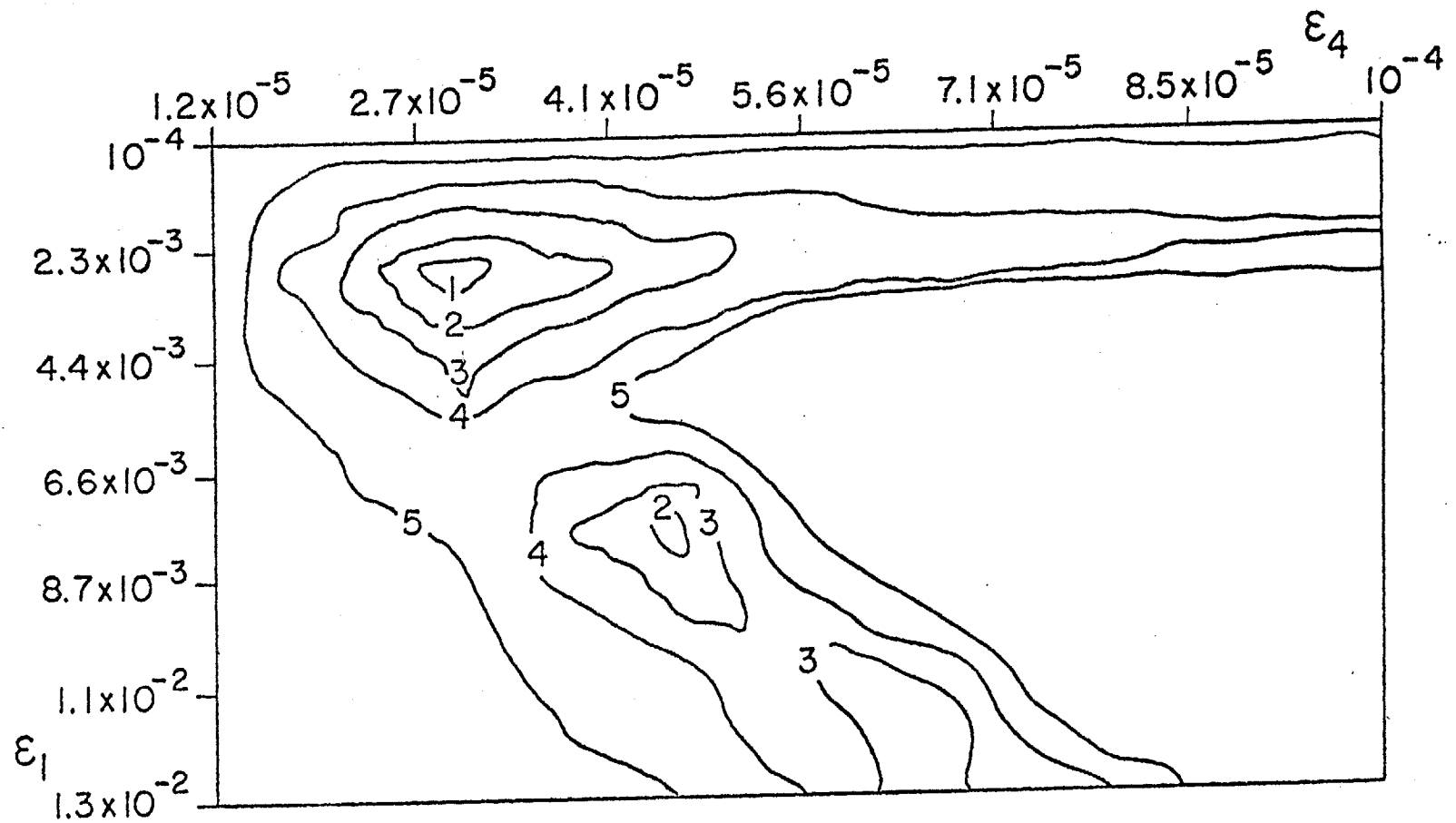


FIGURE 8.18 Absolute proportional average error (E_1). Storm group 3 ($c_1 = 7 \times 10^5$ [KG/M³/SEC]). Contour values: 1 = 0.1, 2 = 0.3, 3 = 0.5, 4 = 0.7, 5 = 0.9

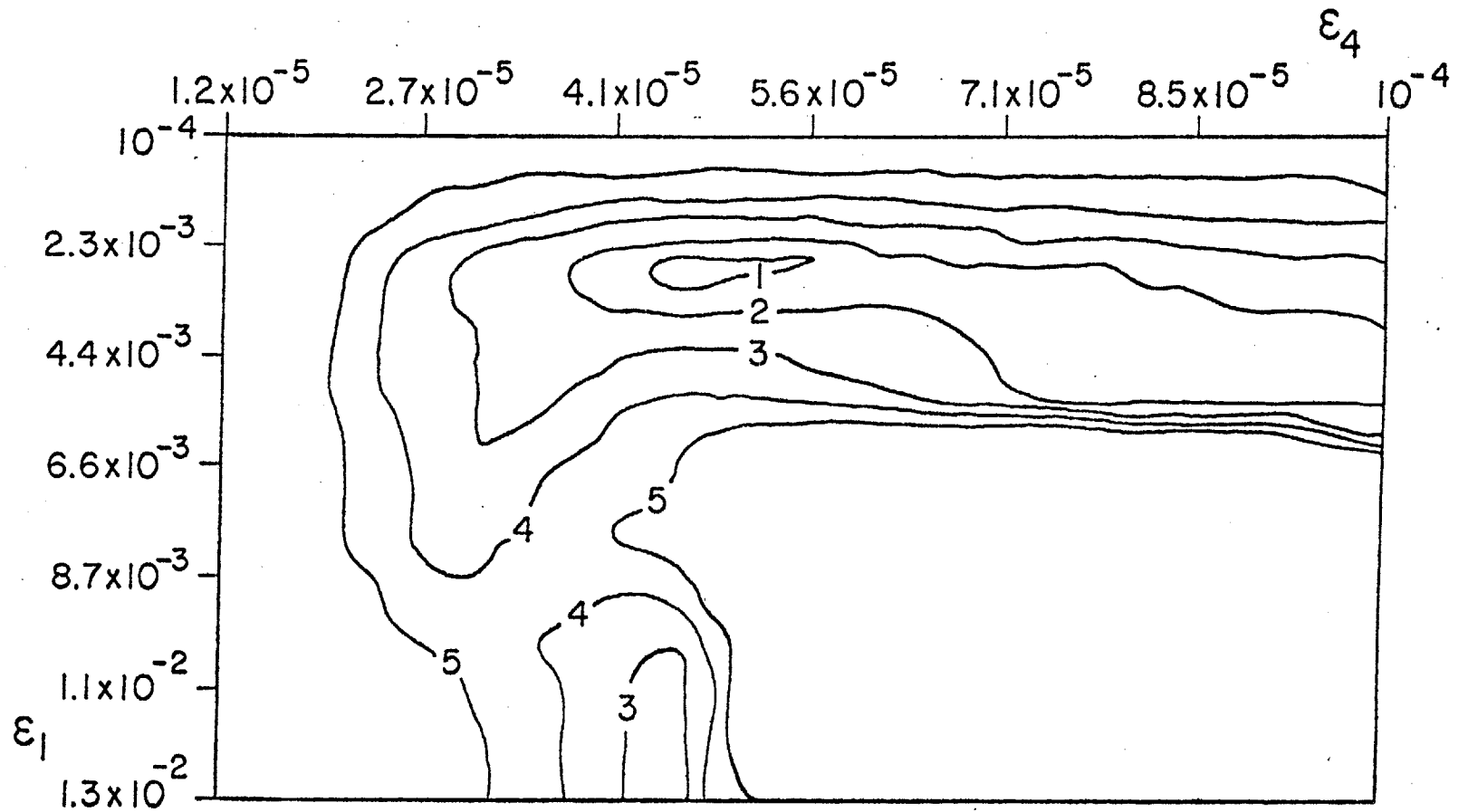


FIGURE 8.19 Proportional standard error (E_2). Storm group 3 ($c_1 = 7 \times 10^5$ [KG/M³/SEC]). Contour values: 1 = 0.84, 2 = 0.87, 3 = 0.90, 4 = 0.93, 5 = 0.96

8.4 Deterministic Station Precipitation Model

The precipitation model developed in the first five chapters was used to forecast the hourly precipitation rate for all storm groups, with the parameters obtained in the previous section. The input at all times was equal to the current observed value for the meteorological parameters. Performance is judged by the values of the following measures:

- 1) residual mean
- 2) residual standard deviation
- 3) lag-1 correlation coefficient of residuals
- 4) coefficient of efficiency
- 5) coefficient of determination
- 6) coefficient of persistence
- 7) coefficient of extrapolation, and
- 8) comparison to the regression runs of section 8.2 that used the same input and were locally calibrated for all storm groups.

The residual at each time is equal to the difference between the predicted precipitation rate and the observed one. The performance indices (4) through (7) were introduced in hydrologic forecasting by Kitanidis and Bras (1980b). The coefficient of efficiency is a measure of the residual squared error, as it compares to the squared error of the quantity to be forecasted. A perfect value is 1. Negative values indicate large residuals relative to the scale of the observations. The coefficient of determination compares the residual

squared error to the squared error of the observations after the linear trends have been removed from the residual time series by regression. Comparison of the coefficients of efficiency and determination allows assessment of the possible model systematic errors. The coefficient of persistence compares the model prediction to a simple model that predicts the previous observation. Thus, negative values of this measure indicate that in the least squares sense the model is worst than no-model persistence. The coefficient of extrapolation compares the model predictions to the observations of a linear extrapolator using the latest observations (in this work the latest two).

The residual mean multiplied by the number of storm time-steps gives the accumulated volume error in predicting precipitation.

Figures 8.20 to 8.24 show the 1-hour lead forecasts of the precipitation rate [MM/HOUR], in dashed lines, together with the corresponding observations, in solid lines, for storm groups 1 to 5, respectively.

Table 8.9 gives the residual mean, standard deviations and three auto-correlation coefficients for each storm group together with the residual standard deviation of the regressions discussed in Section 8.2. Keep in mind that those regressions were calibrated to each group individually, therefore representing the best possible linear fit. Table 8.10 gives the least squares performance measures [items (4) to (7)] for each storm group.

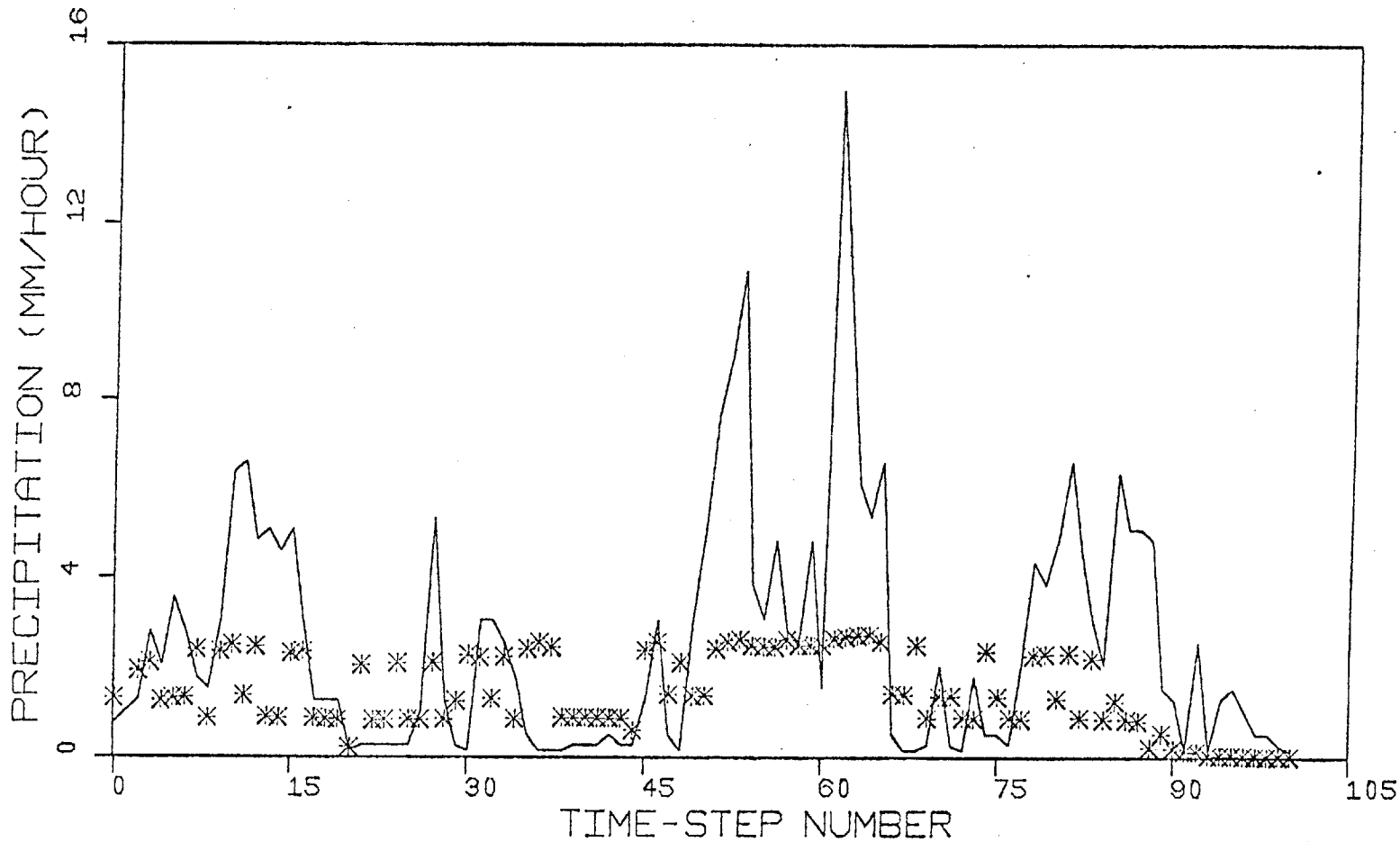


FIGURE 8.20 Deterministic precipitation model hourly predictions (stars) vs. observations (solid line). Storm group 1

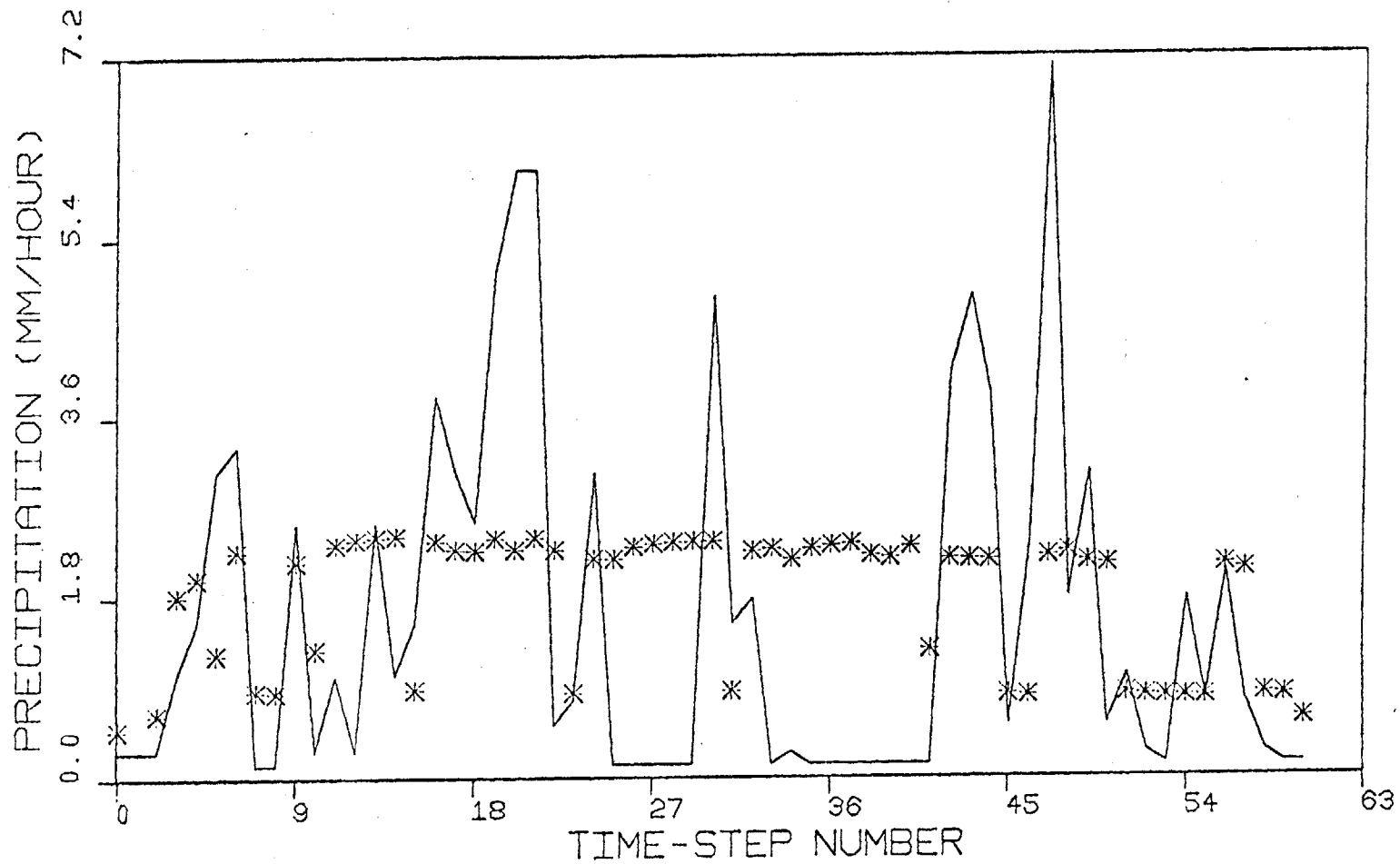


FIGURE 8.21 Deterministic precipitation model hourly predictions (stars) vs. observations (solid line). Storm group 2

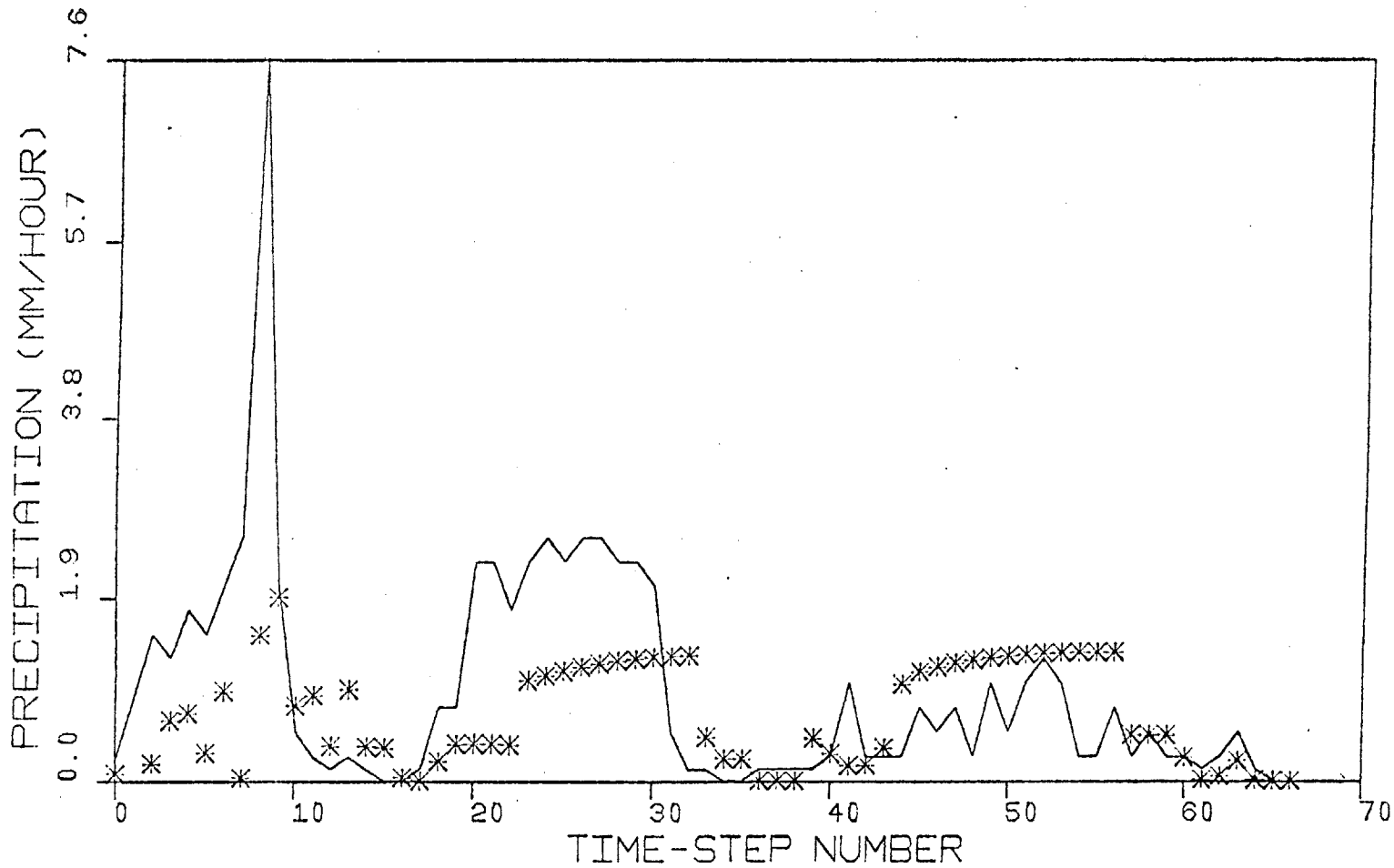


FIGURE 8.22 Deterministic precipitation model hourly predictions (stars) vs. observations (solid line). Storm group 3

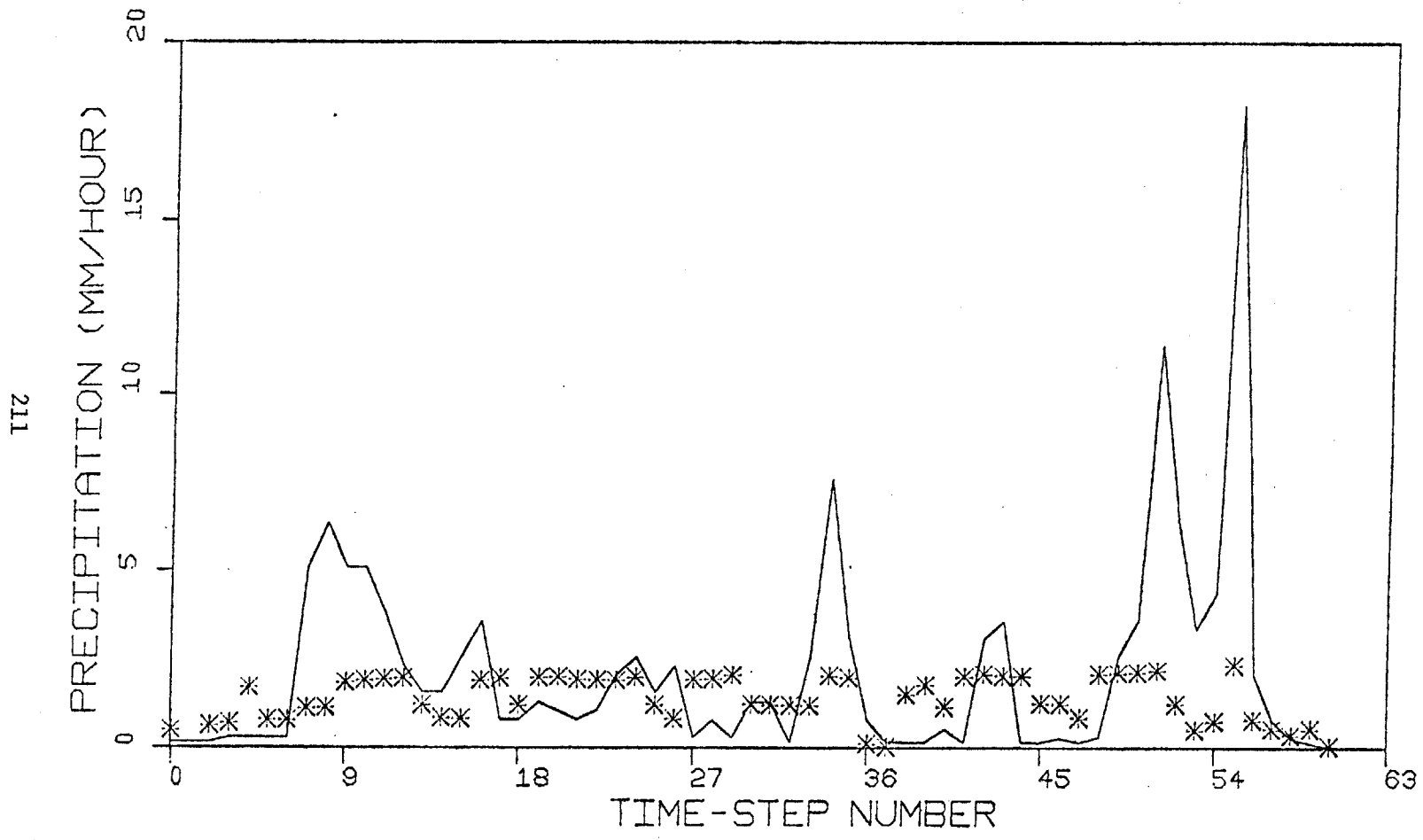


FIGURE 8.23 Deterministic precipitation model hourly predictions (stars) vs. observations (solid line). Storm group 4

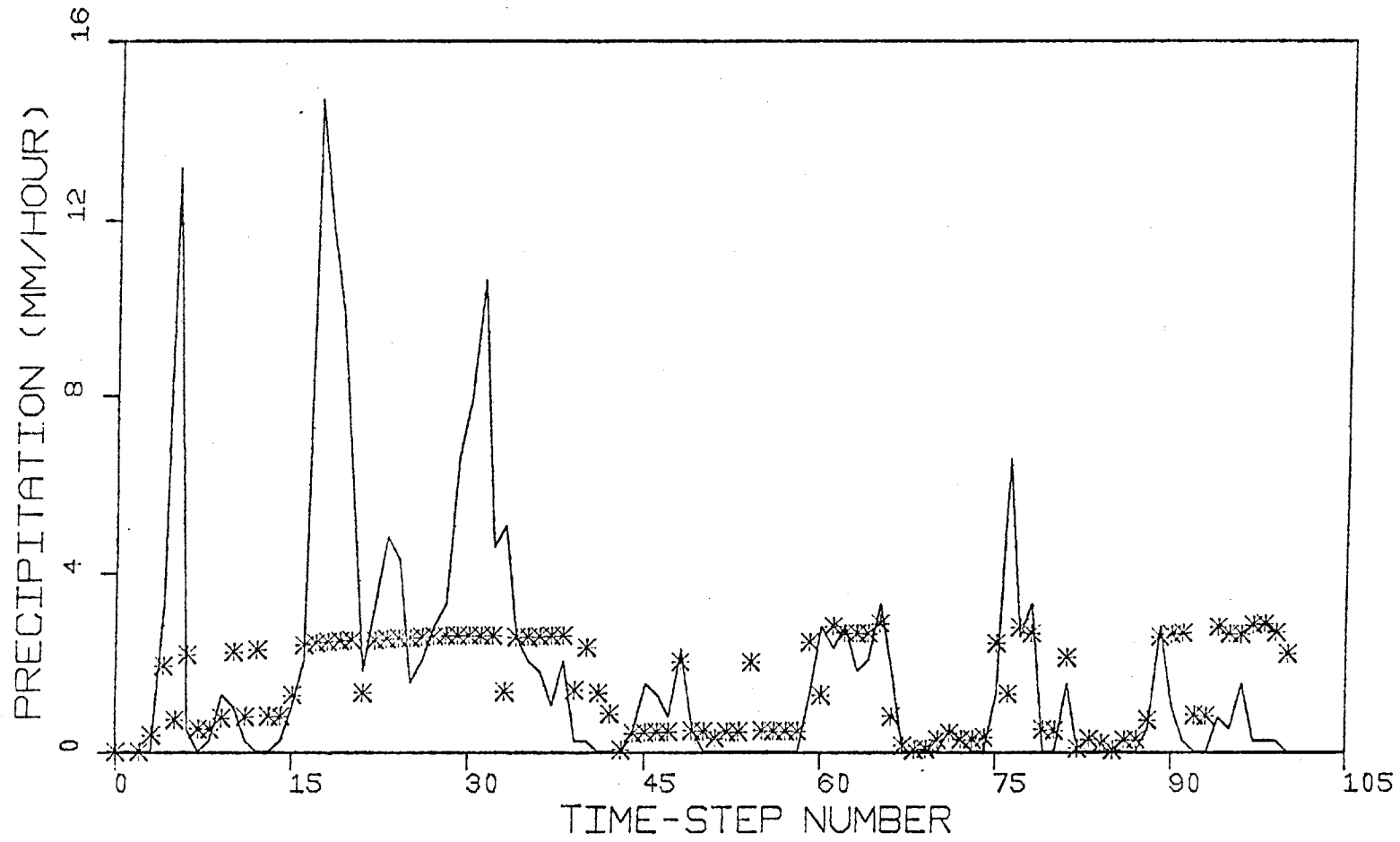


FIGURE 8.24 Deterministic precipitation model hourly predictions (stars) vs. observations (solid line). Storm group 5

Table 8.9

DETERMINISTIC PRECIPITATION MODEL
RESIDUAL STATISTICS FOR STORM GROUPS 1 TO 5

<u>Statistic</u>	<u>Group:</u>	<u>1</u>	<u>2</u>	<u>3</u>	<u>4</u>	<u>5</u>
Mean [MM/HOUR]:		1.09	-0.23	0.28	0.82	0.31
Standard Deviation [MM/HOUR]:		2.49	1.701	1.10	2.91	2.68
Lag-1 Auto-Correlation:		0.56	0.46	0.57	0.41	0.47
Lag-2 Auto-Correlation:		0.34	0.22	0.36	0.20	0.31
Lag-3 Auto-Correlation:		0.21	0.12	0.26	0.16	0.13
Regression Residual Standard Deviation:		2.64	1.63	1.08	2.94	2.60

Table 8.10

DETERMINISTIC PRECIPITATION MODEL
 LEAST SQUARES PERFORMANCE MEASURES FOR STORM GROUPS 1 TO 5

<u>Description</u>	<u>Group:</u>	<u>1</u>	<u>2</u>	<u>3</u>	<u>4</u>	<u>5</u>
Efficiency Coefficient:		0.02	0.10	0.12	0.03	0.15
Determination Coefficient:		0.19	0.12	0.17	0.13	0.16
Persistence Coefficient:		-0.39	0.23	-0.12	0.23	-0.10
Extrapolation Coefficient:		0.44	0.71	0.55	0.70	0.54

Examination of Table 8.9 indicates that the deterministic model performance, with parameters estimated only with data of group 2, is comparable in the least squares sense, to the locally calibrated regressions. In some cases, groups 1 and 4, the precipitation model had better performance. The value of the residual means of Table 8.9 implies that in all cases volume preservation was satisfactory. The relatively high correlation values are indicative of possible improvement when the precipitation model is complemented by a filter.

The performance measures of Table 8.10 point to the low efficiency of the deterministic model. The difference between the coefficient of determination and the coefficient of efficiency indicate systematic errors in some of the predictions. Some cases had negative persistence coefficients, implying poor performance at a 1-hour lead forecast relative to a simple persistence model. The extrapolation coefficient was large for most storm groups, indicating better performance than linear extrapolation.

It should be noted that the precipitation model proposed can predict the beginning and ending of the precipitation based on the temperature and pressure input. Therefore, when the forecasts of no-rain or no-snow are taken into consideration for a continuous period of record, performance is considerably improved.

Characteristic to the deterministic model is its deficiency predicting excessively high precipitation rates. It does a rather good job in predicting the no rain periods. This suggests the examination of values of m , β , and γ other than the

ones arbitrarily selected in this calibration. The diffusion losses part of the model seems to respond properly to observed input.

8.5 Stochastic Station Precipitation Model

The station precipitation model performance in a stochastic feedback mode was studied next. The linear Gaussian filter of Chapter 7 was utilized. The input error standard deviation for temperature and dew point were set to 1 [$^{\circ}$ K], while no error was assumed for the pressure input. Zero correlation in the errors of the different input variables was assumed. The observation error standard deviation took the value 1 [MM/HOUR], while the model error spectral density was set equal to 0.01 [(KG/M)²/SEC]. This spectral density adds about $0.01 \times 3600 = 36$ (KG/M)² to the state variance at each step when the order of magnitude of X is about 10[KG/M]. Such a high value of the model error spectral density was considered necessary in order to avoid filter divergence. The initial state standard deviation was 0.3 [KG/M²]. No sensitivity analysis was performed for any of the filter parameters.

Performance was judged as in the case of deterministic model forecasts. Now, however, the filter predictions are compared to the set of individually fitted regressions in Figures 8.8 to 8.12, that use the previous precipitation value. Figures 8.25 to 8.29 show the model forecasts (dashed line) together with the corresponding hourly precipitation rate (solid line).

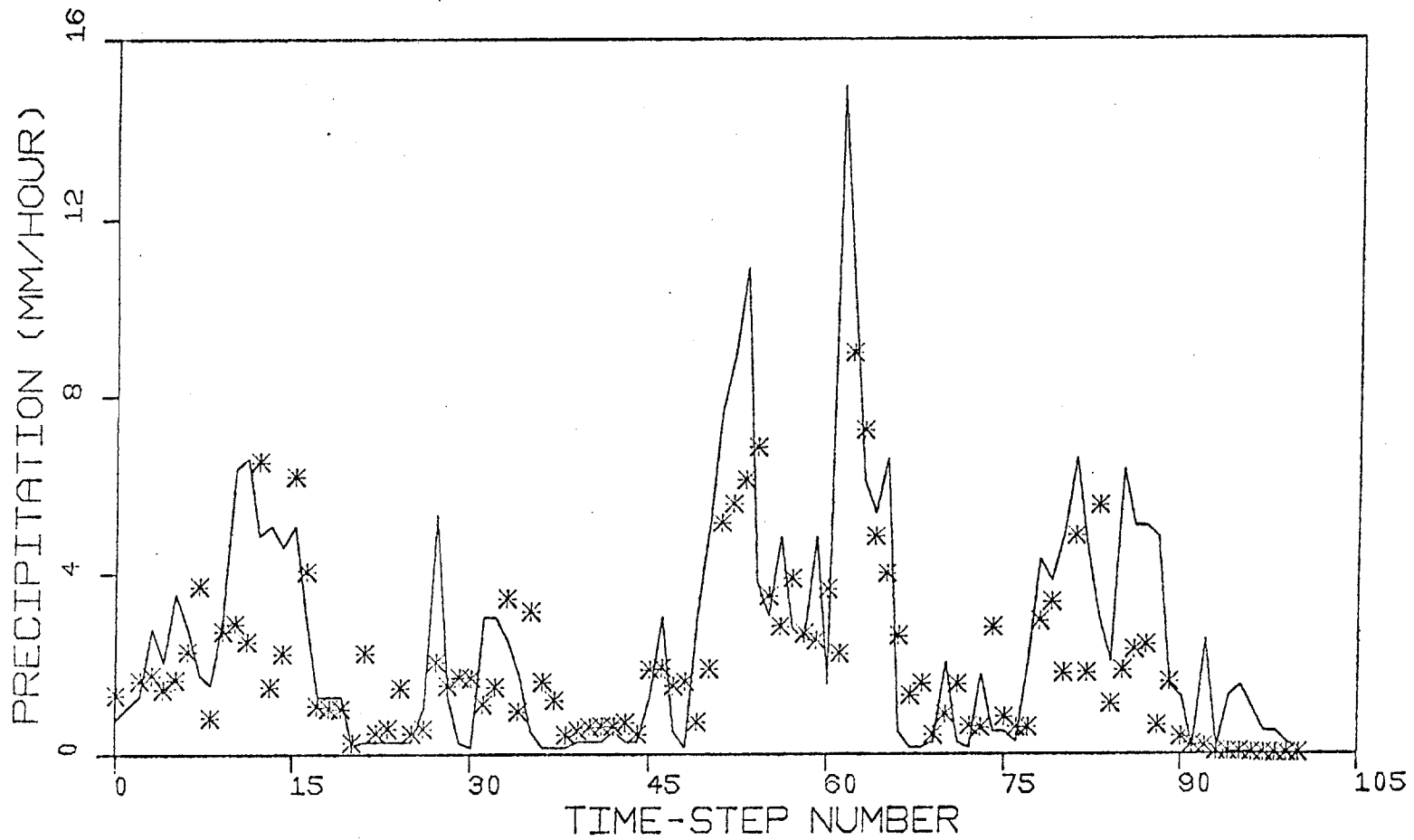


FIGURE 8.25 Stochastic precipitation model hourly predictions (stars) vs. observations (solid line). Storm group 1.

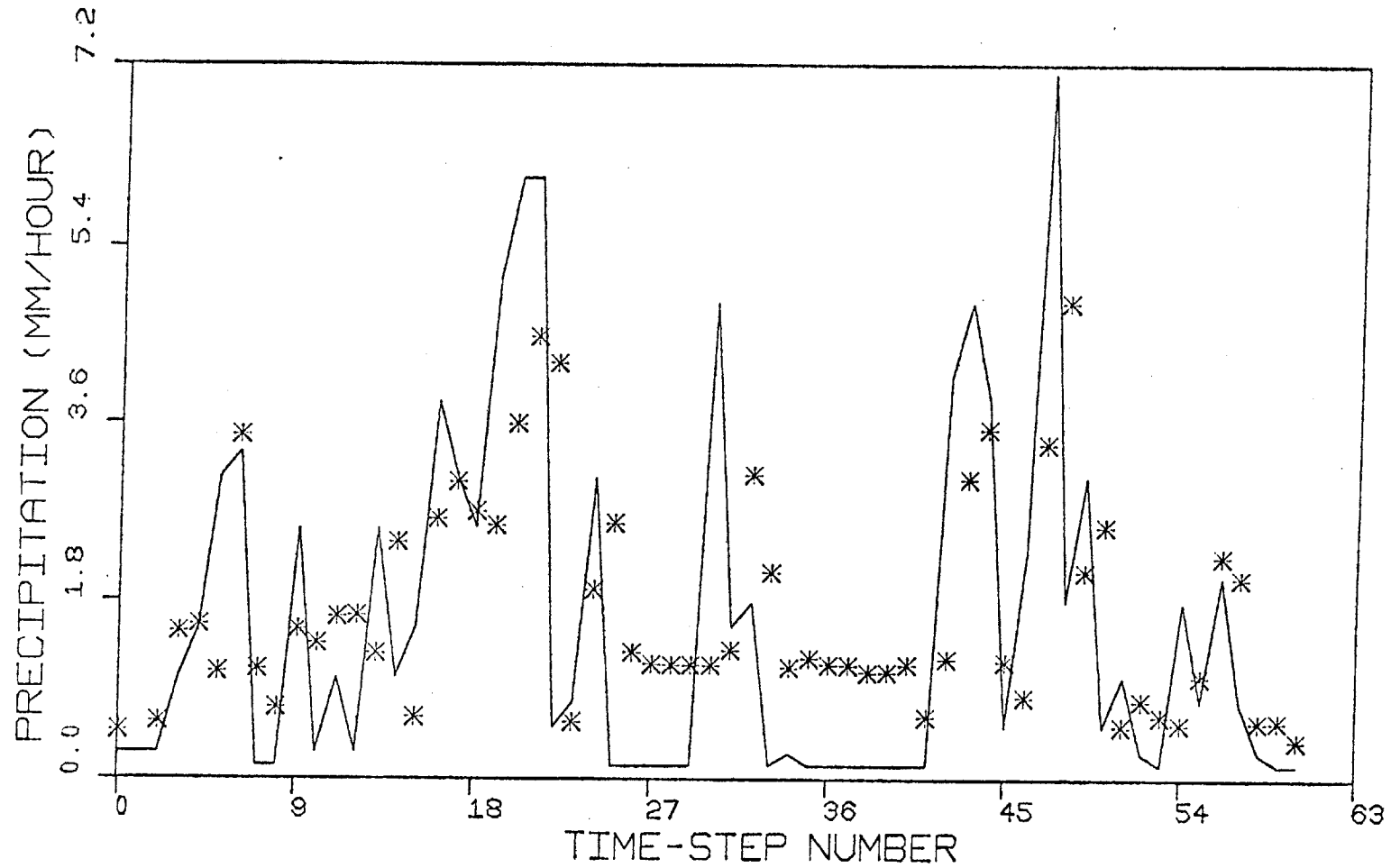


FIGURE 8.26 Stochastic precipitation model hourly predictions (stars) vs. observations (solid line). Storm group 2

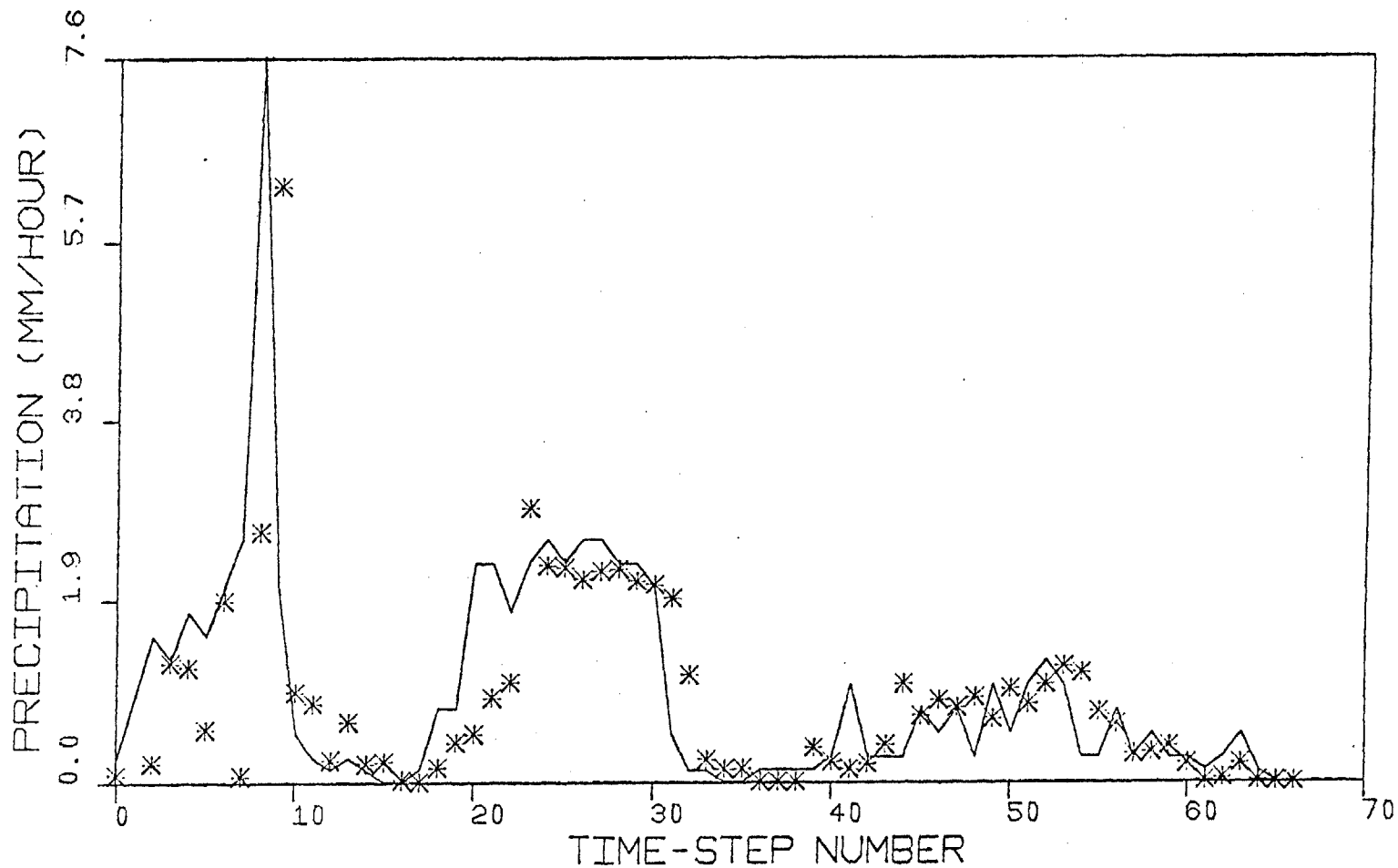


FIGURE 8.27 Stochastic precipitation model hourly predictions (stars) vs. observations (solid line). Storm group 3.

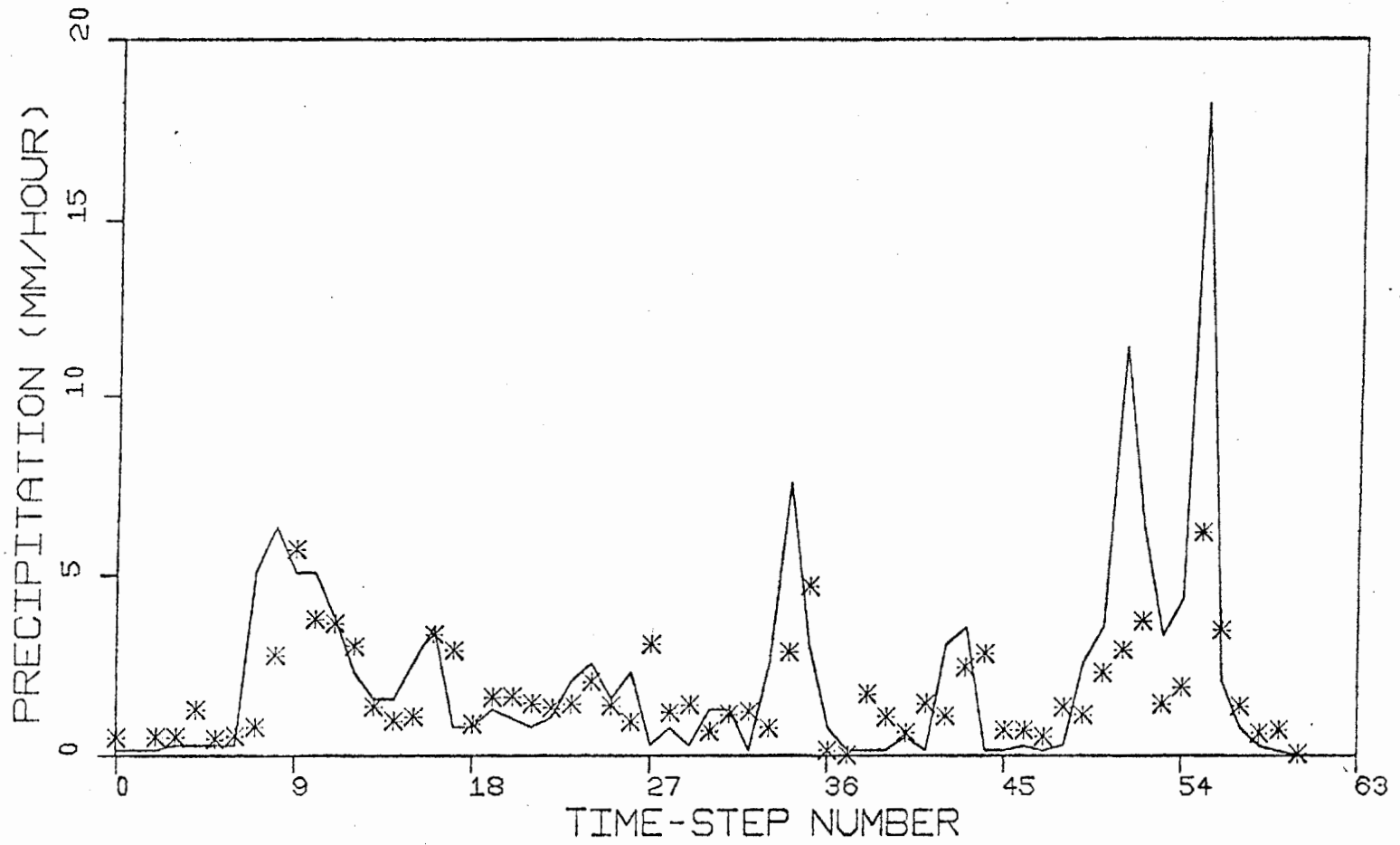


FIGURE 8.28 Stochastic precipitation model hourly predictions (stars) vs. observations (solid line). Storm group 4.

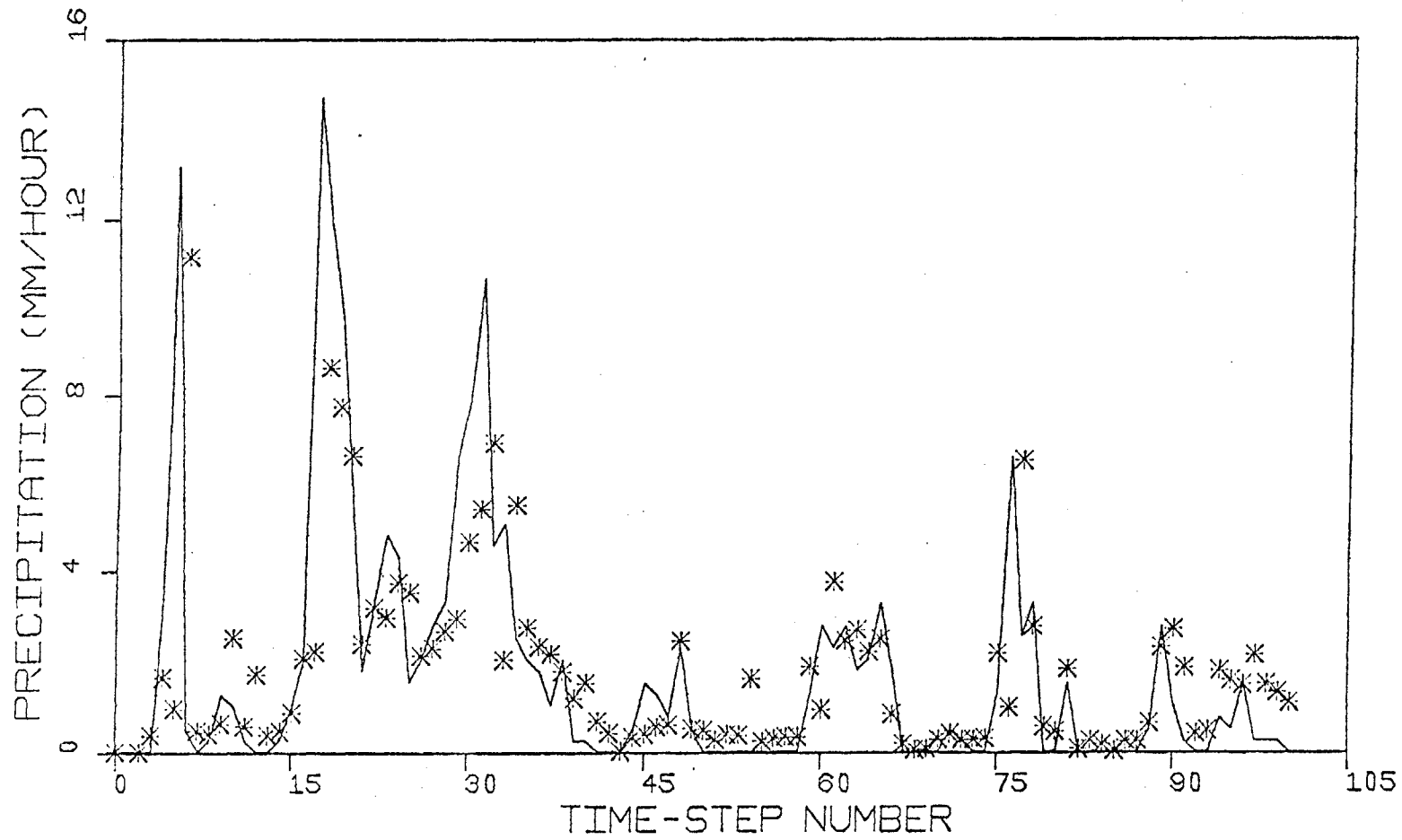


FIGURE 8.29 Stochastic precipitation model hourly predictions (stars) vs. observation (solid line). Storm group 5.

Table 8.11

STOCHASTIC PRECIPITATION MODEL
RESIDUAL STATISTICS FOR STORM GROUPS 1 TO 5

<u>Statistic</u>	<u>Group:</u>	<u>1</u>	<u>2</u>	<u>3</u>	<u>4</u>	<u>5</u>
Mean:		0.58	-0.15	0.104	0.49	0.06
Standard Deviation:		2.01	1.43	0.96	2.20	2.4
Lag-1 Auto-Correlation:		0.058	0.01	-0.003	0.16	-0.12
Lag-2 Auto-Correlation:		0.009	-0.07	-0.058	0.07	0.09
Lag-3 Auto-Correlation:		0.1	-0.05	0.04	0.10	-0.04
Regression Residual Standard Deviation:		2.12	1.51	0.94	2.90	2.30

Table 8.12

STOCHASTIC PRECIPITATION MODEL
 LEAST SQUARES PERFORMANCE MEASURES FOR STORM GROUPS 1 TO 5

<u>Description</u>	<u>Group:</u>	<u>1</u>	<u>2</u>	<u>3</u>	<u>4</u>	<u>5</u>
Efficiency Coefficient		0.36	0.33	0.28	0.38	0.28
Determination Coefficient		0.41	0.33	0.35	0.46	0.30
Persistence Coefficient		0.10	0.43	0.08	0.50	0.07
Extrapolation Coefficient		0.63	0.78	0.63	0.81	0.61

Tables 8.11 and 8.12 correspond to the deterministic forecasts Tables 8.9 and 8.10. Considerable improvement is noted for all storm groups.

The values of the residual mean have all been reduced such that preservation of precipitation volume is even more successful in this case. The standard deviations of the residuals and the auto-correlations confirm good filter performance.

Comparison of the filter forecasts to the locally calibrated regression forecasts (see also standard deviations in Table 8.11) support the robustness and reasonableness of the storm independence of the suggested rainfall model.

Considerable improvement (Table 8.12) in the efficiency measures is observed, relative to the deterministic case.

All persistence coefficients are now positive and the efficiency has risen an order of magnitude in some cases. Examples of the model performance for longer forecast lead times using observed input are given in Tables 8.13 and 8.14. Model forecasts up to a maximum lead time of 6 hours were considered for storm groups 1 and 5. The drop of efficiency is more pronounced in the Boston data (group 1) than in the Tulsa data (group 5). Increase of the persistence coefficient from the low 1-hour lead time value to values of 0.48 and 0.57 supports the forecasting ability of the precipitation model. Table 8.14 suggests that the stochastic model will have good performance with precipitation data from Tulsa for relatively long forecast lead times.

Table 8.13

LEAST SQUARES PERFORMANCE MEASURES FOR
STORM GROUP 1. MAXIMUM LEAD TIME 6-HOURS

<u>Description</u>	<u>Lead Time (HOURS):</u>	<u>1</u>	<u>2</u>	<u>3</u>	<u>4</u>	<u>5</u>	<u>6</u>
Efficiency Coefficient		0.36	0.17	0.08	0.04	0.02	0.02
Determination Coefficient		0.41	0.36	0.31	0.30	0.29	0.30
Persistence Coefficient		0.10	0.26	0.33	0.40	0.47	0.47
Extrapolation Coefficient		0.63	0.53	0.48	0.45	0.44	0.43

Table 8.14

LEAST SQUARES PERFORMANCE MEASURES FOR STORM
GROUP 5. MAXIMUM LEAD TIME 6 HOURS

<u>Description</u>	<u>Lead Time (HOURS):</u>	<u>1</u>	<u>2</u>	<u>3</u>	<u>4</u>	<u>5</u>	<u>6</u>
Efficiency Coefficient		0.28	0.26	0.18	0.34	0.22	0.21
Determination Coefficient		0.30	0.37	0.33	0.40	0.30	0.30
Persistence Coefficient		0.07	0.41	0.43	0.59	0.54	0.56
Extrapolation Coefficient		0.61	0.60	0.55	0.45	0.35	0.35

8.6 Deterministic Rainfall-Runoff Model

The formulation of the general rainfall-runoff model presented in Chapter 6 was used with hydrologic data from the Bird Creek basin and meteorological data from Tulsa in an initial attempt to assess performance. It is not intended to be a definite test.

The outlet of the Bird Creek basin is located about 20 km Northwest of Tulsa with the rest of the basin to the north of it. No temperature and pressure data were available for any location in the basin (2344 km²). The forecast lead time was 6 hours and average temperatures and pressure values over 6 hours, at Tulsa, were used for the prediction of the 6-hour rainfall in the basin. The excessively wet month of May was used as the forecast period. Sharp hydrographs of up to 250 [M³/SEC] are characteristic in this month.

The calibration and initial conditions given in Georgakakos and Bras (1979) for the soil model parameters were used. In addition, m_1 and m_2 took a value equal to 4. The channel model was calibrated as in Georgakakos and Bras (1982). The calibration of the precipitation model, based on hourly data, was that reported in the previous section.

The rainfall predictions (Figure 8.30) from the rainfall-runoff model imply that the precipitation model with Tulsa meteorological input does a poor job in representing mean areal conditions in the Bird Creek Basin as computed by the NWS. The large peak at about the eighth time step of the event has been missed completely. Similarly, the precipitation rates at about the 20th time step have been badly underestimated. The next 2 significant peaks (at 35 and 41 periods) are produced by the model with Tulsa meteorological data, but shifted by about 4 periods. Clearly, the storm movement with respect to the

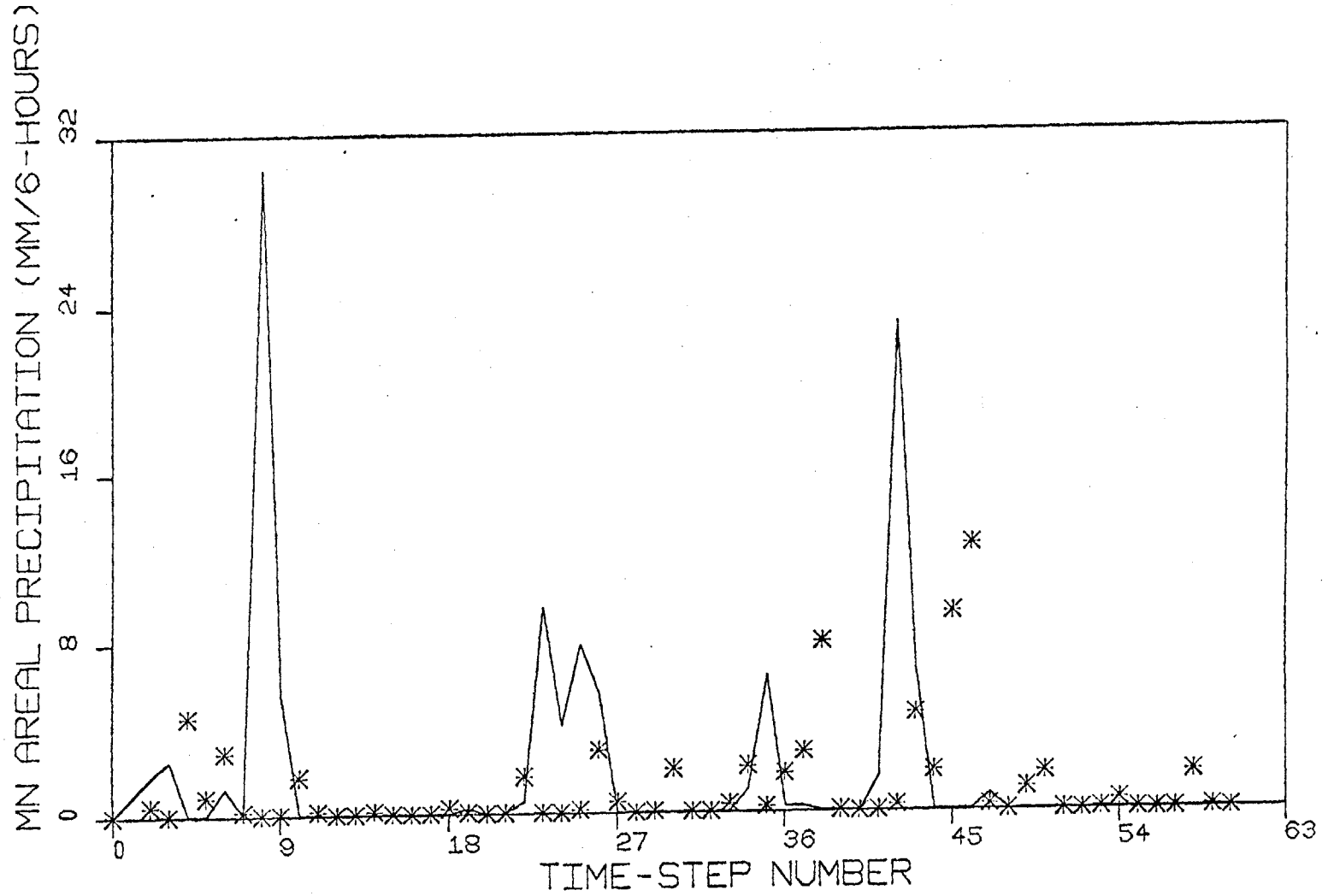


FIGURE 8.30

Deterministic Rainfall-Runoff model precipitation rate 6-hourly predictions (stars) vs. observations (solid line). Bird Creek, May 1959

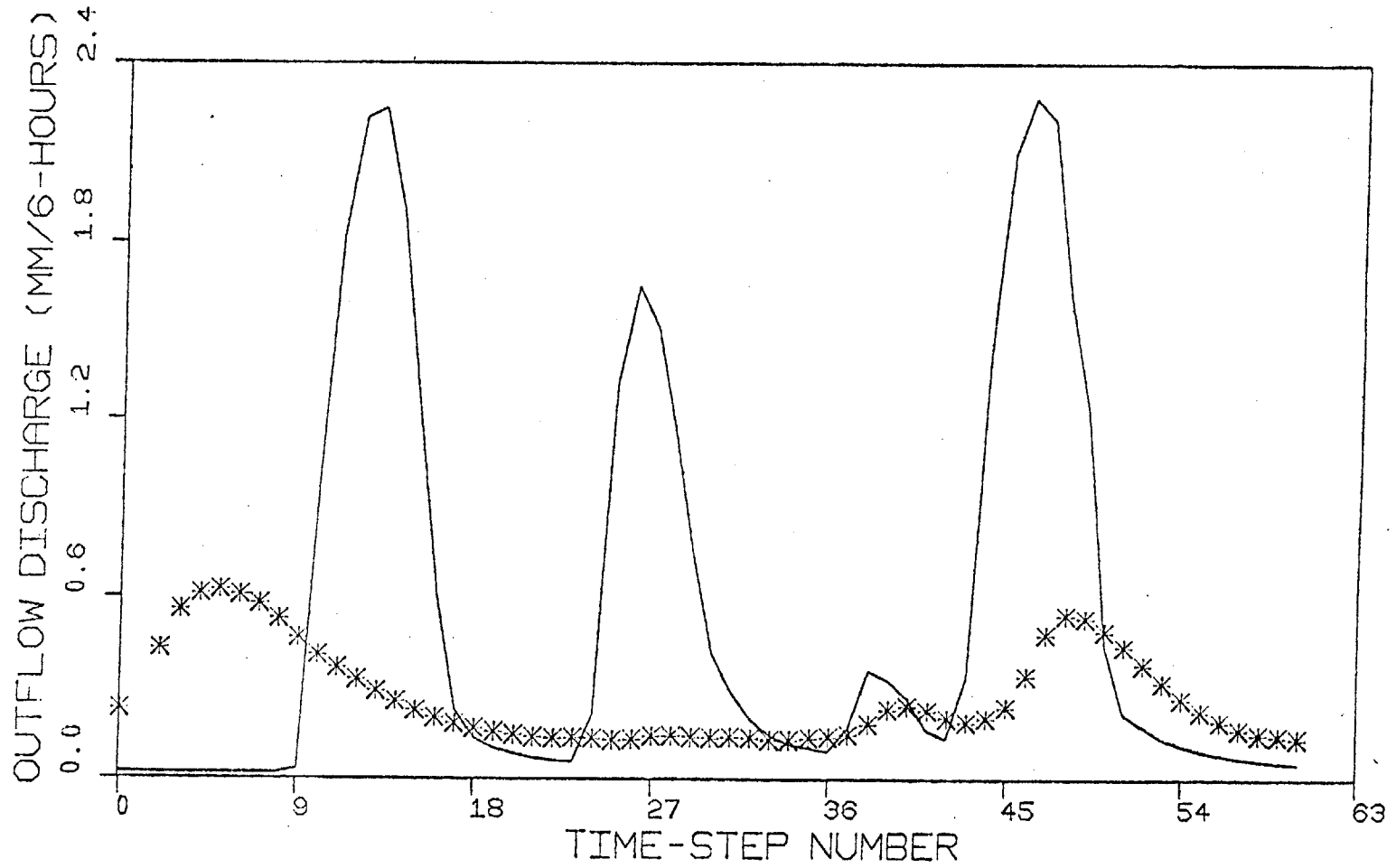


FIGURE 8.31 Deterministic Rainfall-Runoff model discharge rate 6-hourly predictions (stars) vs. observations (solid line). Bird Creek, May 1959

point of meteorological observations and with respect to the basin has an effect on the predictions of basin average conditions.

The corresponding deterministic outflow hydrograph is shown in Figure 8.31. The floods of the 13th and 46th time step of the run appear to be shifted in time. The early peak at about the 4th period is mostly due to the assumed initial conditions of near saturation in the soil model upper reservoirs. No peak was produced to correspond to that observed at the 30th period of the run.

Examination of the daily potential evapotranspiration rates, computed by the NWS for the whole month of May 1959, revealed high rates for the periods prior to the occurrence of the second peak in Figure 8.31. Values ranging from 5 to about 6.5 [MM/DAY] were reported. This fact and the low precipitation activity predicted by the precipitation model, contributed to the low forecasted flows for this period. The relatively low peak flow forecasted by the Rainfall-Runoff model for the 47th time step of the run, in spite of the large precipitation activity predicted (time steps 38 and 45 in Figure 8.30) is mainly due to the reported high evapotranspiration values for this period. The values ranged from a low of 5 to a high of about 8.5 [MM/DAY]. The evapotranspiration potential values used are based on pan evaporation observations adjusted by empirical coefficients. The distribution of the daily to 6-hourly values was done based on weights provided by the NWS, Office of Hydrology. Those are 0 for the first and last 6-hour periods in the day and 0.5 for each of the intermediate periods. The timing of evapotranspiration potential is important due to the dependence of the model response on the time of near saturation conditions for the upper soil

reservoirs. Shifts in the precipitation forecasts could then have a pronounced effect on the model response.

8.7 Stochastic Rainfall-Runoff Model

The purpose of the stochastic rainfall-runoff model runs is to establish the influence of the stochastic precipitation model on overall system performance. At first, a base run with the very low model errors of Table 8.15 was made to establish improvement over the deterministic model behavior. No input error was assumed and the observation error vector statistics of Table 8.16 were utilized. The state initial variances of Table 8.15 served to initiate the filter iterations. The model, observation, and initial covariance matrices were diagonal.

The rainfall-runoff model was then used with data corresponding to the same period, but with increased precipitation model error. This allows the study of the effect of rainfall forecasts uncertainty on streamflow predictions. A value of 25 [MM²/6-HRS] was used in place of the value 2.5×10^{-3} [MM²/6-HRS] of Table 8.15.

The residual statistics for both the mean areal precipitation rate and the outflow is given in Table 8.17 for the two stochastic model runs respectively. For comparison, the corresponding statistics for the deterministic (no update) run of Section 8.5 are also given in Table 8.17. The cross-correlation coefficient of the precipitation and discharge residual errors is also given.

Examination of Table 8.17 supports the following conclusions:

- 1) A small increase in the forecasting ability of the precipitation model, as the precipitation model error was increased, was accompanied by considerable increase in the ability of the Rainfall-

Table 8.15

RAINFALL-RUNOFF INITIAL STATE VARIANCES AND MODEL ERROR
SPECTRAL DENSITY MATRIX DIAGONAL ELEMENTS

<u>State</u>	<u>Initial Variance [MM²]</u>	<u>Model Error Spectral Density [MM²/6-HRS]</u>
X	10 ⁻³	2.5 x 10 ⁻³
x ₁	10 ⁻¹	10 ⁻¹²
x ₂	10 ⁻²	10 ⁻⁶
x ₃	10 ⁻¹	10 ⁻⁴
x ₄	10 ⁻¹	10 ⁻⁴
x ₅	10 ⁻²	10 ⁻⁴
x ₆	10 ⁻²	10 ⁻⁴
s ₁	10 ⁻⁶	10 ⁻⁴
s ₂	10 ⁻⁶	10 ⁻⁴
s ₃	10 ⁻⁶	10 ⁻⁴

Table 8.16

RAINFALL-RUNOFF MODEL OBSERVATION ERROR COVARIANCE MATRIX

	<u>Mean Areal Precipitation</u>	<u>Discharge Outflow</u>
<u>Mean Areal Precipitation:</u>	$1 + 0.01 \cdot z_1^2$	0
<u>Discharge Outflow:</u>	0	$0.05 + 0.01 \cdot z_2^2$

z_1 : Current observation of mean areal precipitation

z_2 : Current observation of the discharge outflow.

Table 8.17

RAINFALL-RUNOFF MODEL RESIDUAL STATISTICS

	<u>Deterministic</u>	<u>Low Precipitation Model Error</u>	<u>High Precipitation Model Error</u>
1) <u>Mean Areal Precipitation</u>			
Mean [MM/6-HRS]	: 0.74	0.70	0.70
Standard Deviation [MM/6-HRS]	: 5.84	5.83	5.82
Lag-1 Auto-Correlation	: 0.206	0.204	0.201
Lag-2 Auto-Correlation	: -0.052	-0.050	-0.052
Lag-3 Auto-Correlation	: -0.170	-0.168	-0.167
2) <u>Outflow Discharge</u>			
Mean [MM/6-HRS]	: 0.32	0.26	0.05
Standard Deviation [MM/6-HRS]	: 0.74	0.73	0.70
Lag-1 Auto-Correlation	: 0.872	0.869	0.864
Lag-2 Auto-Correlation	: 0.586	0.579	0.560
Lag-3 Auto-Correlation	: 0.249	0.237	0.209
Residual Cross-Correlation Coefficient	: -0.261	-0.256	-0.356

Runoff model to predict the outflow discharge rate. This holds true in particular for the preservation of total outflow volume (residual mean).

The improved performance in the prediction of outflow can be seen in Figure 8.33. There, the model predictions (dashed lines) are compared to observations (solid lines) of the outflow discharge for the case of high precipitation model error. Improvement on magnitude and times of occurrence of the first and last peaks was observed. The second peak was again badly forecasted. This points to the fact that bad performance for this case is not dependent on the precipitation model errors.

Figure 8.32 gives forecasted discharges when low precipitation model errors were assumed. There is still an improvement over the no update, deterministic case (Figure 8.31). The precipitation forecasts in the stochastic cases were similar to the deterministic results in Figure 8.30. This is supported by the statistics in Table 8.17. This suggests that improvement in the outflow discharge prediction was due to the propagation of uncertainty rather than to more accurate precipitation rate forecasts.

2) The model error spectral density used was not high enough to account for the abrupt changes of orders of magnitude in the precipitation rates (solid line in Figure 8.30). The relative improvement of the outflow forecasts, however, suggests caution when using excessively high values for this density, if the objective is the accurate prediction of outflow.

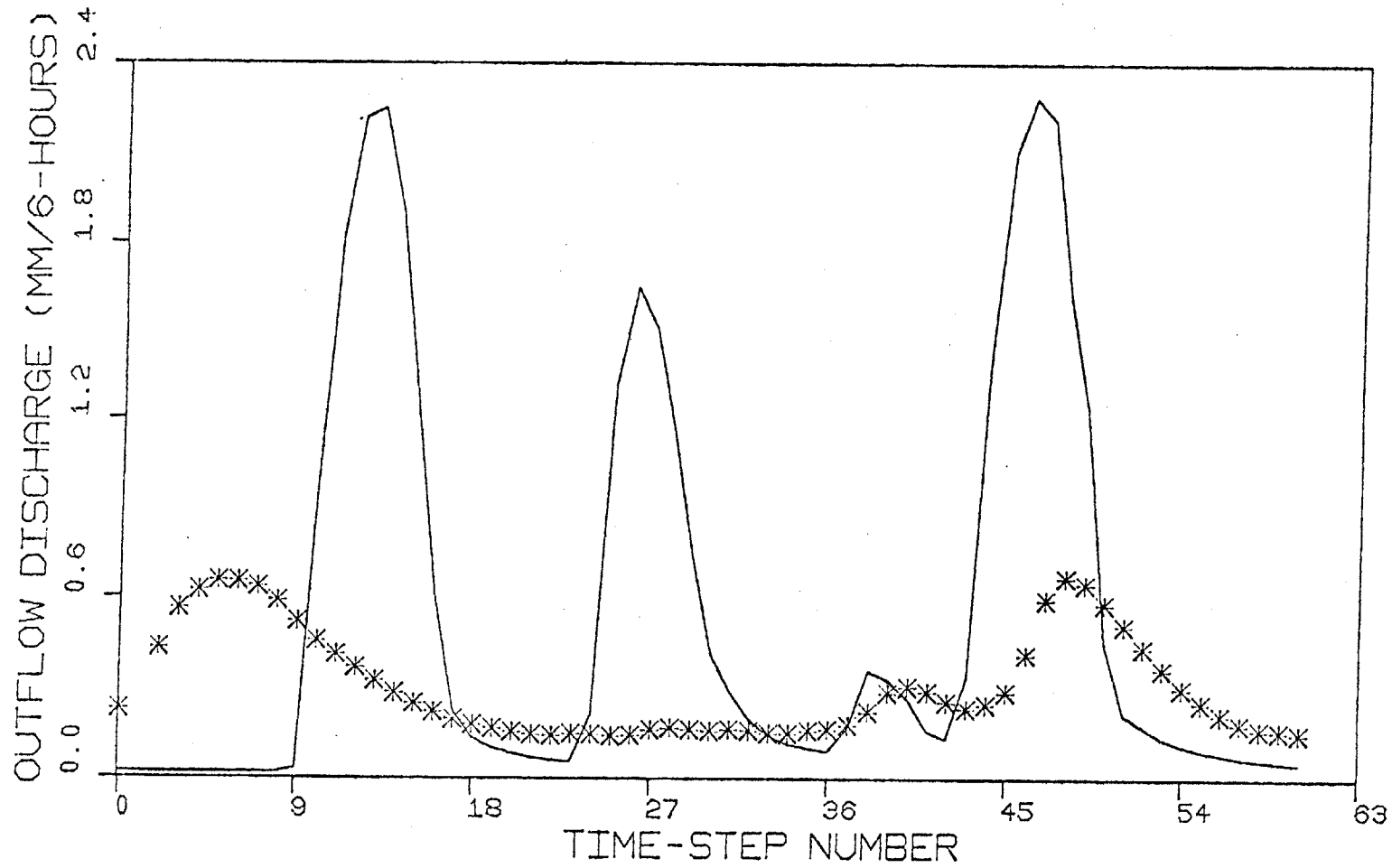


FIGURE 8.32 Stochastic Rainfall-Runoff model outflow discharge 6-hourly predictions (stars) vs. observations (solid line), for a model error of low intensity. Bird Creek, May 1959

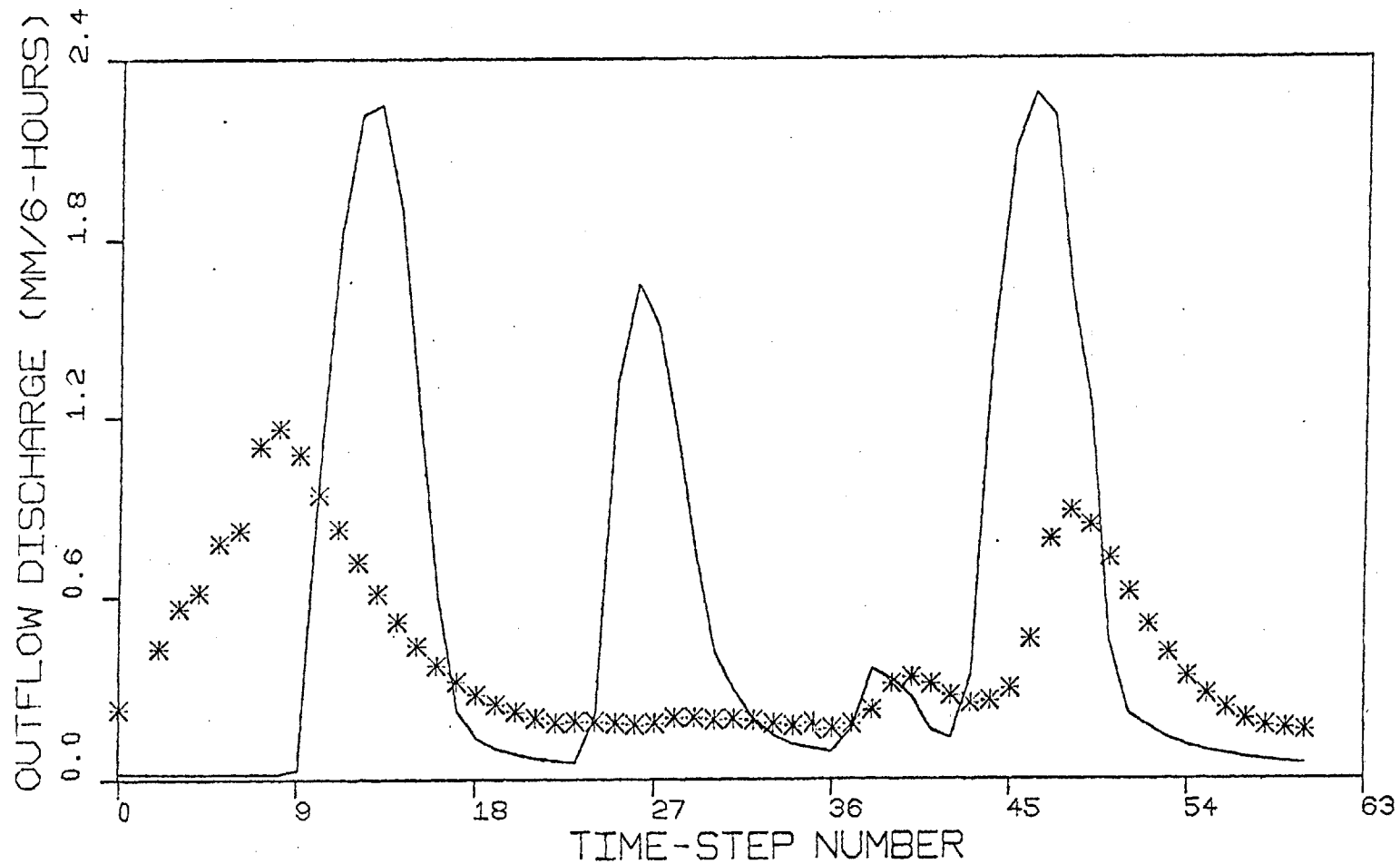


FIGURE 8.33

Stochastic Rainfall-Runoff model outflow discharge 6-hourly predictions (stars) vs. observations (solid line), for a model error of high intensity. Bird Creek, May 1959

3) Due to the difference in the characteristic time constants of the precipitation and drainage-basin processes, the auto-correlation structure of the residuals is drastically different between the two model outputs. Low correlations, of 0.2 and lower for 6-hour lags and longer, prevail in the mean areal precipitation output residuals. Correlations of 0.8 and lower are characteristic to outflow. This difference of order should be taken into consideration when judging filter performance (e.g., discussion in Kitanidis and Bras, 1980b).

CONCLUSIONS AND RECOMMENDATIONS

9.1 Summary of Results

This work developed a stochastic, state-space form, station precipitation model, and formulated the equations for a general rainfall-runoff model suitable for use in the real-time simultaneous precipitation and river flow forecasting.

Tests of the precipitation model involved examination of the deterministic and stochastic model behavior under a variety of meteorological conditions. A set of eleven storms of different type and severity from Boston, Massachusetts and Tulsa, Oklahoma, was the hourly data base for the model tests. Several performance indices were used to quantify behavior of the developed model. Thus, mean, standard deviation and autocorrelation structure of the residual process, together with efficiency, determination, persistence, and extrapolation coefficients were utilized. In addition, the model predictions were compared to the optimistic predictions of linear regressions of same input, calibrated for each storm period separately. In contrast, the physical model parameters were manually calibrated with data from a single storm and remained unchanged during all model tests.

Characteristic to all tests of the deterministic precipitation model was inadequate representation of excessively high precipitation rates and the successful prediction of the no-precipitation periods.

Improved model behavior was observed when the stochastic formulation was used. The filter parameters were based on a priori considerations and remained unchanged for all the stochastic model runs. Again, the model predictions were compared to locally calibrated regression model predictions with rainfall in the last time step as well as meteorologic parameters as explanatory variables. The high extrapolation coefficients indicate superiority of the developed model over linear predictors using the previous two precipitation rates. The low auto-correlations of the residual process suggested near optimal filter performance.

Good stochastic model performance is also confirmed by the positive persistence coefficients. Positive persistence short-range predictions are rather difficult to attain (e.g., Kitanidis and Bras, 1980b).

No significant difference between the Boston and Tulsa hourly forecasts was observed. Nevertheless, when the extended forecasts (up to six hours maximum forecast lead time) performance coefficients were examined for storms of the two locations, the Boston forecasts showed a much more pronounced drop in efficiency with lead time. Efficiency was almost constant for all the lead times for Tulsa.

The full Rainfall-Runoff model was tested with hydrologic data from the Bird Creek basin and with meteorologic data from Tulsa. The basin is of area 2344 [KMxKM] and it is located in the northern part of Oklahoma. Tulsa is located outside of the basin and in a distance of about 20 [KM] to the south of the basin outlet. The outlet is the closest basin location to Tulsa.

Evapotranspiration potential, outflow discharge and computed six-hourly mean areal precipitation data, for the excessively wet month of May 1959 were used. Average temperature and pressure data for the corresponding six-hour periods were computed from observed hourly data.

The deterministic rainfall-runoff model predictions were poor in terms of the basin mean areal precipitation rate and of the outflow discharge. A possible explanation is that the meteorological conditions in Tulsa are not representative of the mean areal precipitation rate computed for the Bird Creek basin.

Two runs of the stochastic rainfall-runoff model were made. In the first, the model error corresponding to all of the states was set equal to a relatively low arbitrary value, simulating perfect model behavior. The results showed improvement over those of a deterministic model with no updating. The effect of the precipitation rate prediction on the discharge forecasts was studied by increasing the error corresponding to the precipitation model while keeping the rest of the model errors small. The results indicated that the coupling of the precipitation to the hydrologic models by the filter is of considerable value to river-flow forecasting. For relatively small improvement in the precipitation forecasts, considerable improvement of the outflow forecasts was observed.

9.2 Future Research

The good behavior of the stochastic precipitation model developed, permits several extensions of this work. They can be grouped as 1) related to the precipitation forecasting per se, and 2) related to the use of the general rainfall-runoff model.

9.2.1 Related to Precipitation Forecasting

Automatic calibration methods of all the model parameters should be used to establish optimal parameter values. The maximum likelihood methodology (Restrepo-Posada and Bras, 1982) and the unbiased sequential estimator in Georgakakos and Bras (1982) are two possible alternatives. The fact that there is only one state, permits the use of elaborate parameter estimation procedures and many data sets. Caution must be exercised, however, to avoid the local optima indicated by the parameter space mapped in Section 8.3. During this effort, all parameters including, m , β , and γ should be calibrated.

The calibrated model, complemented by a filter, should be used with several data sets from different locations and for different storms in a sensitivity analysis of the effect of the filter parameters on model performance. The nonstationarity of the model error should be examined in detail. Similarly, the observation error structure needs examination. Related to this, the theoretical framework in Sharon (1980) will be useful. The extent to which the error in the input variables improves model performance should also be evaluated.

Due to the physical interpretation given to the model components, observations of cloud tops, upper cloud divergence from satellite images, droplet spectra and updraft velocities can considerably improve the stochastic model performance when used in additional observation equations. Perhaps more important will be observations of the model state (cloud moisture) of the type described in Bunting and Conover (1976).

The low order of the precipitation model permits probabilistic forecasts based on the use of the Bayes law and initial probability distributions of the model state. Formulations in Ho and Lee (1964) can be used. This type of forecasts are particularly useful in decision making.

Slight modifications in the model structure can be done to incorporate the effect of the time variation of some parameters. For example, assume a one-parameter Markov model for the time evolution of the average level diameter l/c . Estimating the additional parameter from storm data permits evaluation of the resultant precipitation for varying initial conditions for l/c . This can be done in a filter framework with observations of the precipitation rate and possibly of other physical quantities as described above. This type of research can be valuable in assessing the effects of cloud seeding on the precipitation rate in real time.

9.2.2 Related to River Flow Forecasting

Of primary importance is the collection of a consistent set of data for the applications of the Rainfall-Runoff model. Preferable are situations of drainage basins containing meteorological observations. In the absence of meteorological stations, nodal points of temperature and pressure prediction by the MOS technique (Glahn and Lowry, 1972) can be used, given the high linear auto-correlations of those variables. In the absence of those nodal points, nearby meteorological stations can be used. How-

ever, in this case, re-calibration of the precipitation model might be necessary for good performance. In addition to the meteorological data, hydrological data of high time resolution (six-hours) for the same test basins should be obtained.

Sensitivity analysis of the filter parameters must be performed. It is conceivable that for the short forecast lead times some of the states need not be filtered. The time trace of the filter gains will clarify this. In case only a portion of the state vector needs filtering, the results in Sims (1974) will be of use. An important aspect of the work along this line is the specification of the observation error statistical structure corresponding to the mean areal precipitation. The work of Bras and Iturbe (1976) will provide the guidelines.

Provided that the examination of the Rainfall-Runoff model behavior is complete for a head water basin, as described above, extension to a network of tributary-basins logically follows. The formulation is given in general terms in Appendix C. The major problem and research area in this case is the numerical burden associated with the uncertainty propagation between the different sub-basins. Decomposition theory techniques are unavoidable in this case. The formulations in Noton (1971) and Sims (1974) are relevant. Propagation of uncertainty can also be accomplished with reduced cost by ignoring the model components correlations between different sub-basins, preserving only correlations in each sub-basin, and correlations in the precipitation model states of different sub-basins. Clearly, the effect of each methodology assumptions on model performance should be established.

The precipitation network design methodology of Bras and Iturbe (1976) is applicable. Location and number of meteorological stations or MOS predictions nodal points can be obtained with the stochastic Rainfall-Runoff model developed, for varying accuracy restrictions on the outflow discharge. Consideration of the spatial statistical structure of the input meteorological variables is necessary. It is expected, however, that due to the higher spatial and temporal correlation of those variables compared to the precipitation rate ones, cost efficient designs will result.

REFERENCES

- The Analytic Sciences Corporation, TASC, (1980), "Applications of Kalman Filtering and Maximum Likelihood Parameter Identification to Hydrologic Forecasting," TR-1480-1, Reading, Mass.
- Armstrong, B. L., (1978), "Derivation of Initial Soil Moisture Accounting Parameters from Soil Properties for the National Weather Service River Forecast System," NWS HYDRO-37, NOAA.
- Beard, K. V. (1976), "Terminal Velocity and Shape of Cloud and Precipitation Drops Aloft," Journal of the Atmospheric Sciences, 33, 851-864.
- Beard, K. V. and H. R. Pruppacher (1971), "A Wind Tunnel Investigation of the Rate of Evaporation of Small Water Drops Falling at Terminal Velocity in Air," Journal of the Atmospheric Sciences, 28, 1455-1464.
- Braham, R. R. (1965), "The Aerial Observation of Snow and Rain Clouds," Proc. International Conference on Cloud Physics, May 24 - June 1, 1965, Tokyo and Sapparo, Japan, 494-501.
- Bras, R. L. and I. Rodriguez-Iturbe (1976), "Evaluation of Mean Square Error Involved in Approximating the Areal Average of a Rainfall Event by a Discrete Summation," Water Resources Research, 12(2), 181-184.
- Bras, R. L. and I. Rodriguez-Iturbe (1976), "Network Design for the Estimation of Areal Mean of Rainfall Events," Water Resources Research, 12(6), 1185-1195.
- Bunting, J. T. and J. H. Conover (1976), "Estimates from Satellites of Total Ice and Water Content of Clouds," Preprints International Cloud Physics Conference, July 26-30, 1976, Colorado, 407-412.
- Byers, H. R., (1965), Elements of Cloud Physics, The University of Chicago Press, Chicago, Illinois.
- Charba, J. P. and W. H. Klein (1980), "Skill in Precipitation Forecasting in the National Weather Service," Bulletin American Meteorological Society, 61(12), 1546-1555.

- Coulman, C. E. and J. Warner (1976), "Aircraft Observations in the Sub-Cloud Layer Over Land," Preprints International Cloud Physics Conference, July 26-30, 1976, Boulder, Colorado, 270-274.
- Dingle, A. N. and K. R. Hardy, "The Description of Rain by Means of Sequential Raindrop-size Distributions," Publication No. 59 from the Meteorological Laboratories, University of Michigan, Ann Arbor.
- Dufour, L. and R. Defay (1963), Thermodynamics of Clouds, translated by M. Smyth and A. Beer, Academic Press, New York.
- Eagleson, P. S., (1970), Dynamic Hydrology, McGraw-Hill Book Company, New York.
- Eldridge, R. G. (1957), "Measurements of Cloud Drop-Size Distributions," Journal of Meteorology, 14, 55-59.
- Fletcher, N. H. (1962), The Physics of Rainclouds, Cambridge University Press.
- Fujiwara, M. (1976), "A Cloud Structure and the Rain Efficiency as Observed by Radars and Raindrop Recorder," Preprints International Cloud Physics Conference, July 26-30, 1976, Boulder, Colorado, 494-499.
- Gelb, A., ed., (1974), Applied Optimal Estimation, The M.I.T. Press, Cambridge, Mass.
- Georgakakos, K. P. and R. L. Bras, (1979), "On-Line River Discharge Forecasting Using Filtering and Estimation Theory," Progress Report, Sept. 13, 1978 - Feb. 13, 1979, Ralph M. Parsons Lab. for Water Resources and Hydrodynamics, Dept. of Civil Engineering, M.I.T., Contract No. 7-35112.
- Georgakakos, K. P., and R. L. Bras, (1980), "A Statistical Linearization Approach to Real Time Nonlinear Flood Routing," Ralph M. Parsons Lab. for Water Resources and Hydrodynamics, Dept. of Civil Engineering, M.I.T., TR No. 235.
- Georgakakos, K. P., Restrepo-Posada, P. J. and R. L. Bras, (1980), "On-Line River Discharge Forecasting Using Filtering and Estimation Theory;" Progress Report, Aug. 13, 1979 - Jan. 13, 1980, Ralph M. Parsons Lab for Water Resources and Hydrodynamics, Dept. of Civil Engineering, M.I.T., Contract No. 7-35112.

- Georgakakos, K. P. and R. L. Bras, (1982), "Real Time, Statistically Linearized Adaptive Flood Routing," Water Resources Research, 18(3), pp. 513-524.
- Glahn, H. R. and D. A. Lowry, (1972), "The Use of Model Output Statistics (MOS) in Objective Weather Forecasting," Journal of Applied Meteorology, 11, 1203-1211.
- Gunn, K. L. S. and J. S. Marshall (1958), "The Distribution With Size of Aggregate Snowflakes," Journal of Meteorology, 15, 452-461.
- Ho, Y. C. and R. C. K. Lee, (1964), "A Bayesian Approach to Problems in Stochastic Estimation and Control," IEEE Transactions on Automatic Control, AC-9(5), 333-339.
- Hobbs, P. V., Chang, S. and J. D. Locatelli (1974), "The Dimensions and Aggregation of Ice Crystals in Natural Clouds," Journal of Geophysical Research, 79(15), 2199-2206.
- Hobbs, P. V. and R. A. Houze, Jr., (1976), "Mesoscale Structure of Precipitation in Extratropical Cyclones," Preprints International Cloud Physics Conference, July 26-30, 1976, Boulder, Colorado, 488-493.
- Holton, J. R. (1979), An Introduction to Dynamic Meteorology, second edition, Academic Press, New York.
- Houghton, H. G. (1968), "On Precipitation Mechanisms and their Artificial Modification," Journal of Applied Meteorology, 7(5), 851-859.
- Ingraham, D. V. and S. O. Russell (1981), "Nowcasting Areal Rainfall Over British Columbia from GOES Satellite Images," presented at the International Symposium on Real-Time Operation of Hydro-Systems, University of Waterloo, Ontario, June 24-26, 1981.
- Kalman, R. E. and Bucy, S. B. (1961), "New Results in Linear Filtering and Prediction Theory," ASME, Journal of Basic Engineering 83D, 95-108.
- Kitanidis, P. K. and R. L. Bras, (1980a) "Real-Time Forecasting with a Conceptual Hydrologic Model, 1, Analysis of Uncertainty," Water Resources Research, 16(6), 1025-1033.
- Kitanidis, P. K. and R. L. Bras, (1980b), "Real-Time Forecasting with a Conceptual Hydrologic Model, 2, Applications and Results," Water Resources Research, 16(6), 1034-1044.

- Linsley, R. K., Jr., Kohler, M. A. and J. L. H. Paulhus, (1975), Hydrology for Engineers, second edition, McGraw-Hill Book Co., New York.
- Locatelli, J. D. and P. V. Hobbs (1974), "Fall Speeds and Masses of Some Precipitation Particles," Journal of Geophysical Research, 79(15), 2185-2197.
- Lowry, D. A. and H. R. Glahn, (1976) "An Operational Model for Forecasting Probability of Precipitation -- PEATMOS PoP," Monthly Weather Review, 104, 221-232.
- Magono, C. and C. W. Lee (1966), "Meteorological Classification of Natural Snow Crystals," J. Fac. Sci., Hokkaido University, Ser. 7, 2, 321.
- Marshall, J. S. and W. McK. Palmer (1948), "The Distribution of Raindrops with Size," Journal of Meteorology, 5, 165-166.
- Mason, B. J., (1971) The Physics of Clouds, second edition, Clarendon Press, Oxford.
- National Research Council (1980), "Atmospheric Precipitation: Prediction and Research Problems," prepared by the Panel on Precipitation Processes, Committee on Atmospheric Sciences, National Academy Press, Washington, D. C.
- National Weather Service, (1978) "The Limited-Area Fine Mesh Model (LFM)," NWS Technical Procedures, Bulletin No. 232, NOAA.
- Noton, R. M. A., (1971), "Two-Level Form of the Kalman Filter," IEEE Transactions on Automatic Control," AC-16(2), 128-133.
- Ohtake, T. (1965), "Preliminary Observations of Size Distribution of Snowflakes and Raindrops at Just Above and Below the Melting Layer," Proc. International Conference on Cloud Physics," May 24 - June 1, 1965, Tokyo and Sapporo, Japan, 271-275.
- Peck, E. L., (1976), "Catchment Modeling and Initial Parameter Estimation for the National Weather Service River Forecast System," NWS HYDRO-31, NOAA.

- Pruppacher, H. R. and J. D. Klett, (1978), Microphysics of Clouds and Precipitation, D. Reidel Publishing Co., Boston.
- Restrepo-Posada, P. J. and R. L. Bras (1982), "Automatic Parameter Estimation of a Large Conceptual Rainfall-Runoff Model: A Maximum Likelihood Approach," Ralph M. Parsons Lab. for Water Resources and Hydrodynamics, Dept. of Civil Engineering, M.I.T., TR No. 267.
- Restrepo-Posada, P. J. and P. S. Eagleson, (1979) "Fortran Programs for the Interpretation and Analysis of NOAA Hourly Precipitation Data Tapes," Ralph M. Parsons Lab. for Water Resources and Hydrodynamics, Dept. of Civil Engineering, M.I.T., TN No. 22.
- Rogers, R. R., (1979), A Short Course in Cloud Physics, second edition, Pergamon Press, New York.
- Sharon, D., (1980), "The Distribution of Hydrologically Effective Rainfall Incident on Sloping Ground," Journal of Hydrology, 46, 165-188.
- Sims, C. S., (1974), "An Algorithm for Estimating a Portion of the State Vector," IEEE Transactions on Automatic Control, AC-19(4), 391-393.
- Sulakvelidze, G. K. (1969), Rainstorms and Hail, translated from Russian by the Israel Program for Scientific Translations, Jerusalem.
- Wallace, J. M. and P. V. Hobbs, (1977), Atmospheric Science, An Introductory Survey, Academic Press, New York.

Appendix A

GLOSSARY OF METEOROLOGICAL TERMS USED

Adiabatic or (dry adiabatic) ascent: Rising of air packets that are thermally insulated from their environment.

Dew point temperature, T_d : It is the temperature to which air of temperature T must be cooled at constant pressure (and water content) in order for it to become saturated with respect to a plane surface of water. It holds $T_d \leq T$.

Entrainment: Mixing between the cloud and the environmental air. It results in the cooling of the cloud air mainly due to the evaporation of part of the condensed water that saturates the dry environmental air. This way the buoyancy of the rising air is reduced.

Equivalent potential temperature, θ_e : It is the temperature a parcel of air would have if, expanded pseudo-adiabatically until all the vapor was condensed and fallen out, it was compressed dry adiabatically to the standard pressure of 1000 [MBAR].

Hydrostatic atmosphere: Atmosphere where the upward force acting on a thin slab of air, due to the decrease in pressure with height, is generally very close in balance with the downward force due to the gravitational field.

Irreversible condensation process: Rising of air parcels during which all condensation products immediately fall out of the parcel. This implies rain and no cloud.

Isobaric process: Process under constant pressure.

Isothermal process: Process under constant temperature.

Melting layer: The cloud layer in which melting of the falling ice particles occurs. It corresponds to the upper boundary of the high reflectivity region on a weather radar image of the vertical cloud cross-section.

Mixing ratio, w: It is the ratio of the mass of water vapor in a certain volume of air to the mass of the dry air in the same volume.

Potential temperature, θ : It is the temperature an air parcel would have if it were expanded or compressed dry adiabatically from its existing temperature and pressure to a standard pressure of 1000 [MBAR].

Pseudo-adiabatic ascent: Rising of air parcels with simultaneous condensation of the water vapor forming particles that immediately fall out of the air parcel (irreversible process). The parcel is warmed by the latent heat of condensation which remains in the parcel during the ascent.

Radiosonde observations: Routine temperature observations taken from unmanned balloons carrying relatively inexpensive instrument packages that radio their observations to earth stations. Modern radiosonde systems are capable of making observations up to about 40 km (Wallace and Hobbs, 1977).

Relative humidity in fraction, r: It is the ratio of the actual mixing ratio to the saturation mixing ratio at the same temperature and pressure.

Reversible condensation process: Rising of air parcels with all condensation products retained in them. This process implies cloud and no rain. It is referred to also as a saturated-adiabatic process.

Saturation mixing ratio, $w_s(T,p)$: It is the ratio of the mass of water vapor in a given volume of air saturated with respect to a plane surface of water, and with temperature T and pressure p , to the mass of the dry air.

Saturation vapor pressure, $e_s(T)$: The pressure exerted by the water vapor under equilibrium conditions (balanced rates of evaporation and condensation of the water molecules) with air of temperature T . A plane surface of water is assumed.

Specific humidity, q_h : It is the ratio of the mass of vapor in a certain volume to the total mass of air and vapor in the same volume.

Supercooled rain drops: Drops in a cloud region where the air temperature is below the freezing point, 273.15°K .

Supersaturated air: Cloud regions where the water vapor pressure is higher than the saturation vapor pressure under the same temperature. Supersaturation can be with respect to liquid water or ice.

Wet bulb temperature, T_w : It is the temperature to which a parcel of air is cooled by evaporating water into it at constant pressure until saturation of the air occurs. Due to the fact that the mixing ratio of the air saturated by the above described process is greater or equal to the initial mixing ratio (which is equal to the saturation mixing ratio at temperature T_d), it follows that $T_w \geq T_d$.

Appendix B

SOLUTION OF THE STATION PRECIPITATION MODEL
NONLINEAR ALGEBRAIC EQUATIONS BY THE
NEWTON-RAPHSON ITERATIONS METHOD

Suppose that the nonlinear algebraic equation that a quantity Y obeys is:

$$F(Y) = 0 \tag{B.1}$$

with $F(\cdot)$ a general nonlinear function with continuous derivative.

Then, the root Y^* of Eq.(B.1) can be found iteratively from:

$$Y_k = Y_{k-1} - \frac{F(Y_{k-1})}{\left. \frac{dF(Y)}{dY} \right|_{Y=Y_{k-1}}} \tag{B.2}$$

using a starting value Y_0 . In the previous equation, k is the iteration indicator and Y_k is the current approximation to the root Y^* .

Use of this procedure, called the Newton-Raphson iterations method, requires specification of $F(\cdot)$, $\frac{dF(\cdot)}{dY}$ and of Y_0 . Those quantities are determined next for 1) the pseudo-adiabatic Eq. (3.16), 2) the wet bulb temperature definition Eq. (4.38), and 3) the terminal pressure p_t definition Eq. (5.38).

1) Pseudo-adiabatic equation

The T-root of Eq. (3.16) is sought, for a given pressure p. In this case:

$$F(T) = T \left(\frac{p}{p_0}\right)^{0.286} \cdot \exp \left\{ \frac{L(T) \cdot w_s(T,p)}{c_p \cdot T} \right\} - \theta_e \quad (B.3)$$

with θ_e independent of T.

Denote by E(T) the exponent in Eq. (B.3). Then the derivative of F(T) with respect to T is:

$$\frac{dF(T)}{dT} = [\theta_e + F(T)] \cdot \left[\frac{1}{T} + \frac{dE(T)}{dT} \right] \quad (B.4)$$

with T in [°K], to assure its positiveness.

The derivative of E(T) is:

$$\frac{dE(T)}{dT} = \frac{w_s(T,p)}{c_p \cdot T} \cdot \frac{dL(T)}{dT} + \frac{L(T)}{c_p \cdot T} \cdot \frac{dw_s(T,p)}{dT} - E(T) \cdot \frac{1}{T} \quad (B.5)$$

with:

$$E(T) = \frac{L(T) \cdot w_s(T,p)}{c_p \cdot T} \quad (B.6)$$

Determination of $\frac{dE(T)}{dT}$ requires:

$$\frac{dL(T)}{dT} = -B \quad (B.7)$$

$$\frac{dw_s(T,p)}{dT} = \frac{\epsilon \cdot A_1 \cdot 3.5 (T - 223.15)^{2.5}}{p} \quad (\text{B.8})$$

Eq. (B.7) and (B.8) follow from Eq. (3.15) and Eq. (3.4) with T_0 , p_0 replaced by T and p respectively.

Application of the Newton-Raphson procedure requires a starting value for the temperature T . The value of T resulting from dry-adiabatic ascent to level p (Eq. (3.6) for constant θ taken from Eq.(3.5)), can be used to initialize the iterations.

2) Wet-bulb temperature definition

The function $F(\cdot)$ is now defined as:

$$F(T_w) = T_w - T_0 + \frac{L(T_w)}{c_p} (w_s(T_w, p_0) - w_s(T_d, p_0)) \quad (\text{B.9})$$

Its derivative is given by:

$$\frac{dF(T_w)}{dT_w} = 1 + (w_s(T_w, p_0) - w_s(T_d, p_0)) \cdot \frac{1}{c_p} \cdot \frac{dL(T_w)}{dT_w} + \frac{L(T_w)}{c_p} \cdot \frac{dw_s(T_w, p_0)}{dT_w} \quad (\text{B.10})$$

The derivatives of the right-hand side of Eq. (B.10) are obtained from Eqs. (B.7) and (B.8) for $T = T_w$ and $p = p_0$.

The value of T_d , the dew-point temperature at pressure p_0 , can be used to start the iterations in Eq. (B.2).

3) Terminal pressure definition

In the case of Eq. (5.38), $F(\cdot)$ is given by:

$$F(p_t) = T_m(p_t) \cdot \left(\frac{p_n}{p'(p_t)}\right)^{0.286} \cdot \exp \left\{ \frac{L(T_m(p_t)) \cdot w_s(T_m(p_t), p'(p_t))}{c_p \cdot T_m(p_t)} \right\} - \Theta_e \quad (\text{B.11})$$

where dependence on p_t of T_m , L and w_s is shown.

The derivative of $F(\cdot)$ with respect to p_t is:

$$\begin{aligned} \frac{dF(p_t)}{dp_t} &= \frac{\partial F(p_t, T_m, p')}{\partial p_t} + \frac{\partial F(p_t, T_m, p')}{\partial T_m} \cdot \frac{\partial T_m(p_t)}{\partial p_t} \\ &+ \frac{\partial F(p_t, T_m, p')}{\partial p'} \cdot \frac{\partial p'(p_t)}{\partial p_t} \end{aligned} \quad (\text{B.12})$$

where the notation indicates that $F(\cdot)$ is an implicit function of p_t through T_m, p' . Due to the fact that $F(\cdot)$ does not explicitly depend on p_t , it holds:

$$\frac{\partial F(p_t, T_m, p')}{\partial p_t} = 0 \quad (\text{B.13})$$

The derivative $\frac{\partial F(p_t, T_m, p')}{\partial T_m}$ has been determined in (1) by the set of Eqs. (B.4) through (B.8). In this case $T = T_m$, $p = p'$.

Use of Eq. (5.40) for $T_m(p_t)$ gives:

$$\begin{aligned} \frac{dT_m(p_t)}{dp_t} = & - \frac{2}{c_p \cdot (\epsilon_1 \cdot \epsilon_3)^2} \cdot \frac{(\epsilon_2 - p_t)(\epsilon_2 - p_\ell)}{(p_t - p_\ell)^3} \\ & + 0.0715 \frac{T_0}{p_0} \frac{1}{\left(\frac{3}{4} p_s + \frac{1}{4} p_t\right)^{0.714}} \end{aligned} \quad (\text{B.14})$$

Differentiation of Eq. (5.36) with respect to p_t results in:

$$\frac{dp'(p_t)}{dp_t} = \frac{1}{4} \quad (\text{B.15})$$

Finally, differentiation of Eq. (B.11) with respect to p' gives:

$$\frac{\partial F(p_t, T_m, p')}{\partial p'} = (F(p_t) + \theta_e) \cdot \left(\frac{\partial w_s(T_m, p')}{\partial p'} \cdot \frac{L(T_m)}{c_p T_m} - \frac{0.286}{p'} \right) \quad (\text{B.16})$$

The last derivative in Eq. (B.16) is given by:

$$\frac{\partial w_s(T_m, p')}{\partial p'} = -w_s(T_m, p') \cdot \frac{1}{p'} \quad (\text{B.17})$$

The necessary derivatives for the application of the Newton-Raphson method on the terminal pressure definition equation have now been determined. Use of Eq. (5.40) can be made to determine a starting value p_{t_0} , for the iterations, as a function of the parameters $(\epsilon_1 \cdot \epsilon_3), \epsilon_2$ and the input variables. In this way, p_{t_0} takes the form:

$$p_{t_0} = \frac{\epsilon_2 + \sqrt{c_p \cdot T^0 \cdot (\epsilon_1 \cdot \epsilon_3)} \cdot p_\ell}{1 + \sqrt{c_p \cdot T^0 \cdot (\epsilon_1 \cdot \epsilon_3)}} \quad (\text{B.18})$$

with T^0 a variable with dimensions of temperature. Experiments with a wide variety of input and parameter conditions indicated fast convergence for $T^0 = T_0$.

Appendix C

EQUATIONS FOR LARGE RIVER BASIN NETWORKS

Consider N tributary-basins comprising a large river basin. In this case, the equations for the j^{th} sub-basin in the network can be written as:

$$\frac{d}{dt}(x_p^j) = f_p(x_p^j, \underline{u}^j; \underline{a}_p^j) \quad ; \quad j = 1, 2, \dots, N \quad (\text{C.1})$$

$$\frac{d}{dt}(x_s^j) = f_s(x_p^j, x_s^j, \underline{u}^j, u_e^j; \underline{a}_p^j, \underline{a}_s^j) \quad ; \quad j = 1, 2, \dots, N \quad (\text{C.2})$$

$$\frac{d}{dt}(x_c^j) = f_c(x_p^j, x_s^j, x_c^j, \underline{u}^j, u_e^j; \underline{a}_p^j, \underline{a}_s^j, \underline{A}_c^j) \quad ; \quad j=1,2,\dots,N \quad (\text{C.3})$$

with output:

$$z_p^j = h_p(x_p^j, \underline{u}^j; \underline{a}_p^j) \quad , \quad j = 1, 2, \dots, N \quad (\text{C.4})$$

$$z_c^j = h_c(x_c^j; \underline{a}_c^j) \quad ; \quad j = 1, 2, \dots, N \quad (\text{C.5})$$

Notation in the previous set of equations follows Table 6.2 with upperscript j to identify the tributary basin under consideration. In addition, the vectors \underline{X}_c^j and \underline{A}_c^j , that represent the influence

of the upstream channels on the j^{th} basin equations are defined by:

$$\underline{X}_c^j = [\underline{x}_c^{j_1} \quad \underline{x}_c^{j_2} \quad \dots \quad \underline{x}_c^{j_{M_j}}]^T \quad (\text{C.6})$$

$$\underline{A}_c^j = [\underline{a}_c^{j_1} \quad \underline{a}_c^{j_2} \quad \dots \quad \underline{a}_c^{j_{M_j}}]^T \quad (\text{C.7})$$

with T, as a superscript, to denote the transpose of a vector (or matrix) quantity.

In Eqs. (C.6) and (C.7), the integers $j_1, j_2, \dots, j_{(M_j-1)}$ represent indices of the (M_j-1) tributary-basins, upstream of the j^{th} one, whose output contributes to the input of the j^{th} basin. The indices j, j_i ($i = 1, 2, \dots, M_j$ and $j = 1, 2, \dots, N$) increase following the stream-order of the corresponding tributary. Thus, wherever k tributaries of k different sub-basins, join to form another one of higher stream-order, located in a new sub-basin of index j^* , each of the indices for the k joining tributary-basins is less than j^* .

For illustration purposes, Figure C.2 indicates the flow of the computations related to the precipitation (PREC), soil moisture accounting (SOIL) and channel routing (CHANNEL) models, for the river basin of Figure C.1. In that case, $N = 5, M_1 = 1, M_2 = 1, M_3 = 1, M_4 = 3, M_5 = 3$.

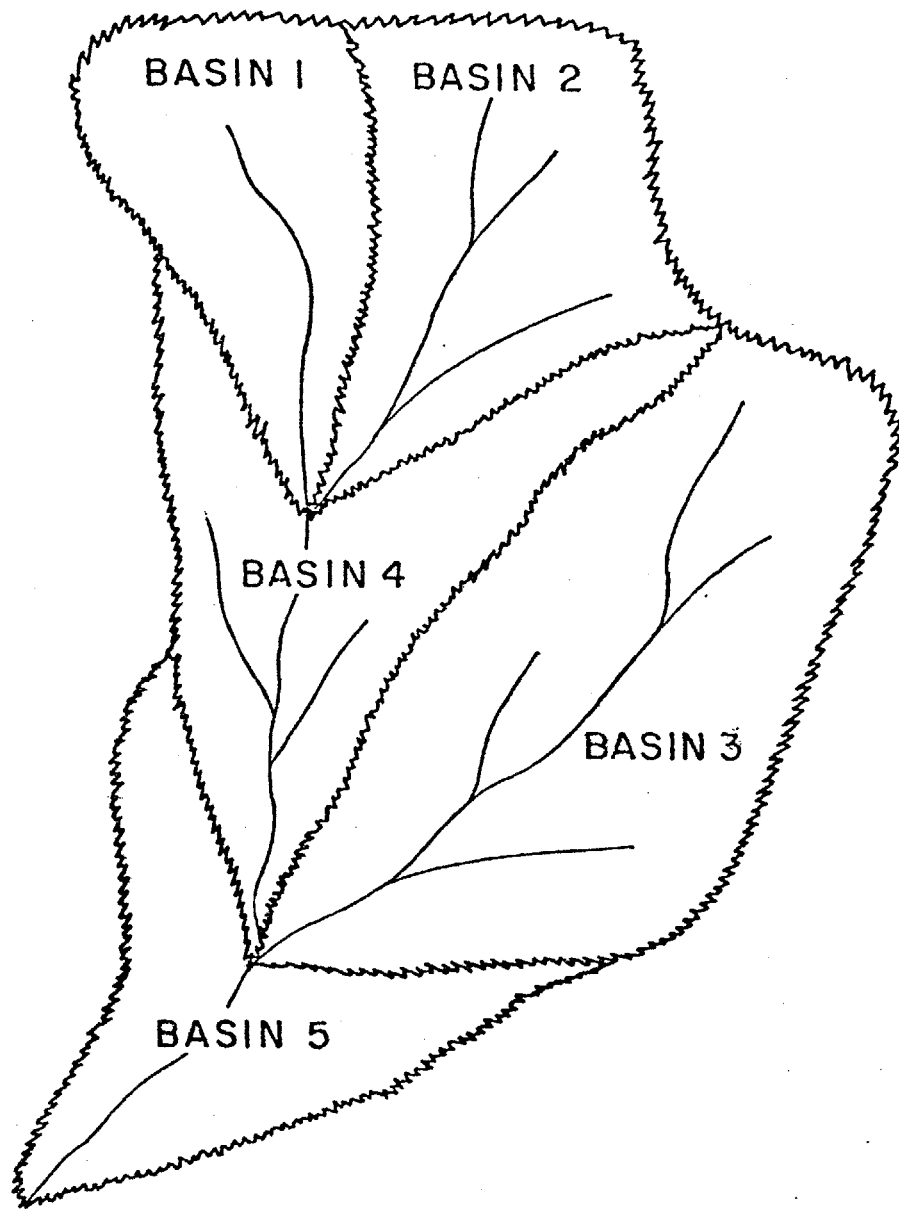


FIGURE C.1

Hypothetical large river basin with five tributary-basins

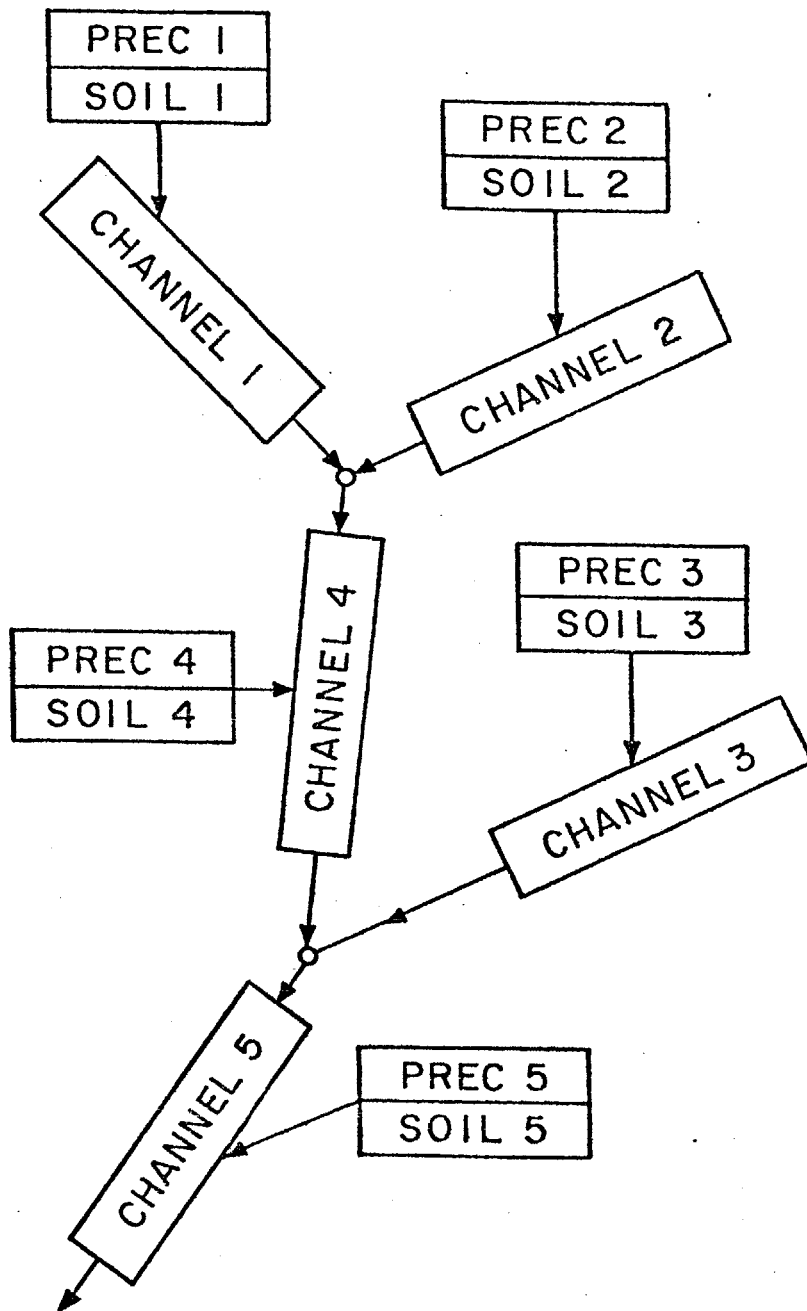


FIGURE C.2

Flow of computation, indicated by arrows, for the tributary-basin network of Figure C.1.

PREC j: Precipitation model computations for basin j

SOIL j: Soil model computations for basin j

CHANNEL j: Channel routing model computations for basin j.

Throughout the previous formulation, each tributary-basin was assumed characterized by one vector \underline{u} of input variables T_0 , T_d , P_0 . In cases with $k(>1)$ different vectors \underline{u} available for a single basin, it is necessary to use k unit area precipitation models, for the areas of influence of each \underline{u} , within the basin. Each predicted precipitation rate is then weighed by the applicable area to obtain the input precipitation rate to the soil model for the basin under consideration. Due to the relatively high sensitivity of the proposed precipitation model to the input vector \underline{u} , a priori averaging of the meteorological input from different areas is not recommended.

Appendix D

STATION PRECIPITATION MODEL LINEARIZED EQUATIONS

The first elements F_1 and G_1 of the rainfall-runoff model vector functions $F(\cdot)$ and $G(\cdot)$ correspond to the dynamics (Eq. (5.32)) and observation (Eq. (6.3)) equations of the precipitation model, respectively.

Omitting time dependence for notational simplicity, F_1 and G_1 can be expressed as:

$$F_1 = f(\underline{u}) - h(\underline{u}) \cdot X \quad (D.1)$$

and

$$G_1 = \phi(\underline{u}) \cdot X \quad (D.2)$$

with $f(\cdot)$, $h(\cdot)$ and $\phi(\cdot)$ showing dependence on the input vector \underline{u} whose u_1 , u_2 , u_3 elements are T_0 , p_0 and T_d , respectively.

Equations (D.1) and (D.2) are linear functions of the state X but nonlinear functions of the input \underline{u} .

The linearized equations for the precipitation model take the form of Eqs. (7.9) and (7.10) with \underline{F}_0 , \overline{N}_F , \overline{M}_F , \underline{G}_0 , \overline{N}_G , \overline{M}_G computed from Eqs. (7.40) through (7.45).

Define \bar{A}_{ij} as the ij^{th} element of a matrix \bar{A} . \underline{B}_i denotes the i^{th} element of a vector \underline{B} . Let $\hat{\underline{B}}$ be the current estimate of a vector \underline{B} .

Differentiation of Eqs. (D.1) and (D.2) with respect to \underline{X} gives:

$$\bar{N}_{F11} = -h(\hat{\underline{u}}) \quad (D.3)$$

$$\bar{N}_{G11} = \phi(\hat{\underline{u}}) \quad (D.4)$$

Also:

$$\underline{F}_{01} = f(\hat{\underline{u}}) - h(\hat{\underline{u}}) \cdot \hat{\underline{X}} \quad (D.5)$$

$$\underline{G}_{01} = g(\hat{\underline{u}}) \cdot \hat{\underline{X}} \quad (D.6)$$

The elements of the matrices \bar{M}_F and \bar{M}_G have to be obtained by differentiation as:

$$\bar{M}_{F1i} = \begin{pmatrix} \frac{\partial f(\underline{u})}{\partial u_i} \\ 0 \end{pmatrix} - \begin{pmatrix} \frac{\partial h(\underline{u})}{\partial u_i} \\ 0 \end{pmatrix} \cdot \hat{\underline{X}} ; \quad i = 1, 2, 3 \quad (D.7)$$

and

$$\bar{M}_{G1i} = \begin{pmatrix} \frac{\partial \phi(\underline{u})}{\partial u_i} \\ 0 \end{pmatrix} \cdot \hat{\underline{X}} ; \quad i = 1, 2, 3 \quad (D.8)$$

with subscript "0" to denote evaluation of a derivative at the current estimates of input and/or state.

D.1 The Derivatives of $f(\cdot)$, $h(\cdot)$ and $\phi(\cdot)$ with Respect to \underline{u}

D.1.1 Derivatives of Condensation Function with Respect to the Input Variables

Define M_{f_i} by:

$$M_{f_i} = \left(\frac{\partial f(\underline{u})}{\partial u_i} \right)_0 ; \quad i = 1, 2, 3 \quad (D.9)$$

By means of Eqs. (D.9), (3.18) and (3.19) it follows ($dA = 1$).

$$\begin{aligned} M_{f_i} = & \left(\frac{\partial(\Delta w)}{\partial u_i} \right)_0 \cdot \hat{\rho}_m \cdot \hat{v} + \left(\frac{\partial \rho_m}{\partial u_i} \right)_0 \cdot \Delta \hat{w} \cdot \hat{v} + \\ & + \left(\frac{\partial v}{\partial u_i} \right)_0 \cdot \Delta \hat{w} \cdot \hat{\rho}_m ; \quad i = 1, 2, 3 \end{aligned} \quad (D.10)$$

I) Differentiation of Eq. (3.17) and use of Eq. (3.1) results in:

$$\left(\frac{\partial(\Delta w)}{\partial u_i} \right)_0 = \left(\frac{\partial w_s(T_d, p_0)}{\partial u_i} \right)_0 - \left(\frac{\partial w_s(T_t, p_t)}{\partial u_i} \right)_0 ; \quad i = 1, 2, 3 \quad (D.11)$$

A) In addition:

$$\left(\frac{\partial w_s(T_d, p_0)}{\partial T_0} \right)_0 = 0 \quad (D.12)$$

$$\left(\frac{\partial w_s(T_d, p_0)}{\partial p_0} \right)_0 = - \frac{D_1 (\hat{T}_d - 223.15)^{3.5}}{\hat{p}_0^2} \quad (D.13)$$

$$\left(\frac{\partial w_s(T_d, p_0)}{\partial T_d} \right)_0 = \frac{D_1 \cdot 3.5 \cdot (\hat{T}_d - 223.15)^{2.5}}{\hat{p}_0} \quad (D.14)$$

with D_1 given by:

$$D_1 = 0.622 \cdot 8 \cdot 10^{-4} = 4.976 \cdot 10^{-4} \quad [\text{KG/M/SEC}^2/\text{K}^{3.5}]$$

B) The second term in the right-hand side of Eq. (D.11) can be written as:

$$\begin{aligned} \left(\frac{\partial w_s(T_t, p_t)}{\partial u_i} \right)_0 &= \left(\frac{\partial w_s(T_t, p_t)}{\partial T_t} \right)_0 \cdot \left(\frac{\partial T_t}{\partial u_i} \right)_0 \\ &+ \left(\frac{\partial w_s(T_t, p_t)}{\partial p_t} \right)_0 \cdot \left(\frac{\partial p_t}{\partial u_i} \right)_0 \quad ; \quad i = 1, 2, 3 \quad (D.15) \end{aligned}$$

1) It holds that:

$$\left(\frac{\partial w_s(T_t, p_t)}{\partial T_t}\right)_0 = \frac{3.5 \cdot D_1 (\hat{T}_t - 223.15)^{2.5}}{\hat{p}_t} \quad (D.16)$$

and

$$\left(\frac{\partial w_s(T_t, p_t)}{\partial p_t}\right)_0 = -w_s(\hat{T}_t, \hat{p}_t) \cdot \frac{1}{\hat{p}_t} \quad (D.17)$$

2) The derivatives $\left(\frac{\partial p_t}{\partial u_i}\right)_0$, $i = 1, 2, 3$, can be obtained from:

$$\left(\frac{\partial F}{\partial u_i}\right)_0 + \left(\frac{\partial F}{\partial p_t}\right)_0 \left(\frac{\partial p_t}{\partial u_i}\right)_0 = 0 \quad ; \quad i = 1, 2, 3 \quad (D.18)$$

which gives:

$$\left(\frac{\partial p_t}{\partial u_i}\right)_0 = - \frac{\left(\frac{\partial F}{\partial u_i}\right)_0}{\left(\frac{\partial F}{\partial p_t}\right)_0} \quad ; \quad i = 1, 2, 3 \quad (D.19)$$

The denominator in Eq. (D.19) was determined in Appendix B (Eqs. (B.12) through (B.17)). The numerator in Eq. (D.19) takes one of the following forms:

a)

$$\begin{aligned}
 \left(\frac{\partial F}{\partial T_0}\right)_0 &= -\hat{T}_m \left(\frac{p_n}{\hat{p}'}\right)^{0.286} \cdot \exp\left\{\frac{L(\hat{T}_m) \cdot w_s(\hat{T}_m, \hat{p}')}{c_p \cdot \hat{T}_m}\right\} \cdot \frac{L(\hat{T}_m)}{c_p \cdot \hat{T}_m} \\
 &\cdot w_s(\hat{T}_m, \hat{p}') \cdot \frac{1}{p'} \cdot \frac{3}{4} \left(\frac{\partial p_s}{\partial T_0}\right)_0 - \left(\frac{\partial \theta_e}{\partial T_0}\right)_0 \\
 &+ \left(\frac{\partial F}{\partial T_m}\right)_0 \cdot \left(\frac{\partial T_m}{\partial T_0}\right)_0 - \frac{0.286}{p'} \cdot (\hat{F} + \hat{\theta}_e) \cdot \frac{3}{4} \left(\frac{\partial p_s}{\partial T_0}\right)_0
 \end{aligned} \tag{D.20}$$

with

$$\left(\frac{\partial p_s}{\partial T_0}\right)_0 = -\frac{3.5}{223.15} \left(\frac{1}{\frac{\hat{T}_0 - \hat{T}_d}{223.15} + 1}\right) \cdot \hat{p}_s \tag{D.21}$$

$$\begin{aligned}
 \left(\frac{\partial \theta_e}{\partial T_0}\right)_0 &= \left(\frac{p_n}{\hat{p}_0}\right)^{0.286} \cdot \exp\left\{\frac{L(\hat{T}_s) \cdot w_s(\hat{T}_s, \hat{p}_s)}{c_p \cdot \hat{T}_s}\right\} \\
 &+ \left(\frac{\partial T_s}{\partial T_0}\right)_0 \cdot \hat{\theta}_e \cdot \left[\frac{D_1 \cdot 3.5 (\hat{T}_s - 223.15)^{2.5}}{\hat{p}_s} \cdot \frac{L(\hat{T}_s)}{c_p \cdot \hat{T}_s} \right. \\
 &\left. - B \cdot \frac{w_s(\hat{T}_s, \hat{p}_s)}{c_p \cdot \hat{T}_s} - \frac{L(\hat{T}_s) \cdot w_s(\hat{T}_s, \hat{p}_s)}{c_p \cdot \hat{T}_s^2} \right] \\
 &- \left(\frac{\partial p_s}{\partial T_0}\right)_0 \cdot \hat{\theta}_e \cdot \frac{L(\hat{T}_s) \cdot w_s(\hat{T}_s, \hat{p}_s)}{c_p \cdot \hat{T}_s \cdot \hat{p}_s}
 \end{aligned} \tag{D.22}$$

Differentiation of Eq. (3.13) results in:

$$\left(\frac{\partial T_s}{\partial T_0}\right)_0 = \frac{\hat{T}_s}{\hat{T}_0} - \frac{\hat{T}_s}{223.15} \cdot \left(\frac{1}{\frac{\hat{T}_0 - \hat{T}_d}{223.15} + 1}\right) \quad (D.23)$$

The derivative $\left(\frac{\partial F}{\partial T_m}\right)_0$ is given in Eqs. (B.4) through

(B.8) with $T = T_m$, $p = p'$ and all quantities evaluated at their mean values.

In order to complete the derivation of $\left(\frac{\partial F}{\partial T_0}\right)_0$, the derivative $\left(\frac{\partial T_m}{\partial T_0}\right)_0$ is needed.

Differentiation of Eq. (5.40) with respect to T_0 gives:

$$\begin{aligned} \left(\frac{\partial T_m}{\partial T_0}\right)_0 &= \frac{1}{p_0} \cdot \left(\frac{3}{4} p_s + \frac{1}{4} p_t\right)^{0.286} + 0.2145 \cdot \frac{T_0}{p_0} \\ &\cdot \left(\frac{3}{4} p_s + \frac{1}{4} p_t\right)^{-0.714} \cdot \left(\frac{\partial p_s}{\partial T_0}\right)_0 \end{aligned} \quad (D.24)$$

with the derivative $\left(\frac{\partial p_s}{\partial T_0}\right)_0$ given by Eq. (D.21).

A similar procedure was followed to obtain the derivatives $\left(\frac{\partial F}{\partial p_0}\right)_0$ and $\left(\frac{\partial F}{\partial T_d}\right)_0$. The relevant equations

are given next.

b)

$$\begin{aligned} \left(\frac{\partial F}{\partial p_0}\right)_0 &= -\frac{0.286}{\hat{p}_0} \cdot \frac{3}{4} \cdot \frac{\hat{p}_s}{\hat{p}_0} \cdot (\hat{F} + \hat{\theta}_e) - (\hat{F} + \hat{\theta}_e) \cdot \frac{L(\hat{T}_m)}{c_p \cdot \hat{T}_m} \cdot w_s(\hat{T}_m, p') \\ &\quad \cdot \frac{1}{\hat{p}'} \cdot \frac{3}{4} \cdot \frac{\hat{p}_s}{\hat{p}_0} - \left(\frac{\partial F}{\partial p_0}\right)_0 + \left(\frac{\partial F}{\partial T_m}\right)_0 \left(\frac{\partial T_m}{\partial p_0}\right)_0 \end{aligned} \quad (D.25)$$

$$\left(\frac{\partial \theta_e}{\partial p_0}\right)_0 = -\frac{0.286}{\hat{p}_0} \cdot \hat{\theta}_e - \hat{\theta}_e \cdot \frac{L(\hat{T}_s) \cdot w_s(\hat{T}_s, \hat{p}_s)}{c_p \cdot \hat{T}_s} \cdot \frac{1}{\hat{p}_0} \quad (D.26)$$

$$\begin{aligned} \left(\frac{\partial T_m}{\partial p_0}\right)_0 &= -\frac{0.286}{\hat{p}_0} \cdot \frac{\hat{T}_0}{\hat{p}_0 \cdot 0.286} \cdot \left(\frac{3}{4} p_s + \frac{1}{4} p_t\right)^{0.286} \\ &\quad + \frac{0.2145 \cdot \hat{T}_0}{\hat{p}_0 \cdot 0.286} \cdot \left(\frac{3}{4} p_s + \frac{1}{4} p_t\right)^{-0.714} \cdot \frac{\hat{p}_s}{\hat{p}_0} \end{aligned} \quad (D.27)$$

c) The derivatives with respect to T_d are:

$$\begin{aligned} \left(\frac{\partial F}{\partial T_d}\right)_0 &= -\frac{1}{\hat{p}'} \cdot (\hat{F} + \hat{\theta}_e) \cdot \frac{3}{4} \cdot \left(\frac{\partial p_s}{\partial T_d}\right)_0 \cdot \frac{L(\hat{T}_m) \cdot w_s(\hat{T}_m, \hat{p}')}{c_p \cdot \hat{T}_m} \\ &\quad - \left(\frac{\partial \theta_e}{\partial T_d}\right)_0 + \left(\frac{\partial F}{\partial T_m}\right)_0 \cdot \left(\frac{\partial T_m}{\partial T_d}\right)_0 - \frac{0.286}{\hat{p}} \cdot \frac{3}{4} \cdot (\hat{F} + \hat{\theta}_e) \cdot \left(\frac{\partial p_s}{\partial T_d}\right)_0 \end{aligned} \quad (D.28)$$

$$\left(\frac{\partial \theta_e}{\partial T_d}\right)_0 = \left(\frac{\partial \theta_e}{\partial T_s}\right)_0 \cdot \left(\frac{\partial T_s}{\partial T_d}\right)_0 + \left(\frac{\partial \theta_e}{\partial p_s}\right)_0 \cdot \left(\frac{\partial p_s}{\partial T_d}\right)_0 \quad (D.29)$$

$$\left(\frac{\partial \theta_e}{\partial T_s}\right)_0 = \left[\frac{B \cdot w_s(\hat{T}_s, \hat{p}_s)}{c_p \cdot \hat{T}_s} + 3.5 \cdot \frac{L(\hat{T}_s)}{c_p \cdot \hat{T}_s} \cdot D_1 \cdot \frac{(\hat{T}_s - 223.15)^{2.5}}{\hat{p}_s} - \frac{L(\hat{T}_s) \cdot w_s(\hat{T}_s, \hat{p}_s)}{c_p \cdot \hat{T}_s^2} \right] \cdot \hat{\theta}_e \quad (D.30)$$

$$\left(\frac{\partial \theta_e}{\partial p_s}\right)_0 = - \frac{L(\hat{T}_s) \cdot w_s(\hat{T}_s, \hat{p}_s)}{c_p \cdot \hat{T}_s} \cdot \frac{1}{\hat{p}_s} \cdot \hat{\theta}_e \quad (D.31)$$

$$\left(\frac{\partial T_s}{\partial T_d}\right)_0 = \frac{1}{223.15} \cdot \frac{\hat{T}_s^2}{\hat{T}_0} \quad (D.32)$$

$$\left(\frac{\partial p_s}{\partial T_d}\right)_0 = \frac{3.5}{223.15} \cdot \hat{p}_s \cdot \frac{\hat{T}_s}{\hat{T}_0} \quad (D.33)$$

$$\left(\frac{\partial T_m}{\partial T_d}\right)_0 = 0.2145 \cdot \frac{\hat{T}_0}{\hat{p}_0} \left(\frac{3}{4} \hat{p}_s + \frac{1}{4} \hat{p}_t\right)^{-0.714} \cdot \left(\frac{\partial p_s}{\partial T_d}\right)_0 \quad (D.34)$$

At this stage, the derivatives $\left(\frac{\partial F}{\partial u_i}\right)_0$, $i = 1, 2, 3$

in Eq. (D.19) have been determined. The derivative

$\left(\frac{\partial F}{\partial p_t}\right)_0$ is given in Eq. (B.12) with all quantities

evaluated at their current estimates. Therefore,

$$\left(\frac{\partial p_t}{\partial u_i}\right)_0 \text{ follows from Eq. (D.19).}$$

3) The derivatives $\left(\frac{\partial T_t}{\partial u_i}\right)_0$ in Eq. (D.15), can be obtained

by differentiation of the function F' with:

$$F' = T_t \cdot \left(\frac{p_n}{p_t}\right)^{0.286} \cdot \exp\left\{\frac{L(T_t) \cdot w_s(T_t, p_t)}{c_p \cdot T_t}\right\} - \theta_e = 0 \quad (\text{D.35})$$

following the pseudo-adiabatic Eq. (3.16).

Differentiation of Eq. (D.35) gives:

$$\left(\frac{\partial F'}{\partial u_i}\right)_0 + \left(\frac{\partial F'}{\partial p_t}\right)_0 \cdot \left(\frac{\partial p_t}{\partial u_i}\right)_0 + \left(\frac{\partial F'}{\partial T_t}\right)_0 \cdot \left(\frac{\partial T_t}{\partial u_i}\right)_0 = 0 \quad ; \quad i=1,2,3 \quad (\text{D.36})$$

Solving for the last derivative one obtains:

$$\left(\frac{\partial T_t}{\partial u_i}\right)_0 = -\frac{\left(\frac{\partial F'}{\partial u_i}\right)_0 + \left(\frac{\partial F'}{\partial p_t}\right)_0 \cdot \left(\frac{\partial p_t}{\partial u_i}\right)_0}{\left(\frac{\partial F'}{\partial T_t}\right)_0} \quad ; \quad i = 1, 2, 3 \quad (\text{D.37})$$

Next, expressions for the right-hand side derivations of Eq. (D.37) are sought.

a) At first, concentrate on $\left(\frac{\partial F'}{\partial u_i}\right)_0$. It holds:

$$\left(\frac{\partial F'}{\partial u_i}\right)_0 = - \left(\frac{\partial \theta}{\partial u_i}\right)_0 ; \quad i = 1, 2, 3 \quad (D.38)$$

with the right-hand side derivatives given in Eqs. (D.22), (D.26), and (D.29), for $u_1 = T_0$, $u_2 = p_0$ and $u_3 = T_d$, respectively.

Differentiation of Eq. (D.35) with respect to p_t gives:

$$\left(\frac{\partial F'}{\partial p_t}\right)_0 = - \frac{0.286}{\hat{p}_t} \cdot (\hat{F}' + \hat{\theta}_e) - \frac{1}{\hat{p}_t} \cdot \frac{L(\hat{T}_t) \cdot w_s(\hat{T}_t, \hat{p}_t)}{c_p \cdot \hat{T}_t} \cdot (\hat{F}' + \hat{\theta}_e) \quad (D.39)$$

Differentiation of the same equation with respect to T_t yields:

$$\begin{aligned} \left(\frac{\partial F'}{\partial T_t}\right)_0 &= \left(\frac{\hat{F}' + \hat{\theta}_e}{\hat{T}_t}\right) + (\hat{F}' + \hat{\theta}_e) \cdot \left[-B \cdot \frac{w_s(\hat{T}_t, \hat{p}_t)}{c_p \cdot \hat{T}_t}\right] \\ &+ \left[\frac{L(\hat{T}_t) \cdot 3.5 \cdot (\hat{T}_t - 223.15)^{2.5} \cdot D_1}{c_p \cdot \hat{T}_t \cdot \hat{p}_t} - \frac{L(\hat{T}_t) \cdot w_s(\hat{T}_t, \hat{p}_t)}{c_p \cdot \hat{T}_t^2}\right] \end{aligned} \quad (D.40)$$

Use of Eqs. (D.38), (D.39), (D.40) and (D.19) in

Eq. (D.37) gives an expression for the derivative

$$\left(\frac{\partial T_t}{\partial u_i}\right)_0, \text{ for } i = 1, 2, 3.$$

At this stage, the derivative $\left(\frac{\partial(\Delta w)}{\partial u_i}\right)_0$, for $i = 1, 2, 3$

can be determined by use of Eqs. (D.11) through (D.40).

II.) Based on the definition of ρ_m and on the ideal gas law, one obtains:

$$\rho_m = \frac{1}{2} \left(\frac{P_t}{R \cdot T_t} + \frac{P_s}{R \cdot T_s} \right) \quad (D.41)$$

where R is the dry air ideal gas constant defined in Chapter 3.

Then, by differentiation of Eq. (D.41) one obtains:

$$\begin{aligned} \left(\frac{\partial(\rho_m)}{\partial u_i}\right)_0 &= \frac{1}{2R} \cdot \left[\frac{\left(\frac{\partial p_t}{\partial u_i}\right)_0 \cdot \hat{T}_t - \hat{p}_t \cdot \left(\frac{\partial T_t}{\partial u_i}\right)_0}{\hat{T}_t^2} \right. \\ &\quad \left. + \frac{\left(\frac{\partial p_s}{\partial u_i}\right)_0 \cdot \hat{T}_s - \hat{p}_s \cdot \left(\frac{\partial T_s}{\partial u_i}\right)_0}{\hat{T}_s^2} \right] \quad (D.42) \end{aligned}$$

All the derivatives in Eq. (D.42), except $(\frac{\partial T_s}{\partial p_0})_0$ and $(\frac{\partial p_s}{\partial p_0})_0$, have already been defined. The remaining two ones are given by:

$$(\frac{\partial T_s}{\partial p_0})_0 = 0 \quad (D.43)$$

$$(\frac{\partial p_s}{\partial p_0})_0 = \frac{\hat{T}}{T_0} \quad (D.44)$$

III) In order to complete the derivation of M_{Fi} in Eq. (D.10) for $i = 1, 2, 3$, one needs to determine $(\frac{\partial v}{\partial u_i})_0$. Use of the definition Eqs. (5.34) and (5.35) and differentiation results in:

$$(\frac{\partial v}{\partial u_i})_0 = \epsilon_1 \cdot \sqrt{c_p} \cdot \frac{1}{2} \cdot (\hat{T}_m - \hat{T}_s)^{-\frac{1}{2}} \cdot ((\frac{\partial T_m}{\partial u_i})_0 - (\frac{\partial T_s}{\partial u_i})_0) \quad (D.45)$$

$i = 1, 2, 3$

Equations (D.24), (D.27) and (D.34) define the derivative $(\frac{\partial T_m}{\partial u_i})_0$. Differentiation of Eq. (5.37) with respect to the input variables gives:

$$\left(\frac{\partial T_s'}{\partial T_0}\right)_0 = \frac{\hat{T}_s'}{\hat{T}_0} + D_2 \cdot \left(\frac{\partial p_s}{\partial T_0}\right)_0 \quad (D.46)$$

with D_2 defined for notational convenience as:

$$D_2 = 0.2145 \cdot \frac{\hat{T}_0}{\hat{p}_0^{0.286}} \cdot \left(\frac{3}{4} \hat{p}_s + \frac{1}{4} \hat{p}_t\right)^{-0.714} \quad (D.47)$$

$$\left(\frac{\partial T_s'}{\partial p_0}\right)_0 = -\frac{0.286}{\hat{p}_0} \cdot \hat{T}_s' + D_2 \cdot \left(\frac{\partial p_s}{\partial p_0}\right)_0 \quad (D.48)$$

$$\left(\frac{\partial T_s'}{\partial T_d}\right)_0 = D_2 \cdot \left(\frac{\partial p_s}{\partial T_d}\right)_0 \quad (D.49)$$

D.1.2 Derivatives of Model Output Function with Respect to the Input Variables

Define M_{h_i} by:

$$M_{h_i} = \left(\frac{\partial h(\underline{u})}{\partial u_i}\right)_0 \quad ; \quad i = 1, 2, 3 \quad (D.50)$$

with $h(\cdot)$ given by Eq. (5.26).

Then:

$$\begin{aligned}
 M_{h_i} = & \left(\frac{\partial h(\underline{u})}{\partial v_p} \right)_0 \cdot \left(\frac{\partial v_p}{\partial u_i} \right)_0 + \left(\frac{\partial h(\underline{u})}{\partial Z_c} \right)_0 \cdot \left(\frac{\partial Z_c}{\partial u_i} \right)_0 \\
 & + \left(\frac{\partial h(\underline{u})}{\partial N_v} \right)_0 \cdot \left(\frac{\partial N_v}{\partial u_i} \right)_0
 \end{aligned} \tag{D.51}$$

I) Differentiation of Eq. (5.26) with respect to v_p , Z_c and

N_v results in:

$$\begin{aligned}
 \left(\frac{\partial h(\underline{u})}{\partial v_p} \right)_0 = & \frac{1}{\hat{Z}_c \cdot \delta} \cdot \left[\frac{1 + \frac{3}{4} \hat{N}_v + \frac{\hat{N}_v^2}{4} + \frac{\hat{N}_v^3}{24}}{e^{\hat{N}_v}} \right. \\
 & \left. + \frac{1 + \frac{3}{4} (\gamma \hat{N}_v) + \frac{(\gamma \hat{N}_v)^2}{4} + \frac{(\gamma \hat{N}_v)^3}{24}}{\gamma^5 \cdot e^{\gamma \hat{N}_v}} + \frac{\hat{N}_v}{4 \cdot \gamma^4} - \frac{1}{\gamma^5} \right]
 \end{aligned} \tag{D.52}$$

$$\left(\frac{\partial h(\underline{u})}{\partial Z_c} \right)_0 = - \frac{h(\hat{u})}{\hat{Z}_c} \tag{D.53}$$

$$\begin{aligned}
 \left(\frac{\partial h(\underline{u})}{\partial N_v} \right)_0 = & - \frac{\hat{v}_p}{\hat{Z}_c \cdot \delta} \cdot \left[\frac{\frac{1}{4} + \frac{\hat{N}_v}{4} + \frac{\hat{N}_v^2}{8} + \frac{\hat{N}_v^3}{24}}{e^{\hat{N}_v}} \right. \\
 & \left. + \frac{1}{\gamma^4} \cdot \frac{\frac{1}{4} + \frac{\gamma \hat{N}_v}{4} + \frac{(\gamma \hat{N}_v)^2}{8} + \frac{(\gamma \hat{N}_v)^3}{24}}{e^{\gamma \hat{N}_v}} - \frac{1}{4 \cdot \gamma^4} \right]
 \end{aligned} \tag{D.54}$$

II) Equations (5.16) and (5.42) differentiated yield:

$$\left(\frac{\partial v}{\partial u_i}\right)_0 = 4\alpha \cdot \varepsilon_4 \cdot m \cdot \hat{v}^{(m-1)} \cdot \left(\frac{\partial v}{\partial u_i}\right)_0 \quad ; \quad i = 1, 2, 3 \quad (D.55)$$

The derivative $\left(\frac{\partial v}{\partial u_i}\right)_0$, $i = 1, 2, 3$ has been determined in

Eq. (D.45).

III) The hypsometric equation (eq. (5.27)) applied to the cloud height Z_c gives:

$$Z_c = \frac{R \cdot \left(\frac{T_t + T_s}{2}\right)}{g} \cdot \ln \left(\frac{p_s}{p_t}\right) \quad (D.56)$$

Differentiation of this equation results in:

$$\begin{aligned} \left(\frac{\partial Z_c}{\partial u_i}\right)_0 &= \frac{R}{2g} \cdot \left[\left(\frac{\partial T_t}{\partial u_i}\right)_0 + \left(\frac{\partial T_s}{\partial u_i}\right)_0\right] \cdot \ln \left(\frac{\hat{p}_s}{\hat{p}_t}\right) \\ &+ \frac{R}{2g} \cdot (\hat{T}_t + \hat{T}_s) \cdot \left[\left(\frac{\partial p_s}{\partial u_i}\right)_0 \cdot \frac{1}{\hat{p}_s} - \frac{1}{\hat{p}_t} \left(\frac{\partial p_t}{\partial u_i}\right)_0\right] \quad ; \quad i=1,2,3 \quad (D.57) \end{aligned}$$

Expressions for all the derivatives of the right-hand side in Eq. (D.57) have been previously given in this Appendix.

IV) In order to complete the evaluation of M_{h_i} , in Eq. (D.51),

the derivative $(\frac{\partial N_v}{\partial u_i})_0$, $i = 1, 2, 3$ has to be determined.

Combining Eqs. (5.14), (5.42) and (5.43) results in:

$$N_v = \frac{\beta}{\alpha \cdot \varepsilon_4} \cdot v^{(1-m)} \quad (D.58)$$

Therefore:

$$(\frac{\partial N_v}{\partial u_i})_0 = \frac{\beta}{\alpha \cdot \varepsilon_4} \cdot \frac{(1-m)}{v^m} \cdot (\frac{\partial v}{\partial u_i})_0 \quad ; \quad i = 1, 2, 3 \quad (D.59)$$

D.1.3 Derivatives of Surface Precipitation Rate Output with Respect to the Input Variables

Define the derivative M_{ϕ_i} as:

$$M_{\phi_i} = (\frac{\partial \phi(u)}{\partial u_i})_0 \quad ; \quad i = 1, 2, 3 \quad (D.60)$$

By means of Eqs. (5.29) and (D.60) one obtains:

$$M_{\phi_i} = (\frac{\partial \phi(u)}{\partial v_p})_0 \cdot (\frac{\partial v_p}{\partial u_i})_0 + (\frac{\partial \phi(u)}{\partial Z_c})_0 \cdot (\frac{\partial Z_c}{\partial u_i})_0 + (\frac{\partial \phi(u)}{\partial N_v})_0 \cdot (\frac{\partial N_v}{\partial u_i})_0 + (\frac{\partial \phi(u)}{\partial N_D})_0 \cdot (\frac{\partial N_D}{\partial u_i})_0 \quad ; \quad i = 1, 2, 3 \quad (D.61)$$

The derivatives of v_p , Z_c , N_v with respect to u_i were determined previously. The rest of the derivatives are given in the following.

- I) The two cases corresponding to whether or not N_D is greater than N_v are treated separately. However, it is noted that at the point \underline{u}_0 where $N_D = N_v$, the function $\phi(\underline{u})$ is continuous and possesses continuous derivatives with respect to the elements of \underline{u} .

A) $N_D \geq N_v$

$$\left(\frac{\partial \phi(\underline{u})}{\partial v_p}\right)_0 = \frac{1}{\hat{Z}_c \cdot \delta} \cdot \frac{\left(1 - \frac{\hat{N}_v}{4}\right) \left(1 + \hat{N}_D + \frac{\hat{N}_D^2}{2}\right) + \frac{\hat{N}_D^3}{8}}{e^{\hat{N}_D}} \quad (\text{D.62})$$

$$\left(\frac{\partial \phi(\underline{u})}{\partial Z_c}\right)_0 = - \frac{\phi(\hat{\underline{u}}(t))}{\hat{Z}_c} \quad (\text{D.63})$$

$$\left(\frac{\partial \phi(\underline{u})}{\partial N_v}\right)_0 = -\frac{1}{4} \cdot \left(1 + \hat{N}_D + \frac{\hat{N}_D^2}{2}\right) \cdot e^{-\hat{N}_D} \cdot \frac{\hat{v}_p}{\hat{Z}_c \cdot \delta} \quad (\text{D.64})$$

$$\left(\frac{\partial \phi(\underline{u}(t))}{\partial N_D}\right)_0 = -\frac{1}{8} \cdot \frac{\hat{N}_D^2 + \hat{N}_D^3 - \hat{N}_v \cdot \hat{N}_D^2}{e^{\hat{N}_D}} \cdot \frac{\hat{v}_p}{\hat{Z}_c \cdot \delta} \quad (\text{D.65})$$

$$\left(\frac{\partial N_D}{\partial u_i}\right)_0 = \left[\frac{\partial \left(\frac{D_c}{\epsilon_4 \cdot v^m} \right)}{\partial u_i} \right]_0 ; i = 1, 2, 3 \quad (D.66)$$

The derivative in Eq. (D.66) is expanded to the following:

$$\left(\frac{\partial N_D}{\partial u_i}\right)_0 = \frac{1}{\epsilon_4} \cdot \frac{\left(\frac{\partial D_c}{\partial u_i}\right)_0 \cdot \hat{v}^m - \hat{D}_c \cdot m \cdot \hat{v}^{m-1} \cdot \left(\frac{\partial v}{\partial u_i}\right)_0}{\hat{v}^{2m}} ; i=1,2,3 \quad (D.67)$$

- 1) It is necessary to determine the derivatives of the characteristic diameter D_c with respect to the input variables T_0 , p_0 , T_d . From Eq. (4.41):

$$\begin{aligned} \left(\frac{\partial D_c}{\partial u_i}\right)_0 &= \frac{4}{3} \cdot \frac{1}{\hat{D}_c^2} \cdot \frac{1}{C_1 \cdot R_v} \cdot \left[\left(\frac{\partial D_{AB}}{\partial u_i}\right)_0 \cdot \hat{Z}_b \cdot \left(\frac{e_s(\hat{T}_w)}{\hat{T}_w} - \frac{e_s(\hat{T}_d)}{\hat{T}_0}\right)\right. \\ &\quad + \hat{D}_{AB} \cdot \left(\frac{\partial Z_b}{\partial u_i}\right)_0 \cdot \left(\frac{e_s(\hat{T}_w)}{\hat{T}_w} - \frac{e_s(\hat{T}_d)}{\hat{T}_0}\right) \\ &\quad + \hat{D}_{AB} \cdot \hat{Z}_b \cdot \left(\frac{0.0028 \cdot (\hat{T}_w - 223.15)^{2.5}}{\hat{T}_w} - \frac{e_s(\hat{T}_w)}{\hat{T}_w^2}\right) \cdot \left(\frac{\partial T_w}{\partial u_i}\right)_0 \\ &\quad \left. - \hat{D}_{AB} \cdot \hat{Z}_b \cdot \left(\frac{e_s(\hat{T}_d)}{\hat{T}_0}\right) \right] \cdot \left(\frac{\partial}{\partial u_i}\right)_0 \end{aligned} \quad (D.68)$$

a) Taking derivatives of Eq. (4.24) with respect to the input variables results in:

$$\left(\frac{\partial D_{AB}}{\partial T_0}\right)_0 = 4.0934 \cdot 10^{-5} \cdot \frac{\hat{T}_0^{0.94}}{T^* 1.94} \cdot \frac{P^*}{\hat{P}_0} \quad (D.69)$$

$$\left(\frac{\partial D_{AB}}{\partial P_0}\right)_0 = - \frac{\hat{D}_{AB}}{\hat{P}_0} \quad (D.70)$$

$$\left(\frac{\partial D_{AB}}{\partial T_d}\right)_0 = 0 \quad (D.71)$$

b) The expression for Z_b is (see also Eq. (5.27));

$$Z_b = \frac{R}{g} \cdot \left(\frac{T_0 + T_s}{2}\right) \ln \cdot \left(\frac{P_0}{P_s}\right) \quad (D.72)$$

Differentiation results in:

$$\begin{aligned} \left(\frac{\partial Z_b}{\partial T_0}\right)_0 &= \frac{R}{2g} \cdot \left[\left(1 + \left(\frac{\partial T_s}{\partial T_0}\right)_0\right) \cdot \ln \cdot \left(\frac{\hat{P}_0}{\hat{P}_s}\right) \right. \\ &\quad \left. - (\hat{T}_0 + \hat{T}_s) \cdot \frac{1}{\hat{P}_s} \cdot \left(\frac{\partial P_s}{\partial T_0}\right)_0 \right] \quad (D.73) \end{aligned}$$

$$\left(\frac{\partial Z_b}{\partial p_0}\right)_0 = \frac{R}{2g} \cdot (\hat{T}_0 + \hat{T}_s) \cdot \frac{1}{\hat{p}_0} \quad (D.74)$$

$$\left(\frac{\partial Z_b}{\partial T_d}\right)_0 = \frac{R}{2g} \cdot \left[\left(\frac{\partial T_s}{\partial T_d}\right)_0 \cdot \ln \cdot \left(\frac{\hat{p}_0}{\hat{p}_s}\right) - (\hat{T}_0 + \hat{T}_s) \cdot \frac{1}{\hat{p}_s} \cdot \left(\frac{\partial p_s}{\partial T_d}\right)_0 \right] \quad (D.75)$$

- c) For the linearization purposes and to avoid the complications arising from the implicit function $T_w(T_0, p_0, T_d)$ in Eq. (4.38), T_w is taken approximately equal to T_0 . Then:

$$\left(\frac{\partial T_w}{\partial T_0}\right)_0 = 1 \quad (D.76)$$

$$\left(\frac{\partial T_w}{\partial u_i}\right)_0 = 0 \quad ; \quad i = 2, 3 \quad (D.77)$$

- d) Finally, to complete the derivation of $\left(\frac{\partial D_c}{\partial u_i}\right)_0$:

$$\left(\frac{\partial \left(\frac{e_s(T_d)}{T_0}\right)}{\partial T_0}\right)_0 = - \frac{e_s(\hat{T}_d)}{\hat{T}_0^2} \quad (D.78)$$

$$\left(\frac{\partial \left(\frac{e_s(T_d)}{T_0}\right)}{\partial p_0}\right)_0 = 0 \quad (\text{D.79})$$

$$\left(\frac{\partial \left(\frac{e_s(T_d)}{T_0}\right)}{\partial T_d}\right) = \frac{0.0028 \cdot (\hat{T}_d - 223.15)^{2.5}}{\hat{T}_0} \quad (\text{D.80})$$

B) $N_v \geq N_D$

$$\left(\frac{\partial \phi(\underline{u}(t))}{\partial v_p}\right)_0 = \frac{1}{\hat{z}_c \cdot \delta} \cdot \left(\frac{1 + \frac{3}{4} \hat{N}_v + \frac{1}{4} \hat{N}_v^2 + \frac{1}{24} \hat{N}_v^3 - \frac{1}{24} \hat{N}_D^3}{e^{\hat{N}_v}}\right) \quad (\text{D.81})$$

$$\left(\frac{\partial \phi(\underline{u}(t))}{\partial N_D}\right)_0 = -\frac{1}{4} \cdot \left(\frac{1 + \hat{N}_v + \frac{\hat{N}_v^2}{2} + \frac{\hat{N}_v^3}{6} - \frac{\hat{N}_D^3}{6}}{e^{\hat{N}_v}}\right) \cdot \frac{\hat{v}_p}{\hat{z}_c \cdot \delta} \quad (\text{D.82})$$

$$\left(\frac{\partial \phi(\underline{u}(t))}{\partial N_D}\right)_0 = -\frac{1}{8} \cdot \frac{\hat{N}_D^2}{e^{\hat{N}_v}} \cdot \frac{\hat{v}_p}{\hat{z}_c \cdot \delta} \quad (\text{D.83})$$

The rest of the necessary derivatives for this case, arising from Eq. (D.61), are as determined in the case when $N_D \geq N_v$.

Appendix E

SOIL MOISTURE ACCOUNTING MODEL
LINEARIZED EQUATIONS

This Appendix presents the linearization, by Taylor's series expansion, of the soil model given by Eqs. (6.5) through (6.12). The matrix subscripts are such that the state of the precipitation model is the first element of the state vector. The soil states follow in the order presented in Table 6.1. The potential evapotranspiration rate input is the fourth element of the input vector $\underline{u}(t)$; the first three input elements correspond to the precipitation model. Only the non-zero elements of the linearization matrices and vectors are given.

Define first:

$$D_3 = C_1 \cdot (1 + \varepsilon \cdot \hat{y}^\theta) \frac{\hat{x}_2}{x_2} \quad (E.1)$$

$$D_4 = C_1 \cdot \frac{\hat{x}_2}{x_2} \cdot \varepsilon \cdot \theta \cdot \hat{y}^{\theta-1} \cdot \left(\frac{1}{x_3^0 + x_4^0 + x_5^0} \right) \quad (E.2)$$

$$D_5 = C_1 \cdot \varepsilon \cdot \theta \cdot \hat{y}^{(\theta-1)} \cdot \left(\frac{1}{x_3^0 + x_4^0 + x_5^0} \right) \cdot \frac{\hat{x}_2}{x_2} \cdot (1 - p_f) \\ \cdot \left[1 - \left(\frac{\hat{x}_3}{x_3} \right)^{m_3} \right] \quad (E.3)$$

$$D_6 = 1 - (1 - P_f) \cdot \left[1 - \left(\frac{\hat{x}_3}{x_3}\right)^{m_3}\right] \quad (\text{E.4})$$

$$D_7 = \left(C_2 \cdot \frac{\hat{x}_5}{x_5} - 1\right) \cdot \frac{\hat{x}_4}{x_4} + 1 \quad (\text{E.5})$$

$$D_8 = D_4 \cdot D_6 \cdot D_7 \quad (\text{E.6})$$

$$D_9 = D_4 \cdot D_6 \cdot (1 - D_7) \quad (\text{E.7})$$

Equation 6.7,

$$F_2 = \left[1 - \left(\frac{x_1}{x_1}\right)^{m_1}\right] \cdot \phi \cdot X - u_e \cdot \frac{x_1}{x_1} \quad (\text{E.8})$$

Then,

$$\bar{N}_{F_{21}} = \left[1 - \left(\frac{x_1}{x_1}\right)^{m_1}\right] \cdot \hat{\phi} \quad (\text{E.9})$$

$$\bar{N}_{F_{22}} = - \frac{m_1 \cdot \hat{x}_1}{x_1^{m_1}} \cdot \hat{\phi} \cdot \hat{X} - \frac{\hat{u}_e}{x_1} \quad (\text{E.10})$$

$$F_{-0_2} = \left[1 - \left(\frac{\hat{x}_1}{x_1}\right)^{m_1}\right] \cdot \hat{\phi} \cdot \hat{X} - \hat{u}_e \cdot \frac{\hat{x}_1}{x_1} \quad (\text{E.11})$$

$$\bar{M}_{F_{2i}} = \left[1 - \left(\frac{\hat{x}_1}{x_1}\right)^{m_1}\right] \cdot \hat{X} \cdot M_{\phi_i} \quad ; \quad i = 1, 2, 3 \quad (\text{E.12})$$

with M_{ϕ_i} , $i = 1, 2, 3$ defined in Appendix D.

$$\bar{M}_{F_{24}} = -\frac{\hat{x}_1}{x_1} \quad (\text{E.13})$$

From Eq. (6.8):

$$F_3 = \left(\frac{x_1}{x_1}\right)^{m_1} \cdot \phi \cdot X \cdot \left[1 - \left(\frac{x_2}{x_2}\right)^{m_2}\right] - d_u \cdot x_2 - C_1 \cdot (1 + \varepsilon y^\theta) \cdot \frac{x_2}{x_2} \quad (\text{E.14})$$

Then:

$$\bar{N}_{F_{31}} = \left(\frac{\hat{x}_1}{x_1}\right)^{m_1} \cdot \hat{\phi} \cdot \left[1 - \left(\frac{\hat{x}_2}{x_2}\right)^{m_2}\right] \quad (\text{E.15})$$

$$\bar{N}_{F_{32}} = \frac{m_1 \cdot \hat{x}_1^{(m_1-1)}}{(x_1^0)^{m_1}} \cdot \hat{\phi} \cdot \hat{X} \cdot \left[1 - \left(\frac{x_2}{x_2}\right)^{m_2}\right] \quad (\text{E.16})$$

$$\bar{N}_{F_{33}} = -\left(\frac{\hat{x}_1}{x_1}\right)^{m_1} \cdot \hat{\phi} \cdot \hat{X} \cdot \frac{m_2 \cdot \hat{x}_2^{(m_2-1)}}{(x_2^0)^{m_2}} - d_u - C_1 \cdot (1 + \varepsilon \hat{y}^\theta) \cdot \frac{1}{x_2} \quad (\text{E.17})$$

$$\bar{N}_{F34} = D_4 \quad (\text{E.18})$$

$$\bar{N}_{F35} = D_4 \quad (\text{E.19})$$

$$\bar{N}_{F36} = D_4 \quad (\text{E.20})$$

$$F_{O3} = \left(\frac{\hat{x}_1}{x_1}\right)^{m_1} \cdot \hat{\phi} \cdot \hat{X} \cdot \left[1 - \left(\frac{\hat{x}_2}{x_2}\right)^{m_2}\right] - d_u \cdot \hat{x}_2 - D_3 \quad (\text{E.21})$$

$$\bar{M}_{F3i} = \left(\frac{\hat{x}_1}{x_1}\right)^{m_1} \cdot \hat{X} \cdot \left[1 - \left(\frac{\hat{x}_2}{x_2}\right)^{m_2}\right] \cdot M_{\phi_i} ; \quad i = 1, 2, 3 \quad (\text{E.22})$$

From Eq. (6.9):

$$F_4 = C_1 (1 + \varepsilon y^\theta) \cdot \frac{x_2}{x_2} \cdot (1 - P_f) \cdot \left[1 - \left(\frac{x_3}{x_3}\right)^{m_3}\right] - u_e \left(1 - \frac{x_1}{x_1}\right) \cdot \frac{x_3}{x_1 + x_3} \quad (\text{E.23})$$

Then:

$$\bar{N}_{F42} = \hat{u}_e \cdot \frac{1}{x_1} \left(\frac{\hat{x}_3}{x_1 + x_3}\right) \quad (\text{E.24})$$

$$\bar{N}_{F43} = C_1 (1 + \varepsilon \hat{y}^\theta) \cdot \frac{1}{x_2} \cdot (1 - D_6) \quad (E.25)$$

$$\begin{aligned} \bar{N}_{F44} &= -D_3 \cdot (1 - P_f) \cdot m_3 \cdot \frac{\hat{x}_3^{(m_3-1)}}{(x_3^0)^{m_3}} \\ &\quad - \hat{u}_e \left(1 - \frac{\hat{x}_1}{x_1^0}\right) \frac{1}{x_1^0 + x_3^0} - D_5 \end{aligned} \quad (E.26)$$

$$\bar{N}_{F45} = -D_5 \quad (E.27)$$

$$\bar{N}_{F46} = -D_5 \quad (E.28)$$

$$\bar{F}_{O4} = D_3 \cdot (1 - D_6) - \hat{u}_e \cdot \left(1 - \frac{\hat{x}_1}{x_1^0}\right) \cdot \frac{\hat{x}_3}{x_1^0 + x_3^0} \quad (E.29)$$

$$\bar{M}_{F44} = -\left(1 - \frac{\hat{x}_1}{x_1^0}\right) \frac{\hat{x}_3}{x_1^0 + x_3^0} \quad (E.30)$$

From Eq. (6.10):

$$\begin{aligned} F_5 &= -d_\ell' \cdot x_4 + C_1 (1 + \varepsilon y^\theta) \cdot \frac{x_2}{x_2} \cdot [1 - (1 - P_f) \cdot [1 - \left(\frac{x_3}{x_3^0}\right)^{m_3}]] \\ &\quad \cdot \left[\left(C_2 \frac{x_5}{x_5} - 1\right) \cdot \frac{x_4}{x_4} + 1\right] \end{aligned} \quad (E.31)$$

Then:

$$\bar{N}_{F53} = C_1 (1 + \varepsilon \hat{y}^\theta) \cdot \frac{1}{x_2} \cdot D_6 \cdot D_7 \quad (\text{E.32})$$

$$\bar{N}_{F54} = D_3 (1 - P_f) \cdot \frac{m_3 \cdot \hat{x}_3^{(m_3-1)}}{(x_3^0)^{m_3}} \cdot D_7 - D_8 \quad (\text{E.33})$$

$$\bar{N}_{F55} = -d'_\ell + D_3 \cdot D_6 \left(C_2 \cdot \frac{\hat{x}_5}{x_5} - 1 \right) \cdot \frac{1}{x_4} - D_8 \quad (\text{E.34})$$

$$\bar{N}_{F56} = D_3 \cdot D_6 \cdot C_2 \cdot \frac{1}{x_5} \frac{\hat{x}_4}{\bar{x}_4} - D_8 \quad (\text{E.35})$$

$$F_{05} = -d'_\ell \cdot \hat{x}_4 + D_3 \cdot D_6 \cdot D_7 \quad (\text{E.36})$$

From Eq. (6.11):

$$F_6 = -d''_\ell \cdot x_5 + C_1 (1 + \varepsilon y^\theta) \cdot \frac{x_2}{x_2} \cdot [1 - (1 - P_f) \cdot [1 - \left(\frac{x_3}{x_3^0}\right)^{m_3}]] \cdot \left(1 - C_2 \cdot \frac{x_5}{x_5}\right) \cdot \frac{x_4}{x_4} \quad (\text{E.37})$$

Then:

$$\bar{N}_{F63} = C_1 (1 + \varepsilon \hat{y}^0) \cdot \frac{1}{x_2} \cdot D_6 (1 - D_7) \quad (E.38)$$

$$\bar{N}_{F64} = D_3 (1 - P_f) \cdot \frac{m_3 \cdot \hat{x}_3^{(m_3-1)}}{(x_3^0)^{m_3}} \cdot (1 - D_7) - D_9 \quad (E.39)$$

$$\bar{N}_{F65} = D_3 \cdot D_6 (1 - C_2 \cdot \frac{\hat{x}_5}{x_5^0}) \cdot \frac{1}{x_4} - D_9 \quad (E.40)$$

$$\bar{N}_{F66} = -d_l'' - D_3 \cdot D_6 \cdot C_2 \cdot \frac{1}{x_5} \cdot \frac{\hat{x}_4}{x_4^0} - D_9 \quad (E.41)$$

$$F_{0_6} = -d_l'' \cdot \hat{x}_5 + D_3 \cdot D_6 (1 - D_7) \quad (E.42)$$

Finally, from Eq. (6.12):

$$F_7 = [1 - (\frac{x_6 - x_1}{x_3^0})^2 \cdot (\frac{x_1}{x_1^0})^{m_1}] \cdot \phi \cdot X$$

$$- u_e (1 - \frac{x_1}{x_1^0}) (\frac{x_6 - x_1}{x_3^0 + x_1^0}) - u_e \cdot \frac{x_1}{x_1^0}$$

$$- [1 - (\frac{x_6 - x_1}{x_3^0})^2 \cdot (\frac{x_2}{x_2^0})^{m_2} \cdot (\frac{x_1}{x_1^0})^{m_1}] \cdot \phi \cdot X \quad (E.43)$$

Then:

$$\begin{aligned} \bar{N}_{F71} &= \left[1 - \left(\frac{\hat{x}_6 - \hat{x}_1}{x_3} \right)^2 \cdot \left(\frac{\hat{x}_1}{x_1} \right)^{m_1} \right] \cdot \hat{\phi} \\ &- \left[1 - \left(\frac{\hat{x}_6 - \hat{x}_1}{x_3} \right)^2 \right] \cdot \left(\frac{\hat{x}_2}{x_2} \right)^{m_2} \cdot \left(\frac{\hat{x}_1}{x_1} \right)^{m_1} \cdot \hat{\phi} \end{aligned} \quad (E.44)$$

$$\begin{aligned} \bar{N}_{F72} &= -\hat{\phi} \cdot \hat{X} \cdot \left[\frac{m_1 \cdot \hat{x}_1^{(m_1-1)}}{(x_1^0)^{m_1}} \cdot \left(\frac{\hat{x}_6 - \hat{x}_1}{x_3} \right)^2 - \frac{2(\hat{x}_6 - \hat{x}_1)}{(x_3^0)^2} \cdot \left(\frac{\hat{x}_1}{x_1} \right)^{m_1} \right] \\ &+ \hat{u}_e \cdot \frac{1}{x_1} \cdot \left(\frac{\hat{x}_6 - \hat{x}_1}{x_3 + x_1} \right) + \hat{u}_e \cdot \left(1 - \frac{\hat{x}_1}{x_1} \right) \cdot \left(\frac{1}{x_3 + x_1} \right) - \frac{\hat{u}_e}{x_1} \\ &- \left(\frac{\hat{x}_2}{x_2} \right)^{m_2} \cdot \hat{\phi} \cdot \hat{X} \cdot \frac{m_1 \cdot \hat{x}_1^{(m_1-1)}}{(x_1^0)^{m_1}} \cdot \left[1 - \left(\frac{\hat{x}_6 - \hat{x}_1}{x_3} \right)^2 \right] \\ &- \left(\frac{\hat{x}_2}{x_2} \right)^{m_2} \cdot \left(\frac{\hat{x}_1}{x_1} \right)^{m_1} \cdot \hat{\phi} \cdot \hat{X} \cdot \frac{2(\hat{x}_6 - \hat{x}_1)}{(x_3^0)^2} \end{aligned} \quad (E.45)$$

$$\bar{N}_{F73} = - \frac{m_2 \cdot \hat{x}_2^{(m_2-1)}}{(x_2^0)^{m_2}} \cdot \left(\frac{\hat{x}_1}{x_1} \right)^{m_1} \cdot \hat{\phi} \cdot \hat{X} \cdot \left[1 - \left(\frac{\hat{x}_6 - \hat{x}_1}{x_3} \right)^2 \right] \quad (E.46)$$

$$\begin{aligned} \bar{N}_{F77} &= -\hat{\phi} \cdot \hat{X} \cdot \frac{2(\hat{x}_6 - \hat{x}_1)}{(x_3^0)^2} \cdot \left(\frac{\hat{x}_1}{x_1}\right)^{m_1} - \hat{u}_e \left(1 - \frac{\hat{x}_1}{x_1}\right) \left(\frac{1}{x_3^0 + x_1}\right) \\ &+ \frac{2(\hat{x}_6 - \hat{x}_1)}{(x_3^0)^2} \cdot \left(\frac{\hat{x}_2}{x_2}\right)^{m_2} \cdot \left(\frac{\hat{x}_1}{x_1}\right)^{m_1} \cdot \hat{\phi} \cdot \hat{X} \end{aligned} \quad (E.47)$$

$$\begin{aligned} \bar{E}_{07} &= \left[1 - \left(\frac{\hat{x}_6 - \hat{x}_1}{x_3}\right)^2 \cdot \left(\frac{\hat{x}_1}{x_1}\right)^{m_1}\right] \cdot \hat{\phi} \cdot \hat{X} \\ &- \hat{u}_e \left(1 - \frac{\hat{x}_1}{x_1}\right) \left(\frac{\hat{x}_6 - \hat{x}_1}{x_3 + x_1}\right) - \hat{u}_e \cdot \frac{\hat{x}_1}{x_1} \\ &- \left[1 - \left(\frac{\hat{x}_6 - \hat{x}_1}{x_3}\right)^2 \cdot \left(\frac{\hat{x}_2}{x_2}\right)^{m_2} \cdot \left(\frac{\hat{x}_1}{x_1}\right)^{m_1}\right] \cdot \hat{\phi} \cdot \hat{X} \end{aligned} \quad (E.48)$$

$$\begin{aligned} \bar{M}_{F7i} &= \left[1 - \left(\frac{\hat{x}_6 - \hat{x}_1}{x_3}\right)^2 \cdot \left(\frac{\hat{x}_1}{x_1}\right)^{m_1}\right] \cdot \hat{X} \cdot M_{\phi_i} \\ &- \left[1 - \left(\frac{\hat{x}_6 - \hat{x}_1}{x_3}\right)^2 \cdot \left(\frac{\hat{x}_2}{x_2}\right)^{m_2} \cdot \left(\frac{\hat{x}_1}{x_1}\right)^{m_1}\right] \cdot \hat{X} \cdot M_{\phi_i}; \quad i=1,2,3 \end{aligned} \quad (E.49)$$

$$\bar{M}_{F74} = -\left(1 - \frac{\hat{x}_1}{x_1}\right) \left(\frac{\hat{x}_6 - \hat{x}_1}{x_3 + x_1}\right) - \frac{\hat{x}_1}{x_1} \quad (E.50)$$

Appendix F

CHANNEL ROUTING MODEL LINEARIZED EQUATIONS

The formulation in Georgakakos and Bras (1982) of the statistically linearized routing model is used with some modification in the treatment of the channel input u_c . They treat u_c as a Gaussian random process with no time correlation. In the present formulation, it is a function of the soil and precipitation model states (by means of Eq. (6.13)). The ordinary Taylor's series expansion is used to linearize u_c with respect to the model states and inputs.

Note that the channel states occupy n positions in the state vector, starting from the eighth element. Adopting the notational convention of Appendix D, the component F_8 of \underline{F} for the first reservoir in the series is written as:

$$F_8 = p_1 \cdot u_c - a_1 \cdot S_1^m(t) \quad (\text{F.1})$$

Then:

$$\bar{N}_{F_{81}} = p_1 \left(\frac{\partial u_c}{\partial X} \right)_0 \quad (\text{F.2})$$

with the derivative given by (see Eq. (6.13)):

$$\begin{aligned}
\left(\frac{\partial u_c}{\partial X}\right)_0 &= \hat{\phi} \cdot \beta_2 + \left(\frac{\hat{x}_6 - \hat{x}_1}{x_3}\right)^2 \cdot \hat{\phi} \left(\frac{\hat{x}_1}{x_1}\right)^{m_1} \cdot \beta_1 \\
&+ \hat{\phi} \left(\frac{\hat{x}_1}{x_1}\right)^{m_1} \left(\frac{\hat{x}_2}{x_2}\right)^{m_2} (1 - \beta_1 - \beta_2) \\
&+ \left[1 - \left(\frac{\hat{x}_6 - \hat{x}_1}{x_3}\right)^2\right] \left(\frac{\hat{x}_2}{x_2}\right)^{m_2} \left(\frac{\hat{x}_1}{x_1}\right)^{m_1} \cdot \hat{\phi} \cdot \beta_1
\end{aligned} \tag{F.3}$$

$$\bar{N}_{F82} = p_1 \cdot \left(\frac{\partial u_c}{\partial x_1}\right)_0 \tag{F.4}$$

with

$$\begin{aligned}
\left(\frac{\partial u_c}{\partial x_1}\right)_0 &= \frac{m_1 \cdot \hat{x}_1^{(m_1-1)}}{(x_1^0)^{m_1}} \cdot \left(\frac{\hat{x}_6 - \hat{x}_1}{x_3}\right)^2 \cdot \hat{\phi} \cdot \hat{X} \cdot \beta_1 \\
&- \frac{2(\hat{x}_6 - \hat{x}_1)}{(x_3^0)^2} \cdot \hat{\phi} \cdot \hat{X} \left(\frac{\hat{x}_1}{x_1}\right)^{m_1} \cdot \beta_1 \\
&+ \hat{\phi} \cdot \hat{X} \cdot \frac{m_1 \cdot \hat{x}_1^{(m_1-1)}}{(x_1^0)^{m_1}} \cdot \left(\frac{\hat{x}_2}{x_2}\right)^{m_2} \cdot (1 - \beta_1 - \beta_2) \\
&+ \frac{m_1 \cdot \hat{x}_1^{(m_1-1)}}{(x_1^0)^{m_1}} \cdot \left[1 - \left(\frac{\hat{x}_6 - \hat{x}_1}{x_3}\right)^2\right] \cdot \left(\frac{\hat{x}_2}{x_2}\right)^{m_2} \cdot \hat{\phi} \cdot \hat{X} \cdot \beta_1 \\
&+ \frac{2(\hat{x}_6 - \hat{x}_1)}{(x_3^0)^2} \cdot \left(\frac{\hat{x}_2}{x_2}\right)^{m_2} \cdot \left(\frac{\hat{x}_1}{x_1}\right)^{m_1} \cdot \hat{\phi} \cdot \hat{X} \cdot \beta_1
\end{aligned} \tag{F.5}$$

$$\bar{N}_{F83} = p_1 \cdot \left(\frac{\partial u_c}{\partial x_2} \right)_0 \quad (F.6)$$

with:

$$\begin{aligned} \left(\frac{\partial u_c}{\partial x_2} \right)_0 &= du \cdot (1 - \beta_1 - \beta_2) + \frac{m_2 \cdot \hat{x}_2^{(m_2-1)}}{(x_2^0)^{m_2}} \cdot \hat{\phi} \cdot \hat{X} \cdot \left(\frac{x_1}{x_1^0} \right)^{m_1} \cdot (1 - \beta_1 - \beta_2) \\ &+ \frac{m_2 \cdot \hat{x}_2^{(m_2-1)}}{(x_2^0)^{m_2}} \cdot \left(\frac{\hat{x}_1}{x_1^0} \right)^{m_1} \cdot \hat{\phi} \cdot \hat{X} \cdot \left[1 - \left(\frac{\hat{x}_6 - \hat{x}_1}{x_3^0} \right)^2 \right] \beta_1 \end{aligned} \quad (F.7)$$

$$\bar{N}_{F85} = p_1 \cdot \left(\frac{\partial u_c}{\partial x_4} \right)_0 \quad (F.8)$$

with:

$$\left(\frac{\partial u_c}{\partial x_4} \right)_0 = \frac{d_\ell'}{1+\mu} \cdot (1 - \beta_1 - \beta_2) \quad (F.9)$$

$$\bar{N}_{F86} = p_1 \cdot \left(\frac{\partial u_c}{\partial x_5} \right)_0 \quad (F.10)$$

with:

$$\left(\frac{\partial u_c}{\partial x_5} \right)_0 = \frac{d_\ell''}{1+\mu} \cdot (1 - \beta_1 - \beta_2) \quad (F.11)$$

and:

$$\bar{N}_{F87} = p_1 \cdot \left(\frac{\partial u_c}{\partial x_6} \right)_0 \quad (F.12)$$

with:

$$\left(\frac{\partial u_c}{\partial x_6} \right)_0 = \frac{2(\hat{x}_6 - \hat{x}_1)}{(x_3^0)^2} \cdot \hat{\phi} \cdot \hat{X} \cdot \left(\frac{\hat{x}_1}{x_1} \right)^{m_1} \cdot \beta_1 \cdot \left(1 - \left(\frac{\hat{x}_2}{x_2} \right)^{m_2} \right) \quad (F.13)$$

For constant channel parameters, Georgakakos and Bras (1982)

give:

$$\bar{N}_{F88} = -a_1 \cdot [m \cdot \hat{S}_1^{(m-1)} + \frac{m \cdot (m-1)(m-2)}{2} \cdot \sigma_{S_1}^2 \cdot \hat{S}_1^{(m-3)}] \quad (F.14)$$

with σ_{S_i} denoting the standard deviation of the state S_i at time T ,
for $i = 1, 2, \dots, n$.

$$\bar{F}_{08} = p_1 \cdot \hat{u}_c - a_1 \cdot \left[\hat{S}_1^m + \frac{m \cdot (m-1)}{2} \cdot \sigma_{S_1}^2 \cdot \hat{S}_1^{(m-2)} \right] \quad (F.15)$$

$$\bar{M}_{F8i} = p_1 \cdot \left(\frac{\partial u_c}{\partial u_i} \right)_0 \quad ; \quad i = 1, 2, 3 \quad (F.16)$$

with:

$$\begin{aligned}
\left(\frac{\partial u_c}{\partial u_i}\right)_0 &= M_{\phi_i} \cdot [\hat{X} \cdot \beta_2 + \left(\frac{\hat{x}_6 - \hat{x}_1}{x_3}\right)^2 \cdot \hat{X} \cdot \left(\frac{\hat{x}_1}{x_1}\right)^{m_1} \cdot \beta_1 \\
&+ \hat{X} \cdot \left(\frac{\hat{x}_1}{x_1}\right)^{m_1} \cdot \left(\frac{\hat{x}_2}{x_2}\right)^{m_2} \cdot (1 - \beta_1 - \beta_2) \\
&+ [1 - \left(\frac{\hat{x}_6 - \hat{x}_1}{x_3}\right)^2] \cdot \left(\frac{\hat{x}_2}{x_2}\right)^{m_2} \cdot \left(\frac{\hat{x}_1}{x_1}\right)^{m_1} \cdot \hat{X} \cdot \beta_1]; \quad i=1,2,3
\end{aligned} \tag{F.17}$$

The non-zero elements of the relevant linearization matrices, regarding the j^{th} ($1 < j \leq n$) reservoir in the series are given next.

Define (see Eq. (6.15)):

$$F_{7+j} = p_j \cdot u_c + a_{j-1} \cdot S_{j-1}^m - a_j \cdot S_j^m \quad ; \quad j = 2, \dots, n \tag{F.18}$$

Then:

$$\bar{N}_{F_{7+j},1} = p_j \cdot \left(\frac{\partial u_c}{\partial X}\right)_0 \quad ; \quad j = 2, \dots, n \tag{F.19}$$

$$\bar{N}_{F_{7+j},i} = p_j \cdot \left(\frac{\partial u_c}{\partial x_{i-1}}\right)_0 \quad ; \quad j = 2, \dots, n, \quad i = 2, 3, \dots, 7 \tag{F.20}$$

$$\bar{N}_{F_{7+j,7+j-1}} = a_{j-1} \cdot [m \cdot \hat{S}_{j-1}^{(m-1)} + \frac{m \cdot (m-1)(m-2)}{2} \cdot \sigma_{S_{j-1}}^2 \cdot \hat{S}_{j-1}^{(m-3)}] \quad j = 2, \dots, n \quad (F.21)$$

$$\bar{N}_{F_{7+j,7+j}} = -a_j \cdot [m \cdot \hat{S}_j^{(m-1)} + \frac{m \cdot (m-1)(m-2)}{2} \cdot \sigma_{S_j}^2 \cdot \hat{S}_j^{(m-3)}] \quad j = 2, \dots, n \quad (F.22)$$

$$\begin{aligned} \bar{F}_{O_{7+j}} &= p_j \cdot \hat{u}_c + a_{j-1} \left[\hat{S}_{j-1}^m + \frac{m \cdot (m-1)}{2} \cdot \sigma_{S_{j-1}}^2 \cdot \hat{S}_{j-1}^{(m-2)} \right] \\ &- a_j \cdot \left[\hat{S}_j^m + \frac{m \cdot (m-1)}{2} \cdot \sigma_{S_j}^2 \cdot \hat{S}_j^{(m-2)} \right] ; j = 2, \dots, n \quad (F.23) \end{aligned}$$

$$\bar{M}_{F_{7+j,i}} = p_j \cdot \left(\frac{\partial u_c}{\partial u_i} \right) ; j = 2, \dots, n, i = 1, 2, 3 \quad (F.24)$$

The outflow of the last reservoir is the second rainfall-runoff model output (the first is precipitation rate). Define (see Eq. (6.16)):

$$G_2 = a_n \cdot S_n^m \quad (F.25)$$

Then:

$$\bar{N}_{G_{2,n}} = a_n \cdot \left[m \cdot \hat{S}_n^{(m-1)} + \frac{m \cdot (m-1)(m-2)}{2} \cdot \sigma_{S_n}^2 \cdot \hat{S}_n^{(m-3)} \right] \quad (\text{F.26})$$

$$\bar{G}_{O_2} = a_n \cdot \left[\hat{S}_n^m + \frac{m \cdot (m-1)}{2} \cdot \sigma_{S_n}^2 \cdot \hat{S}_n^{(m-2)} \right] \quad (\text{F.27})$$